Enhanced ethanol production:
In-situ ethanol extraction using selective adsorption

Rudy Jones

Thesis submitted to the
Faculty of Graduate and Postdoctoral Studies
In partial fulfillment of the requirements PhD for the degree of

Doctorate in Philosophy

In

Department of Chemical and Biological Engineering

University of Ottawa

Abstract

Due to their comparatively lower costs, the widespread availability across a range of climates, and their status as a dedicated energy crop (as opposed to being an important food source), lignocellulosic biomass feeds are ideal raw materials that can be used to produce domestic fuels to partly displace our dependence on non-renewable sources. Although the use of lignocellulosic biomass for ethanol production is often identified as having the greatest potential to meet current and future fuel demands, there exists a technological gap that needs bridging before the conversion of lignocellulosic biomass can be economically competitive with the well-established corn to ethanol production plants of the United States of America and the sugar cane to ethanol plants of Brazil. Due to the mixed sugar composition of the lignocellulosic hydrolysate, genetically-modified microorganisms which are capable of efficiently converting both hexose and pentose sugars to produce ethanol are used for maximum sugar utilization. These recombinant strains have however been shown to have less tolerance to product inhibition, which can result in low sugar utilization, low ethanol production and expensive downstream purification.

In this study, experiments were first performed for adsorbent screening to identify materials that could be used to selectively extract ethanol from fermentation broth. Filtrasorb-600 granular activated carbon (F-600) was selected for further studies due to the combination of relatively high ethanol capacity across the concentration range of interest, rapid kinetics, low cost and availability. The performance of this ethanol-selective adsorbent was first tested on single component systems and later studied in the presence of multiple components (mixed residual sugars/ethanol as well as with actual fermentation broth). Ethanol capacities in multi-component systems were found to be close to the capacity measured during single component studies. The adsorption of sugar was strongly inhibited when appreciable ethanol concentrations were present. Extensive mathematical modelling of the adsorption system was performed.

Studies were then expanded to an *E. coli* KO11 fermentation system in order to assess the impact of a preferential ethanol removal by adsorption. A portion of the fermentation broth was routed through an ethanol selective packed adsorption bed when concentrations of ethanol in the broth reached level known to cause inhibition. By removing ethanol from the broth during the fermentation, inhibition due to the presence of ethanol could be alleviated, enhancing the substrate utilization and ethanol production of the fermentation.

Although inhibition could be avoided by removing ethanol, the fermentation productivity decreased from cycle to cycle. The most likely causes of this measured decline in productivity were the accumulation of other metabolites known to cause inhibition (lactic acid, etc.) and the aging of the cells in the fermenter.

Although desorption and recovery were studied briefly, more schemes must be tested in order to determine the optimum desorption technology once the ethanol has been concentrated on the surface of the adsorbent.

Résumé

En raison de son prix relativement faible, de sa grande disponibilité à travers une variété de climats et de son potentiel comme source d'énergie dédiée (par opposition aux sources d'énergie servant aussi de nourriture), la biomasse lignocellulosique est une matière première pouvant être utilisée avantageusement pour produire des combustibles domestiques, permettant ainsi de contourner partiellement notre dépendance aux sources d'énergie non-renouvelables. Bien que l'utilisation de la biomasse lignocellulosique pour la production d'éthanol offre un grand potentiel pour satisfaire les demandes actuelles et futures en combustible, il existe néanmoins un écart technologique qui doit être comblé avant que la conversion de la biomasse lignocellulosique puisse être une alternative économiquement viable en comparaison aux usines de production d'éthanol des États-Unis d'Amérique basées sur le blé d'Inde et à celles du Brésil basées sur la canne à sucre. Étant donnée la présence de pentoses et d'hexoses dans l'hydrolysat lignocellulosique, des microorganismes génétiquement modifiés, capables de convertir autant les hexoses que les pentoses pour produire de l'éthanol, sont utilisés pour augmenter l'utilisation des sucres et la concentration en éthanol. Ces microorganismes sont toutefois plus susceptibles pour ce qui a trait à leur tolérance aux concentrations élevées en éthanol, menant ainsi à une faible utilisation en sucre, une faible teneur en éthanol et des coûts de purification élevés.

Dans cette étude, des expériences ont été menées pour identifier l'adsorbant ayant le plus grand potentiel pour extraire l'éthanol de manière sélective à partir du bouillon de fermentation. Le charbon activé Filtrasorb-600 (F-600) a été retenu en raison de sa bonne capacité d'adsorption, sa cinétique rapide, son bas prix et sa disponibilité. La performance de cet adsorbant a d'abord été évaluée pour des systèmes aqueux contenant un seul composant et par la suite contenant plusieurs composants. La capacité d'adsorption de l'éthanol dans les systèmes à plusieurs composants est presqu'identique à celle du système eau-éthanol. Par contre, l'adsorption des sucres est fortement inhibée en présence d'éthanol. Un modèle mathématique du système d'adsorption a été développé pour simuler un lit d'adsorption.

Des fermentations avec le microorganisme *E. coli* KO11 ont été faites pour évaluer l'impact de l'adsorption sélective de l'éthanol durant la fermentation. Lorsque le niveau d'inhibition d'éthanol a été atteint, une partie du bouillon de fermentation a été passée à travers un lit d'adsorption pour enlever une certaine quantité d'éthanol. En enlevant une partie de l'éthanol du bouillon pendant la fermentation, l'inhibition est ainsi réduite et la fermentation peut se poursuivre.

Bien qu'il soit possible d'éviter l'inhibition en enlevant une partie de l'éthanol, la productivité de la fermentation a néanmoins diminué de cycle en cycle. Les causes probables de ce déclin de la productivité sont l'accumulation d'autres métabolites pouvant provoquer l'inhibition (l'acide lactique, etc.) et le vieillissement des cellules dans le fermenteur.

Bien que la désorption et la récupération aient été étudiées brièvement, une étude complète est nécessaire afin de déterminer la façon la plus efficace de désorber l'éthanol de la surface de l'adsorbant.

Statement of contributions of collaborators

I hereby declare that I am the sole author of this thesis**.** I was responsible for the experimental design, experimental procedures and all data analysis throughout the project. Project guidance was provided by my co-supervisors: Dr. Handan Tezel and Dr. Jules Thibault.

Graham Morse worked under my guidance on his undergraduate thesis on the development of an adsorption model based on artificial neural networks. Graham is the first author of the paper contained in Chapter 4 and entitled "*Neural Network Modelling of Adsorption Isotherms*". In this publication, I was responsible for generating data for isotherms representing each isotherm type (as defined by IUPAC). I was also responsible for developing and validating the ANN model.

Julie-Anne Gandier worked under my guidance on her undergraduate thesis. Julie-Anne assisted in sample collection for the fermentation and extraction experiments which lasted in some cases more than 100 h. Julie-Anne is listed as the second author of the paper contained in Chapter 6 and entitled "*Enhanced ethanol production through selective adsorption in bacterial fermentation".*

Vinay Mulgundmath is a colleague with whom I assisted in the modelling of gas phase adsorption systems. Vinay built and operated a pressure swing adsorption unit for the purpose of CO_2 adsorption from flue gas mixtures. The model which was developed by the author in Chapter 3 was expanded to include gas phase systems and the impact of temperature on capacity in gas phase systems. Vinay was responsible for experiments and data collection. I was responsible for the model development (mass and energy balances), and the modelling of the experimental data (concentration and temperature profiles within the column). The work appears in the Appendix A.1 as it is not directly related to the work presented in this thesis. Vinay is listed as the first author of the study.

Acknowledgments

I would like to express my heartfelt thanks to my supervisors Dr. Handan Tezel and Dr. Jules Thibault. Without their continued support over the years, this thesis would not have been possible. I was fortunate to have two supervisors to offer critical analysis of my work and moral support in my life.

I would also like to extend a thank you to the technical support team at the University of Ottawa: Louis Tremblay, Franco Ziroldo and Gérard Nina who were always there to solve any unforeseen technical issues.

Thanks to my lab mates Julie-Anne Gandier, Vinay Mulgundmath, Chris Bestfather, Dan Dicaire, Mohamed Hashi, Estela Patcheco, Graham Morse, Muhammad Tawalbeh and Jessica Poupore for their assistance and companionship.

Finally, a special thanks to my loving friends and family.

Contents

List of Tables

Chapter 8

List of Figures

Chapter 1

Chapter 2

Chapter 3

Chapter 4

Chapter 5

Chapter 6

SECTION – I: Introduction

Chapter 1

1.0 Introduction

When conducting research in the field of renewable energy, and in particular when studying the production of bioethanol, it is important to understand the underlying political and economic factors which have shaped the industry to date and stimulated research in this developing field. Historically, scarcity of oil supply (in the short term or long term) and the rise in the price of oil have led to the commissioning of bio-refineries and the proliferation of research groups focused on various aspects surrounding the production of fuel from renewable sources.

In North America, ethanol fuel was first thrust into the media spotlight in 1973 when President Richard Nixon announced "Project Independence" in response to the Arab oil embargo. The stated goal of Nixon's initiative was to achieve energy self-sufficiency for the United States of America by the year 1980. With this strong endorsement from the world's largest consumer of energy, the funding for the development of bio-refineries and research and development rapidly grew. Industrial ethanol from fermentation for the purpose of fuel production in the US sprang to life by the mid-1970s with the commissioning of hundreds of corn-to-ethanol plants over the span of the next decade. Nixon's initial vision was reaffirmed during the second energy crisis in 1979 which began with the Iranian revolution when protests and unrest caused a decline in Iranian oil production, the oil markets were driven higher sharply due in part to the reduced production. The Iraq invasion of Iran in 1980 also contributed to the price of oil being driven even higher during this time as both countries saw dramatic reductions in oil production (Soloman et al., 2007)

The first major wave of bio-refineries for the production of fuel grade ethanol came in the early 1980s, with the majority of the ethanol production capacity using corn as an energy crop. The ethanol capacity of the US rose slowly and steadily during this time from a level of 175 million gallons per year in 1980, to 900 million gallons per year by the end

of the decade (Renewable Fuel Association (RFA), 2011). This production rise in ethanol occurred despite the fact that the world was once again experiencing cheap and abundant oil supply as the situation in the Middle East stabilized and secondary oil exporters like Mexico, Nicaragua and Venezuela ramped up their oil exports.

Nowadays, with the price of oil consistently above 85 USD per barrel, the need for a renewable domestic fuel source has never been more apparent. The demand for oil has risen sharply through the 1990's and 2000's as the per capita energy demand of developing nations like India and China has risen.

Although energy security has always been the primary factor that has driven research in the field of renewable fuels, more recently, the environmental benefits of 'green fuels' has been brought to light. Although some debate still exists about the degree to which greenhouse gases (GHGs) are reduced by using ethanol fuels from renewable sources, it is generally accepted that ethanol particularly from sugar cane and lignocellulosics reduce GHG emissions by anywhere from 50 to 100% (based on a life cycle analysis (LCA) basis) when compared to conventional gasoline and, by an even greater amount, when unconventional sources (Canadian tar sands) are considered (Sims et al., 2010). The reduced level of GHGs is mostly attributed to the CO_2 uptake of the energy crop as it grows. Considering the fact that transport is responsible for 23% of worldwide greenhouse gas emissions, the use of ethanol as a fuel source is an environmentally attractive alternative (Chavez-Rodriguez and Nebra, 2010). Ethanol is an oxygenated fuel that burns cleaner than gasoline. It has been shown that using ethanol-blended fuels can significantly reduce N_2O emissions, a compound that leads to photochemical smog (Tavares et al., 2011). Not all environmental assessments agree that the net impact of ethanol as a biofuel is positive. The greatest environmental criticism levelled at the bioethanol technology is the land and water usage. When examining a life cycle analysis of ethanol from wheat and barley, Lankoski and Ollikainen (2011) found that the net impact of ethanol fuel (economic/environmental) was a negative one. The authors cited the effect the crop growth had on nutrient depletion in the soil and water usage as two problematic issues in Finland due to the production of fuel from these lignocellulosic

crops. Studies with regards to the ecological footprint often have contrasting findings with many studies purporting the benefits of biofuels from an ecological perspective while others oppose these findings. An issue that is less debateable, the commissioning of bio-refineries does have a positive impact on local economies in rural areas, creating jobs and income locally (Chandel et al., 2010).

The raw materials which are most commonly used to produce ethanol through fermentation can be broken into three classifications: sugar crops, starch-based crops and lignocellulosic biomass. For each potential feed source, there are inherent advantages and disadvantages to consider. An overview of the three classifications is provided below:

a) Sugar crops

The most widely used sugar crop for the production of ethanol is sugar cane. Other potential sugar crops include sugar beet and molasses. The pre-processing required when using a sugar crop is the feedstock's greatest competitive advantage. Sugars are readily available in fermentable form. The milling/extraction sections of a sugar cane to ethanol plant are simple, straightforward and have low energy requirements. The concentrated sucrose liquor (as much as 16 %) can be fermented with yeast (the primary organism for fermentative ethanol production) which can consume the disaccharide sugar sucrose and produce ethanol broth with high concentrations (10-12 % wt or more) (Maiorella et al., 1981).

The main drawback of using sugar crop feed is the fact that the crop is also relied upon as a food source (sugar cane is used to produce edible sugar). Furthermore, sugarcane growth is limited to tropical and subtropical climates for the most part.

b) Starch crops

The most common starch-based feedstock for ethanol production is the cereal grain corn. Corn to ethanol plants form the backbone of the current fermentative ethanol industry in the United States. Other starch-based feeds include wheat, rice and barley. Since the carbohydrate starch is not directly fermentable by yeast, a more complex

milling/extraction process is required to obtain the fermentable sugar glucose. The starch polymer is a string of glucose monomers. The bond can be broken and glucose obtained by many methods which could include milling, enzymatic treatment and treatment with weak acids. It has been estimated that as much as 15-20 % of a total capital cost of a starch to ethanol plant is required to build the pre-processing units. Like the production of ethanol from sugar crop, starch based materials also suffer from the fact that the crop used to produce energy is also a food source. Recent rises in the cost of corn (often attributed to corn-to-ethanol plants) have shed negative publicity on the US ethanol industry (Maynard, 2007).

Corn and other potential starch feedstock grow in a wider range of climates than their sugar crop counterparts.

c) Lignocellulosic crops

Lignocellulose to ethanol plants are viewed as the second generation bioethanol plant. The first generation plants (including sugar and starch-based crops) utilize raw materials that can be used for human consumption whereas lignocellulose crops are a dedicated energy crop that is not consumed by humans.

Lignocellulose accounts for the majority of biomass in the world (Singh et al., 2010). These materials are low value feeds that are made up of cellulose, hemicellulose and lignin which are found in almost all plant life. The cellulose, hemicellulose and lignin are bound tightly together and are responsible for providing plants their rigid quality. Cellulose is a crystalline polysaccharide (strong and stable) that is comprised of thousands of glucose molecules. Hemicellulose is also a polysaccharide; it has a weaker structure than cellulose and is comprised of various pentose sugar monomers (xylose, mannose, galactose, and arabinose). The final organic polymer that makes up cellulosic biomass is lignin. Lignin is the organic polymer most responsible for the rigidity of the plant cell wall. With its high heating value, lignin is viewed as a valuable co-product of the extraction process (Zaldivar et al., 2001).

The materials most commonly identified as potential dedicated energy crops include softwoods (poplar and willow), switch grass, and corn stover although various lingocellulose feed alternatives are still being explored.

Depending on the feed selected, the sugar composition can vary dramatically, as a rule of thumb, the ratio of hexose to pentose sugars is about 2:1, with glucose as the hexose sugar and a mixture of pentose sugars of which xylose is the most abundant (Maiorella, 1981).

Due to the rigid nature of the feed, lignocellulosic energy crops suffer from the need for the most intensive pretreatment processing. The biomass first must be pulverized (milling, steam explosion or other methods have been reported) followed by an enzymatic hydrolysis of both cellulose and hemicellulose to obtain sugars in a fermentable form. Due to the nature of the sugar composition (pentose along with hexose sugars), the fermentation becomes more complicated as traditional biocatalyst yeasts cannot metabolise the pentose sugars to produce ethanol. Much research has been ongoing for many years to find microorganisms capable of converting both pentose and hexose sugars to produce ethanol.

Lignocellulosic biomass has major advantages over the more common sugar and starch energy crops:

- Lignocellulosic raw materials are not consumed as food sources like the other more traditional energy crops
- The climates in which these crops grow are incredibly varied, the feed availability is truly world wide
- Crop utilization (assuming all sugars can be consumed) is much greater than that of corn ethanol production where only the head of the corn is used
- The cost of the crops is lower when compared with corn or sugarcane
- Lignocellulose crops can be grown on marginal lands

The drawbacks of lignocellulosic feed lay with the current processing technologies. The current state of the technology leads to very low productivity (typically final ethanol concentrations are below 4 - 6 wt%) and thus expensive downstream processing is required. Significant water use is also a key drawback of current lignocellulosic technologies.

Table 1 - Comparison of feed crops for bioethanol production

	Sugarcane	**Corn**	**Lingo-cellulose**
Availability	limited	moderate	abundant
Feed cost	moderate	moderate	low
Food/Fuel	both	both	fuel
Sugars present	sucrose	glucose	hexose and pentose
Crop utilization	high	low	high
Processing Technology	established	established	under developed
Current Processing costs	low	moderate	high

For the purpose of this research project, the focus has been placed on bench-scale experiments intended to mimic the broth composition in a fermenter that would be found when using lignocellulose feeds (4 - 6 wt% ethanol).

Although the advantages of using lignocellulose over starchy or sugar crop materials for the production of ethanol are obvious, the added technological hurdles that exist in the processing of these feeds currently limit the commercial viability of lignocellulosic ethanol production plants. The low cost of the feed is currently offset by the comparatively higher costs for pretreatment, fermentation, product recovery and waste treatment (Chandel et al., 2010).

Enhancing ethanol production during the fermentation is recognized as one the processing steps, which if improved could potentially have the greatest impact on lowering the energy required to produce fuel grade ethanol from lignocellulose. The majority of research that has been published over the past two decades focuses on finding yeast, fungi or bacteria that exist naturally. Researchers have also developed genetically-

modified variations of these microorganisms that have the ability to produce ethanol using pentose and hexose sugars as a substrate to maximize the productivity of the fermentation (Bothast et al., 1999).

Traditional microorganisms used for the production of ethanol from starch-based or saccharine feeds include *Saccharomyces cerevisiae* and *Zymomonas mobilis*. These microorganisms are well established in industry, having been used successfully for many decades due to the high ethanol yield and productivity in large scale processes. Neither of these traditional ethanol producing microorganisms have the ability to metabolise pentose sugars for ethanol production (Bothast et al., 1999). This is a major drawback for traditional microorganisms since the pentose sugars in lignocellulose can account for more than one third of the total sugar content (Maiorella, 1981).

In the early 1980s, various natural xylose consuming yeasts were discovered and tested for their potential in the processing of mixed sugar feeds. Some of these natural xylose consuming yeasts studied include: *Pachysolen tannophilus* and *Candida shehatae* among others (Bothast et al., 1999). For the most part, these yeasts were reported to have low ethanol productivity and low tolerance to inhibition. The majority of research focused today on finding appropriate microorganisms, surrounds the development of genetically-modified microorganisms. These novel recombinant biocatalysts fall into two categories based on their development philosophy. The first approach is to alter the genetic makeup of traditional ethanol producing microorganisms, which already consume hexose sugar, and produce a xylose metabolic pathway (*S. cerevisiae* and *Z. mobilis*). The other types of recombinant biocatalysts that have been developed involve the modification of microorganisms that are already capable of consuming multiple substrates and enhancing their ability to produce ethanol (*E. coli, Klebsiella oxytoca*) (Bothast et al., 1999). A comprehensive list of studies using recombinant microorganisms was compiled by Xin Li (2009) and has been reproduced with permission in Table 2.1.

Table 2 - Comparison of wild-type and genetically-engineered ethanologenic microorganisms.

Microorganism	**Description**	**Substrates**	**Culture conditions**	**Ethanol yield**	**Overall ethanol productivity**	**Ethanol tolerance**	**References**
Pichia stipitis (ATCC58785)	Wild type	Glucose and xylose	30℃, pH=5 oxygen-limited	0.45 g/g	0.24 g/(L·h)	64 g/L	Agbogbo and Wenger, 2006; Agbogbo et al., 2007
Pichia stipitis (FPL-Shi21)	cyc1-Δmutant strain	Glucose and xylose	25℃, anaerobic	0.46 g/g	0.43 g/(g cells·h)	N/A	Shi et al., 1999
Pachysolen tannophilus CBS 4044	Wide type	Pentose, hexose, and cellobiose	30℃, pH=4.5, aerobic	0.37 g/g	0.62 g/(g cells·h)	50 g/L	Barbosa et al., 1990; Sánchez et al., 2002
Candida shehatae (CSIR-Y492)	Wild type	Glucose and xylose	30℃, pH=4, aerobic	0.37 g/g	0.9 g/(L·h)	48 g/L	du Preez et al., 1986; du Preez et al., 1987
Klebsiella oxytoca (P2)	Containing *pdc*, *adhB* genes from *Z. mobilis*	Pentose, hexose, and cellobiose	32℃-35℃, pH=5.0-5.2, anaerobic	0.46 g/g	1.6 g/(L·h)	36 g/L	Wood and Ingram, 1992; Golias et al., 2002
Fusarium oxysporum (VTT-D-80134)	Wild type	Glucose and xylose	30℃, pH=4.5, oxygen-limited	0.38 g/g	0.15 g/(g cells·h)	50-60 g/L	Ruiz et al., 2007
Saccharomyces cerevisiae BO 15	Wild type	Sucrose	25℃, anaerobic	0.91 g/g	1.0 g/(L·h)	18.7 vol% (147.5 g/L)	Esser and Stahl, 1982
Saccharomyces cerevisiae TMB3001	Carrying *XYL1*, *XYL2* genes from *P. stipitis*	Glucose and xylose	30℃, pH=5.5 anaerobic	0.35-0.38 g/g	0.24-0.30 g/(g cells·h)	N/A	Eliasson et al., 2000

Table 2 (cont.) - Comparison of wild type and genetically-engineered ethanolgenic microorganisms.

Microorganism	**Description**	**Substrates**	**Culture conditions**	**Ethanol yield**	**Overall ethanol productivity**	**Ethanol tolerance**	**References**
Saccharomyces cerevisiae 1400 (pLNH32)	Carrying *XR*, *XDH* genes from *P. stipitis* and over-expressing *XK* gene	Pentose and hexose	30°C, pH=5.5 anaerobic	0.46 g/g	1.6 g/(L·h)	N/A	Moniruzzaman et al., 1998; Ho et al., 1998
Zymomonas mobilis ZM4	Wide type	Glucose	30°C, pH=5, anaerobic	0.50 g/g	3.9 g/(L·h)	16 vol% (126 g/L)	Davis et al., 2006
Zymomonas mobilis ZM4 (pZB5)	Carrying two operons: P_{gap}-*xylA/xylB*, P_{eno}-*tal/tktA*	Glucose, xylose, and arabinose	30°C, pH=5, anaerobic	0.46 g/g	1.29 g/(L·h)	63 g/L	Joachimsthal et al., 1999
Zymomonas mobilis AX101	Insertion 7 genes into the genome.	Glucose, xylose, arabinose,and fructose	30°C, pH=5.5, anaerobic	0.45 g/g	3.3 g/(L·h)	50 g/L	Mohagheghi et al., 2002; Lawford and Rousseau, 2003
Escherichia coli FBR5	Carrying *the* plasmid pLOI297	Pentose and hexose	35°C, pH=6.5, anaerobic	0.46 - 0.51 g/g	0.9 g/(L·h)	50 g/L	Zhang et al., 1995; Qureshi et al., 2006
Escherichia coli KO11	Containing *pdc*, *adhB* genes from *Z. mobilis*	Pentose and hexose	30°C, pH=6.0-6.5, anaerobic	0.53 g/g	1.3 g/(L·h)	50 g/L	Ohta et al., 1991
Clostridium thermocellum SS2	Wild type	Cellulose	60°C, pH=7.5, anaerobic	0.33 g/g	0.021 g/(L·h)	8 vol% (63 g/L)	Sudha Rani et al., 1996; Sudha Rani and Seenayya, 1999
Geobacillus thermoglucosidasius (M10EXG)	Wild type	Pentose and hexose	50-80°C, pH=6-8, anaerobic	0.082 g/g	0.0083 g/(L·h)	10 vol% (79 g/L)	Fong et al., 2006;

E. coli was recognized early as a "platform organism" in the development of genetically-modified biocatalysts as a potential candidate for the conversion of lignocellulosic feed to fuel grade ethanol (Bothast et al., 1999). The bacteria *E. coli*, in its native form can use a wide range of substrates, including all substrates that are present in the lignocellulosic hydrolysate, and it is considered to be stable and strong in a wide range of environmental conditions (Alterthum and Ingram, 1989). The strain *E. coli* KO11 was first produced by genetically modifying the genetic makeup of *E. coli*, with the insertion of genes from a common well known ethanolgenic bacteria (*Z. mobilis*). The genetic alteration for the purpose of ethanol production from mixed substrates was first performed by Dr. Lonnie Ingram and his colleagues at University of Florida in Gainesville, Florida in 1989 (Alterthum and Ingram, 1989). *E. coli* KO11 has been used in many studies on cellulose based feeds including pine wastes (Barbosa et al., 1992), willow (von Sivers et al., 1994), rice hulls (Moniruzzaman and Ingram, 1998), sugar cane bagasse (Takahashi et al., 2000), cotton gin residues (Agblevor et al., 2003), and corn stover (Kim et al., 2006).

In addition to the successful production of ethanol from the mixed sugar hydrolysates noted above, the strain has also displayed a strong resistance to both extreme temperature ranges, and to a wide range of pH (Moniruzzaman et al., 1998). Because of the favourable productivity and yields reported in literature, the environmental robustness, ability to consume a wide range of mixed sugars, and the commercial availability, *E. coli* KO11 was selected among the candidates for this research project.

Ethanol extraction from fermentation broth has become an increasingly popular research topic. The ethanol content in the broth is toxic to the fermentative microorganisms and causes the fermentation to cease at lower ethanol concentration. The genetically-modified microbes used to convert mixed sugar substrates are especially susceptible to the elevated ethanol concentrations (Bothast, 1999). In order to alleviate the inhibition that is witnessed, a number of ethanol selective extraction techniques have been explored. Some of the technologies studied in the literature are highlighted below:

Pervaporation

Pervaporation is a technology that was first utilized in the 1950s (Binning et al., 1961). The technology is a combination of membrane permeation and evaporation at the feed side of the membrane. In recent decades, membrane advancement has seen the production of hydrophobic membranes that are ethanol selective. Permeate streams containing 20-23% w/w have been reported from dilute ethanol feeds (4 - 6% w/w) (Fadeev et al., 2000). The majority of the studies on ethanol extraction from dilute solutions by pervaporation have focused on simple water/ethanol systems. One important issue in the field of membrane pervaporation is the membrane fouling which can significantly reduce membrane performance over time. Membrane fouling causes over time a reduced membrane flux.

Liquid-Liquid Extraction

Liquid-Liquid extraction uses an added solvent to redistribute the ethanol into an organic phase from the aqueous phase. In 1986, Daugulis and Kollerup identified 19 solvents that were suitable for the extraction of ethanol from fermentation broth. The solvents were tested with actual fermentation broth containing biomass and ethanol extraction efficiencies as high as 98% were reported. The liquid-liquid extraction option is complicated by the need to recover the ethanol from the organic phase and the need to regenerate the extracting solvent.

Ethanol removal by carbon dioxide stripping

Ethanol can be removed and recovered from fermentation broth by employing a carrier gas that will not disturb the fermentation. The most common carrier gas employed for this purpose is carbon dioxide which is produced through the conversion of sugars to produce ethanol during the fermentation. The carbon dioxide can be recycled and bubbled through the broth for the purpose of ethanol stripping. The enriched ethanol is later recovered from the carrier gas (Hashi et al., 2010).

Vacuum extraction

Ethanol can be removed by coupling a bioreactor with a vacuum chamber. This design favors the removal of the ethanol molecule (based on volatility) (Cardona and Sanchez, 2007).

.

Adsorption

Much of the available literature in the field of adsorption of ethanol from fermentation broth was published from 1980-1990 during the formative years of the ethanol industry. Chapter 2 of this document outlines a number of studies that explored the extraction of ethanol using hydrophobic adsorbents. The majority of these studies focused on the extraction of ethanol from model broth (as opposed to the actual fermentation broth). This thesis goes on to explore the selective extraction of ethanol from model broth as well as fermentation broth using ethanol selective adsorbents. The benefits of online extraction are explored and modelling of the competitive adsorption is presented.

Compared to the established corn to ethanol industry in the United States and the sugar cane to ethanol industry in Brazil, the lignocellulose conversion to ethanol technology is currently underdeveloped. The key to successful commercialization of the technology is the optimization of the process in a number of areas. Finding cheaper raw materials, increasing crop yields, improving the biomass pretreatment processes, achieving higher fermentation rates, avoiding ethanol inhibition and enhancing the downstream separation of ethanol are some of the key areas of research that will improve the economic viability of ethanol as a gasoline replacement (Chandel et al., 2010).

1.1 Main objectives

The main objectives of the thesis are to:

1. Identify suitable candidates among commercially available adsorbents for the selective extraction of ethanol from fermentation broth.
2. Characterize the key adsorbent performance parameters in batch and dynamic studies of suitable adsorbents
    a. Equilibrium capacity

b. Adsorption kinetics
c. Column performance
d. Ethanol selectivity over residual sugars and broth medium
e. Reversibility of adsorption (Can ethanol be easily desorbed?)
f. Develop and validate a mechanistic model that can use data acquired from simple ethanol adsorption performance in batch systems to simulate the behaviour of dynamic breakthrough experiments over a range of conditions.

3. Design and implement a novel integrated packed bed bio-reactor/packed bed ethanol extraction unit.
4. Develop an integrated model that can predict ethanol production in the bioreactor and subsequent ethanol extraction through a packed bed adsorber.

1.2 Research Methodology

The overriding goal of this research was to enhance ethanol production in fermentation systems by exploiting ethanol selective adsorbents. The structure of the research project is shown in Figure 1.1 which presents the different stages of research that is carried out.

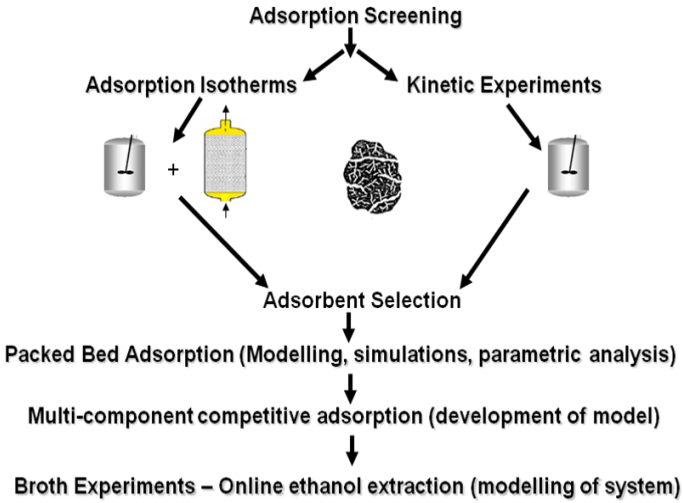

Figure 1 – Stages of the research carried out in this study.

Following a comprehensive adsorption screening, the most promising adsorbent candidates were selected for further research. From the best performing candidates, F-600 activated carbon was selected for further study. Even though F-600 activated carbon did

not have the highest capacity or the fastest kinetics (in part due to its particle size), it performed well in terms of both kinetics and capacity and was commercially available for a reasonable cost (which was not the case for some of the other screened adsorbents). F-600 was first tested extensively in batch systems in order to evaluate the kinetics associated with ethanol adsorption, and the ultimate uptake of ethanol that could be achieved. Based on these batch systems, a finite differences model was developed to describe the mass transfer of ethanol from the liquid bulk phase to the adsorbed phase. This model was later used for simulations of more industrially relevant packed bed experiments with the results of the simulations being validated with actual experiments. Following studies with simple broth, experiments with a more representative fermentation broth were performed (containing residual sugars). The competitive adsorption between ethanol and the sugars known to be present in the greatest proportions (glucose and xylose) were studied in multi-component systems. A competitive adsorption isotherm model based on artificial neural networks was developed and found to appropriately represent the behaviour of the competitive adsorption.

Finally, with an understanding of the competitive nature of the adsorption, actual fermentation runs were carried with an online ethanol extraction scheme exploited to maintain low ethanol levels in the broth. The benefit associated with the online ethanol extraction was explored and a comprehensive model for the fermentation, as well as the ethanol/sugar extraction via adsorption was developed.

1.3 Structure of the thesis

The main body of the thesis is subdivided into six sections: Introduction, Adsorbent screening, modelling of adsorption experiments, Fermentation experiments, Conclusions and Appendicies. Each section is dedicated to a particular sub-topic within the scope of the project. Each chapter within the main body of the thesis is written in a particular journal article format. There are six journal papers included in this document, covering the entire scope of the project. The focus of each section is outlined below along with a description of the contents of each chapter. An overview of the chapter contents is included below:

Chapter 1: "*Introduction*" presents some background on the research topic, the scope and structure of the thesis.

Chapter 2: "*Ethanol removal from water for bioethanol production using silicalite, activated carbon and ZSM-5 adsorbents: Adsorption isotherms and kinetics*" presents the data from an adsorbent screening study which was performed. The paper covers relevant adsorption literature from synthetic and actual fermentation broths for various adsorbent materials. The publication presents new data for various ethanol-water adsorbent systems which were not available in the literature.

Published:

Jones, R.A., Tezel, F.H., Thibault, J., and Tolan, J.S., (2007), Bioethanol production to be blended with gasoline: Improvements in energy use by adsorption. *Inter. J. of Ener. Res.* 31 (15), 1517-153

Presented:

R. Jones, F.H. Tezel, J. Thibault, R. El-Hawary, and J. Tolan, "Adsorption separation of ethanol from water for bioethanol production", presented at the *AIChE Annual meeting* in Cincinnati, Ohio, USA, October 30-November 4, 2005.

Chapter 3: "*Simulation and validation of ethanol removal from water in an adsorption packed bed: isotherm and mass transfer parameter determination in batch studies*" presents a mechanistic model which was developed for the purpose of mass transfer parameter determination and future simulations. Data from both batch systems as well as breakthrough data are presented. Key adsorbent mass transfer parameters are determined and the applicability of the model is discussed.

Published:

Jones, R. A., Tezel, F.H., Thibault, J., 2010, Simulation and validation of ethanol removal from water in an adsorption packed bed: isotherm and mass transfer parameter determination in batch studies. *Can. J. Chem. Eng.* 88 (5), 889 – 898.

Presented:

Jones, R., F.H. Tezel, and J. Thibault, "Enhanced bioethanol production via adsorption – mass transfer modelling and recovery techniques", presented at the *57th Canadian Chemical Engineering Conference* in Edmonton, Alberta, October 28-31, 2007.

Jones R., Tezel F.H. and Thibault J., "In situ bioethanol removal using a packed bed adsorber", presented at the *13th European Congress on Biotechnology* in Barcelona, Spain, September 16-19, 2007.

Chapter 4: "*Neural Network Modelling of Adsorption Isotherms*" presents a novel approach to modelling adsorption systems. A model based on artificial neural networks is used to represent a variety of adsorption systems (Type I – Type V isotherms) and is later extended to temperature dependent isotherms. This work was the basis of the neural network model used in Chapter 5 to model the competitive adsorption between ethanol and residual sugars

Published:

Morse, G., Jones, R., Thibault, J., Tezel, F.H., 2011, Neural network modelling of adsorption isotherms. *Adsorption.* 17 (2), 303-309.

Chapter 5: "*Simulating multi-component liquid phase adsorption systems: ethanol and residual sugar*" presents data for ethanol adsorption in the presence of xylose and glucose. Single component isotherms for each sugar are presented along with multi-component breakthrough data. The adsorption of ethanol is studied in the presence of a wide range of residual sugar compositions. A model based on neural networks for the competitive adsorption of ethanol and sugars is proposed and validated across a range of flow rates and sugar compositions.

Published:

R. Jones, F.H. Tezel, and J. Thibault, "Simulating multi-component liquid phase adsorption systems: Ethanol and residual sugar", Proceedings of International Green Energy Conference to be held in Eskisehir, Turkey, June 5-9, 12 pages (2011). (Conference proceeding: Full refereed paper)

Presented:

R. Jones, F.H. Tezel, and J. Thibault, "Simulating multi-component liquid phase adsorption systems: ethanol and residual sugar", Presented at the International Green Energy Conference held in Eskisehir, Turkey, June 5-9.

Chapter 6: "*Enhanced ethanol production through selective adsorption in bacterial fermentation*" presents batch fermentation data when the microorganism *E. coli* KO11 is used to produce ethanol. The ethanol tolerance of the strain is studied and the impact of online extraction is assessed.

Published:

Jones, R. A., Thibault, J., Tezel, F.H., 2011. Enhanced ethanol production through selective adsorption in bacterial fermentation. *Biotechnol. Bioprocess Eng.* 16 (3), 531-541

Presented:

Jones R.A., Gandier, J.A., Tezel F.H., Thibault J., and Poupore, J. "Adsorption of ethanol from fermentation broth: breakthrough and equilibrium behaviour", presented at the *8th World Congress of Chemical Engineering*, Montreal, Canada, August 23-27, 2009.

Chapter 7: "*Modelling and validation of the continuous production of ethanol with intermittent extraction using a packed bed adsorption column.*" Data from a novel integrated bioreactor/extraction unit is presented. The ethanol productivity achieved is discussed and compared to conventional batch systems. A model is presented for the production and online extraction of ethanol

To be submitted to:

Applied Energy

Presented:

Jones, R., Gandier, J.A., Tezel, F.H., and Thibault, "Enhanced production of bioethanol using *E. coli* KO11 with online ethanol extraction by adsorption", presented at the *10th International Conference on Fundamentals of Adsorption* held in Awaji, Hyogo, Japan, May 23-28, 2010.

Chaper 8: "*Conclusions*" is expanding on the specific conclusions of the respective papers. This chapter identifies the findings that we now know conclusively due to the work contained in this thesis.

Appendix A.1: "*Fixed bed adsorption for the removal of carbon dioxide from nitrogen: breakthrough behaviour and modelling for heat and mass transfer***"** extends the adsorption model to gas phase separations (bulk flue gas separation) where the heat of adsorption and the column temperature are important on the adsorption capacity and thus the concentration profiles.

This thesis consists of six refereed papers which are presented in Chapters 2- 7. In addition to this work, Appendix A.1 is a co-authored article. The work presented in Appendix A.1 was completed with Vinay Mulgundmath (a Ph.D. candidate at the time of the work) and is an extension of the modelling presented in Chapter 3. This work expands the modelling in Chapter 3 to a gas phase system built by Vinay Mulgundmath for CO_2 adsorption. The modelling in this work accounted for temperature dependence of the CO_2 isotherm.

1.4 References

Journals:

1. Agblevor, F.A., Batz, S.,Trumbo, J., (2003) Composition and ethanol production potential of cotton gin residues. *Appl. Biochem. Biotechnol.*105 (1-3); 219-230.
2. Agbogbo, F. K. and K. S. Wenger (2006). Effect of pretreatment chemicals on xylose fermentation by *Pichia stipitis*. *Biotechnol. Letters*, 28: 2065-2069.

3. Agbogbo, F. K., G. Coward-Kelly, M. Torry-Smith, K. Wenger, and T. W. Jeffries (2007). The effect of initial cell concentration on xylose fermentation by *Pichia stipitis*. *Appl. Biochem. Biotechnol.*, 136-140: 653-662.
4. Alterthum, F., Ingram, L.O., (1989) Efficient ethanol production from glucose, lactose and xylose by recombinant *Escherichia coli*. *Appl. Environ. Microbiol.* 55 (8); 1943-1948.
5. Barbosa, M. de F. S., H. Lee, and D. L. Collins-Thompson (1990). Additive effects of alcohols, their acidic by-products, and temperature on the yeast Pachysolen tannophilus. *Appl. Environ. Microbio.*, 56(2): 545-550.
6. Barbosa M.F., Beck, M.J., Fein, J. E., Potts, D., Ingram, L.O., (1992) Efficient fermentation of Pinus sp. Acid Hydrolysates by an Ethanolgenic Strain of *Escherichia coli*. Appl. and Environ. *Microbiol.,* 58 (4): 1382-1384.
7. Binning, R.C., Lee, R.J., Jennings, J.F. and Martin, E.C. (1961) Separation of Liquid Mixtures by Permeation. *Ind. Eng. Chem* 53: 45-58.
8. Bothast R.J., Nichols, N.N., Dien, B.S., (1999) Fermentations with new recombinant organisms. *Biotechnol. Progr*., 15; 867-875.
9. Cardona, C. A., Sanchez, O. J., "Fuel ethanol production: Process design trends and integration opportunities." *Biores. Tech.* 98, 2415-2457 (2007).
10. Chandel, A.K., Singh, O.M., Chandrasekhar, G., Rao, L.V., Narasu, M.L., (2010). Key drivers influencing the commercialization of ethanol-based bio-refineries. *J. of Comm. Biotech.* 16(3), 239-257.
11. Chavez-Rodriguez, M.F., Nebra, S.A., (2010). Assessing GHG emissions, ecological footprint and water linkage for different fuels. *Environ. Sci. Technol.* 44, 9252-9257.
12. du Preez, J. C., M. Bosch, and B. A. Prior (1986). The fermentation of hexose and pentose sugars by *Candida shehatae* and *Pichia stipitis*. *Appl. Microbio. Biotechnol*., 23: 228-233.
13. du Preez, J. C., M. Bosch, and B. A. Prior (1987). Temperature profiles of growth and ethanol tolerance of the xylose-fermenting yeasts Candida shehatae and Pichia stipitis. *Appl. Microbio. Biotechnol.*, 25: 521-525.

14. Eliasson, A., C. Christensson, C. F. Wahlbom, and B. Hahn-Hägerdal (2000). Anaerobic xylose fermentation by recombinant *saccharomyces cerevisiae* carrying XYL1, XYL2, and XKS1 in mineral medium chemostat cultures. *Appl. Environ. and Microbiol*., 66 (8): 3381-3386.
15. Esser, K., U. Schmidt, and U. Stahl (1982). Ethanol and biomass production of wild strains and respiratory deficient mutants of *Saccharomyces cerevisiae* under anaerobic and aerobic conditions. *Euro. J. of Appl. Microbiol. Biotechnol*. 16:161-164.
16. Fadeev, A.G., Meagher, M.M., Kelley, S.S., Volkov, V.V., (2000). Fouling of poly[-1-(trimethylsilyl)-1-propyne] membranes in pervaporative recovery of butanol from aqueous solutions and ABE fermentation broth. *J. Membr. Sci.* 173 (1): 133-144
17. Fong, G. F., C. G. Svenson, K. Nakasugi, C. T. C. Leong, J. P. Bowman, B. Chen, D. R. Glenn, B. A. Neilan, and P. L. Rogers (2006). Isolation and characterization of two novel ethanol tolerant facultative aerobic thermophilic bacteria strains from waste compost. *Extremophiles*, 10: 363-372.
18. Golias, H., G. J. Dumsday, G. A. Stanley, and N. B. Pamment (2002). Evaluation of a recombinant *Klebsiella oxytoca* strain for ethanol production from cellulose by simultaneous saccharification and fermentation: Comparison with native cellobiose-utilising yeast strains and performance in co-culture with thermotolerant yeast and *Zymomonas mobilis*. *J. Biotechnol.*, 96 (2) 26: 155-168.
19. Hashi, M., Thibault, J., Tezel, F. H., (2010). Recovery of ethanol from carbon dioxide stripped vapour mixture: Adsorption prediction and modelling. *Ind. Eng. Chem. Res.* 49, 8733-8740.
20. Ho, N. W. Y., Z. Chen, and A. P. Brainard (1998). Genetically engineered *Saccharomyces* yeast capable of effective cofermentation of glucose and xylose. *Appl.Environ. and Microbiol*., 64(5): 1852-1859.
21. Joachimsthal, E., K. D. Haggett, and P. L. Rogers. (1999). Evaluation of recombinant strains of *Zymomonas mobilis* for ethanol production from glucose/xylose media. *Appl. Biochem. and Biotechnol.*, 77(1-3):147-157.

22. Kim, T. H., Lee, Y. Y., Sunwoo, C., Kim, J. S., (2006) Pretreatment of corn stover by low-liquid ammonia recycle percolation process. *Appl. Biochem. Biotechnol.*, 133; 41-57.
23. Lankoski, J., Ollikainen, M., (2011), Biofuel policies and the environment: Do climate benefits warrant increased production from biofuel feedstocks? *Ecol. Econ.* 70, 676-687.
24. Lawford, H. G. and J. D. Rousseau (2002). Performance testing of *Zymomonas mobilis* metabolically engineered for cofermentation of glucose, xylose, and arabinose. *Appl. Biochem. Biotechnol.*, 98: 429-448.
25. Maiorella, B., Wilke, C.R., Blanch, H.W., (1981). Alcohol Production and Recovery. *Adv. Biochem. Eng./Biotechnol.*, 20: 43-92
26. Mohagheghi, A., K. Evans, Y. C. Chou, and M. Zhang (2002). Cofermentation of glucose, xylose, and arabinose by genomic DNA–Integrated xylose/arabinose fermenting strain of *Zymomonas mobilis* AX101. *Appl. Biochem. and Biotechnol.*, 98-100: 885-898.
27. Moniruzzaman, M., Ingram, L. O., (1998) Ethanol production from dilute acid hydrolysate of rice hulls using genetically engineered *Escherichia coli*. *Biotechnol. Lett.*, 20 (10); 943-947.
28. Moniruzzaman, M., York, S. W., Ingram, L. O., (1998) Effects of process errors on the production of ethanol by *Escherichia coli* KO11. *J. Ind. Microbiol. Biotechnol.*, 20: 281-286.
29. Ohta, K., D. S. Beall, J. P. Mejia, K. T. Shanmugam, and L. O Ingram (1991). Genetic improvement of *Escherichia coli* for ethanol production: Chromosomal integration of *Zymomonas mobilis* genes encoding pyruvate decarboxylase and alcohol dehydrogenase II. *Appl. and Environ. Microbiol*., 57 (4): 893-900.
30. Qureshi, N., B. S. Dien, N. N. Nichols, B. C. Saha, and M. A. Cotta. (2006). Genetically engineered *Escherichia coli* for ethanol production from xylose: Substrate and Product Inhibition and Kinetic Parameters. *Food and Bioprod. Process.*, 84 (C2): 114-122.

31. Ruiz, E., I. Romero, M. Moya, S. Sάnchez, V. Bravo, and E. Castro (2007). Sugar fermentation by *Fusarium oxysporum* to produce ethanol. *World J. of Microbio. and Biotechnol.*, 23: 259-267.
32. Sánchez, S., V. Bravo, E. Castro, A. J. Moya, and F. Camacho (2002). The fermentation of mixtures of D-glucose and D-xylose by *Candida shehatae*, *Pichia stipitis* or *Pachysolen tannophilus* to produce ethanol. *J. Chem. Technol. & Biotechnol.*, 77 (6): 641-648.
33. Shi, N. Q., B. Davis, F. Sherman, J. Cruz, and T. W. Jeffries (1999). Disruption of the cytochrome c gene in xylose-utilizing yeast *Pichia stipitis* leads to higher ethanol production. *Yeast* 15:1021-1030.
34. Sims, R.E.H., Mabee, W., Saddler, J.N., Taylor, M., (2010). An overview of second generation biofuel technologies. *Bioresour. Technol.* 101, 1570-1580.
35. Singh, A., Pant, D., Korres, N.S., Nizami, A-S., Prasad, S., Murphy, J.D., (2010). Key issues in life cycles assessment of ethanol production from lignocellulosic biomass: Challenges and perspectives. *Bioresour. Technol.* 101, 5003-5012.
36. Solomon, B.D., Barnes, J.R., Halvorsen, K.E., (2007). Grain and cellulosic ethanol: History, economics and energy policy. *Biomass and Bioenergy.* 31, 416-425.
37. Sudha Rani, K., M. V. Swamy, and G. Seenayya (1996). High ethanol production by new isolates of *Clostridium thermocellum*. *Biotechnol. Letters* 18, 957-962.
38. Sudha Rani, K. and G. Seenayya (1999). High ethanol tolerance of new isolates of *Clostridium thermocellum* strains SS21 and SS22. *World J. Microbiol. Biotechnol.,* 15 (2): 155-159.
39. Takahashi, C. M., De Carvalho Lima, K. G., Takahashi, D. F., Alterthum, F., (2000) Fermentation of sugarcane bagasse hemicelluloses hydrolysate and sugar mixtures to ethanol by recombinant *Escherichia coli* KO11. *World J. of Microbiol. and Biotechnol*., 16: 829-834.
40. Tavares, J.R., Sthel, M.S., Campos, L.S., Rocha, M.V, Lima, G.R. da Silva, M.G., Vargas, H., (2011), Evaluation of pollutant gases emitted by ethanol and gasoline powered vehicles. *Procedia Enivron. Sci.* 4, 51-60.

41. Von Sivers, M., Zacchi, G., Olsson, L., Hahn-Hagerdal, B., (1994) Cost analysis of ethanol production from willow using recombinant *Escherichia coli*. *Biotechnol. Progr.*, 10 (5): 555-560
42. Wood, B. E. and L. O. Ingram. (1992). Ethanol production from pellobiose, amorphous cellulose, and crystalline cellulose by recombinant *Klebsiella oxytoca* containing chromosomally integrated *Zymomonas mobilis* genes for ethanol production and plasmids expressing thermostable cellulase genes from *Clostridium thermocellum*. *Appl. Environ. Microbio.*, 58(7): 2103-2110.
43. Xin, L., Kinetic study and modelling of ethanol production from glucose/xylose mixtures using the genetically-engineered strain *Escherichia coli* KO11. MASc Thesis, Department of Chemical and Biological Engineering, University of Ottawa, 2008.
44. Zaldivar, J., Nielson, J., Olsson, L., (2001). Fuel ethanol production from lignocellulose: a challenge for metabolic engineering and process integration. *Appl. Microbiol.and Biotechnol.*, 56:17-34.
45. Zhang, M., C. Eddy, K. Deanda, M. Finkelstein, and S. Picataggio (1995). Metabolic engineering of a pentose metabolism pathway in ethanologenic *Zymomonas mobilis*. *Science*, 267: 240-243.

Websites:

1. Maynard, R. (2007). Biofuels report: Against the grain. http://www.theecologist.org
2. Renewable Fuel Association (RFA) (2011): http://www.ethanolrfa.org/

SECTION – II: Adsorbent Screening

Chapter 2

Selective ethanol separation from water using silicalite, activated carbon and ZSM-5 adsorbents: Adsorption isotherms and kinetics

R. A. Jones, F. H. Tezel, J. Thibault and J. Tolan

Abstract

Batch experiments have been conducted to examine the liquid phase adsorption of ethanol from ethanol-water solutions. Experiments were performed to establish the kinetic and equilibrium behavior of the various adsorbents in solution. From the experiments with the ZSM-5 adsorbents, it was found that the silica to alumina ratio had little effect on the ethanol-water separation at low ethanol concentrations. In general, ZSM-5 adsorbents were outperformed by the activated carbon adsorbents, which showed greater capacity. The activated carbon cloth adsorbent showed an high capacity for ethanol, however, the kinetics were slow and likely hinder its usefulness in the industrial setting for the desired separation. XTRUSORB A754 and M-30 activated carbon both showed reasonable capacity and favourable kinetics.

Particle size was found to be the single most influential factor in the uptake rate. The large particle cloths and pellets adsorbents showed sluggish kinetics when compared to their powdered counterparts. When considering kinetic performance and adsorption capacity XTRUSORB A754 and M-30 activated carbon show the most potential for the selective adsorption of ethanol.

1.0 Introduction

Fossil fuels are an exhaustible resource. With the exception of the Persian Gulf nations, oil production in most countries has peaked and already begun to decline (Cooperman, 2004). Estimates place the world peak oil production at or around 2007, after which time the production will fall off, while the demand for fuel continues to rise as major populous' India, China and South-east Asia march towards wide-spread industrialization (Duncan and Youngquist, 1999). The impending energy crisis has initiated much research into sustainable sources of fuel that can be produced and used domestically.

The current impetus is towards bio-fuels; the production of ethanol from biomass such as bio-waste or from corn feedstock, and the production of bio-diesel from soy or sunflower. This paper will focus on bioethanol.

Crops such as corn or waste (wood, corn stover, straw and grass) containing sugars have the potential to be fermented to produce bioethanol. While the paths to production may be slightly different depending on the biomass feed used, the end product is the same. A typical ethanol production from biomass or waste can be schematically represented by Figure 1. The main components of fibrous materials (straw or wood) are cellulose and lignin. The lignin binds the cellulose chains together. A pre-treatment is required to break the bonds in order to recover the available sugars. The sugars are then sent to the fermentation unit where they are converted into ethanol. The sugar solution will yield a final broth with approximately 40 - 60 g/L ethanol after a period of around 36 h. The ethanol solution is then sent to a distillation column to separate the ethanol from aqueous solution. At the top of the column the ethanol solution approaches an azeotrope. Partial condensation at the top of the column is used and the vapor fraction is sent to a PSA adsorption system that dehydrates the alcohol to increase concentration.

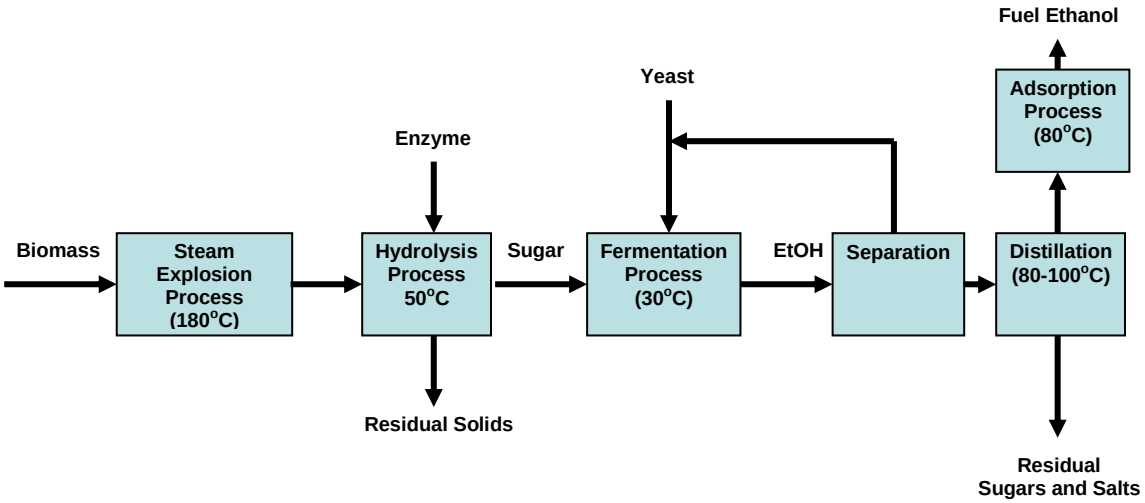

Figure 1 - Typical ethanol production process

There exist technical and economic ch

allenges to overcome in the bioethanol production process, due to the limited ethanol tolerance of the microorganism. The ethanol produced becomes inhibitory as it builds to concentrations of greater than 30 - 50 grams per liter. The inhibition leads to low batch yields, which translates to low bioethanol production capacity (Lencki *et al.,* 1983). The recovery of the ethanol from the fermentation broth appears to be the major economic limiting step which holds back the wide-spread use of bioethanol as a gasoline additive or fuel alternative. While distillation is effective in separating the ethanol from the water, it is not energy efficient. The largest energy inputs in producing ethanol from biomass is the energy used in the fermentation/distillation.

Various researchers claim a positive net energy value (NEV) for the production of ethanol from corn (Shapouri *et al.,* 1995; Shapouri *et al.*, 2004; Marland & Turhollow, 1991; Morris & Ahmed, 1992). Researchers point to the continuing efficiency improvements in farming, and processing techniques as evidence that the technology is becoming more and more viable (Shapouri et al., 1995). As the technology continues to improve, the energy balance of the system improves likewise.

What is not disputed is the fact that improvements in separation technology, particularly during the fermentation or distillation stages have great potential to make bioethanol both

economically and technically appealing. Ideally a more cost effective and less energy intensive separation of ethanol from solution would be employed. Current research includes on-line solvent extraction, pervaporation, and selective adsorption among other techniques being studied. For the purpose of this paper the focus will be on selective adsorption separation.

An optimum separation scheme would remove a small stream from the fermentation broth, and selectively extract ethanol from the broth by passing it through an adsorption column. Extracting the ethanol as it is being produced, could allow the fermentation to continue while suppressing inhibition. The extraction of ethanol would drive the equilibrium to produce more ethanol in accordance with Le Chatelier's principle. Furthermore, the ethanol adsorbed, can be desorbed and the process can be made cyclical by adding parallel columns, and alternating between adsorption and desorption. If the separation is highly selective in its preference for ethanol, the product stream desorbed could be expected to be very concentrated, reducing the burden of energy required for the distillation separation.

The key is finding adsorbents which are highly selective for the ethanol, since ethanol is the dilute component in the broth, this will reduce the quantity of adsorbent required and minimize the costs associated with desorption and regeneration (Walsh *et al.*, 1983).

To be viable, an ideal adsorbent needs to have a low cost, a high ethanol capacity, rapid ethanol uptake, fast desorption kinetics and the ability to be regenerated for re-use. It can be reasonably expected that hydrophobic adsorbents such as activated carbons, silicalite and ZSM-5 would be suitable adsorbents. Silicalite and ZSM-5 have been studied and promising results were obtained (Milestone and Bibby, 1983; Falamaki *et al.*, 2001; Benito *et al.,* 1998; Farhadpour and Bono, 1988, 1996).

In this study a wide variety of adsorbents were screened for their potential to selectively extract ethanol from water. The goal is to determine which adsorbents should be studied further in packed tower adsorption studies with fermentation broth.

2.0 Kinetic Modelling

For this study the first order model, Lagergren's second order and intra-particle diffusion models were tested for their suitability to fit the experimental data obtained.

2.1 Intra Particle Diffusion Model (Pore Diffusion Model)

The intra particle diffusion model is a simple adsorption model based on pore diffusion.

$$q_t = k_{diff} t^{1/2} \tag{1}$$

where

q_t: the uptake at time t, (g ethanol/g adsorbent)

k_{diff}: intra particle diffusion rate, (g ethanol)(day)$^{-1/2}$(g adsorbent)$^{-1}$

t: time, (day)

2.2 Lagergren's second order equation

Being one of the most widely used kinetic models for adsorption kinetics, the Lagergren's second order model is especially effective in modelling liquid phase adsorption from an aqueous phase.

$$\frac{t}{q} = \frac{1}{kq^2_e} + \frac{t}{q_e} \tag{2}$$

where

t: time, (day)

q: uptake, (g ethanol/g adsorbent)

k: pseudo-second order Lagergren's rate constant, (g adsorbent/g EtOH)(day^{-1})

q_e: equilibrium uptake, (g ethanol/g adsorbent – at equilibrium)

3.0 Equilibrium Modelling

An equilibrium isotherm describes the capacity of the adsorbent as a function of the equilibrium concentration of the adsorbate in solution at a constant temperature. Three

isotherm models were used to fit the experimental data in this study: Langmuir, Freundlich and Sips models.

3.1 Langmuir Model

The most widely used model to describe adsorption isotherms is the Langmuir equation. It was originally derived for monolayer adsorption on homogeneous surfaces but its use is not limited to such systems. The Langmuir model is expressed below:

$$q_e = q_s \frac{bC_e}{1+bC_e} \tag{3}$$

where

q_e: adsorption capacity, (g ethanol/g adsorbent)

q_s: saturation capacity, (g ethanol/g adsorbent)

$C_{e:}$ concentration in solution at equilibrium, (g ethanol/L)

b: Langmuir constant, (L/g ethanol)

The equation can be linearized by plotting $1/q_e$ versus $1/C_e$ which will yield a straight line with slope equal to $1/(q_s b)$ and an intercept of $1/q_s$, form which the parameters can be determined.

3.2 Freundlich Model

One of the earliest models in use, and still one of the most common models is the Freundlich isotherm. It was empirically derived and is expressed as follows:

$$q_e = AC_e^{1/n} \tag{4}$$

where

q_e: amount of ethanol adsorbed at equilibrium (g ethanol/g adsorbent)

$C_{e:}$ concentration in solution at equilibrium, (g ethanol/L)

A: Freundlich constant, (g ethanol/g adsorbent) (L/g ethanol) $^{1/n}$

n: Freundlich constant, (dimensionless)

When n = 1 the Freundlich model reduces to a simple linear isotherm (Henry's law).

3.3 Three parameter Langmuir-Freundlich (Sips) isotherm

$$q_e = q_s \frac{(bC_e)^{1/n}}{1+(bC_e)^{1/n}} \quad (5)$$

where

q_e: amount of ethanol adsorbed at equilibrium (g ethanol/g adsorbent)

q_s: saturation capacity, (g ethanol/g adsorbent)

$C_{e:}$ concentration in solution at equilibrium, (g ethanol/L)

b: Langmuir constant, (L/g ethanol)

n: Freundlich constant, (dimensionless)

The parameters for each model were determined from the experimentally determined isotherm data.

4.0 Materials and Methods

4.1 Materials

Solutions were prepared with anhydrous ethyl alcohol (Commercial alcohols inc.) and distilled de-ionized water. The list of adsorbents studied is presented in Table 1 with some important properties.

Table 1 – Adsorbent properties

Adsorbent	Company	Surface Area	Particle Size	Si/Al
	-	m^2/g	µm or mm	-
XTRUSORB A754 - Activated Carbon	Calgon, Mississauga, On.	850	4 mm	-
XTRUSORB HP115 - Activated Carbon	Calgon, Mississauga, On.	850	4 mm	-
Type BPL 4x10 - Activated Carbon	Calgon, Mississauga, On.	850	450-600 µm	-
F – 400 – Activated Carbon	Calgon, Mississauga, On.	900	550-750 µm	-
M-30 Mesobeads – Activated Carbon	Spectracorp, USA	3450	25 µm	-
OLC - Activated Carbon	Calgon, Mississauga, On.	800	3mm	-
Activated Carbon Cloth	Spectracorp, USA	2500	-	-
HiSiv 3000 (High silica ZSM-5)	UOP, USA	400	1/16”	1000+
CBV 28014G (Medium Silica ZSM-5)	Zeolyst, USA	400	500 µm	280
CBV 5524G (Low Silica ZSM-5)	Zeolyst, USA	425	500 µm	50

4.2 Kinetic experiments

Kinetic experiments were carried out to determine the rate of adsorption for each adsorbent in a standard ethanol solution to determine the time at which thermodynamic equilibrium was achieved. The rate of adsorption curve also provided useful information about the initial uptake rate. Aqueous ethanol solutions of around 75 - 80 g of ethanol per liter were prepared in a 1.5 L enclosed flask. The masses of the respective liquids were measured using a standard electronic scale (Denver Instruments, model M-310). The solution was placed on an electric stirrer (Fisher Scientific, Thermix Hot Plate model 210T) to ensure the mixing was sufficient. A pre-determined mass of adsorbent was measured, and then added into the closed vessel. Small samples of approximately 5 mL were removed from the batch system using a syringe at the appropriate time intervals. The temperature and the pH of the system were recorded just prior to removing the liquid sample. The sample was then centrifuged, and filtered (Millipore, MF membrane filters) to ensure no adsorbent particles were within the sample. The density of each sample was measured with a densitometer (Paar, model DMA), which was then used to determine the ethanol mass fraction in the sample. The time after which the composition of ethanol in solution was no longer changing, was taken as the time for the system to reach thermodynamic equilibrium.

4.3 Equilibrium experiments

Equilibrium experiments were carried out to determine the adsorption isotherm for each respective adsorbent. For each adsorbent studied, a known mass of adsorbent was placed in various 125 mL flasks with ethanol solutions of 75 - 80 g of ethanol per liter. The samples were then placed in an isothermal shaker at approximately 29 - 33 ^{o}C to ensure mixing was adequate. When equilibrium was reached, the density of each solution was measured to infer about the ethanol liquid solution concentration. Again, the samples were centrifuged and filtered prior to measuring the density. To account for ethanol losses through evaporation, "blank samples" of approximately the same composition by mass ethanol containing no adsorbent were also placed inside the equilibrium shaker. The density of the blank sample was measured at the start and end of the equilibrium experiment. Any change in the composition of the blank sample could be attributed to evaporation. The loss of ethanol through evaporation was accounted for when determining the actual amount of ethanol adsorbed onto the surface of the adsorbent. A second blank contained only water and the adsorbent, it was found that the presence of the adsorbent in water had no effect on the density of the solution.

4.4 Experimental details

In order to simulate representative ethanol concentration of an industrial fermentation broth, binary aqueous solutions of ethanol were used for both the kinetic and equilibrium experiments. With binary ethanol solutions, it is possible to measure the ethanol concentration using the density of the mixture. From the initial and final ethanol concentration in the mixture, a simple mass balance can provide the amount of ethanol that was adsorbed assuming the total volume of the solution does not change. The following equation provides the amount of ethanol adsorbed per unit mass of adsorbent:

$$q = \frac{V_T (C_o - C_f)}{M_{ads}} \tag{6}$$

where

C_o – initial concentration of solution, (g ethanol/L)

V_T – volume of the solution, (L)

C_f – final concentration of solution, (g ethanol/L)

M_{ads} – mass of adsorbent, (g adsorbent)

While this assumption is valid for the equilibrium experiments which only require the removal of one sample at the end of the experiment, the kinetic experiments required many samples to be removed. The serial removal of samples during the kinetic experiment accounted for less than 3 % of the total initial volume in all trials with the exception of the experiment on activated carbon cloth. For this system, approximately 10% of the total volume was removed for sampling during the 30 days in which the carbon cloth/ethanol-water system required to reach equilibrium.

5.0 Results and discussion

5.1 Kinetic results

The kinetic experiments were performed in order to determine the dynamics of the adsorption. Of greatest interest was the time required to reach equilibrium and the initial uptake rate. Kinetic observations are given in Table 2.

Table 2 - Kinetic Observations

Adsorbent	Particle Type -	Time*, $q=q_e$ (minutes, hours or days)	Time*, $q=0.5q_e$ (minutes, hours or days)
XTRUSORB A754	Pellet	1 day	5 minutes
XTRUSORB HP115	Pellet	1 day	10 minutes
M-30 Mesobeads	Fine powder	10 minutes	3.5 minutes
Activated Carbon Cloth	Cloth fabric	30 days	7 days
HiSiv 3000 (High silica ZSM-5)	Pellet	3 days	250 minutes
CBV 28014G (Medium Silica ZSM-5)	Powder	3.5 hours	3 minutes
CBV 5524G (Low Silica ZSM-5)	Powder	2 days	170 minutes

* Times are approximate.

Table 2 gives a clear indication that the particle form of the adsorbent had an affect on the uptake rate of ethanol by the adsorbent. Typically the powdered adsorbents showed

rapid initial kinetics due to the large surface area that was immediately available for adsorption. In general, for adsorbents in the form of pellets, the initial rate of adsorption was rapid due to the relatively large mass of adsorbent available at the outer portion of the pellets. The rate of adsorption then decreased significantly as diffusion into the porous takes place. The only fabric adsorbent studied was the activated carbon cloth. This adsorbent showed extremely sluggish kinetics, taking nearly 30 days to reach equilibrium. The kinetic parameter of the respective model fits are shown in Table 3. The experimental data from the kinetic screening as well as the corresponding model fits are shown in Figures 2a, 2b and 3. Notice in some instances the appropriate kinetic model is shown to be extrapolated far beyond the data set that is provided. In some cases, the extrapolation is extended well beyond the range of data for a particular adsorbent. The extrapolated curve is not verified beyond the range of data and therefore should be used with caution when predicting performance.

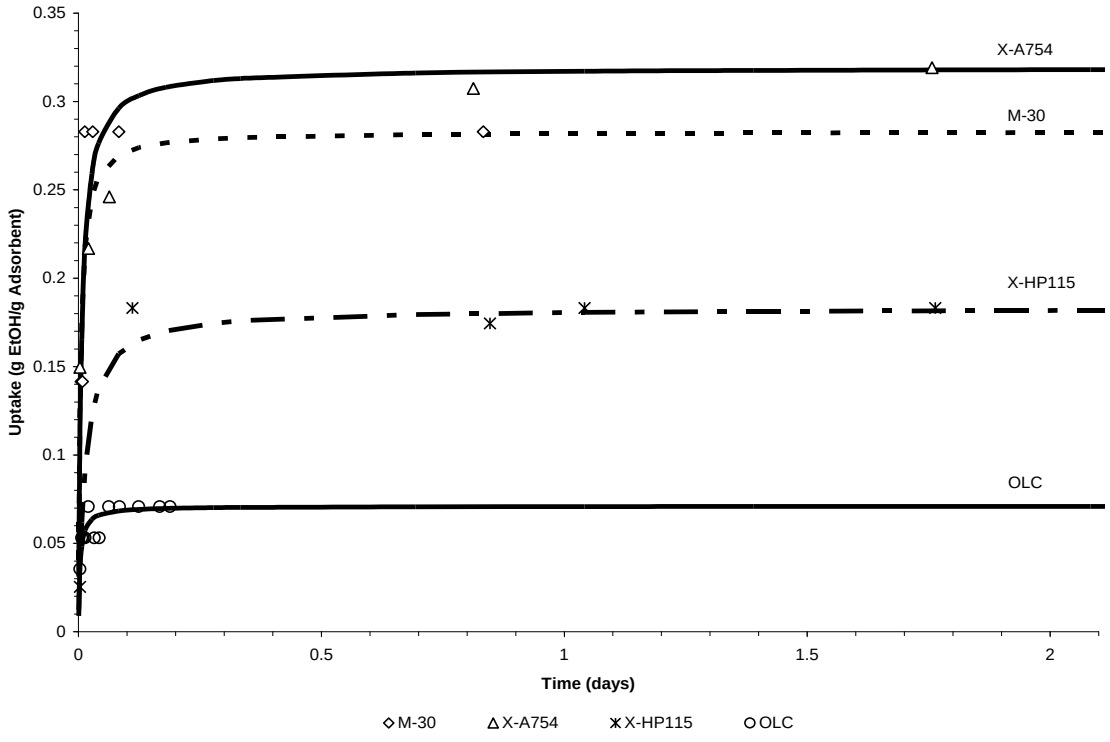

Figure 2a - Ethanol-water adsorption kinetics at 22 ^{o}C with activated carbon adsorbents. Symbols represent experimental data and the lines are fitted kinetic models.

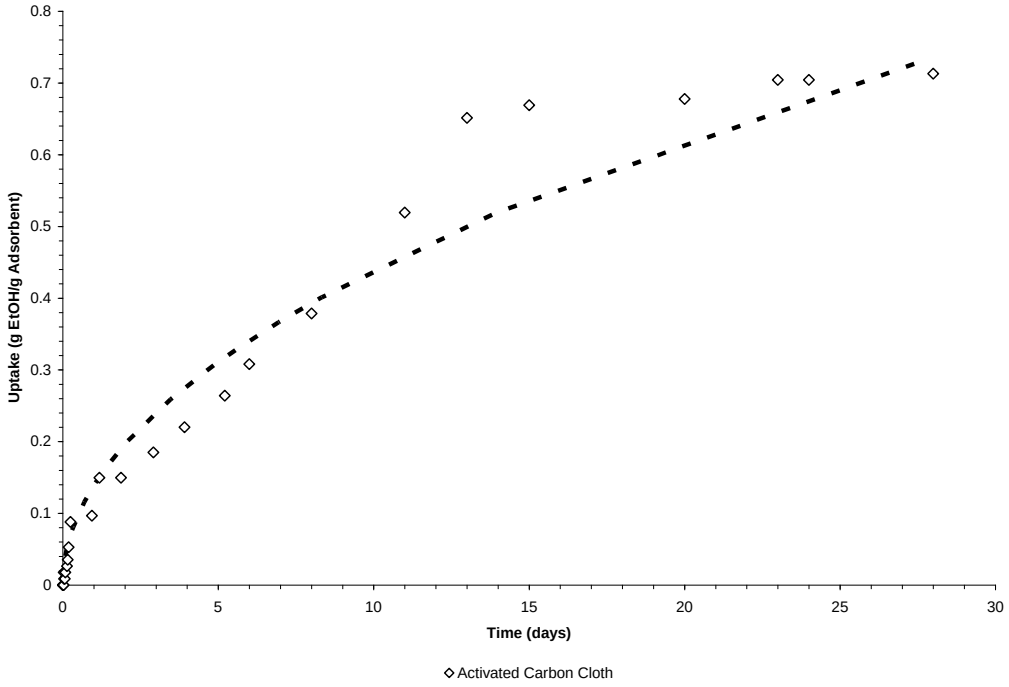

Figure 2b - Ethanol-water adsorption kinetics at 22 ^{o}C with activated carbon cloth adsorbent. Symbols represent experimental data and the lines are fitted kinetic models.

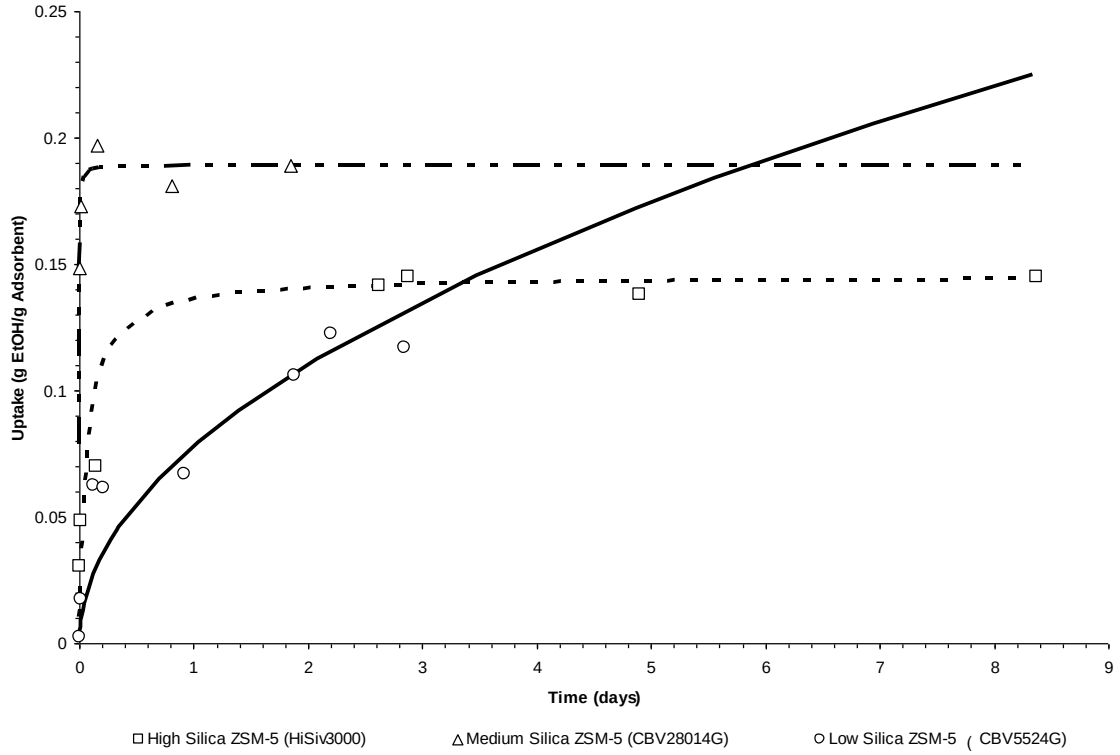

Figure 3 - Ethanol-water adsorption kinetics at 22 ^{o}C with ZSM-5 adsorbents. Symbols represent experimental data and the lines are fitted kinetic models.

Table 3 - Kinetic parameters

Adsorbent	Model: Intra-Particle Diffusion Model k_{diff} (g EtOH)(min$^{-1/2}$)(g ads$^{-1/2}$)	Intra-Particle Diffusion Model R^2 -	Lagergren's Pseudo Second Order Model k_2 (g ads)(g EtOH^{-1})(day^{-1})	Lagergren's Pseudo Second Order Model qe (g EtOh/g Adsorbent)	Lagergren's Pseudo Second Order Model R^2 -
XTRUSORB A754	0.302	0.807	487.09	0.319	0.889
XTRUSORB HP115	0.173	0.519	399.73	0.183	0.978
M-30 Mesobeads	0.457	0.2306	846.6	0.283	0.741
Activated Carbon Cloth	0.139	0.9609	0.274	0.704	0.932
HiSiv 3000 (High silica ZSM-5)	0.077	0.8475	108.19	0.145	0.925
CBV 28014G (Medium Silica ZSM-5)	0.186	0.327	5475.3	0.189	0.897
CBV 5524G (Low Silica ZSM-5)	0.078	0.8937	0.311	0.119	0.672
OCL Activated Carbon	0.0783	0.1976	4276.7	0.071	0.725

The kinetic data for each adsorbent were fitted with the intra-particle diffusion model (Equation 1) and Lagergren's pseudo second order model (Equation 2). The better model in most cases was the Lagergren's pseudo second order model, in particular for systems that showed rapid adsorption dynamics. The intra particle diffusion model was found to be inappropriate for most powder adsorbent systems in which equilibrium was attained rapidly, whereas it was acceptable in modelling the adsorption kinetics of the activated carbon cloth system. This was expected since the adsorption rate in cloth adsorbents is mainly controlled by diffusion.

5.2 Equilibrium results

Adsorption isotherms of ethanol from aqueous solution were determined experimentally. Table 4 shows the values of the parameters for all adsorbents studied. The isotherm parameters for each of these models were also determined and shown in Table 4.

Table 4 - Equilibrium parameters

Adsorbent	Sips (Eq. 5)			Langmuir (Eq. 3)		Freundlich (Eq. 4)	
	Q (g/g ads)	b (l/g)	n	Q (g/g ads)	b (l/g)	A (g/g sol)(l/g)$^{1/n}$	n
XTRUSORB A754	0.2659	1.82×10^{-1}	0.5425	0.2805	0.2682	0.1607	8.2605
OLC	2.0433	1.28×10^{-4}	2.1337	0.2679	0.0379	0.0315	2.2830
BPL 4x10	0.1120	5.68×10^{-2}	0.5301	0.1391	0.0436	0.0222	2.7385
F-400	4.1162	1.01×10^{-4}	1.5339	0.3227	0.0135	0.0106	1.5745
M-30 Mesobeads	6.4273	3.85×10^{-3}	1.3064	0.9468	0.0095	0.0165	1.3483
Activated Carbon Cloth	1.2853	9.37×10^{-3}	1.4149	0.8481	0.0262	0.0785	2.1835
HiSiv 3000 (High silica ZSM-5)	4.0042	2.29×10^{-4}	1.3181	0.4939	0.0072	0.0072	1.3527
CBV 28014G (Medium Silica ZSM-5)	0.3209	2.57×10^{-3}	4.4514	0.1422	0.1413	0.0721	7.2023
Medium Silica ZSM-5**	0.3612	1.61×10^{-4}	4.9730	0.1138	0.1413	0.0577	7.2004
CBV 5524G (Low Silica ZSM-5)	1.1558	3.92×10^{-4}	1.7602	0.2217	0.0208	0.0147	1.9321
Low Silica ZSM-5**	1.9983	5.39×10^{-5}	1.9716	0.1497	0.0356	0.0175	2.3111
XTRUSORB HP115	14.9895	1.02×10^{-4}	1.1538	19.6512	1.5E-04	0.0061	1.2137

**Value was adjusted to predict the effect of using pellet type adsorbent with 20 wt% inert binder.

Figures 4a, 4b, 5 show the experimental capacity of the adsorbents studied along with the most suitable fitted model. It was found that the activated carbon cloth had the highest adsorption capacity for ethanol. M-30 Mesobeads also showed a fairly high adsorption capacity. The ZSM-5 type adsorbents showed less favourable isotherms which were near linear in the case of high and low silica ZSM-5. In most cases, the Sips model was most suitable.

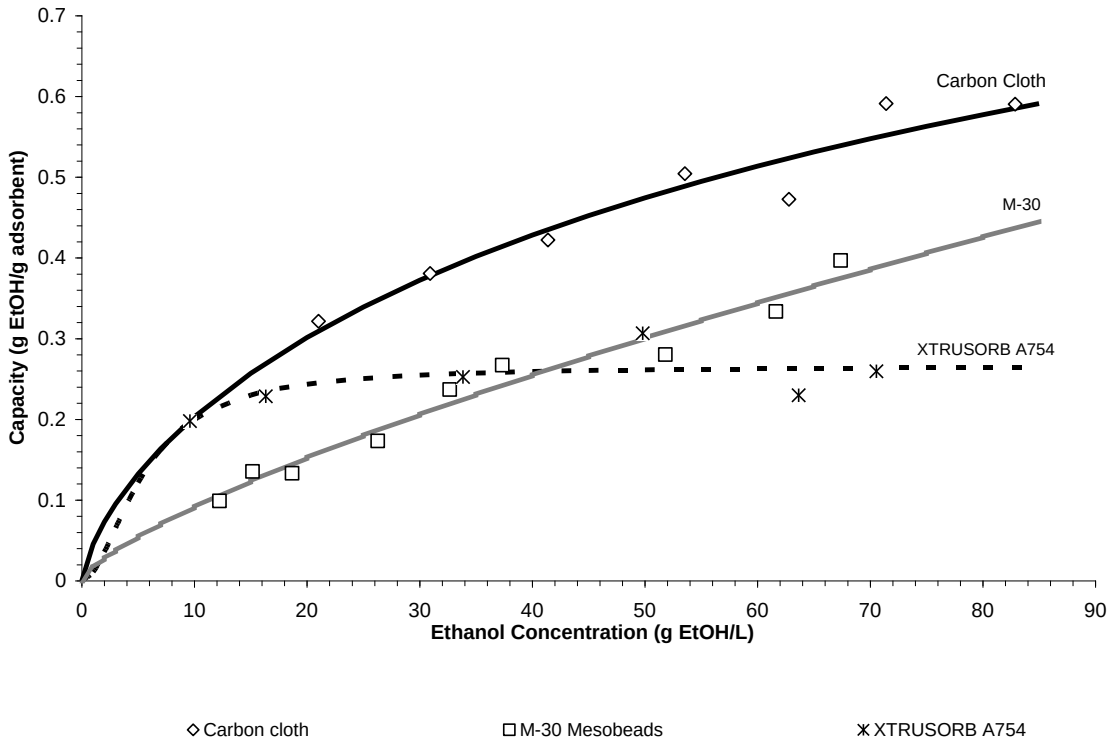

Figure 4a - Ethanol-water adsorption isotherms at 29-33°C with activated carbon adsorbents. Symbols represent experimental data and the lines are fitted isotherm equations.

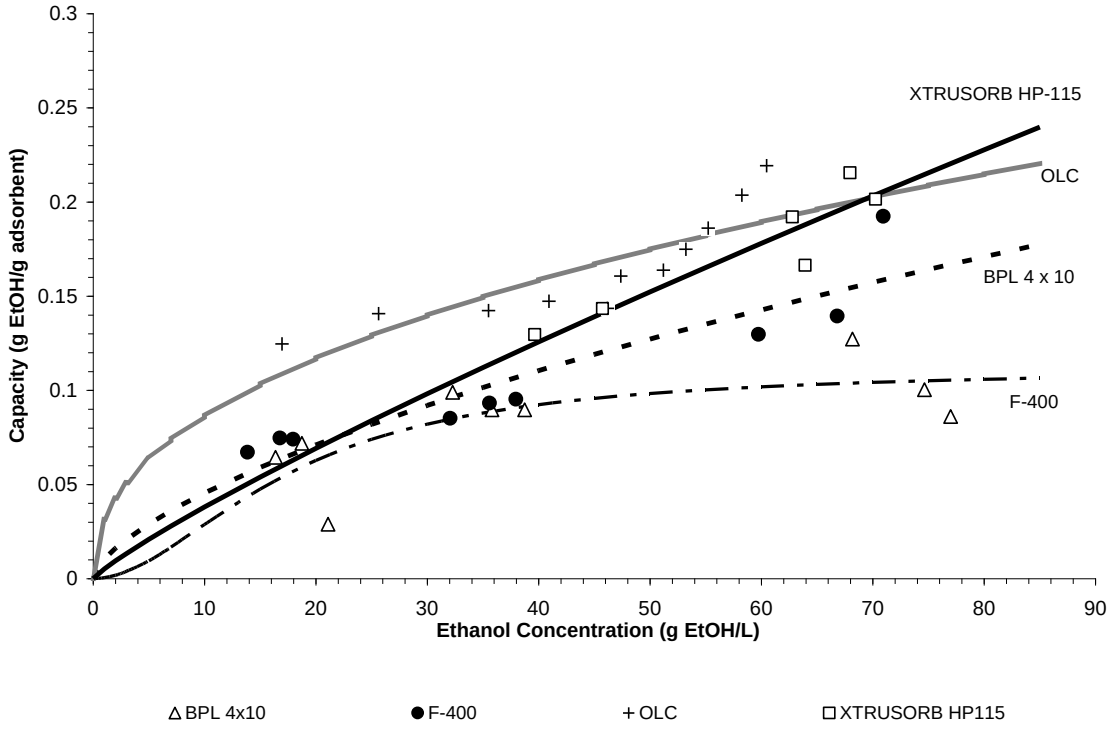

Figure 4b - Ethanol-water adsorption isotherms at 29-33°C with activated carbon adsorbents. Symbols represent experimental data and the lines are fitted isotherm equations.

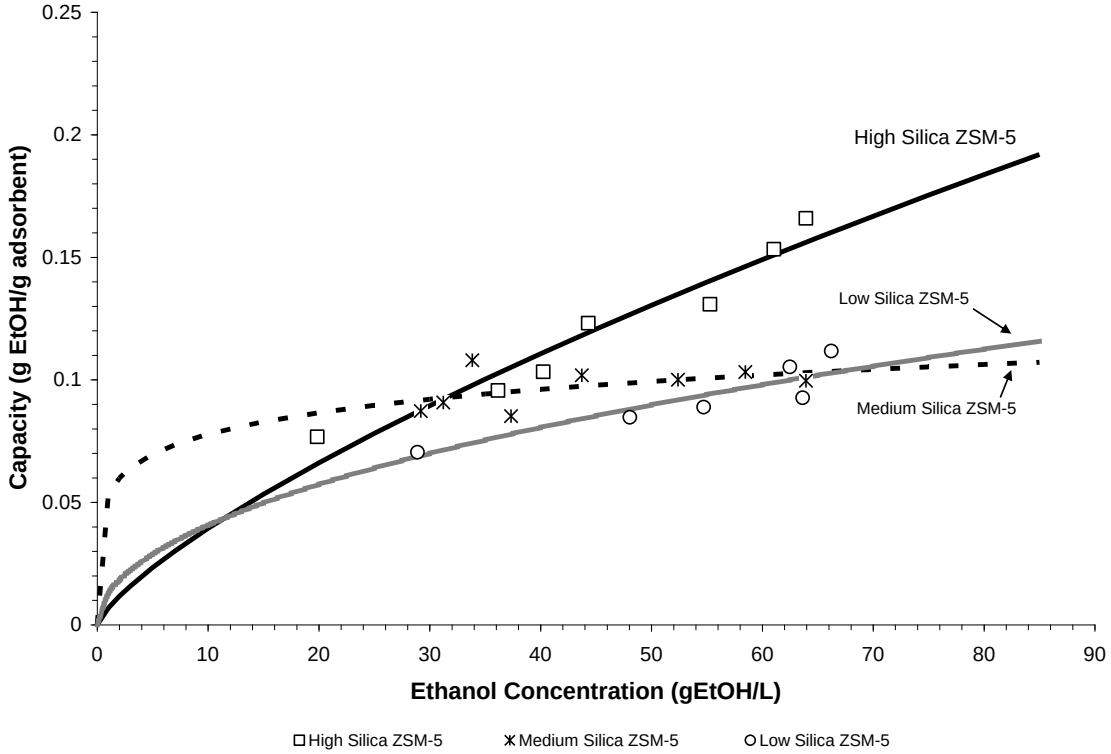

Figure 5 - Ethanol-water adsorption isotherms at 29-33^{o}C with ZSM-5 adsorbents. Symbols represent experimental data and the lines are fitted isotherm equations.

**Capacity of Medium and low silica ZSM-5 adjusted to theoretically include binder (20 wt. %)

5.2.1 Effect of surface area

The ZSM-5 adsorbents studied had lower surface area than the activated carbon counterparts. This observation is likely due in part to the great discrepancy in surface area per unit mass for the ZSM-5 and activated carbon adsorbents (see Table 1). Furthermore, the adsorbents showing the greatest adsorption capacity were the activated carbon cloth and the activated carbon M-30 meso-beads with respective surface areas of 2500 m^2/g and 3450 m^2/g. Surface area per unit mass is clearly not the only factor in determining the capacity. A higher surface area likely can be associated with a greater number of potential adsorption sites, but the affinity of the adsorbate for the particular adsorbent also plays a vital role in the ethanol adsorption capacity of the adsorbent.

5.2.2 Effect of Si/Al ratio

This study monitored the effects of the Si/Al ratio on the capacity of ZSM-5 adsorbents. In order to make a valid comparison between the capacity for high silica ZSM-5, a pellet form adsorbent with 20 wt% inert binder, and the data for the medium and low silica ZSM-5, both powder adsorbents (see Table 2) with no binder the measured capacity had to be adjusted. The data were adjusted by using only 80% of the measured capacity to approximate the adsorption which would take place in the presence of 20 wt% inert binder. This adjustment was introduced because working with powdered adsorbents would not be technically feasible in a packed adsorption tower. Reducing the measured capacity by 20% may be a conservative adjustment. The presence of binder makes the surface less hydrophobic, and may bury possible adsorption sites in addition to the 20 % inert mass not available for adsorption.

From the experiments with silica based adsorbents, the silica to alumina ratio has some impact on the affinity of the adsorbent for the adsorption of ethanol. Results from the equilibrium experiment for high, medium and low silica ZSM-5 in Figure 5, show that in the low concentration range, the capacities were similar. This is can be attributed to the fact both ethanol and water are polar molecules. In studies separating non-polar organics from water, the Si/Al ratio is can have a large effect across all concentrations studied (Ruthven, 1984). However, with this particular system the hydrophobicity of the surface only has a small effect on separating two polar molecules at the high concentration range studied (above 30g/L ethanol). The highest capacity was found with the high silica ZSM-5 in this region, while, the low and medium silica ZSM-5 yielded similar results within this concentration range.

The modelling indicated that the medium silica ZSM-5 showed the most favourable isotherm, however it should be stated that this is not verified by the data, as the concentration does not extend below 20 g ethanol per liter.

This study does not verify the work of Milestone and Bibby (1983) who found that's the capacity decreased slightly with increasing Si/Al ratio (Figure 7). The results of this investigation are contradictory, for the concentration region studied, the high silica ZSM-5 showed the greatest capacity.

5.4 Comparison with literature

There have been numerous attempts at finding adsorbents suitable for the selective separation of ethanol and water. Beginning in the mid-eighties various studies identified ZSM-5 zeolites and activated carbons as possibly suitable adsorption materials for this particular separation. Figures 6 and 7 compare the findings of this study with various adsorbents which have been examined previously. It should be noted that in literature it has been observed that experiments on binary ethanol-water solutions lead to better performance than when using an actual fermentation broth.

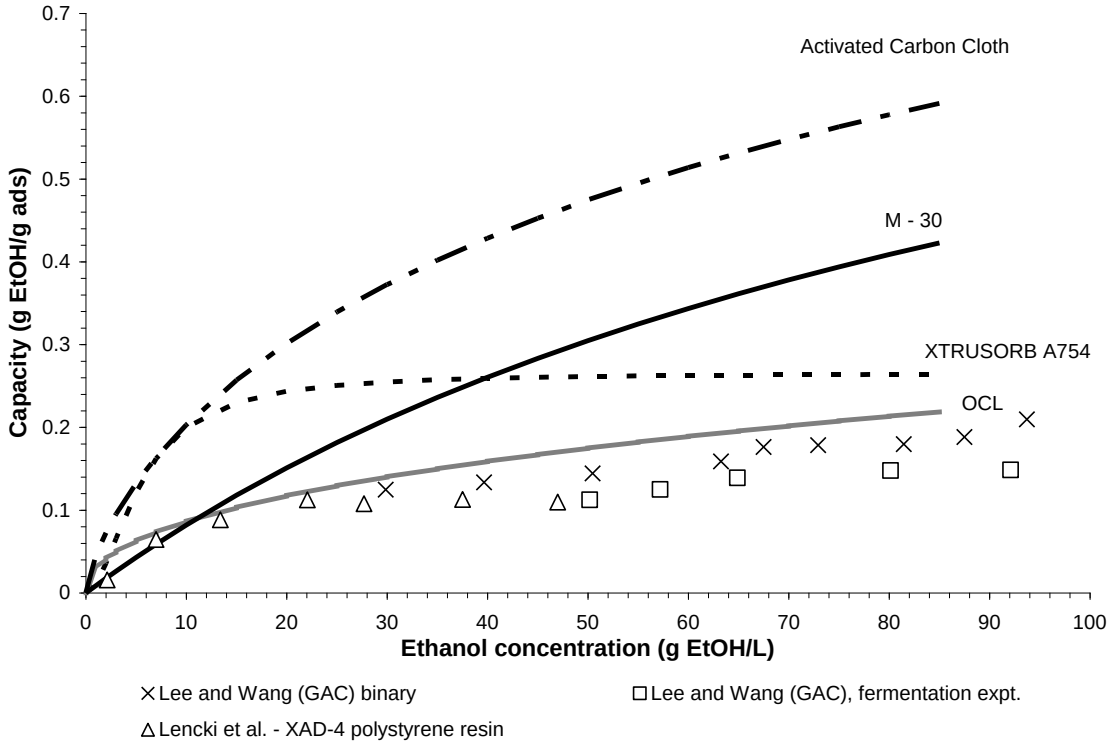

Figure 6 - Activated carbon and polystyrene resin adsorbents: Experimental data from literature at 30 (Lee & Wang, 1982) and 21°C (Lencki et al., 1983). Sips isotherms from Figure 4 are included for comparison of data. Symbols represent experimental data and the lines are fitted isotherm equations.

The work of Lee and Wang (1982) tested beaded activated carbon as an adsorbent for ethanol. In this study, experiments were performed on both binary aqueous solution and fermentation broth. The capacity was slightly lowered when fermentation broth was used. This was explained by citing the adsorption of other fermentation compounds that are required for production. Lencki *et al.* (1983) experimented on XAD-4 a polystyrene resin adsorbent. These experiments were performed on actual fermentation broth. From Figure 6 it is evident from the shape of the isotherm that the XTRUSORB A745 has a more favourable adsorption than the other adsorbents studied in this report, and the data cited in literature. The M-30 meso-bead also showed large capacity by comparison, this may be explained by the very large surface area (3450 m^2/g).

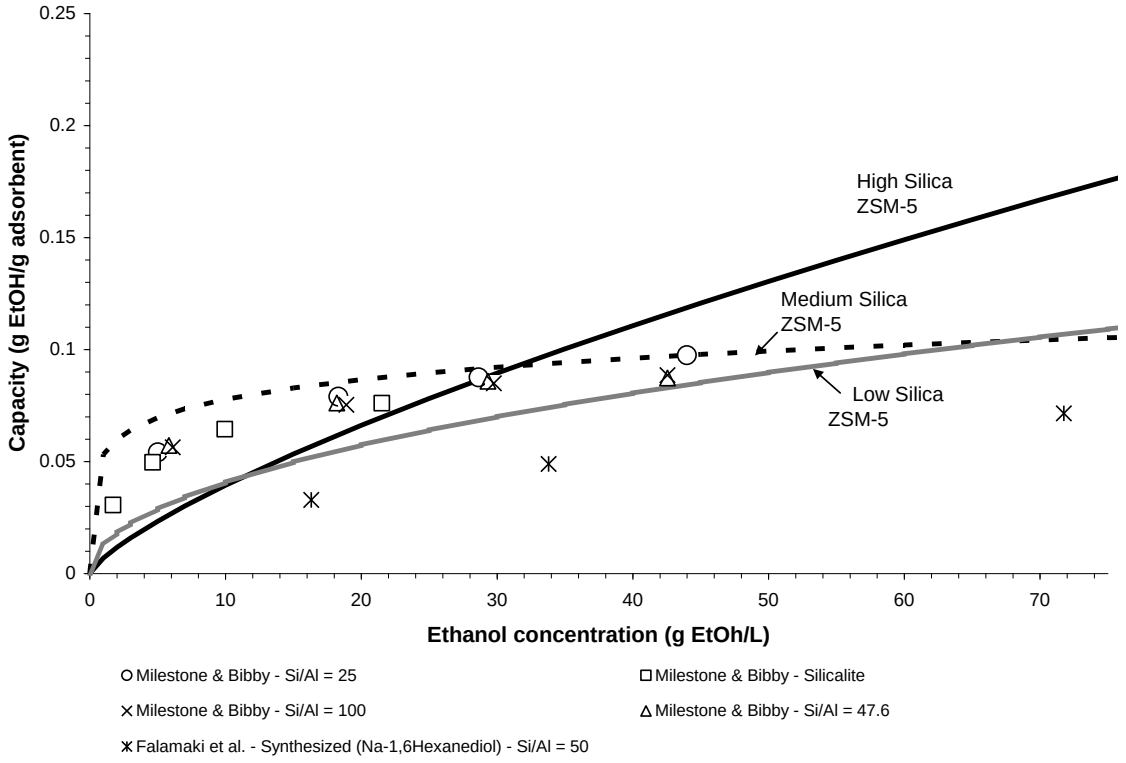

Figure 7 - ZSM-5 Adsorbents: Experimental data from literature at 21 (Milestone & Bibby, 1983) and 25°C (Falamaki et al., 2001). Sips isotherms from Figure 5 are included for comparison of data. Symbols represent experimental data and the lines are fitted isotherm equations.

Figure 7 compares the results of this study with previously reported data (Milestone & Bibby, 1983; Falamaki *et al.*, 2001). In general the results of Milestone and Bibby corresponded reasonably well with the data in this study over the same concentration region. However, the conclusions on the effect of Si/Al were not in agreement. Falamaki

et al. (2001) studied a synthesized ZSM-5 adsorbent with Si/Al of 50, their results were slightly lower than those found for the low silica ZSM-5 (Si/Al = 50) in this study. It should be noted that the use of binder was reported in the preparation of the ZSM-5; however, the weight % of binder was not reported.

6.0 Conclusions

Results from the various kinetic experiments indicated that the particle size had the largest influence on the adsorption rate. The powdered adsorbents reached equilibrium within minutes or hours, while the pellet and cloth adsorbents generally reached equilibrium in days or weeks. Surface area per unit mass has an effect on the adsorption capacity and this explains why the relatively low surface area in the ZSM-5 adsorbents translated into lower capacity. Activated carbon cloth had the largest adsorption capacity, however, the kinetics were extremely sluggish taking more than 30 days to reach equilibrium. The kinetics of this system was best modeled with the intra-particle diffusion model. Activated carbon X-A754 displayed a favourable isotherm, and had a relatively high adsorption capacity. The kinetics were rapid considering the pellet form, 50% of the total adsorption capacity was used in the first five minutes of the kinetic experiment. X-A754 and activated carbon M-30 performed well both for the kinetics and the equilibrium capacities. X-A754 showed a favourable adsorption with a type I isotherm, while the M-30 activated carbon meso-beads had a near linear isotherm. A favourable isotherm indicates the ability to reach high adsorption capacities even at low solution concentrations and this is indeed desirable, however, it indicates a high affinity and thus, desorption from X-A754 is likely to be much more challenging than that from the M-30 adsorbent. These opposing effects must be studied further to understand the economic and technical implications.

There exists enough potential for X-A754 and M-30 to continue experimenting to determine the column dynamics and performance with actual fermentation broth.

7.0 References

1. Benito, G. G., Carton, A., Rey, J. A., de la Fuente, M., 1998. Selection of adsorbents to be used in an Ethanol Fermentation Process. Adsorption Isotherms and Kinetics. *Bio-resources Technology.* 66, 75-78.
2. Cooperman, G., 2004. End of Cheap Oil: When and Why? *Internet Resource: http://www.ccs.neu.edu/home/gene/peakoil/node2.html, December 2004.*
3. Duncan, R. C., Youngquist, W., 1999. Encircling the Peak of World Oil Production. *Natural Resources Research*, 8, 3.
4. Falamaki, C. Sohrabi, M, Talebi, G., 2001. The Kinetics and Equilibrium of Ethanol Adsorption from Aqueous Phase Using Calcined (Na-1,-Hexanediol)-ZSM-5. *Chem. Eng. Tech.* 24, 501-506.
5. Farhadpour, F. A., Bono, A., 1988. Adsorption from Solution of Non-electrolytes by Micro-porous Crystalline Solids: Ethanol-Water/Silicalite System. *J. Coll. Inter. Sci.* 124, 209-227.
6. Farhadpour, F. A., Bono, A., 1996. Sorptive separation of ethanol-water mixtures with a bi-dispersed hydrophobic molecular sieve, silicalite: determination of the controlling mass transfer mechanism. *Chem. Eng. Process.* 35, 141-155.
7. Lee, S. S., Wang, H. Y., 1982. Repeated Fed-Batch Fermentation Using Yeast Cells and Activated Carbon Extraction System. *Biotechnol. Bioeng. Symp.* 12, 221-231.
8. Lencki, W. R., Robinson, W. C., Moo-Young, M., 1983. On-line Extraction of Ethanol from Fermentation Broths Using Hydrophobic Adsorbents. *Biotechnol. Bioeng. Symp.* 13, 617-628.
9. Marland, G. & Turhollow, A. F., 1991. CO_2 Emissions from the Production and Combustion of Fuel Ethanol Corn. *Office of Health and Environmental Research. US Department of Energy, February 1991.*
10. Milestone, N. B, Bibby, D. M., 1983. Adsorption of alcohols from aqueous solution by ZSM-5. *J. Chem. Tech. Biotechnol.* 34A, 73-79.

11. Morris, D. & Ahmed, I., 1992. How Much Energy Does it take to make a Gallon of Ethanol? *Institute for Self Reliance, December 1992.*
12. Pitt, W. W., Haag, G. L. & Lee, D. D., 1983. Recovery of ethanol from fermentation broths using selective sorption-desorption. *Biotechnol. Bioeng.*. 25, 123-131.
13. Shapouri, H., Duffield, J. A., Graboski, M. S., 1995. Estimating the net energy balance of Corn Ethanol. An Economic Research Service Report. *United States Dept. of Agriculture.* Report No. 721.
14. Shapouri, H., Duffield, J., McAloon, A., & Wang, M., 2004. The 2001 Net Energy Balance of Corn-Ethanol (Preliminary). *United States Dept. Agriculture*.
15. Roostaei, N., Tezel, F. H., 2004. Removal of phenol from aqueous solutions by adsorption. *J. Environ. Manag.* 70, 157-164.
16. Ruthven, D. M., 1984. Principles of Adsorption and Adsorption Processes. *Wiley, New York.*
17. Walsh, K. P., Liu, P. C., Findley, E. M., Liaois, I. A. & Siehr, J. D., 1983. Ethanol Separation from Water in a Two-Stage Adsorption Process. *Biotechnol. Bioeng. Symp.* 13, 629-647.

8.0 Authors note

The paper entitled "Selective ethanol separation from water using silicalite, activated carbon and ZSM-5 adsorbents: Adsorption isotherms and kinetics" appears in this thesis as it does in print in the International Journal of Energy Research with minor changes. Following the publication of the manuscript, issues with obtaining bulk supplies of the adsorbents M-30 and X-A754 were discovered. M-30 activated carbon was originally acquired by the authors as a 400 g sample. Although it performed well in the experimental screening in this study (adsorption kinetics and equilibrium capacity), the small particle size of the adsorbent was not appropriate for industrial applications and it was not available from the vendor in other particle sizes. Furthermore, the cost of acquiring a larger quantity of M-30 was significantly greater than all other adsorbents screened and would likely limit the applicability of applying the material in a large scale

adsorption bed. As for X-A754, the product was discontinued by the vendor and thus omitted from future studies.

Additional adsorbents were screened following the publication of this manuscript and among the materials screened F-600 activated carbon was identified as the best candidate for future studies. Equilibrium and kinetic experiments were carried out for F-600 with slightly modified experimental protocols as outlined in Chapter 3. Although the capacity of the F-600 is lower than those reported for M-30 and X-A754, part of the discrepancy was due to the different experimental protocol between the two studies. The adsorption capacity shown for F-600 in Chapter 3 is thought to more accurately represent the capacity that would be available in a packed bed, although it was lower than some results in this study. The methods used to acquire points on the adsorption isotherm of F-600 are reported in Section 2.3 and 2.3.1 of Chapter 3. These sections also discuss why shaker flask experiments (like those performed in Chapter 2) are not always representative of the adsorbent performance in a packed bed system.

The kinetic performance of the F-600 adsorbent is more important than the relatively lower capacity that was measured.

For all studies following the publication of the manuscript in Chapter II, F-600 activated carbon was used as the ethanol selective adsorbent of choice.

SECTION – III: Modelling of adsorption experiments

Chapter 3

Simulation and validation of ethanol removal from water in an adsorption packed bed: Isotherm and mass transfer parameter determination in batch studies

R. A. Jones, J. Thibault, F. H. Tezel

Abstract

Preferential adsorption of ethanol from ethanol/water mixtures in batch equilibrium and kinetic experiments were carried out on a commercially available activated carbon adsorbent Filtrasorb 600 (F-600). A model based on finite difference method was developed and employed to determine the mass transfer parameters and equilibrium behaviour for the adsorption of ethanol from simple batch systems. The estimates of the adsorption isotherm along with the mass transfer parameters were used to simulate the transient performance that could be expected in a packed bed under various operating conditions (feed flow rate, feed concentration, and particle size). The applicability of the simulation results were found to be a good match with experimental packed bed experiments over the entire range of operating conditions tested.

1.0 Introduction

The conversion of biomass feed into a useable ethanol fuel is a complex and energy-intensive process which includes an expensive pre-treatment of feedstock, a fermentation step which yields a dilute ethanol broth and a train of subsequent separation steps. Due to the limitations in the current processing, particularly for the ethanol from lignocellulosic feedstock, the economic viability of ethanol production has come into question. Traditional distillation separation of ethanol from fermentation broth while effective, contributes a significant amount to the overall energy consumption of a typical ethanol from biomass plant, and thus poses an economical challenge. Low energy separation alternatives and technologies that integrate the conversion of fermentable sugars with

subsequent separation are thought to have the greatest potential to significantly reduce processing costs in the bioethanol industry (Cardona and Sanchez, 2007). One technology that shows potential to couple the production of ethanol with the separation and purification of the product is an on-line ethanol adsorption-desorption cycle (Pitt et al., 1983). An envisioned adsorption separation scheme would ideally remove a stream from the fermentation broth when ethanol concentrations rise and the sugar content in the broth is low, and selectively extract ethanol from the broth by passing it through an externally located adsorption column. Extracting the ethanol as it is being produced can allow the fermentation to continue while suppressing product inhibition (Maiorella et al., 1984). As a result, producing fermentation broth with higher substrate utilization and higher reactor productivity is possible. Furthermore, the ethanol adsorbed can be desorbed and the process can be made cyclical by adding parallel columns, and alternating between adsorption and desorption. If the separation is highly selective in its preference for ethanol, the product stream desorbed could be expected to be very concentrated. Pitt et al. (1983) reported that desorbed ethanol fractions of 60 wt% could be obtained from a saturated packed bed of hydrophobic adsorbents when using an adsorption-desorption cycle (from 10 wt% feed). A pre-purification step of selective adsorption-desorption could also be designed to reduce the quantity of feed which needs to be processed through the distillation column. If ethanol is removed as the feed travels the length of the column, the effluent (depleted of ethanol content) can be diverted directly to waste, rather than being processed in the distillation unit. This scheme has the obvious advantage of reducing downstream equipment sizes and costs as well as operating costs. The ability to generate high quality ethanol vapour in the adsorption-desorption unit would reduce the reboiler duty significantly.

Ethanol adsorption studies to date have mainly focused on adsorbent screening studies with the emphasis on finding suitable materials to extract ethanol from the broth with favourable equilibrium capacity and kinetic rates. Various hydrophobic adsorbents capable of extracting ethanol from ethanol-water mixtures have been studied (Benito et al., 1998; Farhadpour and Bono, 1996, 1998; Jones et al., 2007). Similar studies have shown that various alcohols (methanol, propanol and butanol) could be concentrated on

the surface of hydrophobic zeolite adsorbents from miscible alcohol-water solutions (Milestone and Bibby, 1983).

The aforementioned studies used alcohol-water mixtures to simulate fermentation broth. A significant amount of work has also been performed on the extraction of ethanol from actual fermentation broth during operation. Ikegami et al. (2000) reported enhanced substrate utilization and ethanol productivity when activated carbon adsorbents were added directly to fermentation broth. Similarly, a study by Einicke et al. (1991) reported enhanced glucose consumption rates during fermentation when unsaturated hydrophobic adsorbents were present during batch fermentation experiments.

In this study, the development of a mechanistic mass transfer model solved by finite differences for the selective adsorption of ethanol from water is presented. The model is applied for the purpose of mass transfer determination from batch experiments, and the parameters found are used to predict the transient behaviour of a packed bed adsorber. Model validation is performed on a series of small scale experiments, and the applicability of the model is discussed.

The design of packed bed adsorbers is dependent on both the equilibrium isotherm as the departure from the equilibrium represents the driving force for mass transfer in all adsorption processes, and the mass transfer parameters which dictate the rate of mass transfer from the bulk to the adsorbent. Obtaining an accurate adsorption isotherm and a method that can be used for estimating the governing mass transfer resistances are key challenges that will be addressed in this study.

2.0 Materials and methods

2.1 Materials

Solutions used in this study were binary mixtures of ethanol and water and were prepared with anhydrous ethanol (Commercial Alcohols Inc., Brampton, ON, Canada) and distilled de-ionized water. The adsorbent used for this study was F-600 activated carbon

purchased from Calgon Corporation, Bolton, ON, Canada. The approximate BET surface area of the adsorbent was 900 m^2/g.

2.2 Kinetic mixed batch experiments

Kinetic experiments were performed in a mixed batch system. A turbine mixer with as many as six mesh pouches for holding the activated carbon was used to achieve non-destructive adsorbent mixing within the batch. Throughout the experiments, binary mixtures of ethanol and water were used to simulate the fermentation broth. The experiment was performed by introducing a known quantity of activated carbon held in the pouches of the turbine mixer to the batch. The initial volume and composition of the bulk liquid was known, and the change in composition in the bulk was monitored by extracting 0.5 ml samples at defined intervals. Each sample was then centrifuged, and filtered (Millipore, MF membrane filters) to ensure no adsorbent particles were present in the sample. The composition of each liquid sample was determined with a HPLC system **(**Water 501 HPLC pump, Water Differential Refractometer R401 and Waters Dextro-Pak column), which was then used to infer the corresponding ethanol concentration in the solid sample.

The time after which the composition of ethanol in solution was no longer changing, was taken as the time for the system to reach thermodynamic equilibrium. The temperature and pH of the mixture were recorded just prior to removing the liquid samples. Once the system had reached equilibrium, a mass balance on the system was performed, and a single point on the adsorption isotherm was obtained for each kinetic mixed batch experiment.

2.3 Equilibrium experiments

When compiling data to determine the governing isotherm for ethanol adsorption by F-600 activated carbon, data from three separate experimental setups (kinetic mixed batch, re-circulating packed bed, packed bed breakthrough) were used. In addition, a fourth setup was tested (equilibrium flask experiments) and the data was later omitted when estimating the isotherm. Details are discussed below.

2.3.1 Equilibrium flask experiments

The first experimental attempt at determining points on the equilibrium isotherm was carried out in a series of Erlenmeyer flasks. Each flask contained an ethanol water mixture of known volume and initial composition. Varying quantities of adsorbent was placed directly in each of the respective flasks, and the flasks were placed in an equilibrium shaker for a period of 24 hours. After 24 hours, a single sample was extracted from each flask and processed in the same manner as in the kinetic experiments. By performing a mass balance on liquid and solid in the batch, the quantity of ethanol adsorbed was determined.

One problem noted with the equilibrium flask experiments was the destructive nature of the test. It was noted that the activated carbon had undergone significant pulverization during the 24 hour period due to the intense nature of the shaking. Interestingly, the equilibrium capacities observed in the flask experiments were as much as 5 - 40 % higher than the capacity observed using the alternative experimental setups (Sections 2.2, 2.3.2 and 2.4). Particle attrition can contribute to an increase in surface area (particularly external surface area), which is positively correlated with capacity (Jones et al., 2007). However, with activated carbon adsorbents, the vast majority of the surface area is located within the porous structure. The change in particle size and hence the external surface area alone is not thought to contribute significantly to the increased capacity. More likely, the large difference in capacity can be attributed to greater pore accessibility due to the change in particle size and the more vigorous nature of the mixing. In liquid systems, pores can become inaccessible when small air pockets cause dead zones where adsorption does not occur (Zbik et al., 2009). It is thought that the increase in capacity is directly related to the greater pore accessibility in the equilibrium flask experiments.

Since the primary objective was to determine points along the isotherm that represent the capacity found during breakthrough operation, data from the equilibrium flask experiments was omitted when compiling the adsorption isotherm for ethanol on F-600 (Figure 1) as it was not representative of the capacity observed during breakthrough experiments used for model validation.

2.3.2 Re-circulating packed bed equilibrium experiments

A set of experiments was performed to acquire adsorption isotherm data in a re-circulating packed bed system. In these experiments, an ethanol mixture of known composition and volume (approximately 300 mL) was prepared and mixed on a stir plate. The solution was pumped at a fixed flow rate through an adsorption column packed with F-600 and the column effluent was returned back to the feed tank. Small samples (0.5 mL) were removed from the feed tank vessel to monitor the change in composition over time. Once the composition in the feed tank was steady, a sample obtained under thermodynamic equilibrium could provide a single point on the adsorption isotherm. By altering the composition of the batch vessel (by adding ethanol or water) once equilibrium had been obtained, the system could continue to run, and a new equilibrium would be established, providing additional points along the isotherm. This experiment was performed in such a way that initially a low concentration in the batch was used, and the concentration of the batch was elevated periodically (through the addition of ethanol) to produce points on the isotherm at progressively higher liquid phase compositions. Once data was obtained for the entire range of concentration of interest, the vessel was diluted progressively with the addition of water to obtain points on the ethanol desorption isotherm.

2.4 Packed bed breakthrough experiments

Packed bed breakthrough experiments for ethanol adsorption onto F-600 activated carbon were performed over a range of experimental conditions with varying particle size, inlet flow rate and feed concentration. Experiments were carried out in a glass column of radius 0.0127 m and height 0.3 m. The feed solution was prepared and placed on a Stirrer/Hot Plate (Corning). A gear pump (Series GD, Micropump) system was used to feed a defined ethanol solution flow rate for each run. No recirculation was done for these breakthrough experiments. Samples of the column effluent were taken until the adsorbent bed had reached complete saturation. The sample composition was measured as described in Section 2.2. Each experimental run of the packed bed breakthrough experiment was also used to garner more information about the adsorption isotherm. By calculating the

amount of ethanol removed from the effluent at the point of bed saturation, a single point on the adsorption isotherm was also obtained.

2.5 Estimation of the amount adsorbed

For the kinetic mixed batch experiments and the re-circulating packed bed experiments, a simple calculation could be used to determine the quantity of ethanol that had been adsorbed at any time. Knowing the initial and final ethanol concentrations in the mixture, a simple mass balance can provide the amount of ethanol that was adsorbed assuming the total volume of the solution did not change. The following equation provides the amount of ethanol adsorbed per unit mass of adsorbent:

$$q = \frac{V_T (C_o - C_f)}{M_{ads}} \tag{1}$$

While this assumption is valid for the equilibrium experiments which only require the removal of one sample at the end of the experiment, the kinetic experiments required many samples to be removed. The serial removal of samples during the kinetic experiment accounted for less than 1-3% of the total initial volume in all trials. This progressive change in volume was nevertheless considered in the calculation.

3.0 Modelling

3.1 Equilibrium modelling

An equilibrium isotherm describes the capacity of the adsorbent as a function of the equilibrium concentration of the adsorbate in the solution at a constant temperature. The Freundlich isotherm was used to represent the adsorption equilibrium data in this paper. It is one of the most commonly used models for adsorption of liquid solutions and represented the experimental data obtained in this investigation very well. The Freundlich isotherm is expressed as follows:

$$q_e = AC_e^{1/n} \tag{2}$$

3.2 Kinetic mixed batch modelling

Modelling of mixed-batch kinetic experiments was carried out using the set of differential equations presented herein (Equations 3 to 9). The modes of mass transfer for a mixed batch include transfer of ethanol from the bulk liquid to the surface of the adsorbent, intrapellet diffusion within the pores of the pellet and physical adsorption onto the surface of the pores of the solid adsorbent.

The model is based on three governing differential equations: (1) a species balance on adsorbing component (ethanol) within the well mixed bulk fluid, (2) a species balance of the adsorbing component in the mobile phase within the porous structure of the adsorbent particle, and (3) a balance of the physical adsorption onto the surface of the pores of the adsorbent within the pellet. The result is a set of three coupled differential equations describing the mass transfer which occurs within the system. In addition to the governing differential equations, the equilibrium isotherm is required, as with all adsorption systems.

The experimental data could be modeled in two separate ways for the purpose of comparison. Model type #1 assumes instantaneous adsorption once the liquid is in contact with the surface of the adsorbent. Model type #2 includes an adsorption controlled mass transfer resistance.

3.2.1 Mixed batch model assumptions

1. System operates under isothermal conditions
2. The equilibrium is adequately described by the Freundlich isotherm
3. Adsorbent particles are homogenous in size and are spherical in shape
4. Bulk liquid is well mixed
5. Instantaneous adsorption (physical binding of adsorbate to adsorbent) is assumed for model type #1.
6. Adsorption controlled mass transfer is included for model type #2.

3.2.2 Ethanol balance in the liquid bulk

Assuming the bulk liquid is well mixed, the rate of change in concentration in the batch vessel is given by Equation (3). The rate of depletion of ethanol in the liquid phase (the left hand side of the equation) is equal to the disappearance of ethanol moving into the adsorbent particles.

$$\frac{\partial C_L}{\partial t} = -\frac{1-\varepsilon}{\varepsilon} k_L a (C_L - C_P\big|_{r=R_p}) \tag{3}$$

3.2.3 Ethanol balance in the mobile phase in the pellet pores

The rate of concentration change of the mobile phase within the pores of the adsorbent pellets is given by Equation (4).

$$\frac{\partial \boldsymbol{C_p}}{\partial \boldsymbol{t}} + \nabla \cdot (-\boldsymbol{D_{EFF}} \nabla \boldsymbol{C_p}) = \boldsymbol{R} \tag{4}$$

This equation accounts for the diffusion within the pores of the pellet and the rate of adsorption onto the internal surface of the pellet. In this investigation, pellets of spherical shape were used. The model can be expanded using adsorption scenarios, the first of which assumes that the binding of the adsorbate to the surface of the adsorbent occurs very rapidly compared to the other mass transfer steps (instantaneous adsorption). The second includes an additional mass transfer resistance which accounts for the binding of the adsorbate to the adsorbent (non-instantaneous). The two expansions of the equation are shown in Equations (5) and (6), respectively.

$$\left(\varepsilon_p + \left|1-\varepsilon_p\right| \rho_s \frac{\partial q}{\partial C_p}\right) \frac{\partial C_p}{\partial t} = D_{EFF} \left(\frac{1}{r^2} \frac{\partial}{\partial r} \left(r^2 \frac{\partial C_p}{\partial r}\right)\right) \tag{5}$$

$$\frac{\partial C_p}{\partial t} = D_{EFF} \left(\frac{1}{r^2} \frac{\partial}{\partial r} \left(r^2 \frac{\partial C_p}{\partial r}\right)\right) - \frac{k_{ads} a_p (C_p - C_p^*)}{\varepsilon_p} \tag{6}$$

3.2.4 Ethanol balance on the surface of the adsorbent

The equation describing the rate of concentration change on the surface of the solid is derived from a simple mass balance. The rate of ethanol adsorbed onto the surface is simply equal to the rate of transfer from the mobile phase inside the pellet to the solid surface. Equation (7), which implicitly incorporates the Freundlich isotherm (Equation 2), is used when the instantaneous equilibrium is assumed, whereas Equation (8) is used when it is assumed the adsorption contributes significantly to the mass transfer resistance.

$$\frac{\partial q}{\partial t} = \frac{\partial q}{\partial C_p} \cdot \frac{\partial C_p}{\partial t} = \frac{A}{n} C_p^{\left(\frac{1}{n}-1\right)} \frac{\partial C_p}{\partial t} \tag{7}$$

$$\frac{\partial q}{\partial t} = \frac{k_{ads} a_p \left(C_p - C_p^* \right)}{\left(1-\varepsilon_p\right) \rho_s} \tag{8}$$

Where, the rearranged Freundlich isotherm is used to determine the mobile phase concentration that would be in equilibrium with the solid.

$$C_p^* = \left(\frac{q_e}{A} \right)^n \tag{9}$$

3.2.5 Initial and boundary conditions

Solving model type #1 (instantaneous equilibrium) requires the solution of Equations (3), (5) and (7), solving model type #2 (adsorption controlled) requires the solution of Equations (3), (6) and (8).

Initially, the ethanol concentration in the vessel is known. It is also known that ethanol is not present in the pores or on the surface of the adsorbent, initially.

$$At\ t = 0:\ C_L = C_o \text{ (Ex. 60 gEtOH/L)},\ C_P = 0,\ q = 0, \quad \forall\ (r, z) \tag{10}$$

Only the initial conditions are required to solve Equations (3), (7) and (8).

To solve Equations (5) and (6), two boundary conditions are required, along with the initial condition. At the center of the particle, symmetry prevails whereas as at the surface of the sphere the rate of diffusion within the pellet must equal the convective mass flux from the liquid bulk

$$\frac{\partial C_p}{\partial r} = 0 \quad r = 0,\ t \geq 0 \tag{11}$$

$$-D_{EFF}\frac{\partial C_p}{\partial r} = k_L\left(C_L - C_p\big|_{r=R_p}\right) \quad r = R_p,\ t \geq 0 \tag{12}$$

The purpose of the modelling for the kinetic mixed batch system is to obtain an accurate estimate of the internal mass transfer resistances within the adsorbent particles, namely the effective diffusion coefficient and the kinetics associated with the adsorption step. The determined parameters are to be used for simulating and design a packed bed adsorber. The inherent assumption used in this paper is that the internal mass transfer parameters obtained in a mixed-batch system are akin to those that would be found in a packed bed system. The parameters are also assumed to be independent of particle size, adsorbent loading and ethanol composition over the range of variables studied.

3.3 Breakthrough and simulation

Mathematical modelling is required to understand the dynamics of fixed bed adsorbers. A properly working model will allow for a reasonable prediction of the separation which will take place given a set of known operating conditions (inlet feed composition, feed flow rate, adsorber/adsorbent properties).

The governing differential equations and solution for fixed bed is similar to the solution for the mixed batch adsorption study outlined in Section 3.2. Only the equation pertaining to the mass balance on the liquid bulk is changed. The ethanol balance on the bulk phase is altered to account for the axial dispersion and convection within the column. The mass transfer inside the pellet is exactly the same thus Equations (5), (6), (7) and (8) apply depending on whether or not instantaneous equilibrium is assumed.

The mathematical treatment of the model is similar to that of the kinetic experiment. The assumptions outlined in Section 3.2.1 for the mixed batch experiments: isothermal operation, uniform and homogenous particle size, and the applicability of the Freundlich equation are all valid for the packed bed model. In addition to the aforementioned assumptions, for the packed bed simulations, the velocity within the bed is assumed to be constant and uniform.

3.3.1 Ethanol balance on the bulk liquid

Assuming the ethanol concentration is constant in the radial direction, the rate of change in concentration at any position along the column is given by Equation (13). The terms contained in the right-hand side of this equation account for the axial dispersion along the column, the disappearance of ethanol moving into the adsorbent particles, and the amount of ethanol flowing by convection, respectively.

$$\frac{\partial C_L}{\partial t} = D_z \frac{\partial^2 C_L}{\partial z^2} - \frac{1-\varepsilon}{\varepsilon} k_L a (C_L - C_P\big|_{r=R_p}) - u_L \frac{\partial C_L}{\partial z} \tag{13}$$

The mass transfer within the pellet can be described by Equations (5) - (8).

3.3.2 Initial and boundary conditions

Initially, ethanol is not present in the column such that liquid and solid concentrations are zero:

$$At\ t = 0:\ C_L = 0,\ C_P = 0,\ q = 0, \qquad \forall\ (r, z) \tag{14}$$

The two boundary conditions required to solve Equation (13) assume that at the entrance and the exit of the packed bed, the diffusive flux is equal to zero:

$$\frac{\partial C_L}{\partial z} = 0 \qquad z = 0,\ t \geq 0 \tag{15}$$

$$\frac{\partial C_L}{\partial z} = 0 \qquad z = L,\ t \geq 0 \tag{16}$$

The boundary equations for the pellet are the same as the kinetic experiment Equations (11) and (12) apply for this case.

3.3.3 Empirical correlations used to estimate the mass transfer parameters

One objective of this investigation was to determine the minimal number of experimental parameters that are required to allow for the design of a packed bed adsorber. Intuitively, the solid adsorption capacity (i.e. the isotherm), the effective diffusion coefficient and the kinetics of adsorption must be determined experimentally. All other parameters required to solve the differential equations can be estimated. It is desired to see if these estimates are sufficient to adequately simulate adsorption performance in a packed bed adsorber. The empirical equations that are used in the model to determine the external mass transfer resistances, the molecular diffusion coefficient, and the axial dispersion coefficient are discussed below:

3.3.3.1 Average external film resistance

The average mass transfer coefficient between the flowing liquid bulk and the pellet was calculated using the equation of Wakao and Funazkri (1978):

$$\mathrm{Sh} = 2.0 + 1.1\left(\mathrm{Re}\right)^{0.6}\left(Sc\right)^{0.33} \tag{17}$$

$$\frac{k_L D_p}{D_M} = 2.0 + 1.1\left(\frac{D_p \rho u_L}{\mu}\right)^{0.6}\left(\frac{\mu}{\rho D_M}\right)^{0.33} \tag{18}$$

3.3.3.2 Molecular diffusion coefficient

The molecular diffusion of ethanol in water was approximated using the Wilke-Chang equation (Welty et al., 2000).

$$D_M = \frac{7.4x10^{-8}\left(\phi M_B\right)^{0.5} T}{\mu\, v^{0.6}} \tag{19}$$

3.3.3.3 Axial dispersion coefficient

The axial dispersion coefficient was estimated using the following correlation

(Welty et al., 2000).

$$\frac{\varepsilon D_Z}{D_M} = 20 + 0.5\,\mathrm{Re}\,Sc \tag{20}$$

3.4 Numerical methods

The governing differential equations were solved using the finite difference method. Equations (3), (7), (8), (13) and (14) were solved using an explicit scheme. Equation (5) and (6) were solved implicitly and the Thomas Algorithm was used for solving the resulting tri-diagonal matrix (Carnahan et al., 1969).

The influence of the grid size and the time step was assessed to ensure that proper interval sizes were used throughout the modelling in order to accurately solve the system of equations.

4.0 Results and discussion

The primary objective of this paper is to develop a mechanistic mass transfer model describing the adsorption of ethanol onto F-600 activated carbon. The intended use of the model is to simulate packed bed performance over a range of operating conditions. To supplement the model, simple experiments were designed to determine the mass transfer parameters governing the kinetics of the system (kinetic mixed batch experiments) and data from a series of experiments were used to generate an adsorption isotherm that is representative of the adsorption which is observed when operating a packed bed adsorber. Although both model type 1 and model type 2 were used, for the purpose of the results section, only model type 1 is discussed and shown in the figures (instantaneous adsorption). The unknown internal mass transfer parameters: the effective diffusion coefficient and kinetics of adsorption are inherently coupled and without a method to decouple the parameters, using model type 2 with a single unknown internal mass transfer parameter is more appropriate.

The equilibrium isotherm was estimated by compiling data from three primary experimental setups: kinetic mixed batch experiments, re-circulating packed bed

experiments, and experimental breakthrough curves. It should be noted that a fourth experimental setup was tested (equilibrium flask experiments), but the data acquired was not representative of the packed bed performance, and was therefore omitted (see Section 2.3.1). The experimental setups used in the determination of the isotherm were all non-destructive methods and allowed the adsorbent particles to maintain their integrity throughout the experimental run. In fact, it is recommended by the International Union of Pure and Applied Chemistry (IUPAC) to use a fixed bed arrangement to minimize particle "abrasion" and to improve isotherm precision (Everett, 1986). The data obtained through the various non-destructive experimental techniques are shown in Figure 1.

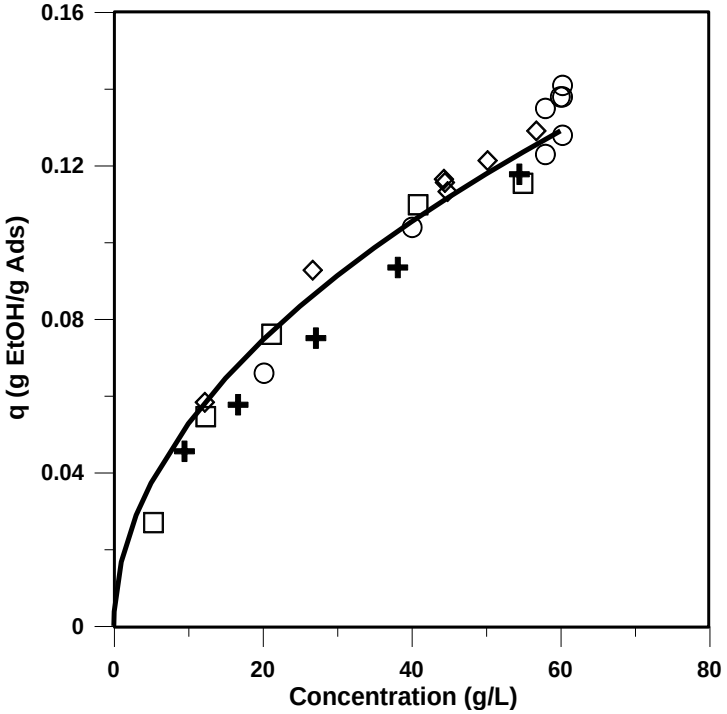

Figure 1 - Ethanol adsorption isotherm on F-600 activated carbon at 23-26°C. Isotherm is comprised of points from the modified mixed-batch kinetic experiments (◊), the packed bed re-circulation experiments (□: adsorption, +: desorption), and the dynamic breakthrough experiments (O).

Figure 1 displays all data from the aforementioned experimental setups. The Freundlich isotherm was used to fit the entire data set yielding a single adsorption isotherm model that was used for all model predicted simulations throughout this paper. The data points used to compile the isotherm do show some degree of scatter (kinetic mixed batch experiments generally had slightly higher capacity, the re-circulating mixed batch

experiments were slightly lower), but the isotherm points from the non-destructive experimental setups showed relatively good agreement. From a practical point of view, using the various techniques to determine a single governing adsorption isotherm model is validated by the close agreement between the isotherm model and the capacity measured during the various breakthrough experiments shown in Figure 1. The adsorption isotherm obtained is believed to be representative of the equilibrium which exists in packed bed operation, and thus fit for the use in the simulation of packed bed adsorption behaviour.

In order to determine the mass transfer resistances which are attributed to the internal portion of the pellet, concentration decay experiments were performed in kinetic mixed batch operation. Experiments were conducted at various initial concentrations, adsorbent to liquid ratios and particle sizes. From the seven unique experimental runs, a single parameter, the effective diffusion coefficient was estimated through an optimization routine by minimizing the total sum of squared residuals from the seven runs. The specific run conditions are presented in Table 1 and the experimental data along with the model fits are found in Figures 2a to 2c.

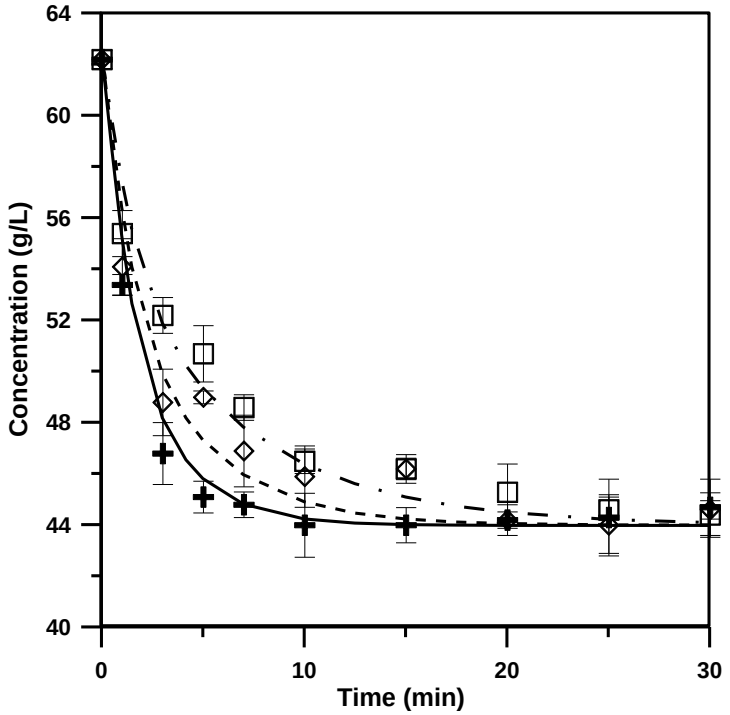

Figure 2a - Ethanol adsorption on F-600 activated carbon. Kinetic experiments performed with varying particle size. Lines represent model fit. Symbols represent experimental data at particle diameters of +: 0.72 mm, ◊: 0.92 mm, and □: 1.21 mm

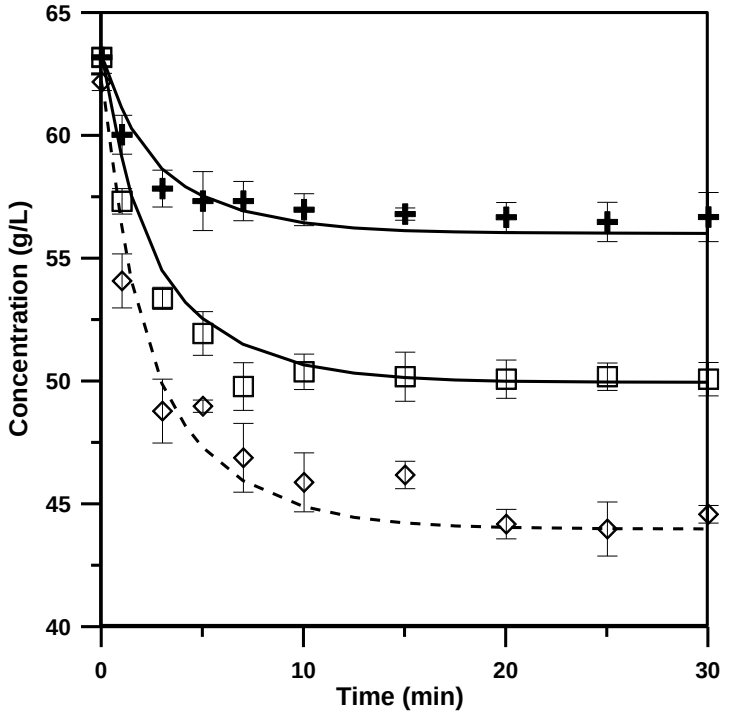

Figure 2b - Ethanol adsorption on F-600 activated carbon. Kinetic experiments performed with varying initial adsorbent to liquid loading ratios. Lines represent model fit. Symbols represent experimental data at adsorbent loading ratios of +: 5g of activated carbon per 100ml of solution, □: 10g/100ml and ◊: 15g/100ml.

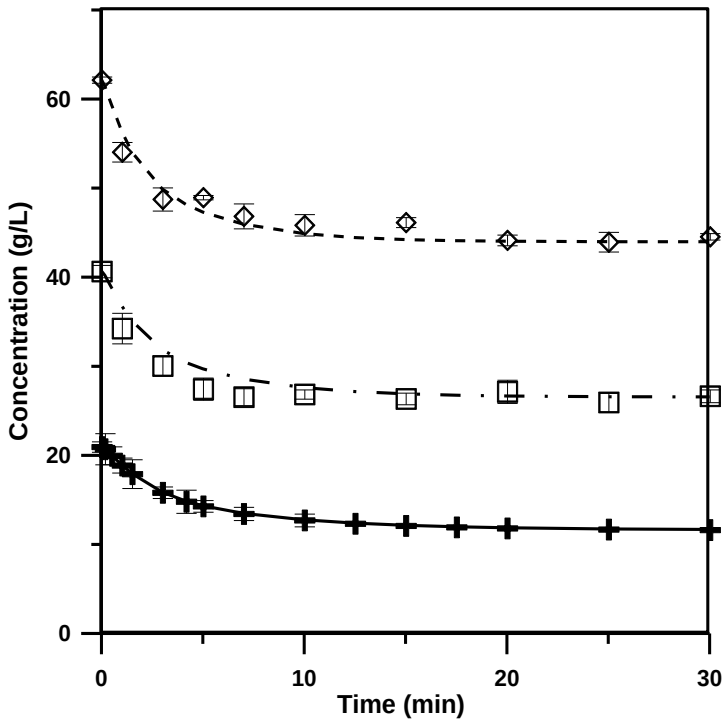

Figure 2c - Ethanol adsorption on F-600 activated carbon. Kinetic experiments performed with varying initial ethanol concentrations. Lines represent model fit. Symbols represent experimental data at initial concentrations of approximately +: 20g/L, □: 40g/L and ◊: 60g/L

In Figures 2a to 2c, seven unique kinetic mixed batch experimental runs are shown in Figure 2a for a variation of particle size, in Figure 2b for a variation in adsorbent loading and in Figure 2c for a variation of the initial batch concentration. For each of the runs, a set of three experiments was performed and the average concentration and the standard deviation error bars are shown. The general concentration decay trend was similar throughout all runs despite differences in initial ethanol concentration, adsorbent loading and particle size. Initially, as the adsorbent was added, a rapid decline in the liquid phase concentration was observed. This rapid decrease is attributed to the readily available adsorption sites at the outer portion of spherical adsorbent pellet becoming occupied. As time progresses, the concentration decline becomes more gradual as ethanol slowly diffuses into the particle and is being adsorbed in the interior portion of the pellets. From Figure 2a, it is evident that as the particle size decreases, the initial rapid drop in concentration is more pronounced. This observation was expected and is explained by the fact that a greater proportion of the adsorption sites for the smallest particle diameter are those sites which are easy to access. Furthermore, pore lengths are generally

shortened on average and thus the ethanol has less distance to diffuse to reach adsorption sites in the center of the pellet. For the larger particles, more time is required for the pellet to saturate. In this case, a greater proportion of the sites are reached only after the ethanol diffuses along the pore.

In Figure 2b, the adsorbent loading ratio was varied. Each of the runs had an initial concentration of approximately 60 g/L ethanol, however, the final concentrations reached varied considerably with varying adsorbent loading. With greater loading, more ethanol was removed from the bulk, and thus a lower final concentration was achieved. The capacity measured in each of the experiments also varied a significant amount which is expected due to the large difference in the final bulk concentration. From each of the runs a single point on the adsorption isotherm was determined (see Figure 1).

In Figure 2c, the initial concentration of the batch was varied. Each run had the same particle size and adsorbent loading. As expected, the batch with the highest initial ethanol concentration experienced the greatest amount of ethanol adsorption (as predicted by the adsorption isotherm).

From the model's fit to the experimental data in Figures 2a to 2c, an effective diffusion coefficient of 3.8×10^{-10} m^2/s was estimated. The model effectively represents the depletion of ethanol in the bulk liquid due to the transfer of ethanol into the activated carbon over a range of concentrations, adsorbent loadings and particle sizes.

It is hypothesized that the internal mass transfer resistance should be independent of the hydrodynamic conditions prevailing outside of the pellet in all cases. This assumption implies that the effective diffusion coefficient estimated from the kinetic mixed batch experiments can be used for the purpose of simulation when considering packed bed operation.

Table 1 - Run conditions for kinetic mixed batch experiments

Run #	$Concentration_{initial}$	Particle diameter	Adsorbent loading
-	g/L	mm	g ads/100 ml
Particle size			
A	62.2	0.72	15
B*	62.2	0.92	15
C	62.2	1.21	15
Adsorbent loading			
D	63.2	0.92	5
E	63.2	0.92	10
B*	62.2	0.92	15
Concentration			
F	20.1	0.92	15
G	40.7	0.92	15
B*	62.2	0.92	15

* Run B – single run with operating conditions defined above

Having obtained an estimate of the adsorption isotherm that governs packed bed operation and an estimate of the effective diffusion coefficient, a series of simulations for varying particle size, inlet flow rate and initial concentration were conducted. In order to evaluate the validity of the model, packed bed adsorption experiments were performed at the same operating conditions for the purpose of comparison. The results of the validation experiments with varying particle size, inlet flow rate and feed composition are shown in Figure 3a to 3c.

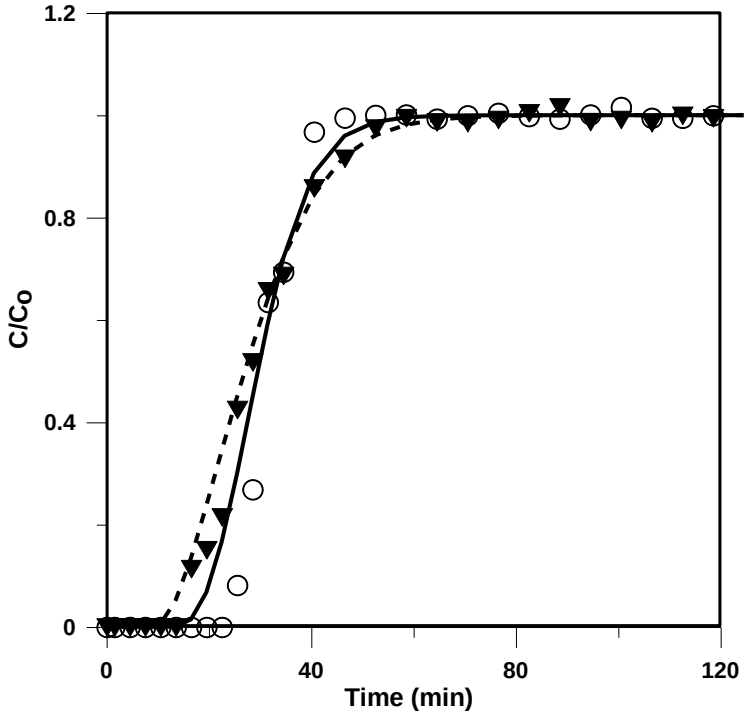

Figure 3a – Ethanol adsorption on F-600 activated carbon during packed bed breakthrough experiment. Breakthrough data are plotted along with model predictions for various particle diameters, (O: 0.72 mm, ▼: 1.21 mm)

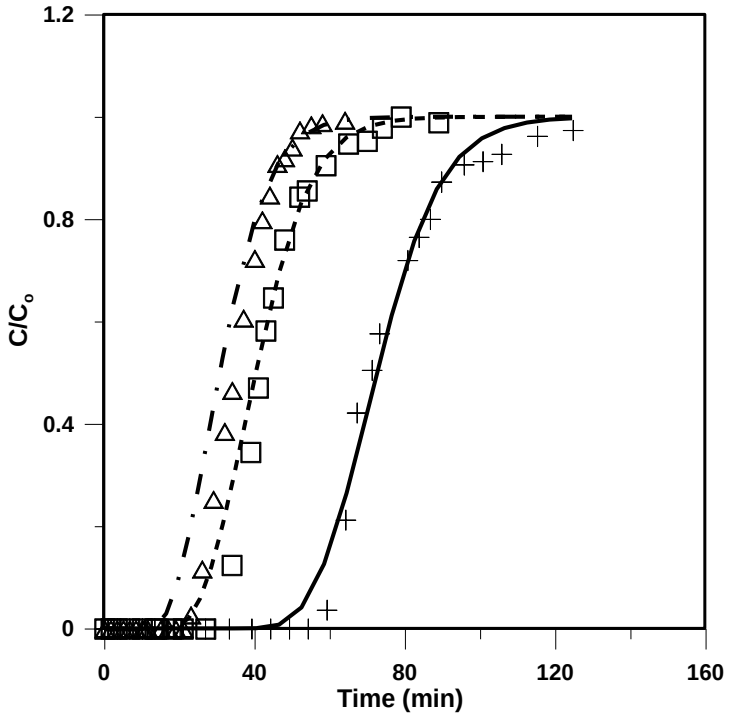

Figure 3b – Ethanol adsorption on F-600 activated carbon during packed bed breakthrough experiment. Breakthrough data are plotted along with model predictions for various inlet flow-rates (+: 4.5 ml/min, □: 8.0 ml/min, Δ 10.1 ml/min)

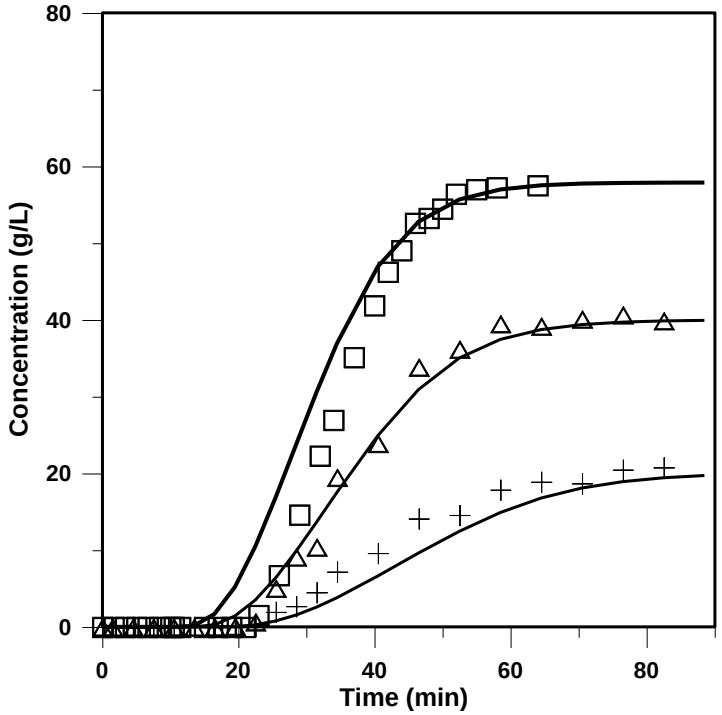

Figure 3c – Ethanol adsorption on F-600 activated carbon during packed bed breakthrough experiment. Breakthrough data are plotted along with model predictions for various inlet ethanol concentrations (+: 20 g/L,: Δ 40 g/L, □: 60 g/L)

In Figures 3a to 3c, eight unique packed bed adsorption experimental runs are shown with particle size varied in Figure 3a, inlet flow rate varied in Figure 3b and the feed concentration varied in Figure 3c. For each of the runs, the mechanistic model developed was used to simulate the packed bed performance with parameters being estimated from empirical correlations (k_L, D_z), or estimated from the mixed batch experimental results (D_{EFF}).

In Figure 3a, only the experimental runs with the smallest and largest particles tested are shown. It was observed that as the particle size decreases, the breakthrough of ethanol at the column effluent was delayed. This delayed breakthrough was not the result of greater ethanol capacity, but rather the result of a sharper ethanol breakthrough profile. A sharp profile with delayed breakthrough is desirable from an operation standpoint, as a greater portion of the saturation bed capacity is used prior to the first appearance of ethanol in the column effluent (useable capacity). Intuitively, as the particle size decreases, the diffusion of ethanol into the porous structure takes less time as the average pore length is

shortened. For the run with the larger particles, the mass transfer resistance attributed to the internal pore diffusion is more pronounced. The experimental data depicts an early breakthrough for the larger particles as the ethanol on average has to travel further along the pore to reach adsorption sites. This fact lengthens the mass transfer zone within the bed and creates a more progressive breakthrough curve. The model simulation qualitatively matches the trend of the experimental data, predicting an earlier breakthrough as the particle size increases. The capacity of the bed measured experimentally and the model predicted capacity were within 5 % for both runs. The model predicted an earlier appearance of ethanol in the column effluent than was observed experimentally for both runs.

In Figure 3b, shorter breakthrough times were experimentally observed when the inlet flow was increased. Experimentally, the shape of the profile does not appear to be altered over the range of flow rates tested. The simulated model profiles predict earlier breakthrough of ethanol in the column effluent when compared to the experimental data. This result is directly related to the slightly higher capacity for these particular breakthrough experimental runs compared to Freundlich isotherm model used in the simulation (observed in Figure 1 as the difference between circles (O) around 60 g/L and the Freundlich isotherm curve). Capacity discrepancies of 5 to 10 % were observed for these data points when comparing the isotherm model and the equilibrium point obtained from the breakthrough curve. In the model prediction, the shape of the profile is changed slightly as the flow increases. The slightly sharper profile at higher flow rates is related to the change in the external mass transfer coefficients that are related to the hydrodynamic properties of the system (see Table 2).

In Figure 3c the effect of feed concentration in packed bed breakthrough experiments is observed. Since the adsorbent capacity is a function of the liquid phase composition, the total amount of ethanol removed to the point of bed saturation is different for each run. Therefore, predicting the point at which ethanol will breakthrough in each run is not intuitive. The model prediction matched the experimental breakthrough points for the 40 g/L inlet concentrations with a very good degree of accuracy. The predictions for the 20

and 60 g/L were slightly off due to a discrepancy in capacity. The model was effective in predicting the order of breakthrough and the general shape of the curves for each of the tested concentrations.

Each of the model simulations were validated by experimental data at the same operating conditions. Deviation between the model and the experiment was caused primarily by a slight lack of agreement between the measured capacity of the bed during the experiment (a single isotherm point), and the Freundlich isotherm model that was used in all simulations. The model comes from a collection of all equilibrium points. The quality of the simulation relies heavily on the proximity of the experimentally measured capacity to the isotherm model. Any slight departure of a single equilibrium point (obtained during the breakthrough experiments) from the determined isotherm model will cause a lack of fit between the breakthrough simulation and the experimental data (characterized as an under-prediction or an over-prediction). Beyond the capacity discrepancy, the slight change of curvature beyond the inflection point of the breakthrough curve was observed in the experimental runs (Figures 3a to 3c), but not adequately addressed by the model. This is a common observation that is well documented in the adsorption literature. In 1959, Scheidegger observed a similar deviation between his model based on the classic convection-dispersion equation (CDE) and his experimental breakthrough results. Scheidegger classified the model error as a systemic deviation of unknown origin. More recent work has shed light on the cause of these deviations for breakthrough curves based upon the CDE. Cortis and Berkowitz (2004) found that many breakthrough curves display “non-Fickian” behaviour (tailing) that cannot adequately be described by the classic CDE. The authors proposed the adoption of a Continuous Time Random Walk theory which better represents the tailing in the experimental data. These authors argue that the failure of the classic CDE based models is due to the assumption of completely homogeneous porous medium, when in reality various studies show that preferential flow patterns persist in packed columns, a trait inherent to heterogeneous systems. Despite the inability to fit the tailing in the experimental data, models based on the CDE equation remain the most popular basis for breakthrough curve models. From a practical standpoint, in terms of general adsorption processes and the process envisioned herein,

predicting the breakthrough point is of greater concern than fitting the observed tailing. The range of operating conditions for the validation experiments are shown in Table 2.

Table 2 - Run conditions for packed bed adsorption experiments

Run #	Flow	Particle size	Concentration	d_c/d_p*	Re	k_L
-	ml/min	mm	g/L	-	-	1/s
Flow						
1	4.5	1.05	57.9	24.2	0.25	7.9×10^{-6}
2	8.0	1.05	59.9	24.2	0.44	1.0×10^{-5}
3	10.1	1.05	57.9	24.2	0.55	1.1×10^{-5}
Particle size						
4	10.0	0.72	60.2	35.3	0.37	1.4×10^{-5}
5	10.0	0.92	60.3	27.6	0.48	1.2×10^{-5}
6	10.1	1.21	60	21.0	0.64	1.0×10^{-5}
Concentration						
7	10	1.05	20.1	24.2	0.55	1.1×10^{-5}
8	10.1	1.05	40	24.2	0.55	1.1×10^{-5}
3	10.1	1.05	57.9	24.2	0.55	1.1×10^{-5}

* d_c/d_p is the ratio of the column diameter to the particle diameter

In addition to the operating conditions, Table 2 also contains the external mass transfer coefficient estimated from empirical correlations used in the model simulation.

5.0 Conclusions

A mechanistic model based upon a modified version of the CDE (convection-dispersion equation) was developed in this paper. Simple experiments were devised to gain information about the kinetic and equilibrium behaviour of ethanol adsorption by F-600 activated carbon. From the experiments, an isotherm that is representative of the equilibrium adsorption capacity observed in a packed bed across all operating conditions tested was obtained. Mixed batch experiments were devised to monitor the rate of ethanol transferred from the bulk to the pores of the adsorbent to study the kinetics. The results gathered from these experiments were used to estimate the mass transfer resistance in the internal portion of the pellet. The effective diffusion coefficient was estimated to be 3.8×10^{-10} m^2/s from the mixed batch experiments by simultaneously modelling seven kinetic experiments carried out under different conditions by assuming

constant diffusion coefficient. This value was then used in simulation of packed bed experiments.

The validation of the packed bed model simulations shows that the model is capable of reliably predicting the breakthrough point of a packed bed adsorber using simulations based entirely on simple batch experiments. Deviations between the experimental and model capacity is a factor that affects the quality of model prediction. It was concluded that obtaining an accurate adsorption isotherm model is the key to a good simulation. Results indicate that experimental techniques that are non-destructive with respect to the adsorbent particles should be used when estimating points on the adsorption isotherm. Simple batch experiments can be used for the determination of the isotherm and with the help of the model developed, for the estimation of the internal mass transfer resistance. The application of the model proposed herein to simulate packed bed performance is a method that can be used as a reliable first estimate in packed bed adsorber design and performance studies.

6.0 Acknowledgments

The authors would like to thank, NSERC (Natural Science and Engineering Research Council of Canada) for their financial contribution for this study.

7.0 Nomenclature

Symbols:

a	Exterior pellet surface area per volume of pellet (m^2 external area/m^3 pellet)
A	Freundlich constant, (kg EtOH/kg adsorbent) (m^3/kg EtOH)$^{1/n}$
a_p	Internal surface area of pellet (m^2 surface area/m^3 pellet)
C_e	Concentration in solution at equilibrium, (kg EtOH/m^3)
C_f	Final concentration of batch solution, (kg EtOH/m^3)
C_L	Ethanol concentration within the liquid bulk (kg EtOH/m^3)
C_o	Initial concentration of batch solution, (kg EtOH/m^3)
C_p	Concentration in the mobile phase in the pellet pores (kg EtOH/m^3)
$C_P\big\|_{r=R_P}$	Concentration at the pellet boundary (kg EtOH/m^3)
C_P^*	Concentration in equilibrium with the solid (kg EtOH/m^3)
D_{EFF}	Effective diffusion coefficient of the adsorbing species (m^2/s)
D_M	Molecular diffusion coefficient of ethanol in water (m^2/s)

D_p Pellet diameter (m)
D_z Axial diffusion coefficient (m^2/s)
k_{ads} Average adsorption mass transfer resistance (m/s)
k_L Average film mass transfer coefficient (m/s)
M_{ads} Mass of adsorbent, (kg adsorbent)
M_B Molecular weight of ethanol (kg/kg.mol)
n Freundlich constant, (dimensionless)
q Amount of ethanol adsorbed (kg EtOH/kg adsorbent)
q_e Amount of ethanol adsorbed at equilibrium (kg EtOH/kg adsorbent)
r Distance in the radial position (m)
R Volumetric rate of adsorption (kg EtOH/m^3.s)
R_p Pellet radius (m)
t Time, (s)
T Temperature, (K)
u_L Superficial velocity (m/s)
V_T Volume of the solution, (m^3)
z Distance in the axial direction (m)

Greek letters:

ε Bed void (m^3 void/m^3 bed)
ε_p Pellet void fraction (m^3 void/m^3 pellet)
ρ Density of solution (kg solution/m^3 solution)
ρ_S Solid density (kg solid/m^3 solid)
μ Viscosity of solution (Pa.s)
ν Solute molal volume (at normal boiling point) (cm^3/mol)
ϕ Association factor specific to the system in question, (dimensionless)

8.0 References

1. Benito, G. G., Carton, A., Rey, J. A., de la Fuente, M., "Selection of adsorbents to be used in an Ethanol Fermentation Process. Adsorption Isotherms and Kinetics." *Bio-resources Technology.* 66, 75-78 (1998).
2. Cardona, C. A., Sanchez, O. J., "Fuel ethanol production: Process design trends and integration opportunities." *Biores. Tech.* 98, 2415-2457 (2007).
3. Carnahan, B., Luther, H.A., and Wilkes, J. O., "Applied Numerical Methods", John Wiley and Sons, New York, (1969).
4. Cortis A., Berkowitz B., "Anomalous Transport in "Classic" Soil and Sand Columns." *Soil Sci. Soc. Am. J.* 68, 1539-1548 (2004).

5. Einicke, W. D., Glaser, B., Schollner, R., "In-situ recovery of ethanol from fermentation broth by hydrophobic adsorbents." *Acta Biotechnologica.* 11., 353-358 (1991)
6. Everett, D. H., "Reporting Data on Adsorption from Solution at the Solid/Solution Interface." *Pure & Appl. Chem.,* 50, 967-984 (1986)
7. Farhadpour, F. A., Bono, A., "Adsorption from Solution of Non-electrolytes by Micro-porous Crystalline Solids: Ethanol-Water/Silicalite System." *J. Coll. Inter. Sci.* 124, 209-227 (1998).
8. Farhadpour, F. A., Bono, A., "Sorptive separation of ethanol-water mixtures with a bi-dispersed hydrophobic molecular sieve, silicalite: determination of the controlling mass transfer mechanism." *Chem. Eng. Process.* 35, 141-155 (1996).
9. Ikegami, T., Yanagishita, H., Kitamoto, D., Haraya, K., "Accelerated ethanol fermentation by *Saccharomyces cerevisiae* with addition of activated carbon." *Biotechnology letters.* 22, 1661-1665 (2000).
10. Jones, R.A., Tezel, F.H., Thibault, J., and Tolan, J.S., "Bioethanol production to be blended with gasoline: Improvements in energy use by adsorption." *Inter. J. of Ener. Res.* 31 (15), 1517-1531 (2007).
11. Maiorella, B. L., Blanch, H. W., Wilke, C. R., "Economic evaluation of alternative ethanol fermentation processes." *Biotechnol. and Bioeng.* 26, 1003-1025 (1984).
12. Milestone, N. B, Bibby, D. M., "Adsorption of alcohols from aqueous solution by ZSM-5." *J. Chem. Tech. Biotechnol.* 34A, 73-79 (1983).
13. Pitt JR., W. W., Haag, G. L., Lee, D. D., "Recovery of ethanol from fermentation broth using selective sorption-desorption." *J. Biotech and Bioeng*. XXV, 123-131 (1983).
14. Scheidegger, A. E., "An evaluation of the accuracy of diffusivity equation for describing miscible displacement in porous media." *In Proc. Theory of Fluid Flow Conf., University of Oklahoma.* 101-116 (1959)
15. Wakao, N., Funazkri, T., "Effect of Fluid Dispersion Coefficients on Particle-to-Fluid Mass Transfer Coefficients in Packed Beds." *Chem. Eng. Sci.* 33, 1375-1384 (1978).

16. Welty, J.R., Wicks, C.E., Wilson, R.E., and Rorrer, G., "Fundamentals of Momentum, Heat and Mass Transfer", John Wiley and Sons, New York, (2000).
17. Zbik, M. S., Du, J., Pushkarova, R. A., Smart, R. St. C., "Observation of gaseous films at solid-liquid interfaces: Removal by ultrasonication." *J. Coll. And Inter. Sci.* 336, 616-623, (2009).

Chapter 4

Neural network modelling of adsorption isotherms

Graham Morse, Rudy Jones, Jules Thibault, and F. Handan Tezel

Abstract

This paper examines the possibility to use a single neural network to model and predict a wide array of standard adsorption isotherm behaviour. Series of isotherm data were generated from the four most common isotherm equations (Langmuir, Freundlich, Sips and Toth) and the data were fitted with a unique neural network structure. Results showed that a single neural network with a hidden layer having three neurons, including the bias neuron, was able to represent very accurately the adsorption isotherm data in all cases. Similarly, a neural network with four hidden neurons, including the bias, was able to predict very accurately the temperature dependency of adsorption data.

Keywords: Isotherms; neural networks; Langmuir; Freundlich; Sips; Toth

1.0 Introduction

Adsorption is a commonly used chemical engineering separation process. It is a process whereby two or more components of a fluid (gas or liquid) stream are separated through contact with a solid surface. The quantity of the component which can bind to the surface of the adsorbent will depend on the temperature and the composition (partial pressure or concentration) as well as various physical and chemical properties of the adsorbate-adsorbent pair. A measurement of the amount adsorbed over a range of compositions at a fixed temperature is known as an adsorption isotherm.

It is difficult to predict a priori the isotherm behaviour of a particular system because of the inherent complexities associated with adsorption. The differing properties of fluids and solids are the key variables affecting this equilibrium. A given fluid or solid can be formed with an infinite variety of differing compositions and components. This creates a myriad of possibilities and scenarios when attempting to model the interactions.

The majority of experimental isotherm data observed can be classified into six defined "types". Brunauer, Deming, Deming and Teller (BDDT) classification in 1940 recognized five distinct isotherm trends (Brunauer et al., 1940), and in 1985 the International Union of Pure and Applied Chemistry (IUPAC) introduced a sixth general isotherm trend which makes up the accepted isotherm classification system (Sing et al., 1985).

Over the years, many adsorption isotherm systems have been modeled using particular equations. These include Langmuir, Freundlich, Sips, and Toth isotherm models among others. Although these classic adsorption isotherm models are capable of representing certain equilibrium data sets by themselves, they also display a considerable lack of fit when modelling non-traditional systems. The variable nature of these adsorption isotherms presents a challenge to the development of an equation that can be used to model the behaviour of all adsorption systems. For example, Padmesh et al. (2006) used a total of ten different isotherm correlations in an attempt to find a suitable equation that

will fit their adsorption data. To date, a single unifying equation to model all types of adsorption isotherms has yet to be constructed.

A general adsorption model must successfully address the following criteria. It must be: (1) flexible enough to deal with the wide variety of isotherms; (2) able to predict the trends between any two data points; (3) fit the visual trends of the data set; and (4) able to include known trends that are characteristic of adsorption.

Because the driving force for all adsorption separations will depend on the existence of a departure from equilibrium, it is imperative that an accurate and versatile adsorption isotherm model for a system is attained before design, simulation or modelling can be accomplished. Artificial neural networks are a general class of nonlinear models that have the potential to address the above criteria.

The scope of this paper is therefore to examine if a single artificial neural network structure can be used as a comprehensive adsorption model. In other words, it is desired to find a suitable model to represent adsorption data where only the parameters of the fixed-structure model will change such that one will not have to search for the most appropriate structure of the model (Langmuir, Freundlich, Sips, Toth, etc.) as it is currently being done in practice. Feedforward neural networks have been successfully used in many applications related to adsorption. It was used to simulate the dynamics of an adsorption column for wastewater treatment of water containing toxic chemicals (Bulsari and Palosaafi, 1993) and to predict the occurrence of breakthrough in an ion-exchange adsorption column (Yang et al., 1993). Lewandoski et al. (1998) developed a method for the simulation and optimization of a pressure swing adsorption process for the separation of nitrogen from air where the neural network model was used to obtain a prediction for the process performance, namely, the specific product and yield, over a wide range of operating conditions. Carsky and Do (1999) predicted the adsorption equilibrium of binary vapour mixtures on activated carbon. Sundaram (1999) used a neural network to analyze the relationship between input and output variables for pressure swing adsorption (PSA) processes for three different applications. Basu et al.

(2002) predicted the effect of temperature on equilibrium adsorption of hydrocarbon gases and vapours on activated carbon. Babu et al. (2003) used a neural network to predict the pollutant removal efficiency based on a large data bank of pollutants and adsorbents whereas neural networks were used by Gao and Engell (2004) to predict the slope, instead of the actual value, of nonlinear isotherms. Mjalli et al. (2005) used neural networks to represent the adsorption data for isopropanol-water system. Giraudet et al. (2006) predicted with a neural network the heat of adsorption from physical characteristics of activated carbons and volatile organic compound molecular properties. Vasina et al. (2009) used neural networks to model protein adsorption. Kumar et al. (2010) used a three-layer feed-forward artificial neural network to model the equilibrium data of hydrogen onto activated carbons. The properties of the activated carbons and the experimental conditions were used as inputs to predict the corresponding hydrogen uptake at equilibrium conditions.

In this paper, it is desired to extend the use of neural network as a universal isotherm model. This paper is divided into sections as follows: it starts with a brief presentation of the most common isotherms that will be used to evaluate the ability of artificial neural networks to represent a wide variety of isotherm data. It is followed by the description of the artificial neural network structure that will be used to obtain these isotherm models. In the subsequent section, results are presented and discussed. Finally, results for temperature-dependent isotherms are presented.

1.1 Common adsorption isotherms

Four of the most common isotherms are used in this investigation to generate different series of adsorption data that will serve as learning data sets to fit artificial neural networks. It is desired to test if a single neural network structure can be used to represent the data of all simulated isotherm data. The four types of isotherms are Langmuir, Freundlich, Sips (Langmuir-Freundlich) and Toth.

The first isotherm, the Langmuir isotherm (Langmuir, 1918) applies to localized adsorption of monolayer surface coverage assuming that each adsorbed molecule

occupies one adsorption site. The derivation of the Langmuir isotherm was obtained by considering both the rates of adsorption and desorption, integrating the net rate of surface coverage and, at equilibrium, the isotherm equation reduces to the simple two-parameter equation presented in Table 1. Another isotherm, the Freundlich isotherm (Freundlich, 1907), is a semi-empirical equation which is widely used to represent adsorption equilibrium data for low to intermediate range of concentration. The Freundlich equation is characterized with two fitting parameters and is presented in Table 1. The Sips isotherm (Sips, 1948) is a combination of the Langmuir and Freundlich isotherms, which represent systems for which one adsorbed molecule could occupy more than one adsorption site (represented by the variable n in the isotherm equation given in Table 1). It has three parameters that could be expressed as a function of temperature which allows easy interpolation and extrapolation of the experimental isotherms to other temperatures and compositions. Another isotherm that has three parameters that could be written as a function of temperature is the Temperature Dependent (TD) Toth isotherm (Toth, 1971). The equation for that isotherm is also given in Table 1.

Table 1 – Modelling results obtained with the four types of isotherms

Isotherm	Equation	Set	Parameters	$\sum(q - \hat{q})^2$
Langmuir	$q = \frac{q_s\ b\ c}{1 + b\ c}$	1	$(q_s, b) = (1, 7)$	8.55×10^{-6}
		2	(1, 100)	1.51×10^{-3}
		3	(150, 0.00670)	3.7×10^{-15}
Freundlich	$q = A\ c^{1/n}$	1	$(A, n) = (1, 1)$	3.97×10^{-15}
		2	(1, 0.1)	9.86×10^{-7}
		3	(1, 10)	2.96×10^{-2}
		4	(1, 0.3)	3.70×10^{-8}
		5	(1, 3)	1.27×10^{-3}
Sips (Langmuir-Freundlich)	$q = \frac{q_s (bc)^{1/n}}{1 + (bc)^{1/n}}$	1	(39.7, 0.273, 0.985)	1.28×10^{-7}
		2	$(q_s, b, t) = (1, 50, 1)$	3.34×10^{-19}
		3	(1, 3, 0.2)	1.49×10^{-3}
Toth	$q = \frac{q_s\ b\ c}{\left[1 + (b\ c)^t\right]^{1/t}}$	1	(3.088, 0.325, 3.60)	1.18×10^{-10}
		2	$(q_s, b, t) = (1, 50, 1)$	3.34×10^{-18}
		3	(1, 3, 3)	7.22×10^{-4}
TD Toth	$q = \frac{q_s\ bc}{\left[1 + (bc)^t\right]^{1/t}}$	40°C	$b_o = 5.685$	3.67×10^{-4}
		70°C	$(Q/RT_o) = 7.029$	3.27×10^{-4}
		80°C	$T_o = 313.15$	2.07×10^{-4}
		100°C	$t_o = 0.706$; $\alpha = 0$, q_{so}	2.36×10^{-4}
		140°C	$= 1.475$; $\chi = 0$	3.79×10^{-4}

To account for temperature dependency, parameters of isotherm equations are correlated as a function of temperature. For instance, the three parameters (q_s, b, and t) for the TD Toth isotherm are expressed as a function of temperature by Equations (1)-(3).

$$b = b_o \exp\left[\frac{Q}{RT_o}\left(\frac{T_o}{T} - 1\right)\right] \quad (1)$$

$$t = t_o + \alpha\left(1 - \frac{T_o}{T}\right) \quad (2)$$

$$q_s = q_{so} \exp\left[\chi\left(1 - \frac{T}{T_o}\right)\right] \quad (3)$$

When these parameters are inserted into the regular Toth isotherm as a function of temperature, then the TD Toth isotherm (q as a function of c) becomes a correlation with a total of seven parameters: b_o, (Q/RT_o), T_o, t_o, α, q_{so}, and χ.

1.2 Neural network models

Neural networks have been the subject of considerable research interest for the past twenty years. Artificial neural networks (ANN) attempt to mimic how a biological system functions and how they can be utilized for their novel architecture to solve highly complex, undefined and nonlinear mathematical problems. ANNs can simply be viewed as general nonlinear models which have the ability to encapsulate the underlying relationship that exists between a series of inputs and outputs of a system. Hoskins and Himmelblau (1988) and Bhat and McAvoy (1989) appear to be the first authors that modelled chemical processes with an artificial neural network. Artificial neural networks are now being used for a wide variety of engineering applications. They possess a high degree of flexibility and plasticity that allows them to easily capture the nonlinear behaviour of a process using input-output data.

Feedforward neural networks (FFNN) are undoubtedly the most popular neural network structure used in engineering applications. It has been shown that a three-layer FFNN can represent any function provided that sufficient number of neurons are present (Cybenko, 1989). A FFNN normally consists of three layers: an input layer, a hidden layer, and an

output layer. The feedforward neural networks that have been used in this investigation are presented in Figure 1. The input layer receives the process inputs and fans out this information to all functional neurons of the hidden layer. Each neuron of the hidden layer essentially performs two tasks: (1) a weighted summation of all process inputs; and (2) a non-linear transformation, via a neuron transfer function, of the weighted summation to produce the output of each neuron of the hidden layer which then serves as inputs to the neurons of the output layer. The output layer performs the same task as the neurons of the second layer to produce the final output of the FFNN. The typical transfer functions that are used in the hidden and output layers are linear, sigmoid or hyperbolic tangent. The input and output to the FFNN are usually scaled between 0 and 1 or -1 to 1. Results obtained with many neural network structures with different transfer functions were very similar such that it was decided to use a conventional structure with sigmoid transfer functions for the hidden layer and a linear transfer function for the output layer. Therefore, the resulting equation for the FFNN with three hidden neurons (including the bias) of Figure 1(a) with scaled input and output is:

$$\bar{q} = \frac{w'_{11}}{1 + e^{-(w_{11}\bar{c} + w_{21})}} + \frac{w'_{21}}{1 + e^{-(w_{12}\bar{c} + w_{22})}} + w'_{31} \tag{4}$$

$$\text{with } \bar{q} = \frac{q - q_{min}}{q_{max} - q_{min}} \text{ and } \bar{c} = \frac{c - c_{min}}{c_{max} - c_{min}} \tag{5}$$

In a neural network, the fitting information lies in the interconnection weights or parameters (W_{ij} and W'_{jk} in Figure 1) between neurons and the topology of the network. Using an ANN to represent experimental data between dependent and independent variables is no different than using any empirical model. The learning process consists of determining the weight matrices, W_{ij} and W'_{jk} that produce the best fit of the predicted outputs over the entire data set. In this investigation, the quasi-Newton optimization algorithm was used to fit the adsorption data (Powell, 1975).

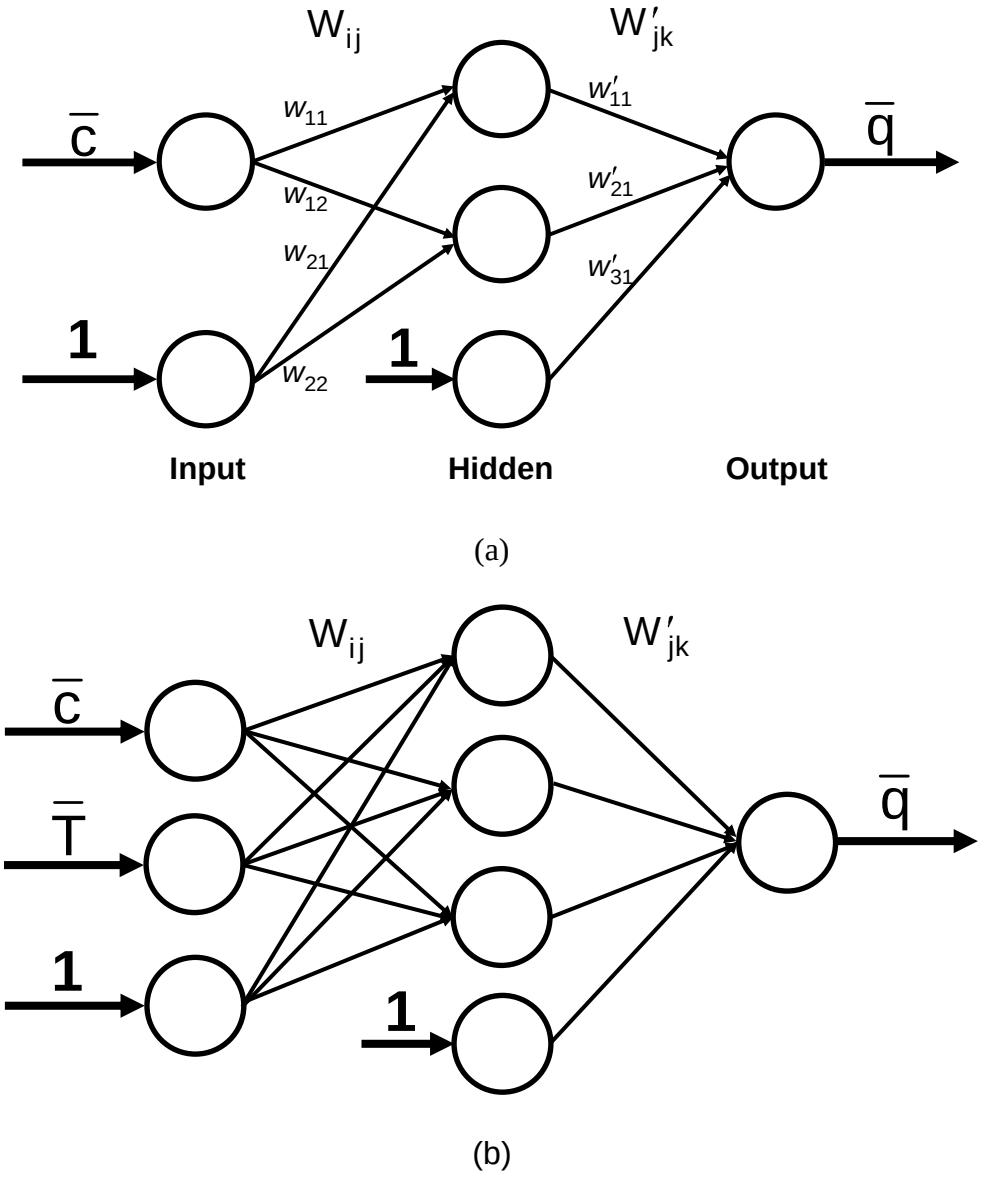

Figure 1 – Feedforward neural networks used to represent (a) all isotherm data sets at a given temperature, and (b) temperature-dependent isotherm data sets.

2.0 Results and discussion

2.1 Neural networks for modelling isotherms

The ultimate goal of this investigation was to test the ability of simple artificial neural network architectures with the least number of parameters to represent a wide variety of isotherm data. The four most commonly used temperature-independent two and three-parameter isotherms (see Table 1) were simulated over a wide range of parameter values and the generated data were fitted using the neural network architecture of Figure 1(a)

with three hidden neurons, including the bias. This neural network consists of one independent variable (the adsorbate fluid concentration, c) and one dependent variable (the adsorbate solids concentration, q). There are a total of seven neural network weights or model parameters.

Figures 2-5 present the results obtained for the four series of isotherm data. The data points in these figures were created by fixing the parameters of the isotherms differently for different data sets as given in Table 1. The FFNN in Figure 1(a) was used to fit these data points. The sums of squares of the differences between the observed or simulated isotherm data and the fitted isotherm data for each set are presented in the fifth column of Table 1. The solid lines on the graphs were obtained by predicting 100 equally distant predicted values in the range of the isotherm data points by using the fitted isotherm neural networks to ensure that the prediction was also good between observed data points that were used to fit the neural network. The 100 equally distributed points were also compared with the isotherm data that were generated from the models of Table 1 and similar prediction average errors were observed than for the points that were used for training the neural network. It is clear that the neural network of Figure 1(a) is able to represent the large majority of isotherm data sets.

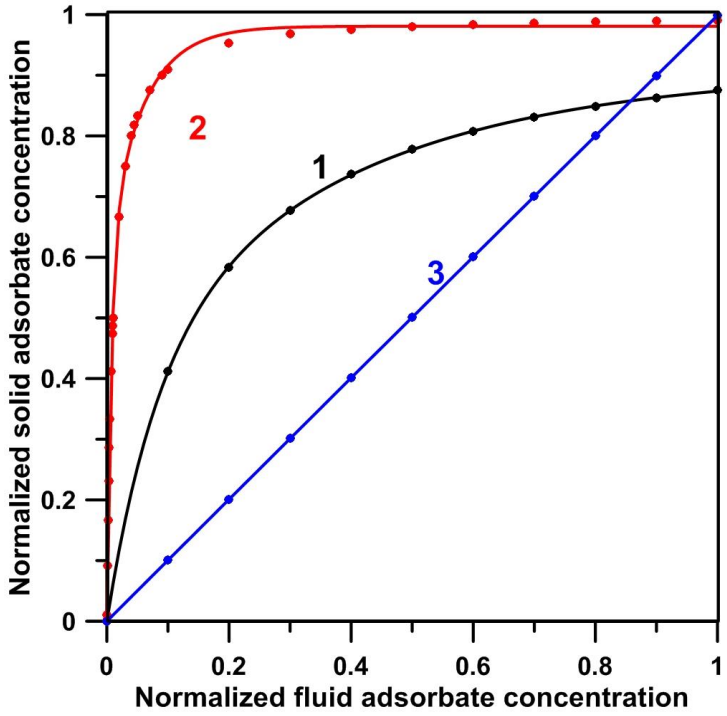

Figure 2 – FFNN for three Langmuir isotherm data sets. Symbols represent isotherm data and curves represent FFNN fits. The numbers refer to the models of Table 1.

The largest deviations are observed when the isotherm is strongly favourable. The most severe discrepancy was for the third set of the Freundlich isotherm data (Figure 3).

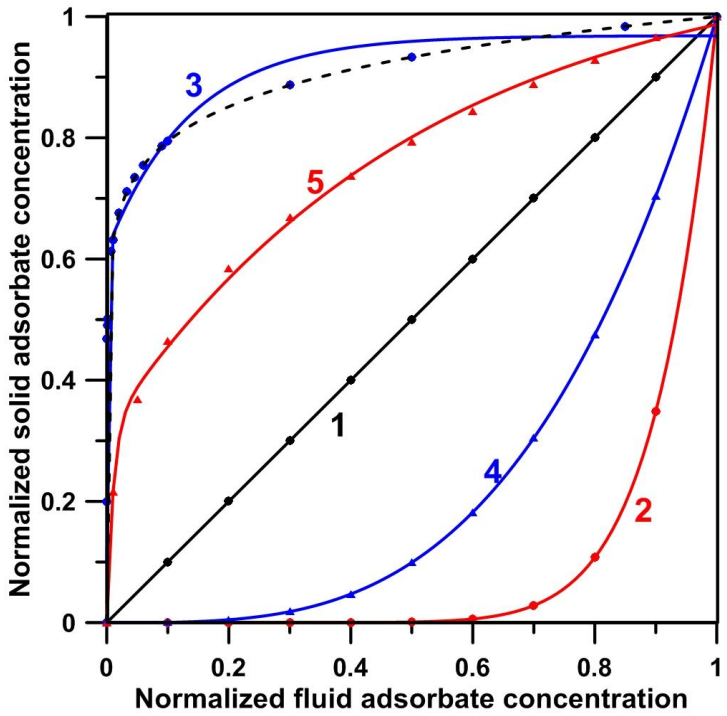

Figure 3 – FFNN for five Freundlich isotherm data sets. Symbols represent isotherm data and curves represent FFNN fits. The numbers refer to the models of Table 1.

With only three hidden neurons (including the bias neuron), the simple neural network architecture of Figure 1(a) was not sufficient to capture the strong nonlinearity that exists between the fluid and solid adsorbate concentrations. By adding a fourth hidden neuron for this particular isotherm data set, the fit was significantly improved as shown by the dotted line in Figure 3. It was only under this extremely steep isotherm that it was necessary to use an additional neural to represent the adsorption data with a very precision. All the other isotherms were very well fitted with the neural network structure of Figure 1(a) such that the predicted isotherm is of sufficient precision to be used with confidence for simulation and design. See Figure 4 and 5 below

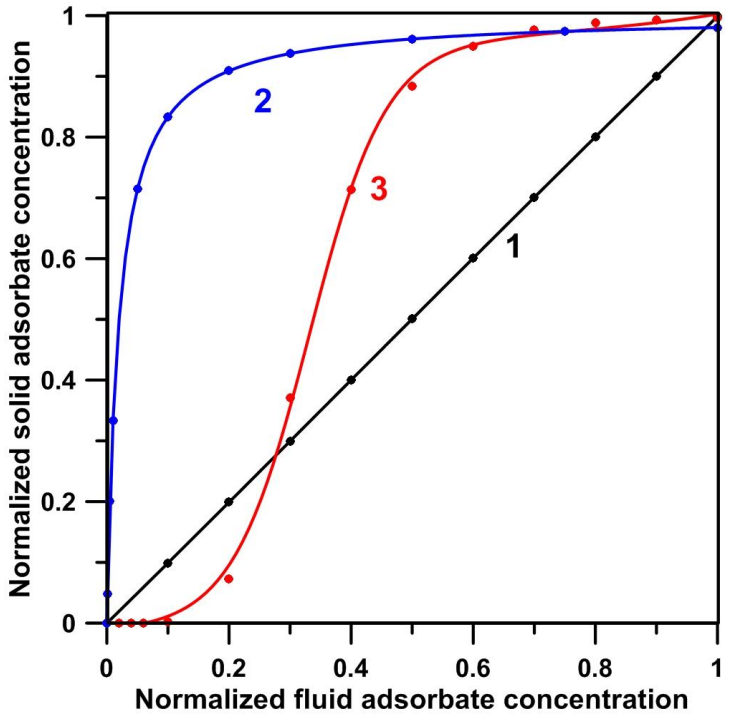

Figure 4 – FFNN for three SIPS isotherm data sets. Symbols represent isotherm data and curves represent FFNN fits. The numbers refer to the models of Table 1.

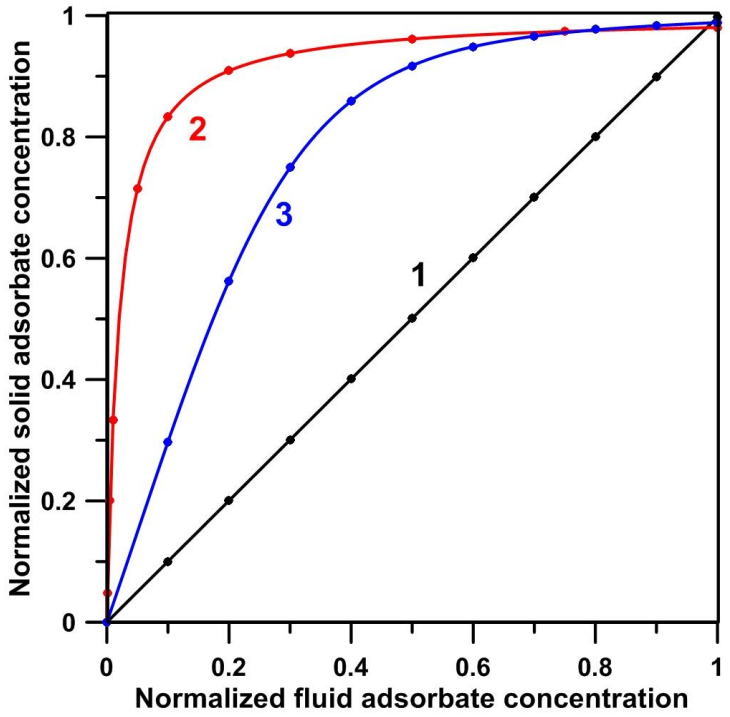

Figure 5 – FFNN for three Toth isotherm data sets. Symbols represent isotherm data and curves represent FFNN fits. The numbers refer to the models of Table 1.

The data of Padmesh et al. (2006) for the adsorption of acid red 88 from an aqueous solution at pH 3 by algal biomass was digitized so that it could be used to evaluate the performance of FFNN to fit adsorption data that deviate from a standard isotherm trend. Indeed, the experimental isotherm is extremely steep at low concentration in solution and has two distinct plateaus for which the most common isotherm equations listed in Table 1 are not able to represent adequately the experimental data by themselves. Figure 6 presents the results obtained with the FFNN with three and four hidden neurons, respectively.

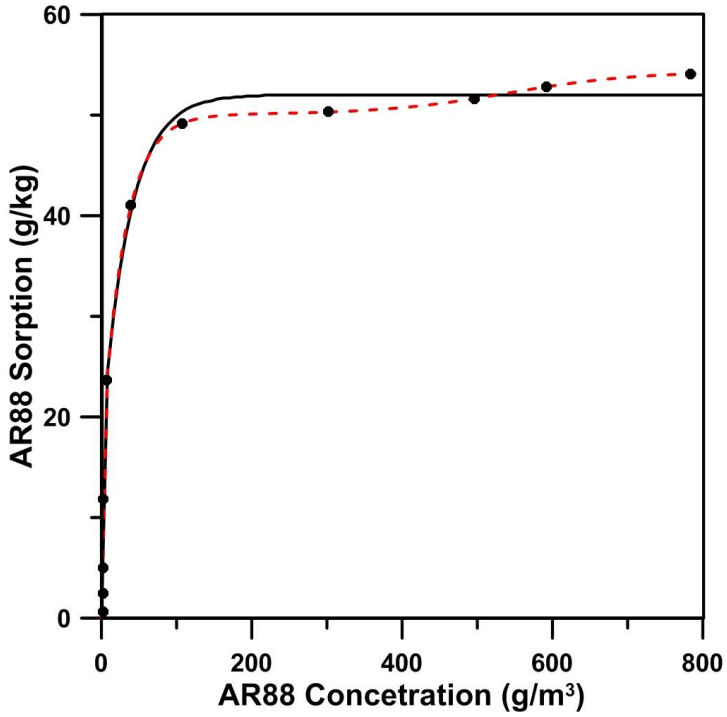

Figure 6 – FFNN for the data of Padmesh et al. (2006). Symbols represent experimental data and curves represent FFNN fits: —— FFNN with three hidden neurons; – – – – FFNN with four hidden neurons.

It is clear that the neural network of Figure 1(a) was not able to perfectly capture the shape displayed by the experimental data. However, by adding another hidden neuron to the FFNN, the fit is excellent. The sums of squares of the errors were 10.5 and 0.012, respectively for the fit with three and four hidden neurons. This example shows clearly the enviable flexibility of neural network isotherm models over more conventional isotherm models.

2.2 Extension to include the temperature effect

In many adsorption applications, temperature effects are important and must be accounted for. It is important to have a reliable model that can fit a temperature-dependent adsorption isotherm over a given range of temperature. Artificial neural networks can be easily adapted to include the effect of temperature by adding an extra input neuron as well as adding one or more neurons in the hidden layer to take into consideration the additional complexity of the adsorption isotherm relationship. The temperature-dependent Toth adsorption isotherm model was used to generate series of isotherm data at five different temperatures, using the 7 parameters given in Table 1. Four of these series (40, 70, 100, and 140^{o}C) were used as the training data set to fit the temperature dependent neural network isotherm and the remaining series (80^{o}C) was used as the validation data set to assess the performance of the neural network predictions for the isotherm data that were not used during the fitting process. Results for these tests are presented in Figure 7 and Table 1 for the neural network architecture of Figure 1(b).

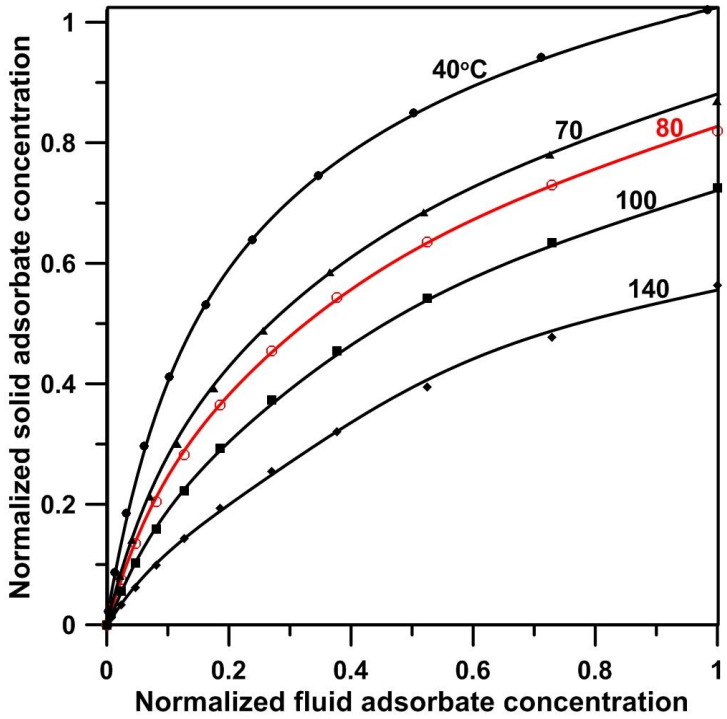

Figure 7 – FFNN for temperature-dependent TD Toth isotherm data sets. Symbols represent isotherm data set at different temperatures and curves represent FFNN fits. Data sets for 40, 70, 100 and 140^{o}C were used for training the neural network whereas the data set at 80^{o}C is used for validation.

The neural network model is able to predict very well the observed data points for both the training and validation data sets. In addition, to ensure that the model is a good representation of the isotherm data over the whole range of concentration and not only at the observed points, 100 equally distant values of the adsorbed concentration in the range of the isotherm data points were generated using the fitted isotherm neural networks. As can be observed, the generated curves (solid lines) are smooth and follow the trend that is expected from the isotherm data.

The accuracy of the fit is truly excellent. As a result, one could use the neural isotherm model with confidence in simulation and design. Here again, parsimony in the number of hidden neurons was targeted in order to have the simplest possible model. The neural network of Figure 1(b) contains four hidden neurons. With five hidden neurons, slightly better predictions were obtained. When six hidden neurons were tested, better predictions were obtained for the learning data set but a weaker predictive ability of the neural network for the validation data set was observed, thereby indicating that overfit prevailed.

3.0 Conclusion

In this study, the ability of neural networks was examined for their effectiveness to represent a wide array of adsorption isotherm data. It was found that the proposed models were highly effective to represent adsorption isotherms at a constant temperature with the flexibility to accurately fit data from all recognized (IUPAC) isotherm types. The extension of the neural network structure to incorporate temperature effects also proved to be excellent. The model proved adept at fitting isotherms of adsorbate-adsorbent systems over a wide range of temperature.

The power of the proposed neural isotherm models lies in the universality of its application. The ability of a single unifying model capable of representing data for all recognized types of adsorption isotherm models is an achievement that classic adsorption isotherm models cannot attain individually.

4.0 Nomenclature

A constant for Freundlich equation (kg ethanol/kg adsorbent) (m^3/kg ethanol) $^{1/n}$

b constant for Langmuir, Toth and Sips equations; temperature dependent variable for the TD-Toth equation (m^3/kg adsorbate)

b_o constant for the TD-Toth equation (m^3/kg adsorbate)

c fluid adsorbate concentration (kg adsorbate/m^3)

n constant for the Freundlich and Sips equations (dimensionless)

q solid adsorbate concentration (kg adsorbate/kg solids)

q_s saturation capacity – constant for Langmuir, Sips, Toth equations; temperature dependent variable for the TD-Toth equation (kg adsorbate/kg solids)

q_{so} constant for the TD-Toth equation (kg adsorbate/kg solids)

Q heat of adsorption (J/mol adsorbed)

R gas constant (8.314 Pa m^3/(mol K) or 8.314 J/(mol K))

t temperature dependent variable for TD-Toth equation (dimensionless)

t_o constant for the TD-Toth equation (dimensionless)

T temperature (^{o}C or K)

T_o reference temperature (^{o}C or K)

W neural network weights between the input and hidden layers
parameters of Equation (6)

W' neural network weights between the hidden and output layers

Greek symbols:

α constant for the TD-Toth equation (dimensionless)

χ constant for the TD-Toth equation (dimensionless)

Upperscript:

$\bar{}$ normalized values

Subcripts:

i neuron number in input layer

j neuron number in hidden layer

k neuron number in output layer

Abbreviations:

ANN	Artificial neural networks
BDDT	Brunauer, Deming, Deming and Teller
FFNN	Feed-forward neural networks
IUPAC	International Union of Pure and Applied Chemistry
TD	Temperature dependent

5.0 Acknowledgement

The authors would like to acknowledge the Natural Science and Engineering Council of Canada (NSERC) for funding this project and for the scholarship awarded to Rudy Jones.

6.0 References

1. Basu, S., Henshaw, P.F., Biswas, N., and Kwan, H.K. (2002). Prediction of Gas-Phase Adsorption Isotherms Using Neural Nets. Can. J. Chem.Eng., 80, 1-7.
2. Bhat, N. and McAvoy, T. (1989). Use of neural nets for dynamic modelling and control of chemical process systems. American Control Conference, Pittsburgh, pp. 1336-1341.
3. Brunauer, S., Deming, L.S., Deming, W.E., and Teller E. (1940). On a Theory of the van der Waals Adsorption of Gases. J. Am. Chem. Soc., 62, 1723-1732.
4. Bulsari, A.B. and Palosaafi, A. (1993). Application of Neural Networks for System Identification of an Adsorption Column. Neural Comput Applic.,1,160-165.
5. Carsky, M. and Do D.D. (1999). Neural Network Modelling of Adsorption of Binary Vapour Mixtures. Adsorption, 5, 183–192.

6. Cybenko, G. (1989). Approximation by superpositions of a sigmoidal function. Math. Control Syst., 2, 303-314.
7. Freundlich, H. (1907). Ueber die adsorption in loesungen. Z. Phys. Chem. 57:385–470.
8. W. and Engell, S. (2004). Neural-network based identification of nonlinear adsorption isotherms. IFAC Dynamics and Control of Process Systems. Cambridge, Massachusetts, USA, 721-724.
9. Giraudet, S., Pré P., Tezel, H., and Le Cloirec, P. (2006). Estimation of adsorption energies using physical characteristics of activated carbons and VOCs' molecular properties. Carbon, 44, 1873–1883.
10. Hoskins, J.C. and Himmelblau, D.M. (1988). Artificial neural network models of knowledge representation in chemical engineering. Computer Chem. Engng, 12(9/10), 881-890.
11. Kumar, K.V. Monteiro de Castro, M., Martinez-Escandell M., Molina-Sabio M., and Rodriguez-Reinoso F. (2010). Neural network and principal component analysis for modelling of hydrogen adsorption isotherms on KOH activated pitch-based carbons containing different heteroatoms. Chem. Eng. Journal 159, 272–279.
12. Langmuir, I. (1918). The Adsorption of Gases on plane surfaces of glass, mica and platinum, J. Amer. Chem. Soc., 40, 1361.
13. Lewandowski, J., Lemcoff N.O. and Palosaari S. (1998). Use of neural networks in the simulation and optimization of pressure swing adsorption processes. Chemical Engineering & Technology, 21, 7, 593-597.
14. Mjalli, F., Al-Asheh, S., Banat, F., and Al-Lagtah, F. (2005). Representation of adsorption data for isopropanol-water system using neural network techniques. Chem. Eng. Technol., 28,12, 1529-1539.
15. Padmesh, T.V.N., Vijayaraghavan, K., Sekaran, G., and Velan, M. (2006). Application of Two-and Three-Parameter Isotherm Models: Biosorption of Acid Red 88 onto *Azolla microphylla*. Bioremediation Journal, 10:1, 37-44.

16. Powell, M.J.D. (1975). Some global convergence properties of a variable metric algorithm for minimization without exact line search. ASM/SIAM Symp. On Nonlinear Programming, New York.
17. Sing, K.S.W., Everette, D.H., Haul, R.A.W., Moscou, L., Pierotti, R.A., Rouquérol, J., and Siemieniewska, T. (1985). Reporting physisorption data for gas/solid systems with special reference to the determination of surface area and porosity. Pure & Appl. Chem., 57, 603-619.
18. Sips, R.J. (1948). On the structure of a catalyst surface. J. Chem. Phys. 16: 490-495.
19. Sundaram N. (1999). Training Neural Networks for Pressure Swing Adsorption Processes. Ind. Eng. Chem. Res., 38, 4449-4457.
20. Toth, J. (1971). State equations of the solid gas interface layer. Acta Chem. Acad. Hung. 69:311-317.
21. Vasina, E.N., Paszek, E., Nicolau Jr., D.V., and Nicolau, D.V. (2009). The BAD project: data mining, database and prediction of protein adsorption on surfaces. Lab Chip, 9, 891–900
22. Yang, M., Hubble, J., Fang, M., Locke, A.D and Rathbone, R.R. (1993). A Neural Network for Breakthrough Prediction in Packed Bed Adsorption. Biotech. Tech., 7, 2, 155-158.
23. Yang, R.T. (1987). Gas separation by adsorption processes, Butterworth Publishers, Stoneham.

Chapter 5

Simulating multi-component liquid phase adsorption systems: Ethanol and residual sugar

R. Jones, F.H. Tezel and J. Thibault

Abstract

A series of multi-component adsorption studies were performed on systems containing ethanol and sugars (xylose and glucose) for applications in ethanol production to be blended with gasoline. These studies were first performed on batch systems in order to develop a model that describes the competition for adsorption sites between ethanol and sugar molecules on the surface of the adsorbent. Three competitive adsorption models (Extended Langmuir, Modified Langmuir and a model based on artificial neural networks (ANN)) were tested for their suitability to fit sets of experimental data across various ethanol and sugar concentrations. By fitting the isotherms to the experimental data sets, the isotherm parameters for each of the models were determined. The isotherm that most adequately described the multi-component equilibrium data was the model based on neural networks. A parity plot comparing the neural network model with the experimental data was generated with a regression coefficient of 0.99.

Following the batch studies, multi-component packed bed adsorption experiments were performed. Experimental results indicate that ethanol capacity was diminished only slightly when compared to single component adsorption studies. The breakthrough profiles for both the xylose and glucose showed significant evidence of sugar displacement from adsorption sites due to this preferential adsorption of ethanol. The capacity for sugars is greatly diminished when appreciable ethanol concentrations were present. The competitive adsorption of xylose and glucose was effectively represented using the neural networks model.

Keywords: Bioethanol, Competitive adsorption, Selective on-line extraction

1.0 Introduction

The use of lignocellulosic feeds to produce ethanol has become an area of emphasis for countries trying to reduce their dependence on fossil fuel sources. Currently, the processing of such feeds is plagued by low ethanol productivity and prohibitive energy requirements during processing and purification of the ethanol. Online ethanol extraction from fermentation systems is one option that is being explored through various avenues to enhance the current processing technology. The selective adsorption of the ethanol as it is produced using hydrophobic activated carbons is one potential separation option. Many studies have focused on the separation of ethanol/Water in binary systems intended to simulate fermentation broth (Pitt et al., 1983; Milestone and Bibby, 1983; Jones et al., 2010). Others have studied the removal of ethanol or other biofuels from fermentation broth without characterizing the adsorption of the minor components in the broth (Ikegami et al., 2000; Einicke et al., 1991, Lencki et al., 1982). Few studies have incorporated adsorption information for minor components known to be present in the broth during the separation (Bui et al., 1985; Bowen and Vane, 2006).

In real adsorption applications such as the removal of ethanol from fermentation broth, there often exist multiple adsorbates competing for the same adsorption sites. The efficiency of an adsorbent to concentrate one or more of the adsorbate molecules from a mixture of solutes depends on the competition between the molecules for available sites. In some cases, the adsorbate molecules having similar properties are in direct competition for the same sites. In these cases, large deviations between single and multi-component isotherm can exist, making the understanding of the competition between the adsorbates of great importance, however, if the properties of the adsorbate molecules differ greatly and the adsorbates target different sites due to size or polarity differences, the competition may not be significant and the single component isotherms may be sufficient to predict adsorption behaviour in a multi-component system (Gun'ko, 2007).

Various models have been developed to describe competitive adsorption of more than one solute from liquid media. Some applications include the competitive adsorption of trace organics modeled by the IAST (Ideal adsorbed solution theory) (Crittenden et. al., 1985), competitive

adsorption of reactive dies from single, binary and ternary systems using models based on the Redlich-Peterson, the Freundlich and the Langmuir adsorption models (Al-Degs, 2007), ethanol, acetic acid and water adsorption for binary and ternary mixtures on hydrophobic zeolites modeled by dual-site extended Langmuir model (Bowen and Vane, 2006).

The majority of the ethanol adsorption studies published to date neglect to report data related to the adsorption of the other primary component within the hydrolysate, namely the sugars xylose and glucose. In this study, single component isotherms for each of the primary constituents of the lignocellulosic hydrolysate (ethanol, xylose and glucose) were examined. In addition, the competitive adsorption that occurs when multiple components are present was studied across the range of interest. Multi-component isotherm models (modified Langmuir model (Equation 3), extended Langmuir model (Equation 4) and a neural network model (Figure 1 and Equation 5) were tested for their suitability in modelling the multi-component adsorption data sets. The resulting isotherms were later used to predict breakthrough profiles over a range of operating conditions.

2.0 Model development

2.1 Single component equilibrium modelling

An equilibrium isotherm describes the capacity of the adsorbent as a function of the equilibrium concentration of the adsorbate in the solution at a constant temperature. The Freundlich isotherm was used to represent the ethanol adsorption equilibrium data in this paper, while the Langmuir isotherm was most appropriate for modelling the equilibrium adsorption of xylose and glucose. The Freundlich and Langmuir models are shown in Equations (1) and (2) respectively.

$$q = AC_e^{1/n} \tag{1}$$

$$q = \frac{q_S b C_e}{1 + b\ C_e} \tag{2}$$

2.2 Modelling equilibrium behaviour of multi-component systems

Experimental results show that the adsorption of ethanol (for the range of interest in this study) is relatively independent of residual sugar concentration. For this reason, the standard Freundlich

model (Equation 1) was used to describe the ethanol adsorption for multi-component systems during the simulations. For the adsorption of sugars, the presence of ethanol has a significant impact on the sugar capacity. A variety of models were tested for suitability for the xylose and glucose adsorption in the presence of ethanol.

2.2.1 Modified Langmuir with correction factor

A modified version of the Langmuir model is proposed for the adsorption of xylose and glucose in the presence of ethanol. This Langmuir model has been modified to incorporate a correction factor related to the amount of ethanol in the adsorbed phase at any given time.

$$q_{SUGAR} = \frac{q_S \ bC_{SUGAR}}{1 + bC_{SUGAR}} \left(1 - \left(\frac{q_{ETOH}}{q_{s,ETOH}} \right)^m \right) \tag{3}$$

2.2.2 Multi-component Langmuir model

The Langmuir adsorption model for a system containing *n* components is expressed as:

$$q_i = \frac{q_{si} C_i}{1 + \sum_{j=1}^{n} b_j C_j} \tag{4}$$

The Langmuir model is among the most common models used for expressing competitive adsorption data (Jacobson and Frenz, 1990).

2.2.3 Neural network model

Recently, neural networks have been the subject of considerable research interest. Artificial neural networks can be used for their novel architecture to solve complex, undefined and nonlinear mathematical problems. ANNs can simply be viewed as general nonlinear models which have the ability to encapsulate the underlying relationship that exists between a series of inputs and outputs of a system. Hoskins and Himmelblau (1988) and Bhat and McAvoy (1989) appear to be the first authors that modelled chemical processes with an artificial neural network. Artificial neural networks are now being used for a wide variety of engineering applications.

They possess a high degree of flexibility and plasticity that allows them to easily capture the nonlinear behaviour of a process using input-output data.

Feedforward neural networks (FFNN) are the most popular structure used in engineering applications. It has been shown that a three-layer FFNN can represent any function provided that sufficient number of neurons are present (Cybenko, 1989). A FFNN normally consists of three layers: an input layer, a hidden layer, and an output layer. The feedforward neural networks that have been used in this investigation are presented in Figure 1. The input layer receives the process inputs and fans out this information to all functional neurons of the hidden layer. Each neuron of the hidden layer essentially performs two tasks: (1) produce a weighted summation of all process inputs; and (2) perform a non-linear transformation, via a neuron transfer function, of the weighted summation to produce the output of each neuron of the hidden layer which then serves as inputs to the neurons of the output layer. The output layer performs the same task as the neurons of the hidden layer to produce the final output of the FFNN. The resulting equation for the FFNN with three hidden neurons in the second layer (including the bias) of Figure 1 with scaled input and output is:

$$\bar{q} = \frac{1}{1+e^{-\left(\frac{W'_{11}}{1+e^{-(W_{11}\bar{C}_S+W_{21}\bar{C}_E+W_{31})}}+W'_{41}+\frac{W'_{21}}{1+e^{-(W_{12}\bar{C}_S+W_{22}\bar{C}_E+W_{32})}}+W'_{41}+\frac{W'_{31}}{1+e^{-(W_{13}\bar{C}_S+W_{23}\bar{C}_E+W_{33})}}+W'_{41}\right)}} \quad (5)$$

In applying a neural network, the fitting information lies in the weights or parameters (W_{ij} and W'_{jk} in Figure 1) between neurons and the structure of the network. Using an ANN to represent experimental data between dependent and independent variables is no different than using any empirical model. The learning process consists of determining the weight matrices, W_{ij} and W'_{jk} that produce the best fit of the predicted outputs over the entire data set. In this investigation, the quasi-Newton optimization algorithm was used to fit the adsorption data (Powell, 1975).

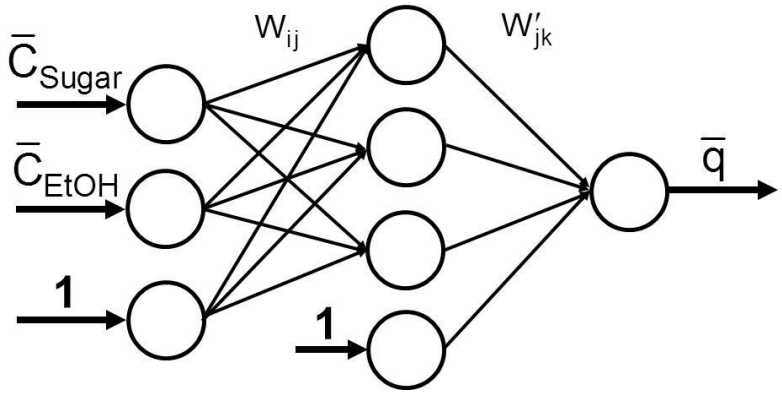

Figure 1 – Neural Network Structure

Inputs to the neural network were scaled using the following equations:

$$\overline{C}_{sugar} = \frac{C_{sugar} - C_{sugar,\max}}{C_{sugar,\max} - C_{sugar,\min}} \tag{6}$$

$$\overline{C}_{EtOH} = \frac{C_{EtOH} - C_{EtOH,\max}}{C_{EtOH,\max} - C_{EtOH,\min}} \tag{7}$$

$$\overline{q}_{sugar} = \frac{q_{sugar} - q_{sugar,\max}}{q_{sugar,\max} - q_{sugar,\min}} \tag{8}$$

2.3 Breakthrough modelling and simulation

The study of column performance for multi component adsorption has been modelled in previous studies. The earliest examples simplified the model by assuming both the solution and the adsorbent phases exist in a state of local equilibrium not accounting for intra-particle mass transfer (Helfferich, 1965). A more comprehensive approach is to recognize the mass transfer that occurs between the liquid phase and the solid by accounting for the mass transfer within the adsorbent pellets (Raymond and Garimella, 2011). The work of Raymond and Garimella accounts for diffusion from the bulk across a thin film, particle diffusion and a resistance due to the kinetics of adsorption. The model used in this study uses a similar treatment. Two variations of the model were used, one accounting for film diffusion, particle diffusion as well as the mass transfer resistance associated with the binding of the adsorbate to an adsorbent site. The second model variant assumes that there is an instantaneous adsorption of the adsorbate once it reaches a site within the particle. For the former case, Equation 10 and 12 are used for the mobile phase of

the pellet and the solid respectively. For the latter case Equation 11 and 13 apply for the mobile phase of the pellet and the solid respectively. The development of these models is discussed in detail in the work by Jones et al., 2010.

2.3.1 Model assumptions

A modified mathematic model based on the work in Jones et al., 2010 was extended to simulate the adsorption of both ethanol and residual sugars under various operating conditions in a packed bed adsorber.

1) The ethanol adsorption is governed by the Freundlich isotherm presented in Equation 1. The presence of sugar at the levels studied has no impact on the adsorption of ethanol (validated by Figure 4).
2) The adsorption of xylose or glucose is governed by a multi-component isotherm model that accounts for the preferential adsorption of ethanol. Three multi-component models were tested for suitability.
3) The balance on the bulk liquid (Equation 5) assumes that the concentration in the column is constant in the radial direction. The component balance in the bulk phase accounts for the axial dispersion along the length of the column, the flow due to convection. The linear driving force model is used to describe the transfer from the bulk phase to the surface of the adsorbent.
4) The balance on the mobile phase within the pores of the pellet accounts for diffusion in the radial direction. In this investigation, the adsorbent particles are assumed to be homogenous spheres in which the adsorbate molecules are transported by diffusion.

   The model assumes that the binding of the adsorbate to the surface of the adsorbent occurs very rapidly compared to the other mass transfer steps (instantaneous adsorption) within the pores.
5) It is assumed that the transfer from the mobile phase within the pellet to the adsorbed phase is instantaneous. That is, there exists an equilibrium condition between the adsorbate on the surface of the activated carbon and the mobile phase of the pellet for all positions within the pellet. The model uses the slope of the appropriate isotherm at a given concentration to predict the surface concentration in equilibrium with the solution.

2.3.2 Bulk liquid phase balance (in the column)

The differential equation showing the mass balance for each species in the bulk flow across the packed bed is shown below:

$$\frac{\partial C_{L,i}}{\partial t} = D_{z_i} \frac{\partial^2 C_{L,i}}{\partial z^2} - \frac{1-\varepsilon}{\varepsilon} k_L a (C_{L,i} - C_{P,i}\big|_{r=R_p}) - u_L \frac{\partial C_{L,i}}{\partial z} \tag{9}$$

Initial condition: $C_L = 0, \ \forall \ Z \text{ at } t = 0$

Boundary conditions: $C_L = C_o, \text{ at } Z = 0 \ (t > 0)$

$$\frac{\partial C_L}{\partial z} = 0 \text{ at } Z = L \ (t > 0)$$

The mass balance in the mobile phase (void) of the pellet is provided in Equation 10. The equation accounts for intraparticle diffusion and mass transfer resistance due to the kinetics of adsorption.

$$\varepsilon_p \frac{\partial C_p}{\partial t} = \varepsilon_p D_{EFF} \left(\frac{1}{r^2} \frac{\partial}{\partial r} \left(r^2 \frac{\partial C_p}{\partial r} \right) \right) - k_{ads} a_p (C_p - C_p^*) \tag{10}$$

The mass balance for the adsorbed phase is given by the following equation:

$$(1-\varepsilon_p) \rho_s \frac{\partial q}{\partial t} = k_{ads} a_p (C_p - C_p^*) \tag{11}$$

In the case of instantaneous adsorption, Equations (10) and (11) can be amalgamated into a single equation:

$$\left(\varepsilon_p + \ 1-\varepsilon_p \ \ \rho_s \frac{\partial q_i}{\partial C_{p_i}} \right) \frac{\partial C_{p_i}}{\partial t} = \varepsilon_p D_{EFF_i} \left(\frac{1}{r^2} \frac{\partial}{\partial r} \left(r^2 \frac{\partial C_{pi}}{\partial r} \right) \right) \tag{12}$$

The following initial and boundary conditions apply to both Equations (10) and (12):

Initial condition: $C_P = 0, \ \forall \ R \text{ at } t=0$

Boundary conditions: $\frac{\partial C_{p_i}}{\partial r} = 0 \quad r = 0, \ t \geq 0$

$$- D_{EFF} \frac{\partial C_{p_i}}{\partial r} = k_L \left(C_{L\,i} - C_{p\,i}\big|_{r=R_p} \right) \quad r = R_p, \ t \geq 0$$

In addition to the mass balances on the liquid bulk, the pellet mobile phase and the surface of the adsorbent, an accurate isotherm model is required to determine change which occurs in the

adsorbed phase with respect to the change occurring in the mobile phase of the pellet. For this study, the Freundlich isotherm was used for ethanol adsorption and for glucose/xylose, three competitive adsorption models (Extended Langmuir, Modified Langmuir and a model based on ANN) were tested.

3.0 Results and discussion

3.1 Single component adsorption isotherms

The adsorption isotherms for ethanol, xylose and glucose with F-600 activated carbon as the adsorbent are plotted in Figure 2 a, b respectively. The pure ethanol adsorption isotherm (not shown here) was previously published in Jones et al. (2010) (Chapter 3). In the case of the single component ethanol isotherm, the Freundlich adsorption model was the most appropriate to fit the data. For the xylose and glucose single component adsorption data, the Langmuir model was selected. The model parameters are provided in Tables 1 and 2.

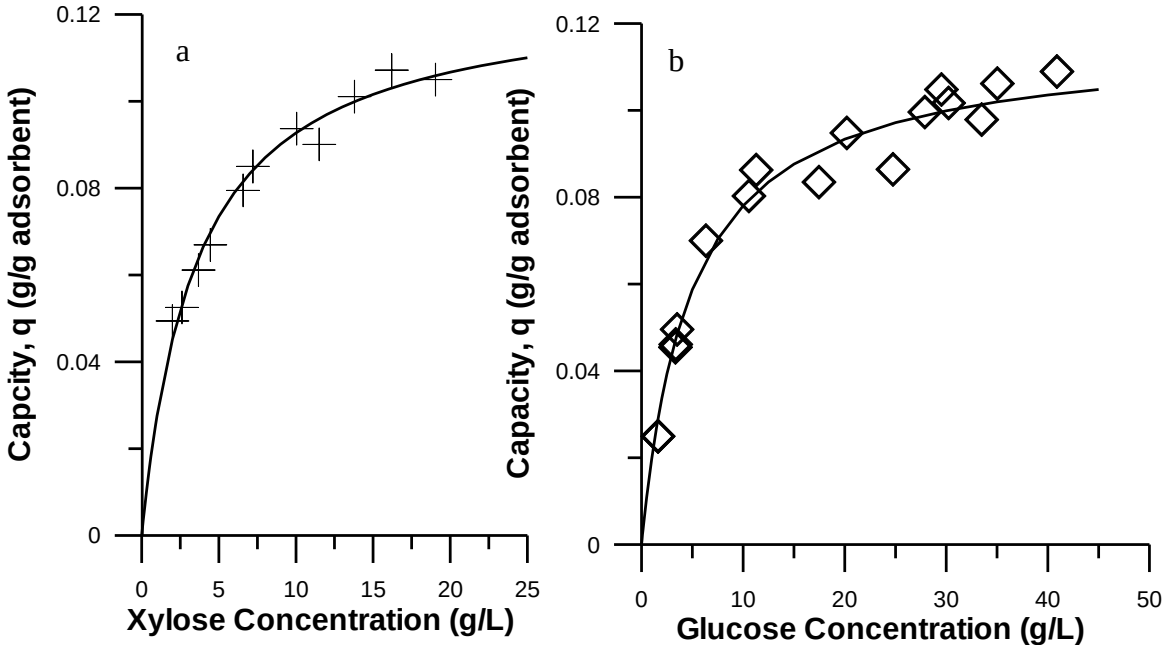

Figure 2 (a) - Xylose (+) and (b): Glucose (◊) adsorption isotherms on F-600 activated carbon at 23-26^{o}C. Langmuir model fit is shown as solid line.

From Figure 2, it can be seen that the adsorption of each sugar is favourable across the entire concentration range studied. The xylose isotherm is shown from about 2 to 20 g/L and the glucose isotherm is shown for concentration from 2 to 45 g/L. This concentration range studied

for each sugar is in-line with the sugar concentration that could be expected during processing of lignocellulosic biomass.

The fitted parameters for each single component isotherm are shown in Tables 1 and 2 below:

Table 1 - Freundlich parameters for pure component isotherm

Component	**Parameters**	
-	**A**	**n**
Ethanol	0.15	1.98

Table 2 - Langmuir parameters for pure component isotherms

Component	**Parameters**	
-	**q_s**	**b**
Glucose	0.11	0.24
Xylose	0.11	0.21

3.2 Multi-component adsorption

Multi-component adsorption equilibrium data for ethanol in the presence of sugars (xylose and glucose) is shown in Figure 3.

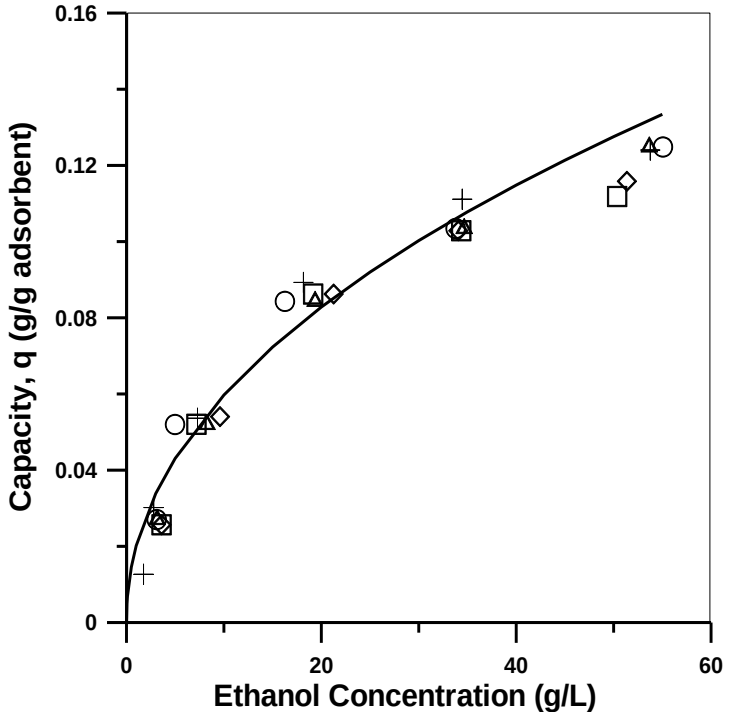

Figure 3 - Ethanol adsorption isotherm with F-600 activated carbon in the presence of sugar at 23-26^{o}C. Freundlich model fit for pure system is shown as solid line. Symbols represent data points, the initial sugar concentration for each run is provided: +: Pure ethanol (0g/L sugar), ◊: Ethanol with xylose (20g/L), □: Ethanol with 20 g/L glucose, ○: Ethanol with 5g/L glucose and 15 g/L xylose, Δ: Ethanol with 15g/L glucose and 5 g/L xylose

From this figure it is evident that the uptake of ethanol is not greatly impacted by the presence of residual sugars (combined concentrations below 20 g/L). This is a significant finding, as the proposed ethanol extraction scheme would operate under a similar range of residual sugar concentrations. The ability to maintain high ethanol capacity even in the presence of residual sugars is due to a preferential adsorption of ethanol over the sugars that remain in the broth. Furthermore, Figure 3 suggests that the Freundlich model used to predict ethanol adsorption from single component systems is an adequate model to predict ethanol adsorption in the presence of sugar concentrations below 20 g/L (xylose, glucose or a combined sugar concentration).

To further study the competitive nature of the adsorption between ethanol and the sugars, adsorption isotherms for each of the sugars (xylose and glucose) were prepared under various levels initial ethanol concentrations. Shown in Figure 4 is the set of adsorption isotherms for

glucose when ethanol is present at different concentration. A similar plot was generated for each of the three competitive adsorption models used, but the model based on ANN was most appropriate and is shown in Figure 4. A similar plot was generated for xylose adsorption (not shown here).

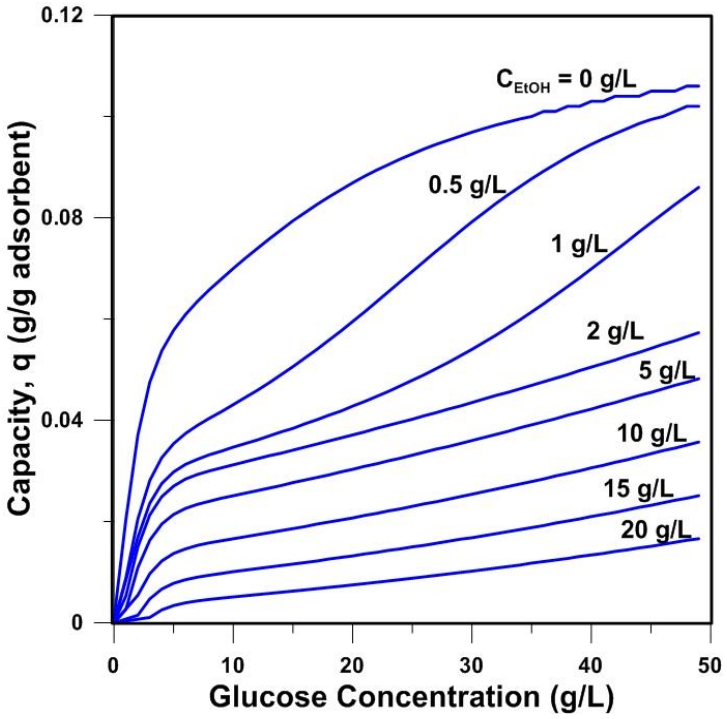

Figure 4 - Glucose isotherms in the presence of ethanol.

The adsorption model shown is for constant equilibrium ethanol concentration as indicated on the plot. The plots generated have been simulated as it is not possible to maintain constant equilibrium ethanol concentration experimentally. The model simulation was used to predict the isotherm from 0 to 20g/L of ethanol in solution at equilibrium. Each of the three competitive adsorption models used was fit to sets of experimental data (sugar adsorption in the presence of varying ethanol levels). The quality of the model fit is displayed in the form of a parity plot (Figure 5).

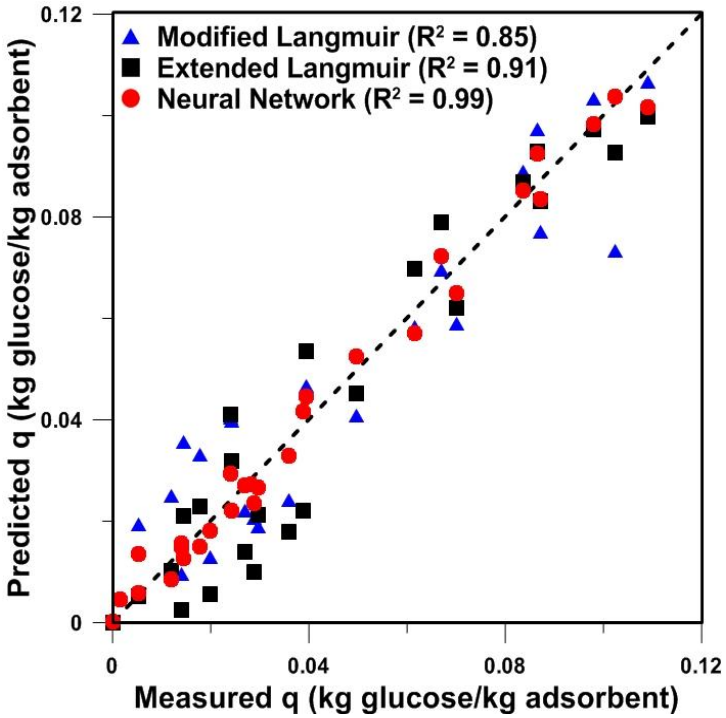

Figure 5 - Parity plot of model predictions versus experimental adsorption data.

From the parity plot for glucose it is obvious that the model based on ANN was superior to the Extended and the Modified Langmuir models over the concentration range studied. The same was found for the experimental data with xylose (not shown here). With a regression coefficient of 0.99 on the parity plot, the model is believed to appropriately represent the competitive adsorption between ethanol and residual sugars.

3.3 Multi-component isotherm data: Breakthrough behaviour in the column

The adsorption of ethanol from synthetic fermentation broth was studied for various flow-rates, and various residual sugar concentrations (both xylose and glucose). The prevailing trend across the experimental runs, was that for sugar concentrations studied (as high as 20 g/L), the sugar present had little effect on the total equilibrium capacity of ethanol. Meanwhile, sugar adsorption was greatly diminished when compared to the single component sugar studies. As sample multi-component breakthrough profile is shown in Figure 6.

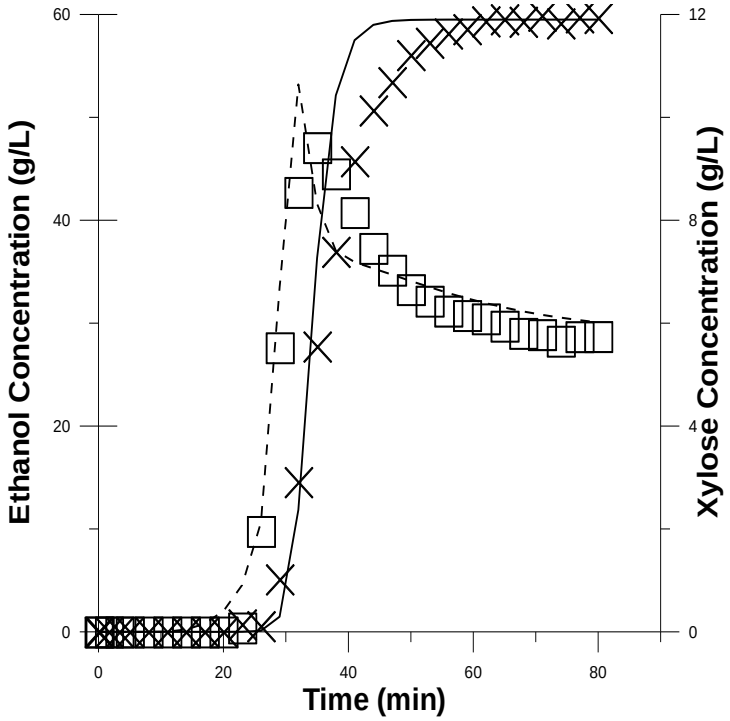

Figure 6 - Ethanol-Xylose multi-component breakthrough profile – symbols represent experimental data, lines represent the model predictions. Run was performed with a feed composition of approximately 60g/L EtOH and 6 g/L Xylose.

From Figure 6, it is evident that the adsorption of ethanol is favoured over the adsorption of xylose. This selectivity for ethanol over residual sugars is most likely due to the comparatively higher carbon ratio of the ethanol adsorbate compared to the sugars. As the feed travels the length of the column, ethanol is preferentially removed by the activated carbon. This allows the mass transfer zone for the sugar to travel ahead of the ethanol mass transfer zone within the bed. When the ethanol reaches portions of the bed that are partially saturated with sugar, a displacement of xylose molecules occurs as ethanol is adsorbed.

The dynamic adsorption model proposed for the competitive adsorption of ethanol in the presence of residual sugars can be used to simulate the ethanol adsorption over a wide range of operating conditions. The model input for the simulation is provided in Table 3.

Table 3 - Fixed-bed parameters used for simulation

Parameters	Values
Bed length	0.3 m
Feed flow	10 mL/min
Carbon particle diameter	1.0 mm
Superficial velocity	3.0×10^{-4} m/s
Ethanol feed concentration	59.7 g/L
Xylose feed concentration	5.8 g/L

4.0 Conclusions

A model based on ANN was found to be most appropriate to describe the competitive adsorption that occurs when sugars are present with ethanol. The ANN model was excellent at representing the adsorption of sugar was across the entire range of concentrations studied for both xylose and glucose. The model was then applied to simulate competitive adsorption in dynamic breakthrough experiments. The model adequately predicted breakthrough behavior of both ethanol and sugar across a wide range of operating conditions.

5.0 Acknowledgement

The authors would like to thank, NSERC (Natural Science and Engineering Research Council of Canada) for their financial contribution for this study.

6.0 Nomenclature

a Exterior pellet surface area per volume of pellet (m^2 external area/m^3 pellet)
A Freundlich constant, (kg adsorbate/kg adsorbent) $(m^3/kg\ adsorbate)^{1/n}$
a_p Internal surface area of pellet (m^2 surface area/m^3 pellet)
b Langmuir constant, (m^3/kg adsorbate)
C_e Concentration in solution at equilibrium, (kg adsorbate/m^3)
C_L Ethanol concentration within the liquid bulk (kg adsorbate/m^3)
C_p Concentration in the mobile phase in the pellet pores (kg adsorbate/m^3)
$C_P|_{r=R_p}$ Concentration at the pellet boundary (kg adsorbate/m^3)
C_P^* Concentration in equilibrium with the solid (kg adsorbate/m^3)
D_{EFF} Effective Diffusion coefficient of the adsorbing species (m^2/s)
D_z Axial diffusion coefficient (m^2/s)

k_{ads} Average adsorption mass transfer resistance (m/s)
k_L Average film mass transfer coefficient (m/s)
m Modified Langmuir constant, (dimensionless)
n Freundlich constant, (dimensionless)
q Amount of adsorbate adsorbed (kg EtOH/kg adsorbent)
q_s Langmuir constant, (kg adsorbate/kg adsorbent)
r Distance in the radial position (m)
t Time, (s)
u_L Superficial velocity (m/s)
z Distance in the axial direction (m)

Greek Letters

ε Bed void (m^3 void/m^3 bed)

ε_p Pellet void fraction (m^3 void/m^3 pellet)

ρ Density of solution (kg solution/m^3 solution)

ρ_S Solid density (kg solid/m^3 solid)

Subscripts

i Used as index number
j Used as index number
k Used as index number
w Weighted parameter for ANN
EtOH Used to denote the species of interest (pertains to ethanol)
Sugar Used to denote the species of interest (pertains to xylose or glucose)

7.0 References

1. Al-Degs, Y., Khraisheh, M.A.M., Allen, S.J., Ahmad, M.N., Walker, G.M., 2007, Competitive adsorption of reactive dyes from solution: Equilibrium isotherm studies in single and multisolute systems. *Chem. Eng. J.* 128, 163-167
2. Bhat, N. and McAvoy, T., 1989, Use of neural nets for dynamic modelling and control of chemical process systems. *American Control Conference*, Pittsburgh, pp. 1336-1341.
3. Bowen, T.C., Vane, L.M., 2006, Ethanol, acetic acid and water adsorption from binary and ternary liquid mixtures on high-silca zeolites. *Langmuir* 22, 3721-3727
4. Bui, S., Verykios, X., Mutharasan, R., 1985, In Situ Removal of Ethanol from Fermentation Broths. 1. Selective Adsorption. *Ind. Eng. Chem. Process Des. Dev.* 24, 1209-1213
5. Crittenden, J.C., Luft, P., Hand, D.W., Orvaitz, J.L., Loper, S.W., Arl, M.,1985. Prediction of multicomponent adsorption equilibria using ideal adsorbed solution theory. *Environ. Sci. Technol*. 19, 1037–1043

6. Cybenko, G., 1989, Approximation by superpositions of a sigmoidal function. *Math. Control Syst*., 2, 303-314.
7. Einicke, W.D., Rwschetilowski, W., Heuchel, M., Szombathely, M.V., Bräuer, P., Schöllner, R, 1991, Liquid-phase adsorption of binary ethanol–water mixtures on high-silica adsorbents. *J. Chem. Soc.* Faraday Trans. 87(8), 1279–1282
8. Gun'ko, V. M., 2007, Competitive Adsorption. *Theor. Exp. Chem.*43 (3), 139-183
9. Helfferich, F., 1965, Ion-exchange kinetics. V. Ion exchange accompanied by chemical reactions. *J. Phys. Chem.* 69, 1178-1187
10. Hoskins, J.C. and Himmelblau, D.M.,1988, Artificial neural network models of knowledge representation in chemical engineering. *Computer Chem. Engng*, 12(9/10), 881-890.
11. Ikegamai, T., Yanagishita, H., Kitamoto, D., Haraya, K., 2000, Accelerated ethanol fermentation by Saccharomyces cerevisiae with addition of activated carbon**.** *Biotechnology Letters* 22 (21), 1661-1665
12. Jacobson, J. M., Frenz, J., 1990, Determination of competitive adsorption isotherms for modelling large-scale separations in liquid chromatography. *J. of Chrom.* 499, 5-19
13. Jones, R. A., Tezel, F.H., Thibault, J., 2010, Simulation and Validation of Ethanol Removal from Water in an Adsorption Packed Bed: Isotherm and Mass Transfer Parameter Determination in Batch Studies. *Can. J. Chem. Eng.* 88 (5), 889 – 898
14. Lencki, R.W., Robinson, C.W. and Moo-Young, M., 1983, On-line extraction of ethanol from fermentation broths using hydrophobic adsorbents. *Biotechnol. Bioeng. Symp.* 13, 617–628
15. Milestone, N. B, Bibby, D. M.,1983, Adsorption of alcohols from aqueous solution by ZSM-5. *J. Chem. Tech. Biotechnol.* 34A, 73-79.
16. Pitt, W. W, Haag, G. L., Lee, D. D., (1983), Recovery of ethanol from fermentation broth using selective sorption-desorption. *J. Biotechnol. Bioeng.* 25 (1), 123-131
17. Raymond, A., Garimella, S., 2011, Intraparticle mass transfer in adsorption heat pumps: Limitations of the linear driving force approximation. *J. Heat Transfer.* 133 (4), 128-141.

SECTION – IV: Fermentation Experiments

Chapter 6

Enhanced ethanol production through selective adsorption in bacterial fermentation

R. A. Jones, J. A. Gandier, J. Thibault, F. H. Tezel

Abstract

To alleviate the ethanol inhibition of *Escherichia coli* KO11 (ATCC 55124) during fermentation, online ethanol sequestration was achieved using F-600 activated carbon. Two separate schemes were tested, one involving direct addition of activated carbon to the fermentation flask for the purpose of in-situ adsorption and a second involving an externally located activated carbon packed bed.

For the in-situ ethanol adsorption experiments, varying amounts of adsorbent were added to the medium, at the start of the fermentation. The addition of the activated carbon in the fermentation broth resulted in increased glucose utilization and ethanol production for all flasks containing activated carbon. For the control flasks, approximately 75% of the available substrate was utilized before the fermentation was completely inhibited. The entire glucose supply of flasks containing activated carbon was depleted. Ethanol production was also increased from 28 g/L for the control containing no activated carbon to nearly 45 g/L (including the ethanol in the adsorbed phase) for the flasks containing activated carbon.

The implementation of an externally located packed bed adsorber for the purpose of on-line ethanol removal was tested over a number of adsorption cycles to evaluate the performance of the adsorption bed and the ethanol productivity. Results indicate that maintaining ethanol fermentation medium concentrations below 20 to 30 g/L extends and enhances ethanol productivity. After 3 cycles over a period of 180 h, an additional 80% ethanol was produced when compared to the control experiments, despite the suboptimal acidic pH of the medium.

Keywords: ethanol, adsorption, fermentation, *Escherichia coli* KO11, production of ethanol

1.0 Introduction

Today, bioethanol is primarily produced from either sucrose or starch based biomass. First generation bioethanol industries (sugar crop and starch) are mature and established which have roots dating to the 1970s and the Arab oil embargo [1]. Recently, attention has shifted to the production of ethanol from lignocellulosic biomass due to inherent advantages related to lower crop cost, greater biomass availability across varied climates, and a potential for greater crop utilization and thus ethanol yield per unit of crop. Furthermore, the fact that lignocellulosic biomass can be viewed as a dedicated energy crop as opposed to a food source is advantageous [2].

Despite such advantages, significant challenges must be overcome to render the conversion of lignocellulosic biomass to ethanol economically feasible. Currently, the lower cost of this feedstock is offset by costly feed pre-treatments and waste treatments [3]. Unlike starch based feeds, which are easily depolymerised into monomeric glucose, the hydrolysis of lignocellulosic biomass requires greater energy input and results in a complex mixture of hexose and pentose sugars. Typically, corn stover hydrolysate contains 37.4% glucose, 21.1% xylose, 2.9% arabinose, 2.0% galactose and 35% other organic compounds; pentose sugars accounting for more than one third of total sugar content [4]. Traditionally microorganisms used for bioethanol production, such as *Saccharomyces cerevisiae* and *Zymomonas mobilis*, are unable to metabolize pentose sugars [3].

Naturally occurring *E. coli* has the ability to metabolize a wide range of substrates, including all those present in lignocellulosic hydrolysate. It is considered to be a stable bacteria well adapted to operating in a wide range of environmental conditions [5]. Ingram et al. of the University of Florida (Gainesville, Florida) introduced the *Z. mobilis* pyruvate to ethanol pathway through homologous recombination into the *E. coli* genome, creating a strain (KO11) in which the main product of fermentation is ethanol. *E. coli* KO11, has since been used in numerous studies with a range of cellulose derived mixed sugar feeds including pine waste [6], willow [7], rice hulls [8], sugar cane bagasse [9], cotton gin residues [10], and corn stover [11].

In addition to the successful production of ethanol from the mixed sugar hydrolysates noted above, the strain has also displayed a strong resistance to both extreme temperature ranges, and wide range of pH [12]. Due to the reported favourable productivity and yield, its ability to consume a wide range of mixed sugars, and its commercial availability, *E. coli* KO11 was selected amongst numerous candidates in this investigation to conduct in-situ ethanol recovery via adsorption.

Cellular immobilization is a technology with applications ranging from tissue culture [13] to fermentation [14]. Notably, bacterial immobilization is used in continuous production of non-growth related products. By sequestering biomass within the reactor, its desired concentration can be maintained at a lower growth rate necessary than that of a planktonic culture. By thus decreasing the growth rate, there is less genetic drift in the culture over time [15]. This phenomenon is particularly useful when dealing with recombinant strains which can lose their engineered characteristics with time.

Alginate, a linear unbranched polysaccharide made up of 1,4-linked β-D-mannuronic acid (M) and α-L-guluronic acid (G) residues [16], has the ability to gel in the presence of divalent cations such as calcium [17]. A microorganism can be added to an aqueous alginate mixture, which can then be gelled by a solution of divalent salts such as calcium. This gel formation is nontoxic and does not require heating, resulting in no decrease in viability. However, a major drawback in using this gel is its incompatibility with buffers, such as phosphate buffers, which have the ability to sequester divalent cations [18].

The objective of this work is to alleviate the inhibition caused by elevated ethanol concentrations using an online extraction technique. The experiments presented herein were performed with model broth containing pure glucose as a substrate. The model broth was used to best assess the inhibitory nature of ethanol in the broth. The fermentation system used a microorganism (*E. coli* KO11) that is tailored for use with lignocellulosic hydrolysate and has documented limitations when ethanol concentrations are elevated.

2.0 Materials and methods

2.1 Microorganism

Escherichia coli KO11 (ATCC 55124) was purchased from the American Type Culture Collection and stored at -80°C in 30% glycerol, 0.1M $MgSO_4$, 0.025 TRIS (pH 8.0). The bacteria were revived on Luria Broth (LB) agar (10 g/L tryptone, 10 g/L NaCl, 5 g/L yeast extract, 15 g/L agar) plates with 0.2 g/L xylose as carbon source, containing 40 mg/L chloramphenicol (*E. coli* KO11 has known resistance to chloramphenicol). The plates were kept in a refrigerator at 5°C for a maximum of two weeks.

2.2 Sterilization

All materials and solutions utilized were sterilised in an autoclave at a temperature of 116^{o}C and 175 kPa for 20 minutes then left to cool.

2.3 Analytical methods

Relative cell concentration was determined by measuring the optical density (OD) at a wavelength of 600 nm (Perkin Elmer Lambda 25 UV/Vis). A standard curve was prepared that showed a linear relationship between the OD measured and the dry weight of the cell mass. When performing OD measurements, samples were diluted in order to ensure that the readings fell within the linear range (below 0.8) of the prepared standard curve.

The pH was determined using the Barnant ATC probe and meter.

Glucose and ethanol concentrations were determined by high pressure liquid chromatography (HPLC), using the Waters Sugar-Pak I cation-exchange column (6.5 mm x 300 mm) (Waters Ltd., On, CA) equipped with a Waters Breeze system and a Waters 2414 refractive index detector. Separation was performed at 90°C using a distilled deionised water mobile phase at a flow rate of 0.5 ml/min.

Fermentation broth samples for HPLC analysis were centrifuged at 13000 rpm for 6 min to remove cells. The supernatant was then filtered with a 0.45 µm nitrocellulose Millipore (Billerica,

MA) membrane filter. Samples were diluted with distilled deionised water for sugar concentration to be within 0.01-3g/L range and for the organic solvent content (such as ethanol and organic acids) to be below 5%. Concentrations were determined by integrating peaks using the Waters Breeze software. Glucose and ethanol standards were run with each sample in order to confirm the accuracy of the determined concentrations.

2.4 Adsorbent

The adsorbent used for ethanol extraction from the fermentation broth was F-600 activated carbon purchased from Calgon Corporation (Calgon, Mississauga, ON, Canada). The physical properties of F-600 adsorbent are given in Table 1. This adsorbent was selected as the best candidate among more than a dozen activated carbon adsorbents and hydrophobic zeolites that were screened in a previous study [19]. F-600 was selected based on the combination of high equilibrium ethanol capacity, fast adsorption kinetics observed, and high selectivity for ethanol over residual sugars and broth medium. Although F-600 did not have the highest capacity or the fastest kinetics, the availability and the comparatively low cost made it the most attractive option [19-20]. Previous unpublished work has also shown that F-600 activated carbon is rugged and durable and thus can be re-used following regeneration. Additionally, the equilibrium can easily be reversed as demonstrated by water flushing (Chapter 3) or column heating (Appendix A.2).

Table 1: Properties of activated carbon F-600

Property	**F - 600**
Particle diameter (mm)	1.0
Bulk density (kg/m^3)	674
Particle density (kg/m^3)	1036
Solid density (kg/m^3)	2270
Particle void fraction (m^3/m^3)	0.54
BET surface area (m^2/g)	906
Cumulative Pore Volume (cm^3/g)	0.52

2.5 Calcium-alginate encapsulation

Sodium alginate (Fisher scientific, Alginic acid sodium salt from brown algae for the immobilization of microorganisms) was dissolved in water by vigorous agitation at 300 rpm in a rotary shaker overnight to achieve a 2% (wt.) solution. The solution was then left to degas for 12

hours. The required volume of Na-alginate solution was poured into a flask which was then sealed with a foam stopper covered in aluminum foil. A second sealed flask contained a 1% (wt.) calcium chloride solution with a magnetic stir bar. The two flasks were connected using a silicon tube (Tygon, 1 m length x 0.16 cm diameter). One end of the tube was sealed in the Na-alginate containing flask, resting at the bottom of the solution, while the other end was sealed in the $CaCl_2$ containing flask, suspended 12 cm above the surface of the solution. The resulting beads had an average diameter of 4.68 mm ± 0.05 mm. The setup was sterilised by autoclave as previously described.

Inoculum, consisting of *E. coli* KO11 was grown in LB broth until the exponential phase. A volume of inoculum was added directly into the sterile alginate solution as to obtain a 2.4 mg/L bacteria/Na-alginate mixture which was then gently stirred rotationally. A peristaltic pump was used to pump the bacteria/Na-alginate mixture into the $CaCl_2$ solution. The Na-alginate formed drops at the end of the tube which fell from a height of 12 cm into the moderately agitated $CaCl_2$ solution. As each drop hit the solution, it gelled and formed Ca-Alginate beads containing *E. coli* KO11. The resulting beads were then hardened for 2 hours in the $CaCl_2$ solution, agitated at 100 rpm to keep the beads suspended. The beads were then rinsed with 200 ml of sterile distilled deionised water and aseptically transferred to the fermentation broth prepared as described in the fermentation methodology.

2.6 Fermentation

Fermentations were carried out in 300 mL Erlenmeyer flasks fitted with rubber stoppers and topped by a water trap. The water traps were filled with sterile distilled water, maintaining anaerobic conditions inside the flasks. Each flask contained 100 mL fermentation broth consisting of 25 g/L Miller Luria-Bertani (LB) broth (10 g/L tryptone, 10 g/L NaCl, 5 g/L yeast extract; Fisher Scientific Ottawa, ON, CA) supplemented with glucose as carbon source. Glucose concentration varied between experiments performed in this investigation. A sodium phosphate buffer (79 g NaH_2PO_4/L, 138.6 g Na_2HPO_4/L, pH 7.4) (Sigma Aldrich, Oakville, ON, Canada) was also included, unless otherwise stated, to maintain the pH at a relatively constant value. For experiments involving free bacteria, each flask was inoculated to provide a concentration of 1.2 mg/L of bacteria.

The flasks were kept in a MaxQ 5000 rotary shaker (Geneq Inc., Montreal, QC, Canada) and maintained at 30^{o}C. An orbital rotation of 150 rpm was used to agitate the fermentation broth for all experiments. A 2 mL sample was aseptically taken at regular time intervals which were subsequently analysed to determine pH, cell density, and ethanol and glucose concentrations as previously described.

2.7 Ethanol inhibition experiment

Two series of experiments were conducted under the previously described fermentation conditions. In the first series of experiments, ethanol was added to the flasks at the same time as the inoculum to obtain initial ethanol concentrations of 35, 50 and 65 g/L. In the second set of experiments, ethanol was added after 3 h of uninterrupted fermentation in order to produce a concentration of additional ethanol of 15, 30 and 40 g/L.

2.8 In-situ ethanol adsorption

The goal of the extraction experiments was to determine if the fermentation could be extended and enhanced with the selective on-line removal of ethanol from fermentation broth. In the first attempt at ethanol extraction, sterilized activated carbon was added to the fermentation flasks simultaneous with the inoculum in an attempt to recover in-situ a fraction of the ethanol being produced and thereby reducing its inhibitory effect. Four concentrations of activated carbon were tested: 0, 5, 10 and 15 g per 100 mL of initial broth volume. For each experimental condition, three replicate flasks were monitored throughout the duration of the experiment. The ethanol and biomass concentrations were measured along with the pH. Because of the presence of the activated carbon, the optical density could not be measured accurately and it was not possible to predict the biomass concentration.

2.9 External extraction experiments

A second extraction scheme was performed with a packed bed adsorption column, located outside of the bioreactor. Plastic columns from Fisher Scientific, 12 cm long and 1.3 cm ID, were used for the external packed bed extraction units. The columns were filled with F-600 adsorbent. A small portion of cheese cloth was inserted at both ends of the columns to retain the adsorbent

packing within the columns. For each extraction, the packed adsorption column contained 10 g of activated carbon.

The extraction of ethanol was performed only after ethanol reached levels demonstrated to be inhibitory (25-30 g/L range). The fermentation broth was pumped through the packed bed adsorption column at a low flow rate (1-2 mL/min) until all broth had been treated through the packed bed. Samples were taken immediately prior to and following the extraction and analysed. In order to allow the fermentation to continue, a concentrated substrate solution was added following the extraction in order to replenish the substrate supply. Following the extraction cycle, the flasks were placed back in the shaker for 2 additional fermentation cycles.

3.0 Results and discussion

3.1 Ethanol tolerance

It has been well established that the recombinant strain *E. coli* KO11 has a relatively low ethanol tolerance in comparison to the conventional microorganisms used in the bioethanol industry. Ethanol inhibition of *E. coli* strains have been reported at concentrations ranging from 35 to 50 g/L [21-23] and in some cases even lower, whereas the inhibition of the yeast *Saccharomyces cerevisiae* has been observed to occur at concentrations as high as 150 g/L of ethanol (where glucose is the only substrate) [24]. In this study, the tolerance of ethanol was tested by the instantaneous addition of anhydrous ethanol, to obtain different ethanol concentrations in the fermentation medium.

For the first set of experiments, ethanol was added immediately after seeding the flasks, to obtain initial ethanol concentrations of 35, 50 and 65 g/L respectively. A fourth set of flasks with no ethanol present was used as a control. The results of this experiment are shown in Figure 1. For all results presented in this section, three replicate flasks were used. The average result was plotted along with the standard deviation error bars. In a second set of experiments, ethanol was added three hours after seeding the flask to obtain concentrations 15, 30 and 40 g/L in the fermentation medium (Figure 2). This was done to allow the bacteria to enter into a growth phase before the addition of ethanol. While the addition of exogenous anhydrous ethanol is not perfectly representative of the effect of natural inhibition that occurs due to the slow production

of ethanol within the vessel, the technique used, can still provide useful insight into the response and resiliency of the cells in the presence of ethanol.

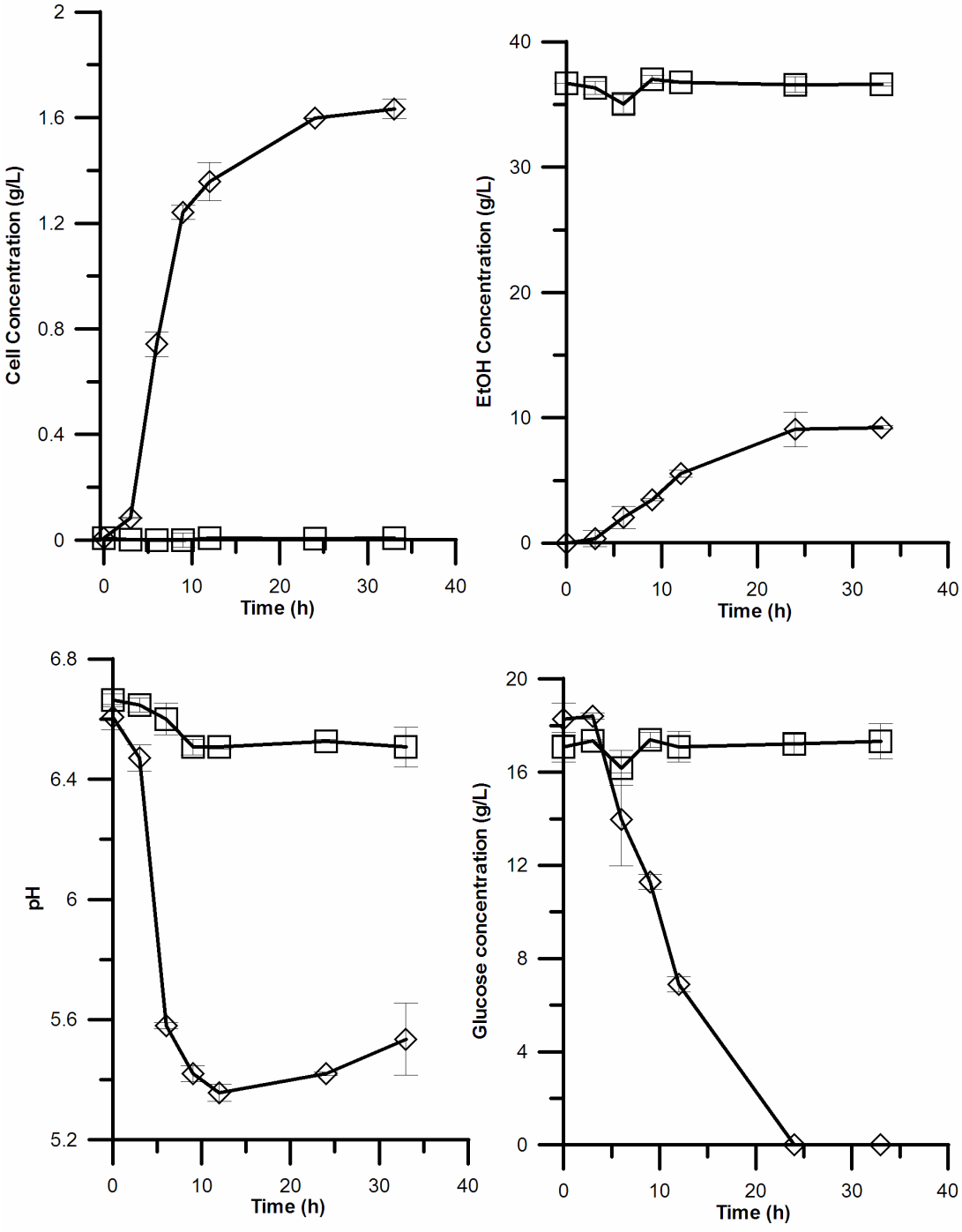

Figure 1 - Cell, ethanol and glucose concentrations in addition to pH with respect to time for ethanol addition immediately after seeding for flask fermentation carried out at 30^{o}C and 150rpm. Squares represent the runs with ethanol addition (35 g/L) and the diamonds correspond to the control flasks where no ethanol was added.

The trend for the control flasks and the flasks with the lowest level of ethanol loading (35 g/L) are shown in Figure 1. The trends for the high levels of ethanol loading (50 and 65 g/L) are omitted since they do not significantly differ from the results obtained for 35 g/L loading. At all ethanol concentrations tested, it was found that cell growth, substrate consumption and ethanol production were negligible. In addition, the pH remained almost constant throughout these runs. These results indicate, at levels as low as 35 g/L ethanol, *E. coli* KO11 cell growth, substrate utilization and ethanol production were inhibited by the presence of ethanol. As for the control where no ethanol was initially present, the substrate was consumed entirely within 24 hours and the ethanol concentration rose to approximately 10 g/L within the same time frame. Cell concentration in the control flasks reached a maximum concentration of approximately 1.6 g/L.

The second set of experiments was performed to further explore the impact of ethanol on the bacteria. For this set of experiments, the fermentation flasks were seeded and ethanol added to each of the flask after three hours in order to obtain concentrations in the fermentation medium of 15, 30 and 40g/L. Again, the set of experiments also included a series of control flasks for which no ethanol was added.

Figure 2 provides the glucose and cell concentrations, the pH and the differential ethanol concentration.

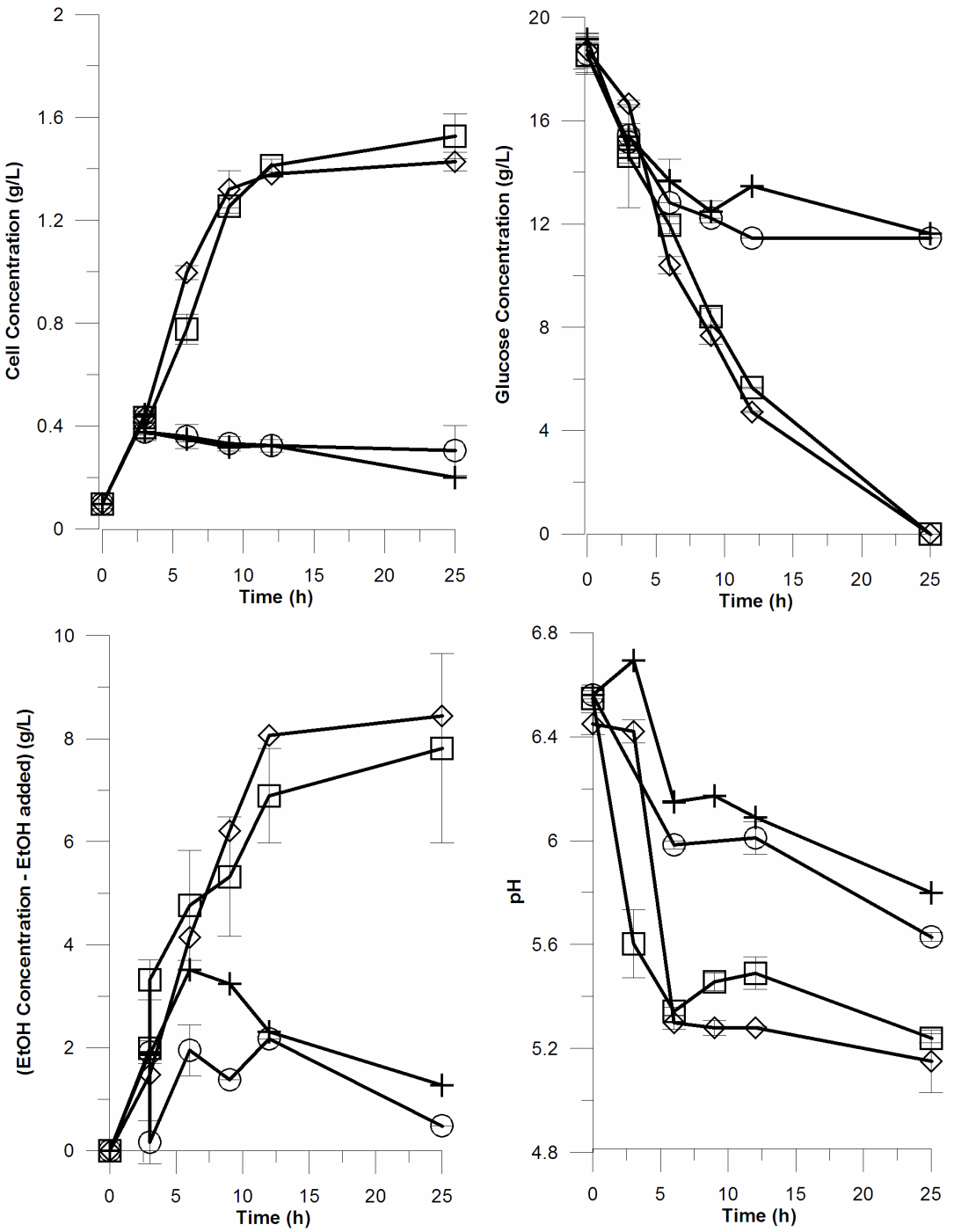

Figure 2 - Cell concentration, ethanol differential concentration and glucose concentration along with flask pH are plotted vs. time for ethanol addition three hours after seeding for flask fermentation carried out at 30°C and 150 rpm. Diamonds represent the control for which no ethanol was added. For the other runs, ethanol was added at the following loading levels (□: 15, +: 30 and O: 40 g/L) three hours subsequent to seeding.

The differential ethanol concentration corresponds to the amount of ethanol produced by the fermentation. It was determined by subtracting from the total concentration the initial exogenous addition. As demonstrated in Figure 2, the cell concentration for all flasks was approximately the

same up until 3 hours, the time at which ethanol was added. Following the addition of different amounts of ethanol, the rate of cell growth differed greatly. For the two highest ethanol concentrations, 30 g/L and 40 g/L, the cell density in the flask did not increase. In fact a slight decrease in the cell density was observed for these trials. For the control fermentation for which no ethanol was added, and for the lowest level of ethanol loading (15 g/L), the cell concentrations were very similar throughout the 24 h run. Both sets of flasks reached a maximum cell concentration of approximately 1.6 g/L. For the substrate concentration, again, the two highest levels of loading showed similar trends with more than 50% of the available substrate going unused as the fermentation shut down at around 10 h fermentation time for both cases. The control flasks along with the low level of ethanol loading followed a similar trend for the substrate concentration. After a period of 24 h, the substrate was completely exhausted in both cases. As for the amount of ethanol produced, the control and the low ethanol loading both reached levels around 8 g/L produced while the 30 g/L and the 40 g/L flasks produced only 1-3 g/L of ethanol. If the differential ethanol concentration is added to the amount of ethanol introduced at 3 h, the total ethanol content in each flask can be determined. For the lowest amount added (15 g/L), a total ethanol concentration of around 23 g/L was present without witnessing any ethanol inhibition. Above 30 g/L, ethanol inhibition is observed as the fermentation shut down despite ample availability of substrate and a pH that was still in the optimal range. These results clearly show that the ethanol tolerance of *E. coli* KO11 is low. Even in the relatively low ethanol concentration of 30 g/L, inhibition of cell growth and substrate utilization was observed. For this reason, the online extraction of ethanol as it is produced will be extremely important. Although in this study, inhibition was observed earlier than previous work which reported inhibition in the range of 35 to 50 g/L [21-23], it should be noted that exogenous anhydrous ethanol was added to the flasks in this study while the aforementioned works dealt with ethanol produced through fermentation. Intuitively, the direct addition of ethanol is likely more detrimental to the cells as they may not have sufficient time to acclimate to ethanol and thus the sudden addition of ethanol is a shock to the fermentation system. Nevertheless, the work in this study confirms that product inhibition is a major restriction when *E. coli* KO11 is used to produce ethanol. The limited ethanol tolerance of *E. coli* KO11 is a major bottleneck for its industrial use.

3.2 *In-situ* ethanol extraction

Following the ethanol tolerance experiments, a series of experiments were conducted to perform the extraction of ethanol from the fermentation broth using activated carbon added directly into the fermentation flasks. Experiments were performed for three activated carbon loadings: 5, 10 and 15 g/100 mL. A series of control experiments were also conducted in parallel with a number of flasks without the addition of activated carbon. Results of these experiments are presented in Figure 3.

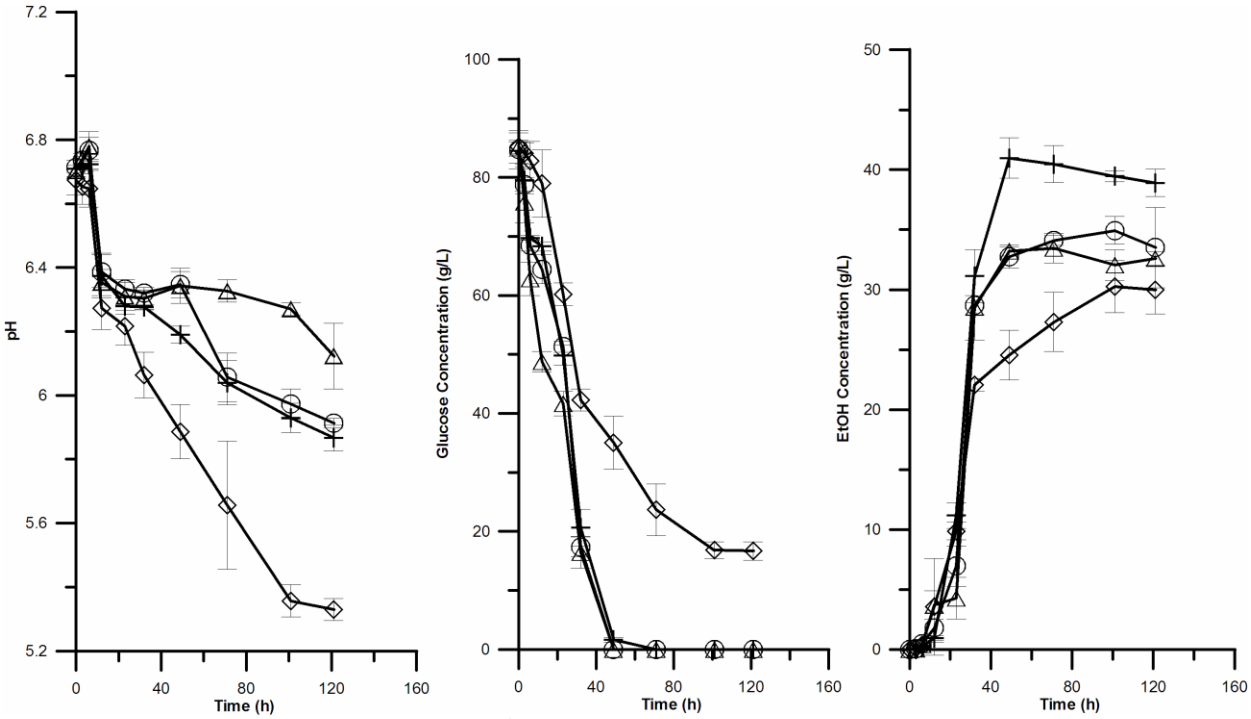

Figure 3 - Flask fermentations carried out at 30°C and 150 rpm. Ethanol and glucose concentrations along with pH are plotted vs. time for different amounts of F-600 activated carbon: ◊: 0; +: 5; O: 10; and Δ: 15g of adsorbent/100 mL of solution.

For this set of experiments, all flasks started with nearly identical glucose concentrations of 85 g/L. The results of Figure 3 show that for the flasks containing activated carbon, a rapid drop in the concentration of glucose was observed across all activated carbon loading levels. This depletion of sugar in the liquid phase during the first few hours can be attributed to glucose being adsorbed by the activated carbon. Over the same time frame, the control flask shows little change in the glucose level. After 6 h of fermentation, the production of ethanol started for all flasks. For the control flasks, glucose utilization to produce ethanol continued until approximately 100 h where the fermentation appears to be inhibited as a significant portion of the substrate

(approximately 20 g/L) still remained unused. The ethanol concentration for the control reached nearly 30 g/L up until that point. It should be noted that the pH of the control flasks was still at a level conducive to ethanol production when the fermentation ceased. Interestingly, the flasks containing activated carbon (across all loading levels) showed complete substrate exhaustion between 40 and 60 h. The rate of substrate utilization for flasks containing activated carbon was much greater than the control over the same time period. It is not possible to decouple the quantity of substrate which has been consumed and the quantity of substrate that is in the adsorbed phase at any given time by measuring only the substrate concentration in the liquid phase. However, it is reasonable to deduce (based on the high ethanol concentrations attained) that most if not all of the substrate that is initially in the fermentation system is consumed to produce ethanol within 40 to 60. The activated carbon also had an impact on the pH of the solution. For all levels of activated carbon loading, the pH remained higher when compared to the control despite the fact that more substrate was metabolized for these runs. A fraction of fermentation by-products such as lactic and acetic acids that are known to cause the pH to decline were possibly adsorbed by activated carbon [25]. When monitoring the ethanol concentration for flasks containing activated carbon, the rate of ethanol production was enhanced when the activated carbon was added. Following a period of 40-60 h, the ethanol concentration in the liquid phase was the highest for the 5 g/100 mL flask, while the 10 and 15 g/100 mL flasks had similar final liquid phase ethanol compositions.

It should also be noted that the amount of ethanol in the bulk solution is not entirely representative of the total ethanol present in the flask when activated carbon is present. A portion of the ethanol that was produced during the fermentation is bound in the adsorbed phase in equilibrium with the corresponding liquid phase concentration. The amount of ethanol in the adsorbed phase is related to the equilibrium capacity and the total quantity of activated carbon in each flask. Figure 4 shows the equilibrium relationship between the quantities of ethanol in the adsorbed phase with the corresponding liquid phase composition.

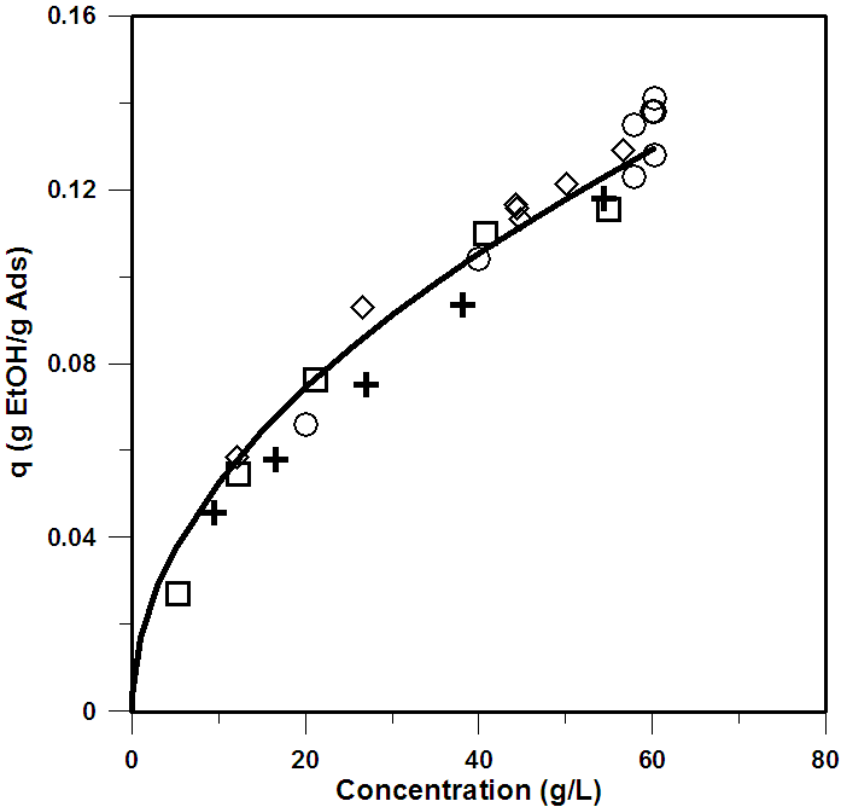

Figure 4 - Ethanol adsorption isotherm on F-600 activated carbon at 23-26°C. Isotherm is comprised of points from the modified mixed-batch kinetic experiments (◊), the packed bed re-circulation experiments (□: adsorption, +: desorption), and the dynamic breakthrough experiments (O), Freundlich model fit is shown as solid line (Jones et al., 2010).

Based on a wide range of equilibrium experiments performed in a previous study [20], it is possible for each experiment with different activated carbon loading levels to estimate the total amount of ethanol produced by taking into account the adsorbed ethanol. The isotherm model shown in Figure 4 was used to estimate the ethanol present in the adsorbed phase for each of the flasks. This amount was combined with the ethanol measured in the liquid to determine the equivalent amount of ethanol that would be in solution if all adsorbed ethanol was unbound. The measured amount of ethanol in the liquid phase along with the total estimated amount of ethanol is shown in Figure 5.

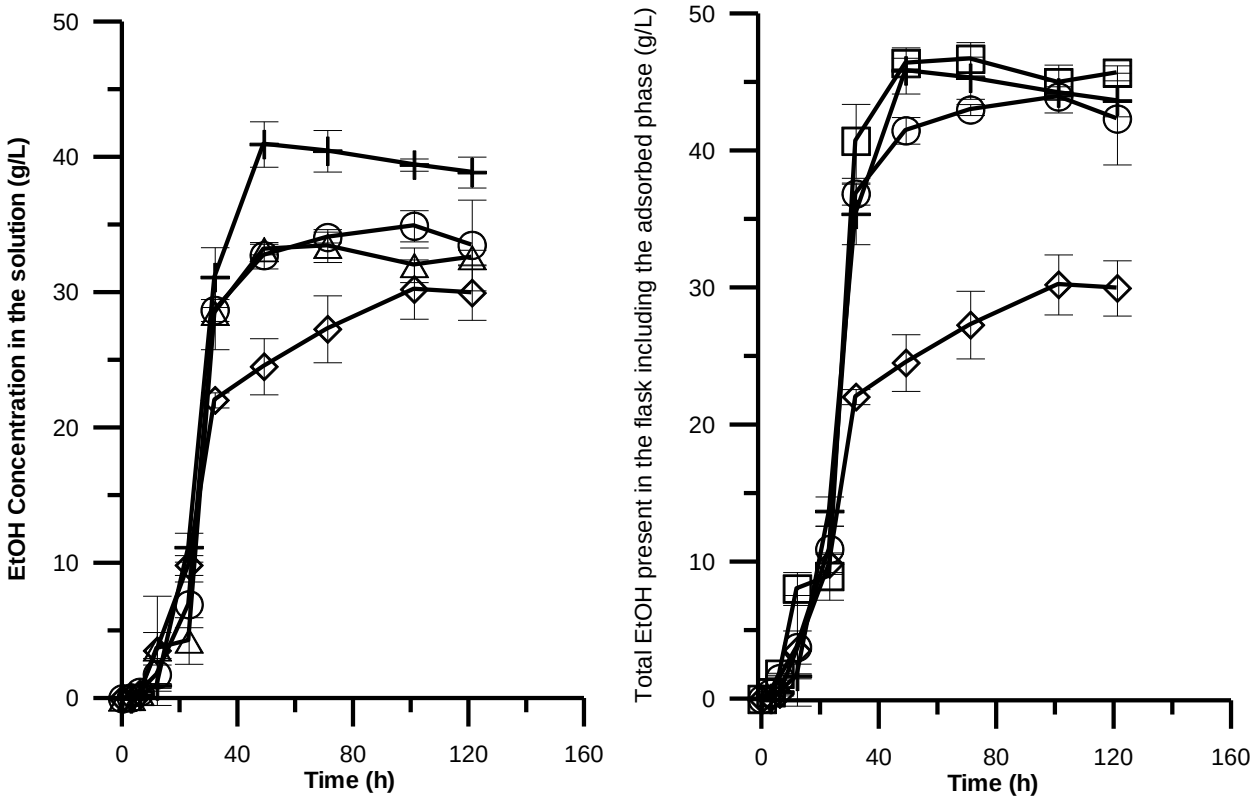

Figure 5 - The measured ethanol composition (on the left) and the total ethanol present in the flask (measured plus ethanol predicted to be in the adsorbed phase) (on the right) vs. time for different amounts of F-600 activated carbon: ◊: 0, +: 5, O: 10, and Δ: 15g of adsorbent/100ml of solution for flask fermentation carried out at 30°C and 150 rpm.

Figure 5 shows that a significantly higher ethanol concentration was achieved through the addition of as little as 5 g of activated carbon per 100 mL of broth. Overall, the flasks with the presence of activated carbon seem to indicate that the loading of the activated carbon (5, 10 or 15 g/100 mL) had little impact on the total amount of ethanol that was produced. In all cases with adsorbent present, the substrate was completely consumed. It should be noted, that the data in the graph on the right hand side of Figure 5 is the result of the combination of the measured liquid composition (on the left) and the adsorbed phase concentration predicted from the isotherm. Based on this combination, the total ethanol produced is approximately 50% higher for the fermentations where adsorbent was present. The ethanol yield predicted through the combination of the model and experimental data is in the range of 0.50 to 0.54 g of ethanol per gram of glucose which is close to the theoretical ethanol yield of 0.51 g/g. The yields reported in this study are comparable to those reported in a similar study from 1991 where a system using *E. coli* KO11 was reported to have an ethanol yield of 0.53 g/g [21].

3.3 External ethanol extraction

In addition to the introduction of activated carbon directly in the fermentation flasks to perform the in-situ partial extraction of ethanol, an alternative method for ethanol extraction was also studied. In this method, rather than adding the activated carbon directly to the flasks, experiments were performed with externally located activated carbon packed beds. Inherently, the in-situ addition of activated carbon has limited potential. One major drawback of this system would be the challenge of recovering the ethanol from the surface of the adsorbent upon saturation. In theory, the activated carbon could be separated from the broth and the ethanol desorption could subsequently be performed. However, this step would require additional solid handling which can be costly. With the activated carbon bed located outside of the bioreactor, the solid handling issue is circumvented. The results of the fermentation experiments for the case where the column was located outside the bioreactor are shown in Figure 6.

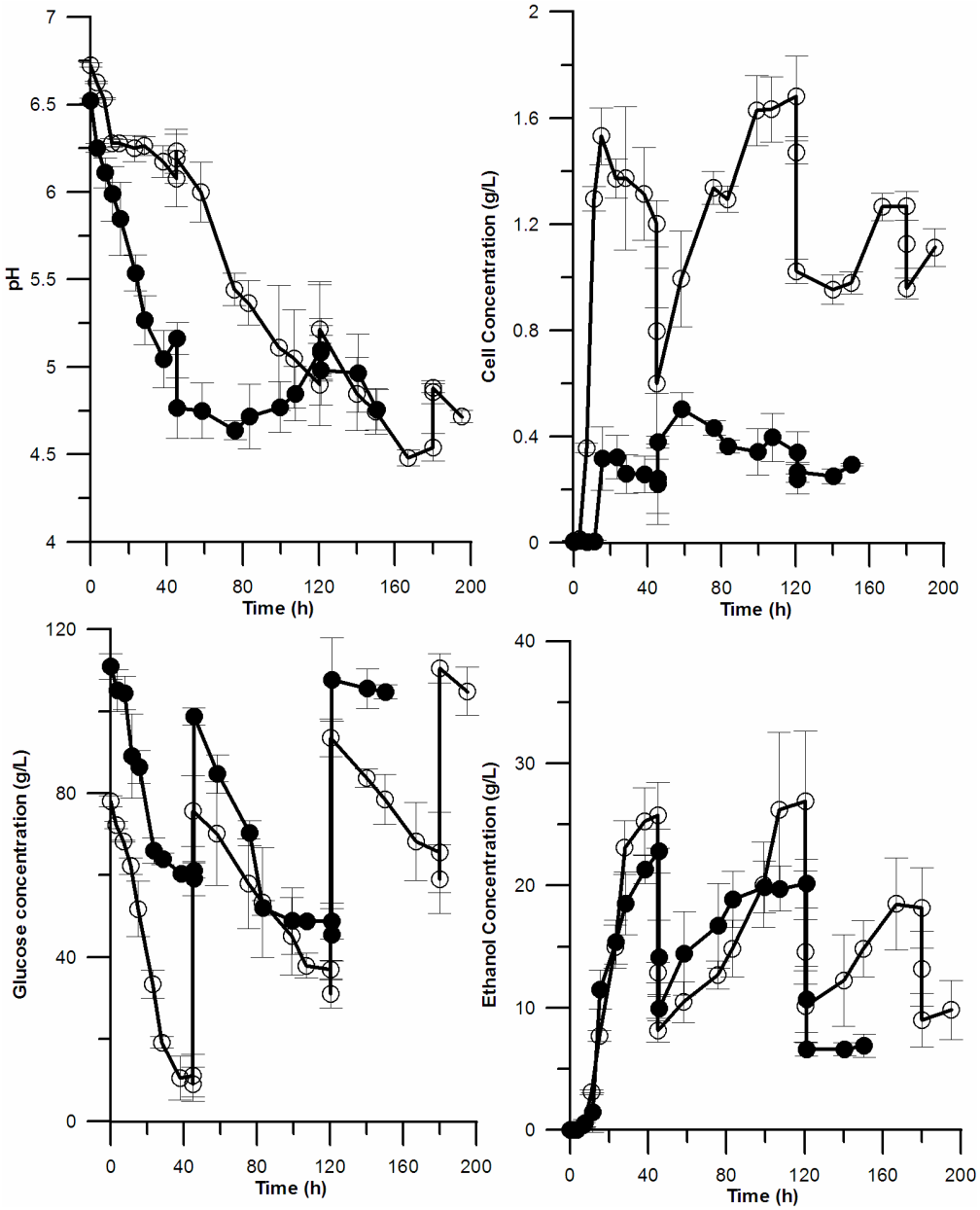

Figure 6 - Ethanol, cell and glucose concentrations of medium along with pH for planktonic (open circles) and encapsulated (solid circles) flask fermentations carried out at 30°C and 150 rpm. Ethanol extractions were performed on the entire fermentation broth at 45, 120.5 hr for both encapsulated and planktonic bacteria. An additional extraction was performed on the planktonic bacteria at approximately 180 h. Following the extraction, a concentrated substrate solution was added to the fermentation mixture.

Figure 6 depicts the cell, ethanol and glucose concentrations along with the pH of the medium for the planktonic and encapsulated fermentations, through three separate extraction cycles over a period of nearly 200 h. Initially starting with a neutral pH, a low cell concentration and a substrate concentration of approximately 80 g/L and 110 g/L glucose (planktonic and encapsulated, shown as hollow and solid circles, respectively, in Figure 6), the progression of the

fermentation was monitored by periodic sampling of the bulk solution. The fermentation was allowed to proceed until an ethanol concentration approaching 30 g/L (45 hours) was achieved, at which time the first partial ethanol extraction was performed. A sample was taken prior to the extraction and immediately after the extraction in order to characterize the effects of the passage of the bulk liquid phase through the adsorption unit. A sample was also taken after the introduction of fresh substrate (a pure aqueous glucose solution) in order to evaluate its diluting effect on broth composition.

Within 45 h, the ethanol concentration had reached approximately 27 g/L with approximately 10 g/L glucose remaining in the planktonic fermentation broth. In the encapsulated fermentation, 23 g/L ethanol and 60 g/L of glucose were present at the same time. The rate of glucose consumption had slowed significantly in both sets and the concentration of both the glucose and ethanol appeared to be reaching a plateau similar to those observed with the control flasks shown in Figure 3. During the first extraction process, a third of the biomass present in the planktonic fermentation was retained in the adsorbent of the external unit. Due to the sequestration of biomass within the gel beads, this phenomenon was not observed in the encapsulated fermentation. Following the addition of the substrate solution, cell and ethanol concentrations were decreased due to the dilution of the medium. The residual glucose concentrations of the flasks remained relatively constant before and after the first extraction suggesting little glucose was adsorbed by the activated carbon. Nearly half of the ethanol in the planktonic and encapsulated fermentation medium was adsorbed by the activated carbon of the first extraction. The fermentations were then continued; the inhibition caused by the presence of high ethanol concentrations being alleviated.

As can be observed in Figure 6, the rate of ethanol production was significantly reduced after the removal of ethanol *via* adsorption in the planktonic (free) bacterial fermentation. This reduction is correlated to the reduction in biomass concentration also observed post adsorption. As the fermentation broth is passed through the activated carbon bed, a fraction of the biomass is adsorbed along with ethanol. The point at which maximal ethanol production is achieved corresponds to the maximal allowable population represented by the plateau of biomass concentration versus time.

In the case of the encapsulated fermentation, it can be observed in the second adsorption cycle that the rate of ethanol production was maintained higher than that of the planktonic bacteria post adsorption. The sequestration of the bacteria within the beads partially alleviated the decrease in the rate of ethanol production. In order to properly characterize this phenomenon, more work must be conducted.

Additionally, throughout the entire 200 h experiment, a trend of declining pH contributed to the reduced fermentation rate observed with time. The optimal pH is reported to be 6 [13]. After a period of approximately 60 h, the pH of the planktonic fermentation medium remained below this optimal value and reached a final value of 4.5 to 4.75 after nearly 200 h. It can be noted that for each extraction cycle, a small change in pH was observed when comparing the measurement just prior and after the extraction. It is important to note that no buffer was used in the encapsulated fermentation due to its incompatibility with the gel beads. As a result, the pH in the encapsulated fermentation medium attained 4.75 within 40 hours. Fermentation occurs past 40 hours due to the buffering ability of the carboxyl groups present on the residues of the alginate polymer which make up the encapsulation matrix.

Over the second cycle, in both sets of fermentations, an additional 40 g/L of glucose was consumed and approximately 20 g/L of new ethanol was produced.

The third cycle, occurring from 120.5 to 180 hours, with an initial residual ethanol concentration of 10 g/L resulted in the consumption of nearly 30 g/L of the glucose in solution and produced an additional 10 g/L of ethanol in the case of the planktonic fermentation. The pH reached a range of 4.5 to 4.7, a level at which inhibition of fermentation is observed, approaching the end of the cycle. No consumption of glucose or production of ethanol was observed in the encapsulated fermentation during this cycle.

The final extraction, performed at 180 hour on only the planktonic fermentation medium, was less effective in terms of ethanol removal. The likely cause of the diminished ethanol capacity on the adsorbent is the concentration of glucose that remained in solution and the competition for

adsorption sites. For the final extraction, the concentration of glucose in solution was approximately 65 g/L prior to the extraction and the ethanol concentration was only 17 g/L. Adsorption capacity is a function of liquid phase concentration (as shown by Figure 4). By measuring the composition just before and after the extraction, it was observed that glucose was indeed adsorbed (as much as 6 g/L removed) during this third extraction causing a comparatively lower amount of ethanol to be removed.

Through the cycles performed, a total of approximately 52 g/L of ethanol was produced by the planktonic fermentation with the ethanol production diminishing from cycle to cycle (26, 18 and 8 g/L of new ethanol for the respective cycles). Although a buffer was added to each flask to help regulate the pH initially, pH control by way of NaOH addition or other means may have prolonged the fermentation and enhanced the ethanol production rate. For the flasks having undergone three extraction cycles, 80% more ethanol was produced when compared to the control data shown in Figure 3.

In the case of the encapsulated fermentation, 33 g of ethanol was produced per litre of broth, ethanol production diminishing from cycle to cycle (23, 10 and 0 g/L of new ethanol respectively).

When comparing the extraction schemes tested, the second extraction technique, having an externally located activated carbon packed bed is likely a more practical approach to on-line extraction and recovery of ethanol. Having the adsorbent located externally in a packed column would minimize the solid handling required when performing adsorption and desorption cycles. The external column would allow the extraction to be performed intermittently as ethanol concentration builds up. The adsorption cycle could continue until column saturation. The ethanol could then be recovered from the surface of the activated carbon as a concentrated vapour. The process could then be made cyclical by alternating between ethanol adsorption and column desorption. The adsorption of planktonic bacteria by the activated carbon, resulting in fouling of the adsorbent in addition to a reduced bacterial concentration of the fermentation broth, can be partially alleviated by the sequestration of the bacteria within macroscopic gel beads.

4.0 Conclusions

Ethanol inhibition plays a key role in the conversion of lignocellulosic hydrolysate to ethanol by *E. coli* KO11. By maintaining lower concentrations of this toxic product in the fermentation medium through the recovery of ethanol via adsorption, greater conversions of substrate to ethanol can be achieved. By adding ethanol directly to fermentation flasks, it was found that even at levels as low as 30 g/L, the growth of cells and the production of ethanol ceased. The addition of activated carbon inside the flask was found to increase the rate of substrate consumption and ethanol production. Furthermore, the addition of activated carbon enhanced the total quantity of substrate that was consumed and the total quantity of ethanol produced.

Intermittent ethanol extraction was shown to be effective in prolonging and enhancing the production of ethanol in the fermentation broth. Eighty percent more ethanol was produced during the experiment with externally located activated carbon columns. It was also demonstrated that the rate of ethanol production could be maintained post adsorption through the encapsulation of the microorganism within Ca-alginate beads. One problem that remains in the flask experiments was the continually declining pH. In order to best demonstrate the impact of on-line ethanol removal, the pH should be maintained at a level that is conducive to additional ethanol production. This could be achieved through the application of pH control by NaOH addition.

5.0 Nomenclature

ATCC – American Type Culture Collection
E. coli – *Escherichia coli*
HPLC – high pressure liquid chromatography
EDTA – ethylenediaminetetraacetic acid
F-600 – Filtrasorb 600 (commercial name)
LB – Luria-Bertani
EtOH – ethanol
OD – optical density
BET – Brunauer-Emmett-Teller

6.0 References

1. Durbin, R.J., (1988). Ethanol a home grown answer to a host of problems. *Forum for Appl. Res. and Pub. Pol.* 3 (4); 66-68.
2. Hahn-Hagerdäl, B., Galbe, M., Gorwa-Grauslund, M.F., Lidén G., Zacchi, G., (2006) Bioethanol – the fuel of tomorrow from the residues of today. *Trends Biotechnol.*, 24 (12); 549-556.
3. Bothast R.J., Nichols, N.N., Dien, B.S., (1999) Fermentations with new recombinant organisms. *Biotechnol. Progr*., 15; 867-875.
4. Maiorella, B. L., C. R., and Blanch, H. W., (1984) Economic evaluation of alternative fermentation processes. *Biotechnol. Bioeng.*, 26, 1003-1025.
5. Alterthum, F., Ingram, L.O., (1989) Efficient ethanol production from glucose, lactose and xylose by recombinant *Escherichia coli*. *Appl. Environ. Microbiol.* 55 (8); 1943-1948.
6. Barbosa M.F., Beck, M.J., Fein, J. E., Potts, D., Ingram, L.O., (1992) Efficient fermentation of Pinus sp. Acid Hydrolysates by an Ethanolgenic Strain of *Escherichia coli*. Appl. and Environ. *Microbiol.*, 58 (4): 1382-1384.
7. Von Sivers, M., Zacchi, G., Olsson, L., Hahn-Hagerdal, B., (1994) Cost analysis of ethanol production from willow using recombinant *Escherichia coli*. *Biotechnol. Progr.*, 10 (5): 555-560
8. Moniruzzaman, M., Ingram, L. O., (1998) Ethanol production from dilute acid hydrolysate of rice hulls using genetically engineered *Escherichia coli*. *Biotechnol. Lett.*, 20 (10); 943-947.
9. Takahashi, C. M., De Carvalho Lima, K. G., Takahashi, D. F., Alterthum, F., (2000) Fermentation of sugarcane bagasse hemicelluloses hydrolysate and sugar mixtures to ethanol by recombinant *Escherichia coli* KO11. *World J. of Microbiol. Biotechnol*., 16: 829-834.
10. Agblevor, F.A., Batz, S.,Trumbo, J., (2003) Composition and ethanol production potential of cotton gin residues. *Appl. Biochem. Biotechnol.*105 (1-3); 219-230.

11. Kim, T. H., Lee, Y. Y., Sunwoo, C., Kim, J. S., (2006) Pretreatment of corn stover by low-liquid ammonia recycle percolation process. *Appl. Biochem. Biotechnol.*, 133; 41-57.
12. Moniruzzaman, M., York, S. W., Ingram, L. O., (1998) Effects of process errors on the production of ethanol by *Escherichia coli* KO11. *J. Ind. Microbiol. Biotechnol.*, 20: 281-286.
13. Karuppusamy, S., (2009) A review on trends in production of secondary metabolites from higher plants by in vitro tissue, organ and cell cultures. *J. Med. Plan. Res.* 3 (13); 1222-1239.
14. Skoog, K., Hahn-Hagerdal, B., (1988) Xylose Fermentation. *Enz. and Microb. Technol.* 10 (2); 66-80.
15. Nasri, M., Sayadi, S., Barbotin, J.N., Thomas D., (1987) The use of the immobilization of whole living cells to increase stability of recombinant plasmids in Escherichia coli. *J. of Biotechnol.* 6 (2); 147-157.
16. Qin, Y., (2008) Alginate fibres: an overview of the productions processes and applications in wound management. *Polym. Int.* 57; 171-180.
17. Smidsrod, O., Skjaok-Br, G., (1990) Alginate as immobilization matrix for cells. *Trends Biotechnol*. 8; 71-78.
18. Yang, C.Y., Chiu, C.T., Chang, Y.P., Wang, Y.J., (2009) Fabrication of Porous Gelatin Microfibers Using an Aqueous Wet Spinning Process. Artif. Cells, Blood Substitutes, *Immobil. Biotechnol.* 37 (4); 173-176.
19. Jones, R.A., Tezel, F.H., Thibault, J., Tolan, J.S., (2007) Ethanol production to be blended with gasoline: Improvements in energy use by adsorption. *Int. J. Green Energy* 31 (15); 1517-1531
20. Jones R.A., Thibault, J., Tezel, F.H., (2010) Simulation and validation of ethanol removal in an adsorption packed bed: Isotherm and mass transfer parameter determination in batch studies. *Can. J. Chem. Eng.* 88: 889-898
21. Ohta K., Beall, D. S., Mejia, J. P., Shanmugam K. T., Ingram, L. O., (1991) Genetic improvement of Escherichia coli for ethanol production: Chromosomal integration of *Zymomonas mobilis* genes encoding pyruvate decarboxylase and alcohol dehydrogenase II. *App. Env. Microbiol.*, 57, (4):893-900.

22. Zhang, M., Eddy, C., Deanda, K., Finklestein, M., Picataggio, S., (1995) Metabolic engineering of a pentose metabolism pathway in ethanologenic *Zymomonas mobilis*. Science,267:240-243
23. Qureshi, N., B. S. Dien, N. N., Nichols, B. C., Saha and M. A. Cotta (2006) Genetically engineered *Escherichia coli* for ethanol production from xylose: Substrate and product inhibition and kinetic parameters. *Food Bioprod. Proc.* 84:114-122
24. Esser K., Schmidt, U., Stahl, U., (1982) Ethanol and biomass production of wild strains and respiratory deficient mutants of Saccharomyces cerevisiae under anaerobic and aerobic conditions. *Euro. J. of Appl. Microbiol. And Biotechnol.*, 16 (2-3); 161-164.
25. Rao, M.B., Sircar, S., Golden T.C., (1991) Equilibrium and kinetics for liquid phase adsorption of bulk acetic acid from water on activated carbon. Extended abstract and programs, Bienniel Conference on Carbon, 54-55.

Chapter 7

Modelling and validation of the continuous production of ethanol with intermittent extraction using a packed bed adsorption column

R. Jones, J. Thibault and F.H. Tezel

Department of Chemical and Biological Engineering
University of Ottawa
Ottawa, Canada K1N 6N5.

Jules.Thibault@uottawa.ca

Abstract

In order to produce ethanol derived from lignocellulosic feeds at a cost that is competitive with current gasoline prices, the fermentation process, converting sugars to produce ethanol and the subsequent purification steps, must be enhanced. Researchers have identified the fermentation/ethanol extraction step as one of the key areas of the process where cost savings are attainable. In this study, in-situ extraction of ethanol from fermentation broth was studied in order to assess the benefits of removing ethanol from the fermenter as it is produced.

The in-situ extraction scheme used ethanol selective sorbents for the removal of ethanol from a fermentation system using the ethanol sensitive microbe *Escherichia coli* KO11. Extractions were carried out intermittently when concentration reached levels that cause fermentation to cease. Upon extraction of the inhibitory ethanol, the substrate concentration was replenished in order to allow the fermentation to continue unimpeded. Experiments indicate that fermentation can be prolonged by removing ethanol as it reaches concentrations around 30 g/L. Results suggest that while the fermentation was prolonged, allowing for a greater amount of ethanol to be produced per batch, there was a decline in substrate utilization and ethanol productivity from cycle to cycle. Following

two consecutive cycles, the substrate utilization and ethanol production levels dropped off dramatically at the start of the third cycle.

To validate experimental results, the combined batch fermentation of glucose by *E. coli* KO11 and ethanol adsorption cycles were modelled. Monod kinetic model with product inhibition was used to represent batch fermentation and ethanol extraction was modelled using a pore diffusion model for multi-component competitive adsorption. The fermentation model was used to identify potential causes of the observed decline in productivity (cycle to cycle). Results suggest that cell growth becomes severely inhibited as a function of the number of cycles due to the accumulation of inhibitory metabolites (including but not limited to ethanol) in the fermentation system.

While fermentation was extended by online removal of ethanol, the decline in productivity observed cycle to cycle negates some of the benefit achieved from extending the fermentation. Cell age and accumulation of inhibitory metabolites are likely the reason for the loss of productivity over time.

1.0 Introduction

A dramatic rise in the cost of liquid transport fuels coupled with projections of future oil scarcity has given rise to a new generation of bio-refineries intended to meet ever growing worldwide energy demands. Ethanol produced from lignocellulose is one among many renewable fuels currently studied for its potential to be produced in large scale plants domestically (Cheng and Timilsina, 2011). Lignocellulose to ethanol technology has the potential to produce a truly global fuel that can help to partly alleviate the pressure on the demand of liquid fuels. Lignocellulosic feedstock grows rapidly across varied climates, is widely available and requires little to no outside intervention for the crops to flourish. In addition, a large source of lignocellulosic biomass comes from agricultural residues such as straw and corn stovers, thereby avoiding the food-to-fuel debate. For these reasons, lignocellulose, the most abundant biopolymer on earth, has lower feed cost when compared to starch or sugarcane based ethanol plants (El Bassam, 1998).

While there are inherent advantages to using lignocellulose biomass to produce ethanol, the current processing technology is still relatively young with roots dating back only to the 1980s when the first demonstration plant was commissioned by Iogen Corporation (Solomon et al., 2007). The mixed sugar composition of the lignocellulosic feedstock, a mixture of pentose and hexose, makes the associated processing plants more complicated than ethanol plants based on sugar cane or corn. First, to be able to recover fermentable sugars from biomass fibrous materials, it is necessary to break the bonds in order to increase the availability of complex-carbohydrate polymer chains for hydrolysis. Secondly, conventional microorganisms used in the fermentative ethanol industry (*Zymomonas mobilis and Saccharomyces cerevisiae*) can easily metabolize glucose but are not capable of converting the pentose sugars present in the resulting mixture. In order to convert all sugars present in the hydrolysate into ethanol, various recombinant microbes have been produced using *Z. mobilis*, *E. coli*, or *S. cerevisiae* as a platform (Bothast et al., 1999). *E. coli* KO11 is one genetically-modified microbe that has the

ability to consume all sugars present in lignocellulosic feeds to produce ethanol, but this strain akin to the Purdue *S. cerevisiae* is highly sensitive to the presence of ethanol and other inhibitors (Palmqvist and Hahn-Hägerdal, 2000). The recombinant *S. cerevisiae* developed at Purdue University and licensed by Iogen Corporation is being harnessed to make commercial quantities of ethanol using straw collected from farms (Ho and Tsao, 1995; Ho et al., 1998).

To increase the ethanol productivity, a fermentation-extraction hybrid process is envisioned to partly circumvent product inhibition. In this hybrid process, the fermentation is carried out until ethanol concentration reaches levels, in the vicinity of 30 g/L, that are known to be inhibitory (Jones et al., 2011). Upon reaching inhibitory ethanol concentration levels, the fermentation broth are passed through an external bed of activated carbon where ethanol is preferentially adsorbed. The depleted fermentation broth is returned to the fermenter. With lowered ethanol concentration, the fermentation can continue with reduced inhibition. Additional substrate can be added to the semi-batch process to allow the continued production of ethanol by *E. coli* KO11. The process arrangement is similar to the one that have been researched for butanol fermentation systems where inhibition is a major process concern (Maddox, 1982). Online removal of butanol from such systems using adsorbents or other means has shown to enhance sugar utilization and the productivity of the fermentation (Ennis et al., 1987).

Ethanol adsorbed on the activated carbon bed can later be recovered and concentrated using a number of different separation techniques such as microwave desorption (Menendez et al, 1999; Ania et al., 2004, Bradshaw et al., 1998), vacuum swing adsorption (Cruz et al., 2003), and gas stripping (Walsh et al., 1983), and sent for additional downstream processing, namely, distillation and pressure swing adsorption to produce fuel grade ethanol.

To validate experimental results and to gain a better understanding in the operation of the hybrid fermentation/extraction system, a model was developed in this study to simulate the performance of a semi-batch fermentation unit with intermittent ethanol extraction.

The comprehensive fermentation/extraction model was developed in phases, the first being a classic unstructured kinetic model to describe the ethanol production by *E. coli* KO11 in a glucose medium. The kinetic parameters of the fermentation model were determined using weighted sum of squared residuals (WSSR) by fitting the model equations to experimental data sets from single substrate fermentations. Having obtained the parameter estimations for the kinetics, the model was expanded to incorporate the impact of online ethanol selective extraction. The competitive adsorption model predicts the transfer of ethanol and sugar to and from the surface of the activated carbon adsorbent. The goal of this study is to assess the applicability of online ethanol removal from fermentation broth using ethanol selective adsorbents.

2.0 Materials and methods

2.1 Microbe

Escherichia coli KO11 (ATCC 55124) was purchased from the American Type Culture Collection. The microorganism was preserved at -80°C in 30% glycerol, 0.1M $MgSO_4$, 0.025 TRIS (pH 8.0). A small portion (0.3 mL) of freeze dried material received from ATCC was aseptically transferred to a test tube of the broth medium (5 to 6 mL total). The last few drops of this suspension were transferred to an agar slant. The slant and the tube were incubated at 30^{o}C under the appropriate conditions for a few days.

2.2 Culture media and operating conditions

Prior to each experiment, *E. coli* KO11 was taken from the freezer and warmed to room temperature. The bacteria were grown on plates of Luria Broth (LB) agar (10 g/L tryptone, 10 g/L NaCl, 5 g/L yeast extract, 15 g/L agar) with 0.2 g/L glucose as carbon source and containing 40 mg/L chloramphenicol (to which *E. coli* KO11 is resistant). The plates were kept in a refrigerator at 5°C for a maximum of two weeks. Plates were incubated at 35^{o}C overnight. Cells from an isolated colony were transferred aseptically to 100 mL of sterile culture broth containing 2 g/L glucose and 25 g/L LB broth (10 g/L tryptone, 5 g/L yeast extract, 5 g/L NaCl). The culture was incubated for 10 h at 35^{o}C at 100 rpm in an elliptical rotary shaker. After 10 h incubation, 0.5 mL of the culture broth was transferred to a second fresh sterile culture broth. The optical density (OD) of the

broth was monitored until the late log phase of the growth curve was reached. These cells were used for inoculation of the fermentation broth.

2.3 Fermentation conditions

Fermentations were performed in bioreactors constructed in our laboratory. The constructed bioreactor had a total volume of 1.5 L, with a 1 L working volume. A thermostat was used to maintain the fermentation temperature at 30^{o}C, and the pH monitored by the insertion of an autoclavable pH probe (Broadly James Corporation, USA) and maintained above 6.0 by the addition of 1M NaOH (pH controller). The vessel was topped with a rubber stopper with holes for the insertion of the pH electrode, the NaOH addition port, a fermentation sampling port and CO_2 gas vent. Agitation was carried out with a magnetic stirrer and rod at an rpm between 100 and 150. The initial cell mass following inoculation was 1.2 mg/L of bacteria (dry weight). Fermentation experiments were carried out under anaerobic conditions.

2.4 Fermentation medium

The fermentation medium was prepared with 25 g/L LB broth. The fermentation medium contained glucose as a carbon source. The quantity of glucose initially present in the medium is specified for each of the fermentation experiments performed.

2.5 Analytical procedures

Dry cell concentration was determined by measuring the optical density (OD) at a wavelength of 600 nm (Perkin Elmer Lambda 25 UV/Vis). A standard calibration curve was prepared and clearly showed a linear relationship between the OD measured and the dry weight of the cell mass. When performing OD measurements, samples were diluted in order to ensure that the readings fell within the linear range of the standard curve.

The pH of the fermentation was monitored using the F-635 Fermprobe by Broadley James Corporation. The probe was connected to Labview and a controller was used to add 1M NaOH to maintain the pH at 6.0. The pH was verified intermittently with a

secondary pH meter during sampling in order to ensure that the fermentation was indeed operating near the pH set point of 6.0.

Glucose and ethanol concentrations were determined by high pressure liquid chromatography (HPLC), using the Waters Sugar-Pak I cation-exchange column (6.5 mm x 300 mm) (Waters Ltd., ON, CA) equipped with a Waters Breeze system and a Waters 2414 refractive index detector. Separation was performed at 90°C using distilled deionised water containing 50 mg/L calcium ethylenediaminetetraacetic acid (EDTA) as per the column operating requirements.

Fermentation broth samples for HPLC analysis were centrifuged at 13000 rpm for 6 min to pelletize the cells. The supernatant was then filtered with a 0.45 μm nitrocellulose Millipore (Whatman, CAN) membrane filter. Samples were diluted with distilled deionised water for sugar and ethanol concentrations to be within 0.01-3 g/L range as per column operating instructions. Concentrations were determined by integrating peaks using the Waters Breeze software. Glucose and ethanol standards were run with each sample in order to confirm the accuracy of the determined concentrations.

2.6 Ethanol extraction/substrate addition

During fermentation, concentrations of ethanol, substrate and cell mass were monitored by extracting 1 mL samples at defined time intervals. When the ethanol concentration reached levels known to be inhibitory, an ethanol extraction cycle was performed. The extraction was carried out using an external adsorption column using Filtrasorb 600 (F-600) granular activated carbon from Calgon Corporation.

The entire content of the fermenter was passed through the external bed of activated carbon at a flow rate of 5 mL/min. Samples were collected just prior to extraction and just after the extraction in order to assess the removal of ethanol, sugar and cells by the activated carbon. Following the extraction, the substrate level was replenished to 70 – 80 g/L glucose in order to promote the continued production of ethanol. The addition of substrate had a dilution effect that further reduced the ethanol concentration in the fermenter. For each experiment, the fermenter was operated for two full cycles

(fermentation, extraction, substrate addition) and stopped following the fermentation step of the third cycle.

3.0 Process modelling

3.1 Kinetic model of ethanol production by engineered *Escherichia coli* KO11

Fermentation models are employed to help understand and predict the behaviour of bacterial fermentation systems. Batch systems were used exclusively when modelling fermentation kinetics. For the purpose of this study, the kinetics of ethanol production by *E. coli* KO11 was studied in laboratory with a medium consisting of LB Broth and glucose. The mathematical treatment of the system was adapted from a study by Olsson et al. (1995) and the work of Jones et al. (1981).

The mass balance on the cell, ethanol and substrate results in a set of ordinary differential equations given in Equation 1-3. The balance on the cell is expressed using a modified version of the Monod kinetic equation (includes product inhibition and limitations on maximum cell density that can be achieved). The ethanol balance includes a term accounting for ethanol production due to cell growth and a term that accounts for the ethanol production of existing cells. The substrate balance includes substrate utilization due to cell growth, production of ethanol and cell maintenance.

$$\frac{1}{X}\frac{dX}{dt} = \mu = \frac{\mu_m S}{K_S + S}\left(1 - \frac{P}{P_m}\right)^n \left(1 - \frac{X}{X_m}\right)^\gamma \tag{1}$$

$$\frac{dP}{dt} = \alpha\frac{dX}{dt} + \beta X \tag{2}$$

$$-\frac{dS}{dt} = \frac{1}{Y_{X/S}}\frac{dX}{dt} + \frac{1}{Y_{P/S}}\frac{dP}{dt} + mX \tag{3}$$

In this study, the values of parameters μ_m, K_S, P_m, X_m, n, γ, α, β, $Y_{X/S}$, $Y_{P/S,}$ and m in the set of equations were determined by minimizing the weighted sum of squared residuals

(WSSR) between predicted values of ethanol, glucose and biomass concentrations and their respective experimental values.

For the minimization, normalized values of the concentrations of ethanol, glucose and cell mass were used. Weights correspond to the inverse of the maximum values of the three variables. The WSSR was calculated using the following equation:

$$WSSR = \mathrm{w}_1 \sum \left(P_e - P_p \right)^2 + \mathrm{w}_2 \sum \left(S_e - S_p \right)^2 + \mathrm{w}_3 \sum \left(X_e - X_p \right)^2 \tag{4}$$

3.2 Competitive adsorption: ethanol and glucose

To model the extraction of ethanol from the fermentation broth using activated carbon, a competitive adsorption isotherm was developed. Experiments have shown that the adsorption of ethanol was not affected by the presence of sugar (Jones et al., 2011) and the adsorption of ethanol on activated carbon F-600 was well represented using a standard Freundlich isotherm (Equation 5). Sugar substrate (glucose and/or xylose) is also adsorbed during the extraction process. However, the adsorption of sugar is greatly impacted by the presence of ethanol. When an appreciable ethanol concentration is present along with sugar, the final amount of sugar adsorbed is a small fraction of the amount that would be adsorbed for a pure sugar solution (Jones et al., 2011). To represent the isotherm for the competitive adsorption, the artificial neural network of Figure 1 was used successfully to capture the change in adsorption characteristics of glucose for various concentration of ethanol. Equation (6) represents the corresponding mathematical expression of the three-layer feed-forward neural network of Figure 1 where the concentrations of sugar and ethanol in solution are used to predict the adsorbed sugar concentration. Morse et al. (2011) have shown that a simple neural network could represent a wide range of types of isotherms.

$$q = AC_e^{1/y} \tag{5}$$

$$\bar{q} = \frac{1}{1+e^{-\left(\frac{W_{11}'}{1+e^{-(W_{11}\bar{C}_S + W_{21}\bar{C}_E + W_{31})}} + W_{41}' + \frac{W_{21}'}{1+e^{-(W_{12}\bar{C}_S + W_{22}\bar{C}_E + W_{32})}} + W_{41}' + \frac{W_{31}'}{1+e^{-(W_{13}\bar{C}_S + W_{23}\bar{C}_E + W_{33})}} + W_{41}'\right)}} \tag{6}$$

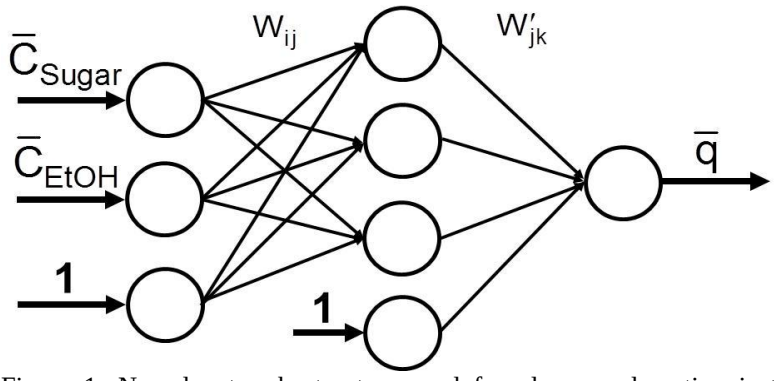

Figure 1: Neural network structure used for glucose adsorption isotherm in the presence of ethanol. Variables with a macron indicate normalized concentrations.

To account for the change in concentrations of sugar and ethanol throughout the packed bed adsorber, three differential equations are required. Equation (7) provides the mass balance for each species in the bulk flow across the packed bed. The first term on the right-hand side accounts for the axial dispersion whereas the second term gives the rate of mass transfer from the bulk to the surface of the solid particles and the third term represents the fluid flow across the bed:

$$\frac{\partial C_{L,i}}{\partial t} = D_{z_i} \frac{\partial^2 C_{L,i}}{\partial z^2} - \frac{1-\varepsilon}{\varepsilon} k_L a (C_{L,i} - C_{P,i}\big|_{r=R_p}) - u_L \frac{\partial C_{L,i}}{\partial z} \tag{7}$$

With the following initial and boundary conditions:

Initial condition: $C_L = 0, \ \forall z \ at \ t = 0$

Boundary conditions: $C_L = C_o$, $at \ z = 0 \ (t > 0)$

$$\frac{\partial C_L}{\partial z} = 0 \ at \ z = L \ (t > 0)$$

Equation 8 provides the mass balance of each species in the mobile phase (void) within the pellet. The rate of change of each species depends on the intraparticle diffusion and the rate of adsorption onto the surface of the solid.

$$\varepsilon_p \frac{\partial C_p}{\partial t} = \varepsilon_p D_{EFF} \left(\frac{1}{r^2} \frac{\partial}{\partial r} \left(r^2 \frac{\partial C_p}{\partial r} \right) \right) - k_{ads} a_p (C_p - C_p^*) \tag{8}$$

Initial condition: $C_P = 0, \ \forall r \ at \ t = 0$

Boundary conditions: $\frac{\partial C_{p_i}}{\partial r} = 0 \quad at \;\; r = 0,\; t \geq 0$

$$-D_{EFF}\frac{\partial C_{p_i}}{\partial r} = k_L\left(C_{Li} - C_{p_i}\Big|_{r=R_p}\right) \; at \; r = R_p,\; t \geq 0$$

The mass balance for the adsorbed phase is given by Equation (9):

$$1-\varepsilon_p \;\; \rho_s \frac{\partial q}{\partial t} = k_{ads} a_p \;\; C_p - C_p^* \tag{9}$$

Initial condition: $q = 0, \;\forall r \; at \; t = 0$

4.0 Results and discussion

4.1 Kinetics of *E. coli* KO11 fermentation

To determine the kinetic parameters of *E. coli* KO11 fermentation, four control experiments were carried out over a 60 h period. Starting with a substrate concentration of approximately 80 g/L, the fermentation vessel was inoculated and samples were taken to determine the concentrations of ethanol, glucose and cell mass. Four replicate experiments were performed and the kinetic fermentation model shown in Equations 1 - 3 were fitted to the experimental data in order to determine the parameters of the model that would best represent these four experiments. Figure 2 shows the experimental data (only two runs shown) and the corresponding model fit that was obtained by minimizing the optimization function given in Equation (4). These results show that the kinetic model is able to represent the concentrations of ethanol, glucose and biomass for single batch experiments. A summary of the kinetic parameters that resulted in the lowest WSSR is provided in Table 1.

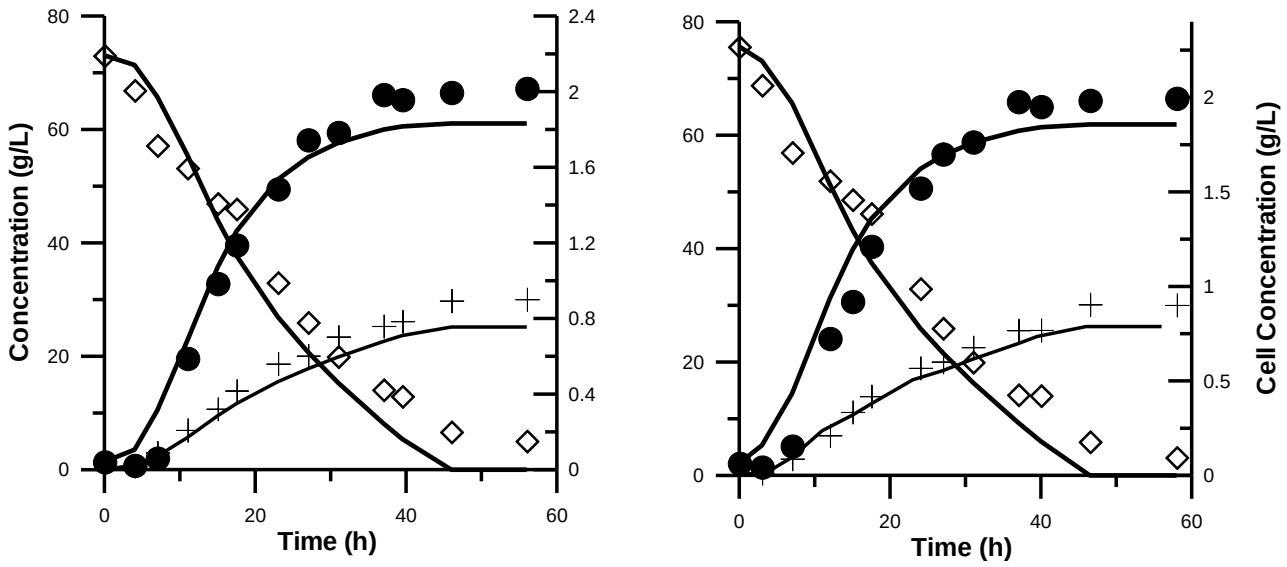

Figure 2 - Two examples of single sugar batch fermentation performed at 30°C and a pH of 6 with *E. coli* KO11. Symbols represent experimental data (◊: glucose concentration, •: cell concentration, +: ethanol concentration) and lines represent the fitted model described in Equations (1) to (3).

The results from Figure 2 show that the substrate, initially at a concentration of 80 g/L, was not fully depleted following 60 h of fermentation. The ethanol concentration approached 30 g/L for all experimental trials whereas the maximum cell concentration was in the vicinity of 2.0 g/L of dry cell mass. The fact that substrate was not completely consumed even after 60 h suggests that the ethanol concentration was sufficiently high to hinder further substrate consumption and ethanol production.

Table 1 - Fitted kinetic parameters from control experiments

Parameters	**Fitted Value**
μ_m	0.36
K_m	5.64
α	7.84
β	0.23
$Y_{X/S}$	0.14
$Y_{P/S}$	0.45
P_m	64.61
X_m	2.30
n	0.95
γ	1.71
m	0.0002

4.2 *E. coli* KO11 fermentation with extraction

Following the control experiments used to determine the kinetic parameters, experiments were conducted with the objective to enhance the longevity and productivity of the fermentation by selectively extracting ethanol as it was produced. To test the technical feasibility of selective ethanol extraction during fermentation, experiments were conducted in cycles: (1) a fermentation cycle where substrate is depleted to produce cells and ethanol, (2) an extraction cycle using a packed bed adsorber to reduce ethanol concentrations, and (3) the replenishment of the substrate to approximately the initial concentration to pursue with another cycle of fermentation. Four experiments were carried out, each consisting of two full cycles and ending the experiment with the fermentation step of the third cycle. The experimental result of a typical trial is presented in Figure 3 along with the model prediction.

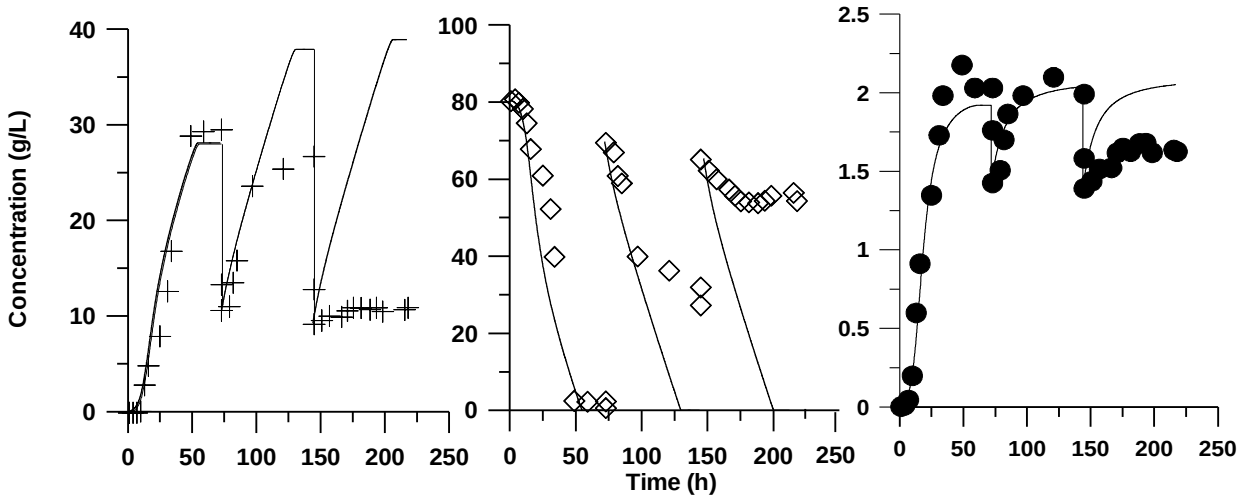

Figure 3 - Example of a multiple fermentation/extraction cycle experiment at 30°C and a pH of 6 with *E. coli* KO11. Symbols represent experimental data (+ - ethanol concentration, ◊ - glucose concentration, • - cell concentration) and lines represent the simulation using Equations 1 to 3 with kinetic parameters in Table 1. Extraction cycle was predicted with Equations 5 to 9.

Figure 3 shows two full cycles and the subsequent fermentation step of the third cycle. This figure has been broken into three panels showing the concentrations of ethanol, glucose and cells. Much like the control experiments presented in Figure 2, the substrate concentration started around 80 g/L and was nearly depleted in the first cycle as cells and later ethanol were produced. After 72 h, the ethanol concentration was nearly 30 g/L, a level known to be inhibitory. The cell concentration reached 2.2 g/L and less than 3 g/L

of substrate remained in the fermentation broth. The first extraction cycle was carried out at 72 h. The entire fermentation broth was passed through the external adsorption column where a good fraction of ethanol, and to a lesser degree the sugar, was removed. Following the extraction cycle, the ethanol concentration of the resulting solution was slightly above 10 g/L, a concentration level that is not associated with product inhibition even for microbe *E. coli* KO11.

The amount of ethanol removed during the extraction cycle depends on the ethanol adsorption isotherm as well as the quantity of activated carbon in the adsorption bed relative to the total amount of ethanol produced in the fermenter. According to a previous study at a concentration of 30 g/L, a capacity of 0.078g EtOH/g of adsorbent can be expected (Jones et al., 2010).

Samples were collected just prior to and just after the extraction of ethanol as well as after the addition of substrate. No samples were collected during the ethanol extraction. In lieu of data, the extraction model (Equations 5-9) was used to predict the concentration of the adsorbent column effluent from the adsorption bed. The result of the extraction simulation is shown in Figure 4.

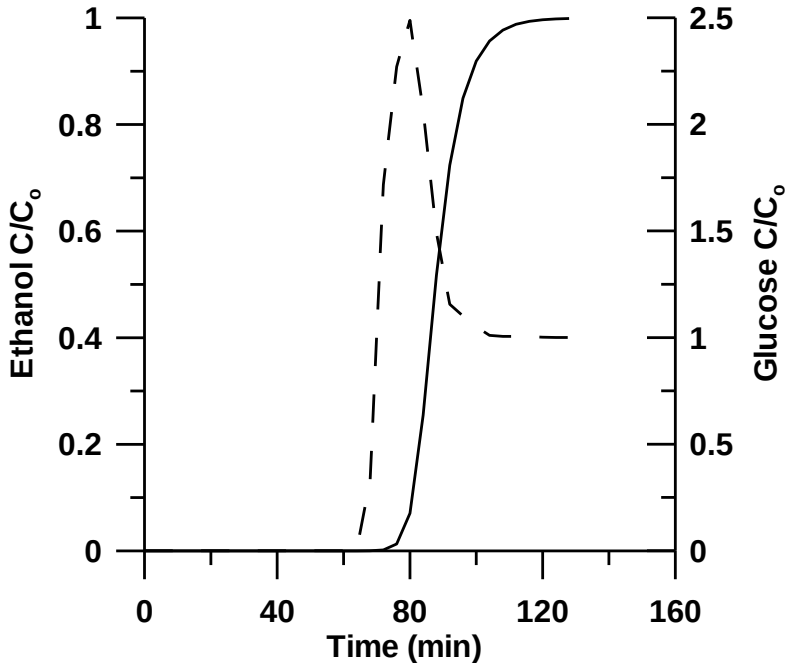

Figure 4 - Model predicted breakthrough profile for ethanol and glucose as a function of time. Solid line represents the predicted profile for ethanol. The broken line represents the prediction for glucose.

Figure 4 shows the normalized concentration (the effluent concentration divided by the inlet concentration) for the ethanol and glucose at exit of the activated carbon extraction bed as a function of time. Ethanol, which is preferentially adsorbed by the activated carbon, displays a typical breakthrough profile, with the first appearance of ethanol breaking through around 70 minutes. By 120 minutes, the entire bed is saturated and no longer has capacity for ethanol adsorption. The glucose breakthrough profile is typical of a weakly adsorbed component. The profile predicts the first appearance of glucose just after 60 minutes, the glucose concentration at the effluent rapidly rises to nearly 2.5 times the inlet concentration. This rise in the effluent concentration is due to the displacement of glucose molecules as ethanol, the component which is preferentially adsorbed, claims the adsorption sites and causes desorption of glucose molecules. Due to the preferential adsorption of ethanol, the mass transfer zone for glucose travels ahead of the mass transfer zone for ethanol causing an early breakthrough.

Following the extraction cycle, fresh substrate was added to the solution to allow the fermentation to proceed. The addition of a concentrated substrate solution further

decreased the concentration of ethanol in the vessel (dilution). Having added more substrate, the first cycle was complete and the second cycle was allowed to continue. Again, throughout the second cycle fermentation, small samples were collected every few hours to monitor the concentrations of ethanol, glucose and biomass. Even though more ethanol was produced, the rate of substrate utilization and ethanol production declined significantly in the second cycle compared to the first. Furthermore, after 72 h of fermentation for the second cycle (144 h total fermentation), more than 20 g/L of substrate remained and the ethanol concentration still had not reached 30 g/L. The cell concentration was reduced following the extraction and addition of substrate, but returned to approximately the same final value of 2 g/L.

At the 144 h mark, the second cycle of extraction and substrate replenishment was performed. Following the extraction and addition of glucose, the ethanol concentration was again equal to approximately 10 g/L. For the fermentation portion of the third cycle, a further decline in the rate of substrate utilization and ethanol production was observed. For this fermentation cycle, the final cell population stabilized at a lower cell density than for the first two cycles. In the end, the production of ethanol and cells completely ceased and, throughout the complete third fermentation cycle, very little ethanol and cells were produced. This was accompanied by very low substrate utilization.

Although the intermittent extraction of ethanol did allow the fermentation to continue with less inhibition after one complete cycle, the productivity declined from cycle to cycle. The reason for the decline of productivity is not fully understood. Ethanol levels were sufficiently low in the third cycle for the fermentation to proceed. It is likely that the cell age reduced cell productivity (Madigan et al., 2009). The accumulation of metabolites could also contribute to the observed inhibition (Liu and Qureshi, 2009). However, metabolites other than ethanol were not quantified in this study.

When the fermentation model described in Equations 1-3 was used to predict the experimental data using the kinetic parameters reported in Table 1, results show that excellent agreement was observed for the first cycle of fermentation. The ethanol,

glucose and cell concentrations were accurately represented up until 72 h. At the end of 72 h fermentation, the adsorption model was used to predict the amounts of ethanol and glucose that were extracted. Results of Figure 3 for the ethanol for the first extraction cycle is very well predicted by the model described by Equations 7-9. On the other hand, the model cannot predict the amount of cells trapped by the adsorption bed.

Following the addition of substrate at the end of the first cycle, the fermentation model was used to simulate the second cycle. In this case, the model showed a significant lack of fit particularly when comparing the simulation prediction for the glucose and ethanol concentrations. The model predicted a complete exhaustion of the substrate and an ethanol concentration of nearly 40 g/L following the fermentation. The fit of the third cycle was worse yet since the model does not predict the decline of productivity from cycle to cycle.

The problem with the model was easy to identify. The simulation predicted the same rate of glucose utilization and ethanol production in the first, second and third cycles. Experimentally this was not the case. In order to enhance the predictive ability of the model and to better comprehend the effect of time or the number of cycles on the fermentation, some parameters had to be updated to account for the decline in productivity from cycle to cycle. In a first attempt, parameter β of Equation (2), representing the ethanol productivity of existing cells, was adjusted from cycle to cycle to minimize the WSSR of each individual cycle. Results of the model fitting are shown in Figure 4.

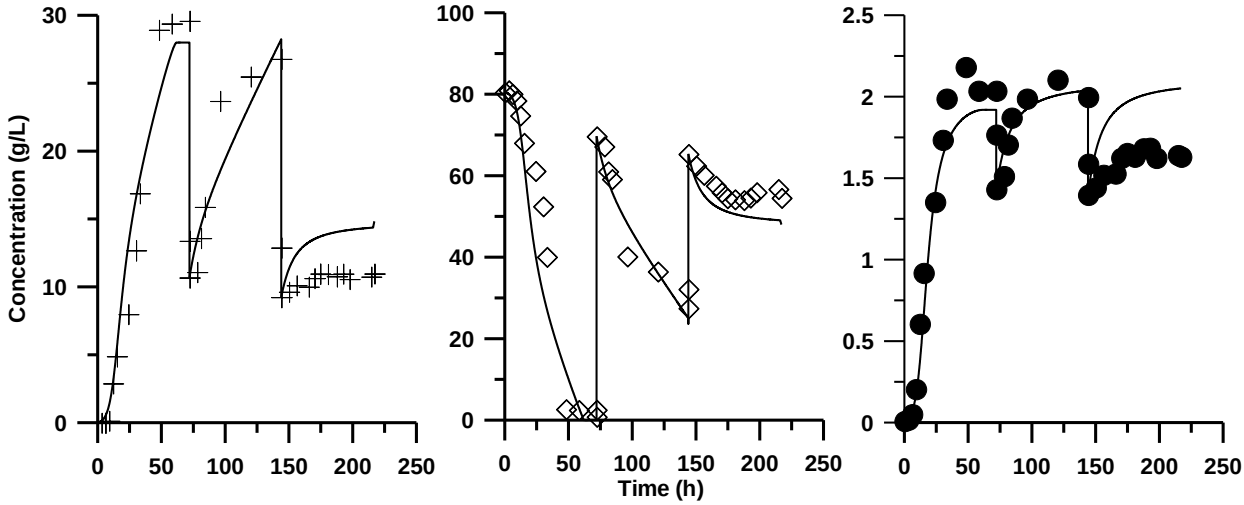

Figure 5 - Example of multiple fermentation/extraction cycle experiment at 30°C and a pH of 6 with *E. coli* KO11. Symbols represent experimental data (◊ - glucose concentration, • - cell concentration, + - ethanol concentration) and lines represent the simulation described in Equation 1 to 3 when using kinetic parameters in Table 1 (fermentation kinetics), while only modifying the cell productivity term (β). Extraction predicted with Equations 5 to 9.

By varying the value of β from cycle to cycle, and maintaining all other parameters at their nominal values shown in Table 1, the model prediction was significantly improved. In Figure 5, results show that the ethanol concentration is modelled well through the first two cycles, with an over prediction of the ethanol produced during the fermentation during the third cycle. Likewise the fit of the prediction for the substrate is excellent through the first two cycles, but in the third cycle the model over predicts the amount of substrate utilized. In the cell concentration plot, the model fit is strong for the first two cycles but fails to accurately represent the cell level that was reached during the experiments. The model predicts a cell concentration rising to above 2.0 g/L while in reality an observed concentration of approximately 1.5 g/L was reached.

The cycle to cycle value of β is shown in Table 2. These results suggest that existing cells gradually become less productive in terms of ethanol production from cycle to cycle. In fact, by the third cycle existing cells halt all ethanol production. This suggests that only the new cells formed are responsible for ethanol production.

Table 2 - Fitted values of β by cycle

Cycle #	β (1/g cell mass)
1	0.182
2	0.095
3	0

To better describe the decline observed during the subsequent fermentation cycles, the model had to be further adjusted to adequately represent the actual cell growth that was observed in the third and final cycle, which was over predicted when only β was varied. In order to account for the cell growth inhibition, the parameter P_m which is a product inhibition term was varied along with parameter β. The two parameters were varied for each cycle and the results of the model fit are presented in Figure 6.

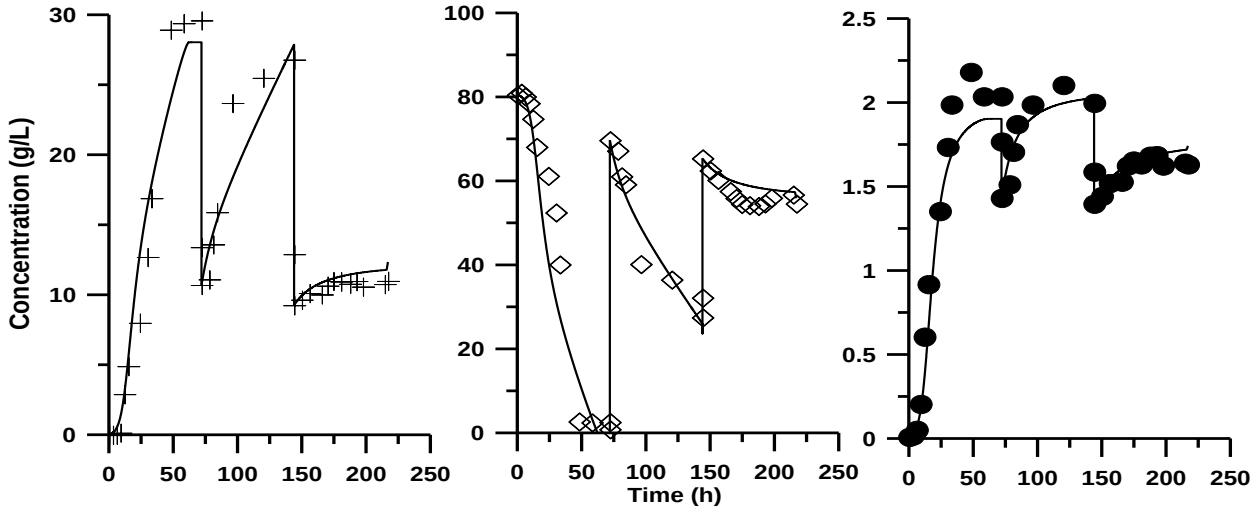

Figure 6 - Example of multiple fermentation/extraction cycle experiment at 30°C and a pH of 6 with *E. coli* KO11. Symbols represent experimental data (◊ - glucose concentration, • - cell concentration, + - ethanol concentration) and lines represent the simulation described in Equations 1 to 3 when using kinetic parameters in Table 1 (fermentation kinetics), while modifying the cell productivity term (β) and the product inhibition term (P_m). Extraction predicted with Equations 7 to 9.

By varying both the values of P_m and β, the model fit was able to sufficiently represent the trend of the ethanol, glucose and cell concentration profiles across all cycles. Although P_m is a parameter that accounts for product inhibition, in some sense, it can be viewed as a lump parameter incorporating the inhibitory nature of any species that accumulate in the broth (ethanol, lactic acid, etc.). The values of parameters β and P_m that minimize the WSSR for each cycle are shown in Table 3. It is important to point out that

the two parameters were obtained by fitting simultaneously the four experiments performed with the hybrid fermentation/extraction system.

Table 3 - Fitted values of β and P_m by cycle

Cycle #	β (1/g cell mass)	P_m (g EtOH/L)
1	0.185	52.9
2	0.098	47.2
3	0.008	18.5

From Table 3, the value of β again drops from cycle to cycle to the point where the value is almost zero in the final cycle (almost no ethanol production from existing cells). Parameter P_m also declines from cycle to cycle. The smaller the value of P_m, the more strongly new cell growth is inhibited. The model as it stands, following the fitting of β and P_m, provides evidence that cell productivity significantly declined from cycle to cycle. The second contributing factor causing a lack of ethanol production was the observed inhibition of new cell growth. Because ethanol is a primary metabolite, the production of ethanol is strongly linked to cell growth (Madigan et al., 2009). In the absence of growth due to the accumulation of components that are inhibitory to the cells, the fermentation shuts down.

5.0 Conclusions

By using an external adsorption bed, ethanol can be selectively removed from fermentation broth. *E. coli* KO11 is highly sensitive to moderate concentrations of ethanol. By maintaining the concentration below 30 g/L the fermentation, the life was extended and the total amount of ethanol produced was enhanced. Although the production was extended, a troubling decline in productivity was observed from cycle to cycle.

After two full cycles, further extraction of ethanol (even to as low as 10 g/L) had little impact on producing more ethanol. It is hypothesized that the two primary reasons for the decline in substrate utilization, cell growth and ethanol production is the decline in productivity by existing cells, and the lower cell density reached due to the elevated concentration of inhibitory compounds.

6.0 Nomenclature

a Exterior pellet surface area per volume of pellet (m^2 external area/m^3 pellet)
A Freundlich constant, (kg adsorbate/kg adsorbent) (m^3/kg adsorbate)$^{1/y}$
a_p Internal surface area of pellet (m^2 surface area/m^3 pellet)
C_e Concentration in solution at equilibrium, (kg adsorbate/m^3)
C_L Ethanol concentration within the liquid bulk (kg adsorbate/m^3)
C_p Concentration in the mobile phase in the pellet pores (kg adsorbate/m^3)
$C_P\big|_{r=R_P}$ Concentration at the pellet boundary (kg adsorbate/m^3)
C_P^* Concentration in equilibrium with the solid (kg adsorbate/m^3)
D_{EFF} Effective diffusion coefficient of the adsorbing species (m^2/s)
D_z Axial diffusion coefficient (m^2/s)
k_{ads} Average adsorption mass transfer resistance (m/s)
k_L Average film mass transfer coefficient (m/s)
K_s Half saturation constant (g/L)
m Cell maintenance coefficient (g substrate/(g cell.s))
n Constant in product inhibition model (dimensionless)
P Product concentration (g/L)
P_m Product concentration above which cells do not grow (g/L)
q Amount of adsorbate adsorbed (kg EtOH/kg adsorbent)
r Distance in the radial position within the pellet (m)
S Substrates concentration (g/L)
t Time, (h)
u_L Superficial velocity (m/s)
w weighted parameter for ANN or sum of squared residuals
X Cell mass concentration (g/L)
y Freundlich constant, (dimensionless)

$Y_{P/S}$ Ethanol yield coefficient (g ethanol/g substrate)
$Y_{X/S}$ Cell mass yield coefficient (g cell/g substrate)
z Distance in the axial direction (m)

Greek Letters

α Growth associated production coefficient (g EtOH/g cell mass)
β Cell productivity coefficient (1/g cell mass)
ε Column void fraction (m^3 void/m^3 column)
ε_p Pellet void fraction (m^3 void/m^3 pellet)
μ_m Maximum specific growth rate in Monod equation (h^{-1})
ρ_S Solid density (kg solid/m^3 solid)
γ Constant in cell inhibition model (dimensionless)

Subscripts

e Denotes experimental value
i Used as index number
j Used as index number
k Used as index number

p Denotes model predicted value
E Used to denote the species of interest (pertains to ethanol)
S Used to denote the species of interest (pertains to xylose or glucose)

7.0 References

1. Ollson, L., Hahn-Hägerdalt, B., Zacchi, G., (1995), Kinetics of Ethanol Production by Recombinant *Escherichia coli* KO11. *Biotechnol. Bioeng.,* Vol. 45, Pp. 356-365
2. Underwood, S.A., Zhou, S., Causey, T.B., Yomano, L.P., Shanmugam, K.T., and Ingram, L.O., (2002) Genetic Changes To Optimize Carbon Partitioning between Ethanoland Biosynthesis in Ethanologenic *Escherichia coli. Appl. Environ. Microbiol.* , Dec. 2002, p. 6263–6272.
3. Trinh, C.T., Huffer, S., Clark, M.E., Blanch, H.W., Clark, D.S., (2010) Elucidating Mechanisms of Solvent Toxicity in Ethanologenic *Escherichia coli*. *Biotechnol. Bioeng.*, Vol. 106, No. 5, 721-730
4. Jones, R. P., N. Pamment, and P. F. Greenfield (1981). Alcohol fermentation by yeast – The effect of environmental and other variable. *Process Biochem.y*, 16: 42-49.
5. El Bassam, N., 1998. Energy plant species: their use and impact on environment and development. *Earthscan Publications (London UK).*
6. Cheng, J.J, Timilsina, G.R., 2011, Status and barriers of advanced biofuel technologies: A review. *Renewable Energy.* 36 (12), 3541-3549.
7. Solomon, B.D., Barnes, J.R., Halvorsen, K.E., 2007. Grain and cellulosic ethanol: History, economics and energy policy. *Biomass Bioenergy.* 31, 416-425.
8. Jones, R. A., Tezel, F.H., Thibault, J., 2010, Simulation and Validation of Ethanol Removal from Water in an Adsorption Packed Bed: Isotherm and Mass Transfer Parameter Determination in Batch Studies. *Can. J. Chem. Eng.* 88 (5), 889 – 898.
9. Morse, G., Jones, R., Thibault, J., Tezel, F.H., 2011, Neural network modelling of adsorption isotherms. *Adsorption.* 17 (2), 303-309.
10. Jones, R. A., Thibault, J., Tezel, F.H., 2011. Enhanced ethanol production through selective adsorption in bacterial fermentation. *Biotechnol. Bioprocess Eng.* 16 (3), 531-541.

11. Menéndez, J.A., Menéndez, E.M., Garcia, A., Parra, J.B., Pis, J.J., 1999. Thermal treatment of activated carbons: comparison between microwave and electrical heating. *Inter. Microwave Power.* 34 (3), 137-143.
12. Ania, C.O., Menéndez, J.A., Parra, J.B., Pis, J.J., 2004. Microwave induced regeneration of activated carbon polluted with phenol. A comparison with conventional thermal techniques. *Carbon*. 42, 1377-1381.
13. Bradshaw S.M., van Wyk, E.J., de Swardt, J.B., 1998. Microwave heating principles and the application the regeneration of granular activated carbon. *The Journal of South African institute of mining and metallurgy.* 98 (4), 201-210.
14. Cruz P., Santos, C., Magalhães, F.D., Mendes, A., 2003. Cyclic adsorption separation processes: analysis strategy and optimization procedure. *Chem. Eng. Sci.* 58, 3143-3158.
15. Walsh, P.K., Liu, C.P., Findley, M.E., Liapis, A.I., Siehr, D.J., 1983. Ethanol Separation from water in a two-stage adsorption process. *1983 Symposium on biotechnology for fuels and chemicals*. 629-647.
16. Palmqvist, E., Hahn-Hägerdal B., 2000.Fermentation of lignocellulosic hydrolysate I: Inhibition and detoxification. *Bioresour. Technol.* 74 (1), 17-24.
17. Bothast, R.J., Nichols, N.N, Dien, B.S., 1999. Fermentation with new recombinant organisms. *Biotechnol. Prog.* 15 (5), 867-875.
18. Zhang, M. Eddy, C. Deanda, K. Finkelstein, M. Picataggio,, 1995. S. Metabolic engineering of a pentose metabolism pathway in ethanologenic *Zymomonas mobilis*. *Science*, 267, 240-243.
19. Stevis, P. E.; Ho, N. W. Y. Overproduction of D-xylose isomerase in Escherichia coli by cloning the D-xylose isomerase gene. *Enzyme Microb. Technol.* 1985, 7, 592-596.
20. Ho, N. W. Y.; Tsao, G. T. Recombinant yeasts for effective fermentation of glucose and xylose. *PCT Patent No. WO95/13362*, 1995.
21. Ho, N. W. Y.; Chen, Z.; Brainard, A. P. Genetically engineered *Saccharomyces* yeast capable of effective cofermentation of glucose and xylose. *Appl. Environ. Microbiol.* 1998, 64, 1852-1859.

22. Madigan, M.T., Martinko, J.M., Dunlap, P.V., Clark, D.P., 2009. Brock Biology of microorganisms. Published by Benjamin Cummings New York.
23. Liu, S., Qureshi, N., 2009. How microbes tolerate ethanol and butanol. New *Biotechnol.* 26 (3/4), 117-121.
24. Maddox I.S., (1982). Use of silicalite for the adsorption of n-butanol from fermentation liquids *Biotechnol. Lett*, 4 759-760.
25. Ennis B.M., Qureshi N., Maddox I.S., (1987) In-line toxic product removal during solvent production by continuous fermentation using immobilized *Clostridium acetobutylicum*, *Enzyme Microb. Technol.*,9 672-675.

SECTION – V: Conclusions

Chapter 8

Conclusions

> "To truly transform our economy, protect our security, and save our planet from the ravages of climate change, we need to ultimately make clean, renewable energy the profitable kind of energy".
>
> - Barack Obama February 24th, 2009

To improve ethanol productivity, more importantly from cellulosic biomass, this thesis has examined the use of hydrophobic adsorbents for their ability to selectively adsorb ethanol continuously or intermittently from fermentation broth. The application targeted by this research project is the integration of an online ethanol extraction unit that can remove ethanol intermittently to alleviate ethanol inhibition. The main accomplishments of the thesis, suggested future work and the final remarks are provided below.

1.0 Main accomplishments and contributions

A brief summary of the major thesis accomplishments and an assessment of how the objectives were met are presented below. The introduction of the objectives can be found in Chapter I: Introduction

1) Adsorbent screening – 15 commercially available adsorbents were screened for their ability to selectively adsorb ethanol from model fermentation broth. Adsorption performance was characterized based on the kinetics of adsorption and the equilibrium capacity. Among the adsorbents screened, Filtrasorb 600 activated carbon (F-600) was selected for further studies due to its strong performance in the adsorbent screening as well as its availability and low cost.
2) Determination of multi-component isotherms - Models for multi-component adsorption isotherm for ethanol and sugar (the major components present in fermentation broth) were determined. The ethanol isotherm was found to be effectively modeled by the Freundlich isotherm, while a new isotherm based

on artificial neural networks was developed to adequately predict sugar (glucose and xylose) adsorption in the presence of ethanol.

3) Adsorption model development – A mechanistic model based on finite differences method was developed and used to predict the mass transfer of ethanol in a packed adsorption bed. Isotherm models were incorporated into a model, consisting of a series of differential equations, used to simulate the performance of adsorbents in a packed bed where multiple components were present. The model used parameters and estimations of physical variables to predict the performance of the packed adsorption column instead of fitted parameters. The only parameters that necessitated experimental determination and fitting were the isotherms for pure and multi-component systems. This model proved adept to represent experimental data. The model was effective at simulating ethanol and sugar adsorption across a wide range of operating conditions. The model can be used as a basis to simulate ethanol extraction in industrial size equipment. Development of an online extraction scheme – Experiments with a hybrid system was performed where a fermentation system was coupled with on an online extraction unit. Results of these experiments suggested that inhibition of the ethanol intolerant microbe *E. coli* KO11 could be delayed by maintaining low ethanol concentrations in the fermentation broth. By selectively removing ethanol as it is produced, the fermentation can continue for a time unimpeded by elevated ethanol concentrations.
4) Development of a kinetic model for fermentation model – a kinetic model was developed in order to predict the utilization of sugar, the production of biomass and the production of ethanol as a function of time during the fermentation. The model was effective in simulating fermentation systems and was validated experimentally.
5) Development of a hybrid fermentation/extraction system model – A comprehensive model incorporating the fermentation kinetics and the subsequent extraction of ethanol in an external packed bed was finalized. The

model was validated by experimental trials and is thought to be a valuable for scale-up and design of an industrial size system.

6) Publications, Conference Proceedings and Presentations – The experimental findings of this work were shared with academic peers internationally through the published work in refereed journals, conference papers and presentations outlined in Appendix A.4

2.0 Future work

Desorbing concentrated ethanol from the surface of the adsorbent remains a challenge that was not addressed in detail in this particular study. Vacuum swing adsorption with purge gas and microwave adsorption schemes were tested and proved effective in regenerating activated carbon in small scale preliminary tests (less than 500 g of activated carbon).

Microwave regeneration of activated carbon showed that the adsorption capacity remained unchanged even following five consecutive saturation/desorption cycles (data shown in Appendix A.2). Although these schemes were only tested briefly to examine the technical feasibility, a setup that would be industrially relevant for large scale operations would need to be tested to better study ethanol extraction in an industrial context. This study did not aim to determine the ideal desorption technology that would be employed industrially. More work is needed on this front and in particular the design of a suitable microwave heating system taking into account the low penetration of microwave into a packed bed of solids. In addition, an economic analysis of such a system should be performed in future studies.

3.0 Final remarks

The advent of oil drilling and refining in the early 1900s started the liquid transport fuel age. The availability of liquid transport fuels such as gasoline and diesel made possible the widespread use of automobiles, highways, marine and air travel. Worldwide, oil exploration began in the 1900s and new oil reserve discoveries grew each decade

reaching a peak in the 1960s; after this time, there has been a steady decline in the discovery of conventional oil reserves (Simmons, 2006).

Oil prices respond like all commodities: prices increase during supply shortages and fall in times of oversupply. However, few commodities have the direct impact on our day to day lives like that of oil. The oil market has historically been volatile. In the 1970s conflict in the Middle East saw oil prices more than quadruple in a period of less than a month. The supply domestically is also sensitive. Extreme weather such as hurricanes in the Gulf Coast have been known to disrupt the supply chain and cause sharp short term price surges for liquid fuels domestically (Solomon et al., 2007).

In response to the volatile nature of the supply chain for oil, for decades, private and public dollars have been directed at developing domestic fuels from renewable sources aimed at alleviating our economic dependence on oil. First commercialized in the 1970s and 1980s, ethanol produced from food crops (corn and sugarcane) represented the first generation bio-refineries (Sims et al., 2010). Today, ethanol from corn and sugar cane are considered mature technologies. From 2000 to 2008, global production of ethanol from first generation ethanol plants more than quadrupled from 400 PJ to 1750 PJ (IEA, 2009).

Though energy supply has been the primary driver for the development of biofuels, supporters of the biofuel industry cite the added advantages of economic impact (adding agriculture and industry jobs in rural communities where the crops are grown), and the mitigation of greenhouse gases (Chandel et al., 2010).

Today, the future of first generation of bioethanol plants are considered limited. Though they are capable of producing a domestic fuel source, high crop cost, and high land usage are problems that plague the process making profitability difficult to attain without government subsidies (OCED, 2008). In 2009, global production of biofuel represented only 1.5 % of all transport fuel used with the majority using corn or sugarcane as a feed.

Research into non-food biomass (lignocellulose) has risen to prominence over the past two decades. Dedicated energy crops and are known to have better energy yields per land usage, to be available at lower cost and to grow on marginal land across varied climates (Singh et al., 2010). Biofuels from these non-conventional sources were brought to the forefront of the public's conscience by Barack Obama's Presidential Address in 2009, and today are considered the future of the ethanol industry.

Significant strides have been made in the development of the ethanol from lignocellulose technology since the first demonstration plant in the 1980s. Despite these advancements, today only 0.1% of the world's biofuels are produced from lignocellulose sources. Technological hurdles still stand between the current processing technology and profitable commercialization of the technology. In order to overcome these hurdles, research into increasing crop yield, improving pre-treatment of biomass, engineering new microbes capable of high ethanol yield and enhancing separation efficiency is required (IEA, 2009)

The importance of fuels derived from renewable sources will continue to rise as known fossil fuel reserves are depleted. The price of transport fuels will also rise as consumption trends in developing nations outpace the production. Bioethanol from lignocellulose feeds will be a major source of renewable liquid transport fuel going forward. Significant commitments to lignocellulosic ethanol by the US and Canadian governments have pushed second generation biofuel plants to the forefront of North America's renewable energy plan. Major energy corporations such as Chevron, BP, Shell and Exxon have also made major investments in biofuel technologies. Given these public and private investments, wide spread commercialization of the technology is coming, though it may still be years if not decades away.

4.0 References

1. Chandel, A.K., Singh, O.M., Chandrasekhar, G., Rao, L.V., Narasu, M.L., (2010). Key drivers influencing the commercialization of ethanol-based bio-refineries. *J. of Comm. Biotech.* 16(3), 239-257.
2. IEA Bioenergy (2009). Sustainable bioenergy – a reliable option. *Report prepared for IEA Bioenergy Implementing Agreement.* www.ieabioenergy
3. OCED (2008). Economic assessment of biofuel support policies. Organisation for economic co-operation and development. www.oced.org/tad
4. Simmon, R.M., (2006). Twilight in the Desert. Wiley, New York
5. Sims, R.E.H., Mabee, W., Saddler, J.N., Taylor, M., (2010). An overview of second generation biofuel technologies. *Bioresour. Technol.* 101, 1570-1580.
6. Singh, A., Pant, D., Korres, N.S., Nizami, A-S., Prasad, S., Murphy, J.D., (2010). Key issues in life cycles assessment of ethanol production from lignocellulosic biomass: Challenges and perspectives. *Bioresour. Technol.* 101, 5003-5012.
7. Solomon, B.D., Barnes, J.R., Halvorsen, K.E., 2007. Grain and cellulosic ethanol: History, economics and energy policy. *Biomass and Bioenergy.* 31, 416-425

Section VI: Appendices

Appendix A.1

Fixed bed adsorption for the removal of carbon dioxide from nitrogen: breakthrough behaviour and modelling for heat and mass transfer

Mulgundmath, V.P., Jones, R.A., Tezel, F.H. [$] and Thibault, J.

Abstract

Concentration and temperature profiles for CO_2 adsorption from a CO_2-N_2 gas mixture (10 % CO_2 by vol in N_2) have been studied in a dynamic adsorption pilot plant unit to better understand the breakthrough behaviour. The scope of the present work is to study the adsorption characteristics and heat effects of this CO_2-N_2 gas mixture and to develop a simple model for the dynamic simulation of non-isothermal adsorption in a fixed bed.

Results indicated that adsorption heat effects were significant for this mixture while the breakthrough time obtained with Ceca 13X adsorbent was independent of the initial bed temperature. The cooling step that follows the thermal regeneration of the adsorption bed could be omitted entirely without affecting the adsorption performance. An earlier breakthrough time was observed for a higher feed flow rate of 6.6 SL/min compared to 4 SL/min. Cooling during the adsorption cycle decreased the width of the mass transfer zone and led to a longer breakthrough time. The study also indicated that online measurements of temperature at different locations along the column bed could be used to predict the concentration breakthrough for this CO_2-N_2 gas mixture. The novel two-population model used in this study provided an adequate representation of the temperature and concentration breakthrough profiles within the adsorption column.

Keywords: Fixed bed adsorption, modelling, carbon dioxide, flue gas, 13X.

1.0 Introduction

Carbon dioxide is an omnipresent species that has generated enormous attention since the turn of the century because of its contribution to the greenhouse gas effect. Combustion of fossil fuels is a major source of these harmful emissions which is the result of ever increasing worldwide population and an increased per capita demand for energy. According to the International Energy Agency Working Party on Fossil Fuels [1], more than 85% of the world's energy needs are met by fossil fuels which account for the annual emission of 25 billion tons of CO_2 into the atmosphere. Fossil fuel-fired power generation facilities account for one-third of the global CO_2 emission to the atmosphere [2]. This has resulted in a global research effort to mitigate the emissions of CO_2 and examine ways to capture CO_2 directly from power plant flue gases [3].

For the purpose of reducing CO_2 emissions to the atmosphere, IEA WPFF [1] outlines the utilisation of Zero Emission Technologies (ZET) which virtually eliminate emissions from the conversion of fossil fuels and their consequences on health and environment. ZET promote the increase of the overall plant efficiency, the use of lower-carbon or carbon free energy sources, oxy-fuel combustion, CO_2 fixation using algae and the development of new power cycles. However, these are innovative technologies that cannot be easily used to retrofit existing power plants. Carbon sequestration involving the carbon dioxide capture and storage (CCS) has become a major focus of reducing point-source emissions. For CO_2 to be sequestered, it must be relatively pure (>95%) to find useful applications in the food refrigeration industry, fire extinguishers, enhanced oil recovery, beverage carbonation, metals fabrication, urea production and to reduce the volume of stored CO_2 in deep saline aquifers, depleted oil and gas reservoirs and unminable coal/mineral beds [4].

Cryogenic distillation, liquid phase absorption and gas separation membranes compete with adsorption processes for CO_2 removal applications [5, 6]. The flue gas concentration ranges from 8-15 vol% for typical coal fired plants. Absorption using amines is the currently widely employed commercial technology but there is a significant energy

penalty required to regenerate the solvent. Cryogenic distillation is only feasible for CO_2 concentrations greater than 90 vol% whereas membranes exhibit low fluxes, degradation, high cost and fouling [7]. Adsorption processes are increasing being used as they tend to utilise less resources and energy and are highly efficient [8-12].

The scope of the present work is to study the adsorption breakthrough characteristics and heat effects of a gas mixture (10 % CO_2 in 90% N_2 by vol) that resembles the concentration of CO_2 found in typical dry flue gases and to develop a simple model for the simulation of a non-isothermal adsorption in a fixed bed.

Selection of a suitable adsorbent is one of the important issues in an adsorption process. This adsorbent must possess a high selectivity for CO_2 over N_2 along with faster uptake rates in order to achieve a higher throughput. The most widely used adsorbents for CO_2 removal are zeolites, with 4A, 5A, and 13X being the most popular from this class [13, 14], although activated carbon and activated alumina are also used for PSA applications [15, 16]. Reynolds et al. [7] used a high temperature PSA with potassium promoted hydrotalcite (HTlc) as adsorbent which exhibited higher capacity at elevated temperatures and good water insensitivity. Attempts have been made to develop and commercialise novel MCM-41 polymer modified molecular basket adsorbents for CO_2 removal [17] and amine impregnated pore expanded (PE) MCM-41 adsorbents [4]. Most recently activated Alumina composites are being developed in combination with zeolite 13X. The alkaline treated Alumina has better resistance against moisture and 13X with a narrow pore size distribution provides a selective adsorptive separation. The adsorbent candidates chosen for this study included Ceca 13X zeolite, Alcan activated alumina AA320-AP and a composite of activated alumina/13X adsorbent, Alcan 650 PCAP.

Pure gas adsorption isotherms for CO_2 and N_2 were measured at 40^oC and 100^oC for each adsorbent in a constant volume system (Accusorb 2100 Physical Adsorption Analyzer supplied by Micromeritics Instrument Corporation) for Ceca 13X, Alcan AA320-AP and Alcan 650 PCAP. This method involves measuring pressure changes in a known volume of gas exposed to an adsorbent sample. As the gas is adsorbed and allowed to reach

equilibrium, the measured decrease in the closed system pressure yields the amount of gas adsorbed under given operating conditions [18]. The pure gas isotherms of CO_2 and N_2 are displayed in Figure 1a for 13X and AA 320-AP and Figure 1b for 13X and 650 PCAP. Isotherm data for 13X are repeated in these figures for comparison with other tested adsorbents. The experimentally determined pure gas isotherms have been fitted with the Langmuir model.

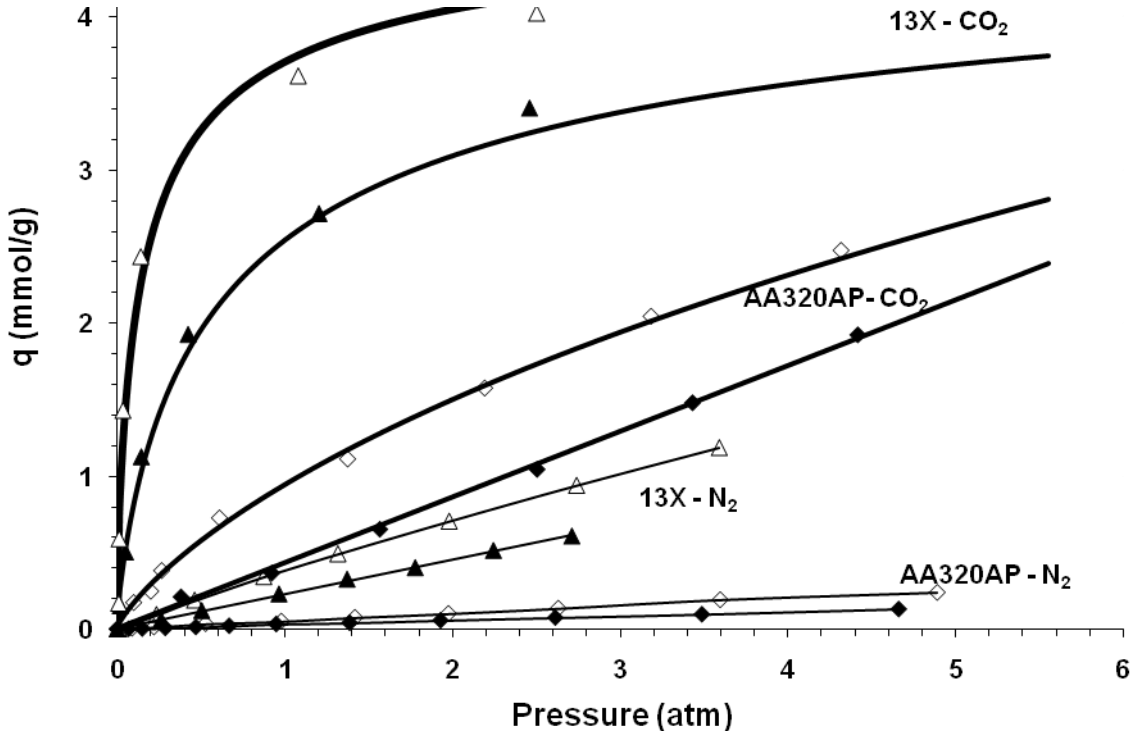

Figure 1a - Pure isotherms of CO_2 on 13X and AA 320-AP at 40°C (hollow symbols) and 100°C (filled symbols). Lines represent the Langmuir fit.

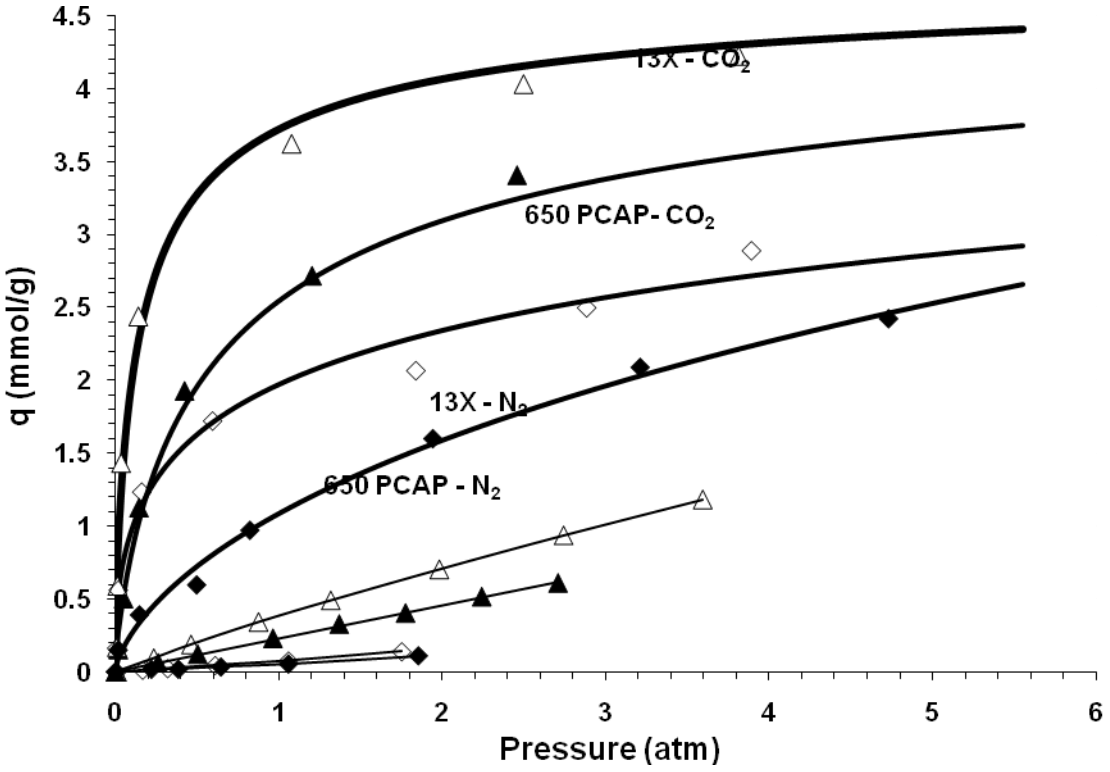

Figure 1b - Pure isotherms of CO2 on 13X and 650 PCAP composite at 40oC (hollow symbols) and 100oC (filled symbols). Lines represent the Langmuir fit.

From Figures 1a and 1b, it was observed that the shape of the CO_2 isotherms on 13X was very rectangular whereas the N_2 adsorption isotherms were linear. The initial slope of the CO_2 isotherm is very high when compared to that of N_2 isotherm. This indicates more interactions between CO_2 molecules and the heterogeneous surface of 13X adsorbent. CO_2 favours a more heterogeneous surface due to its higher quadrupole moment compared to N_2. At a lower temperature of 40°C, the capacities of all tested adsorbents were greater than at 100°C, as expected, and consistent with always exothermic physical adsorption behaviour. Our previous studies on binary adsorption isotherms of CO_2 and N_2 with 13X zeolite indicated that the binary adsorption behaviour of this pair of gases were completely dominated by the adsorption of CO_2 [19].

13X had a large working capacity for CO_2 when compared to 650PCAP composite and AA320-AP. This observation indicates higher interactions between CO_2 and the more heterogeneous Ceca 13X structure which is highly desirable for the removal of CO_2 from

flue gas. A lower column pressure (6.44 atm) was arbitrarily chosen since flue gas is available at low pressures. Operating the column at a much higher pressure would increase the number of moles adsorbed and thus the heat generated within the column, leading to a higher cooling demand required.

Nitrogen capacities observed were slightly higher for Ceca 13X followed by Alcan 650 PCAP and Alcan 320-AP. Higher N_2 capacities are not desirable for this gas separation since it will be recovered as a product when CO_2 is adsorbed on the adsorbent. When all the above tested adsorbents were compared, Ceca 13X exhibited the larger differences in the adsorption capacities between CO_2 and N_2 at the operating pressure (6.44 atm) and feed concentration (10% CO_2 by vol) at 40^oC. These pure gas isotherm observations suggest that 13X is a suitable adsorbent for the separation of CO_2 in a flue gas application followed by 650 PCAP composite and AA320-AP.

From the literature binary isotherm data, it was observed that 13X adsorbent is a promising adsorbent for CO_2 flue gas separations [19]. Also, the equilibrium phase diagrams obtained for this binary mixture on 13X adsorbent indicated that better separation of CO_2 and N_2 was achieved at high temperatures when compared to 40°C. This observation also indicates that Ceca 13X is suitable for flue gas separation applications. This finding is similar to the observation made on commercial 13X zeolite by Zhang et al. [3]. 13X was chosen in this investigation as the adsorbent for the lab scale dynamic adsorption unit to study the breakthrough behaviour.

2.0 Experimental section

A two column dynamic adsorption analysis unit has been designed and built to separate CO_2-N_2 mixtures using zeolite Ceca 13X as the adsorbent supplied by Honfleur, France. The properties of the adsorbent and the fixed bed are given in Table 1 while Figure 2 shows a simplified schematic diagram of the apparatus built in-house.

Table 1 - Properties of the adsorbent and fixed bed

Bed Length (m)	0.61
Column internal diameter (m)	0.044
Column wall thickness (m)	0.0029
Port 1 position[1] (m)	0.102
Port 2 position[1] (m)	0.305
Port 3 position[1] (m)	0.507
Ceca 13X pellet radius (m)	0.00103
Ceca 13 X bulk density ($kg.m^{-3}$)	705

[1] Tap location from the column inlet

This experimental system was designed to allow easy in-situ regeneration of the saturated adsorbent. It primarily consists of the following components: two identical adsorption columns, feed and purge gas , heating tape, an in-line gas heater, a vacuum pump, copper heating/cooling tubes wrapped around the column, solenoid three-way and two-way valves, 1/4" and 1/8" outside diameter stainless steel tubing, a data acquisition system, customized control software, thermocouples, a multiposition valve, pressure transducers, mass flow controllers, a mass flow meter, a gas mixing chamber (MC), a gas chromatograph (GC), a non dispersive infrared analyzer (NDIR) and an Edwards high vacuum pump.

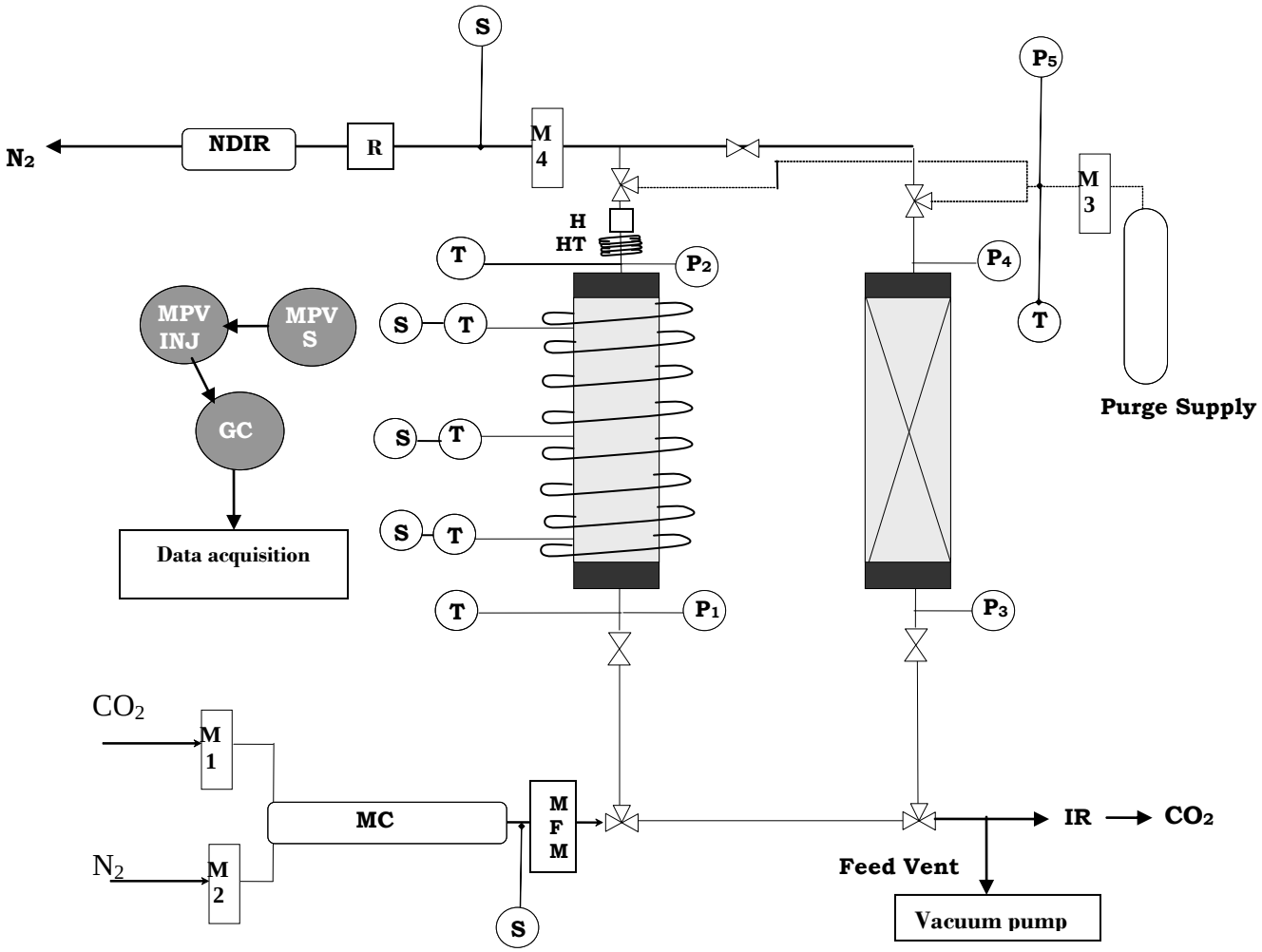

GC- Gas Chromatograph ; H- Heater ; HT- Electrical heating tape ; INJ - Injection valve ; NDIR- Non Dispersive Infrared analyzer ;M- Mass flow controller ; MC- Mixing chamber ; MFM- Mass flow meter ; MPV- Multiposition valve ; P - Pressure transducer ; R- Rotameter ; S- Sample port ; T- Thermocouple

Figure 2 - Schematic diagram of the two bed Thermal Pressure Swing Adsorption (TPSA) system

The two adsorption columns are made of 316 stainless steel which is known for its corrosion resistance, toughness even at elevated temperatures and for fast heat dissipation. The inside diameter of the column is 4.4 cm, and the length available for the adsorption bed is 61.0 cm.

The columns are fitted to inlet and outlet stainless steel conical flow distributors in order to favour plug flow conditions. VCR® fittings and Teflon O-rings formed the seals between the column and the flow distributors. One of the columns has three ports that were simultaneously used for temperature and concentration measurements from column centre axis location. These sample ports were connected to a VALCO model SD 32-port micro-electric actuated multiposition valve. This multiposition valve had 32 ports (16 inlet and 16 outlet ports) and had the capability of connecting 16 different sample ports at any time A 6-port micro-electric actuated injector valve housed the sample gas cell (500 µL) and connected the 32-port micro-electric actuated multiposition valve to a Varian 3400 Series Gas Chromatograph (GC) for concentration measurements through 0.32 cm (1/8") outside diameter stainless steel tubing. The sample gas cell within the 6-port micro-electric actuated injector valve was purged with UHP helium for 5 seconds followed by injecting the CO_2-N_2 gas mixture sample from the desired sample port for a period of 3s. Each gas sample took 1 min to be analysed in the GC to obtain the CO_2 composition. Therefore, experimental composition data points from the GC were obtained every minute. Since there were three sample location ports along the column, the data point at each sample location was obtained every 3 minutes. Using a GC provided the flexibility of experimenting with various gases. Disadvantages with the GC included the difficulty in obtaining continuous gas detection at each sample port immediately, as there is a time lag involved with the GC detector. Along with the GC, a non dispersive infrared analyzer (NDIR) was used for continuous CO_2 gas detection (0-20% by vol) at the adsorber column exit. The zero and span drifts were less than ± 1% of the full scale. Accurate temperature measurements were obtained by using Omega type-K exposed tip thermocouples.

The two adsorption columns were each equipped with two 590 Barocel pressure transducers at the entrance and the exit of the columns for measuring pressures up to 10 atm with an accuracy of 1% of the reading. The average of the inlet and outlet column pressures was taken as the average column pressure. Due to the low pressure drops (0.26 - 0.44 kPa) in the range of flow rates studied (4 - 6.6 SL/min), it represented the true column pressure. A Proportional-Integral-Derivative (PID) controller was built into LABVIEW software (from National Instruments) that was used to control this average column pressure by manipulating

column exit mass flow rate via the mass flow controller (MFC) M4. The feed, purge and sample flow rates were controlled by MKS type M100B mass flow controllers (0-10 SL/min) which had an accuracy of 1.5% of the full scale.

The column was fitted with flexible copper coils and a thermostat controlled 50:50 (vol/vol) ethylene glycol-water mixture circulated inside the coils in order to achieve near isothermal conditions for the process. In this study, an attempt is made to replicate a cooling jacket adsorber since it promotes higher adsorption efficiency when compared to beds without jackets [20]. Various components of this system were connected by 0.64 cm (1/4") outside diameter stainless steel tubing. A data acquisition system in conjunction with LABVIEW software from National Instruments was used to collect and record the pressure, temperature, concentration and flow rate data. For the adsorption of carbon dioxide from nitrogen, nitrogen was used both as a feed component and as a purge gas.

At the beginning of the set of experiments used in this study, the adsorption column was isolated from the set up and packed with the Ceca 13X adsorbent. Uniform distribution of the adsorbent pellets inside the column was ensured by continuous tapping of the sides of column. The adsorbent was regenerated in an electric oven at 200^{o}C under nitrogen flow in order to remove any impurities present in its structure followed by cooling it overnight. Then the two ends of the column (inlet and outlet) were plugged to prevent any leaks and it was connected back to the rest of the experimental set up.

Prior to each run, the NDIR analyzer was calibrated with span gas, UHP N_2 and a standard calibrated gas mixture of 10% (by vol) CO_2 and 90% (by vol) N_2. During pressurisation and after NDIR calibration, the feed gas mixture was prepared in the mixing chamber (MC) filled with glass beads using two pre-calibrated mass flow controllers (MFC) M1 and M2. This gas mixture was sampled through NDIR and GC to establish the variability in concentration.

Before each run, the column was pressurised using UHP N_2 to the desired column pressure and maintained at the same pressure using the PID controller. During this cycle,

N_2 is adsorbed by the adsorbent and heat is liberated which raises the temperature within the column to about 55-60^oC. The column was cooled to ambient temperatures (40^oC) using ethylene glycol-water mixture that circulated in the copper coils that surrounded the column. When ambient column temperatures (40^oC) were attained, the adsorption cycle was started by introducing the feed gas mixture (10% CO_2 bal. N_2) into the column. For each run, the CO_2 concentration, flow rates, pressures and temperatures were continuously monitored and the data were recorded in an MS-Excel worksheet.

When the gas concentration at the last sample port reached the feed concentration (10 % CO_2 bal. N_2), the feed flow was stopped. A complete regeneration of the saturated adsorbent was performed by combining high temperature (120^oC) and vacuum in-situ, between different experimental runs. During the regeneration cycle, UHP N_2 gas was allowed to flow through the column. The completion of this step was verified by stopping the vacuum and analysing the desorbed gas coming out from the column for CO_2 concentration using the NDIR analyzer. Complete regeneration of the adsorbent was achieved when the desorbed gas contained no traces of CO_2. The column was then allowed to cool under UHP N_2 purge. It was then isolated from the rest of the setup by closing the column inlet and the outlet valves.

Prior to the start of the next run, the column was re-pressurised to the desired column pressure and the adsorption cycle was repeated. Adsorption column breakthrough experiments were conducted at a constant adsorption column pressure of 6.44 atm (absolute).

3.0 Mathematical modelling of the process

The objective of this study was to accurately describe the mass and heat transfer taking place within a packed bed adsorber. The model outlined here describes both the mass and heat transfer in the bulk fluid flowing within the bed, as well as the transport phenomena occurring within the porous solid adsorbent pellets. The model is intended to simultaneously fit three concentration profiles and three temperature profiles at different locations within the packed column. Therefore, the principal assumptions made in the development of the model are as follows:

- Bulk concentration and temperature in the column does not change in radial direction.
- Mass transfer between the surface of the pellet and the fluid is described by a linear driving force model, while the intra-particle mass transfer is described by pore diffusion.
- Within the adsorbent pellets, instantaneous equilibrium is assumed between the mobile fluid phase and the solid surface.
- The adsorption process is non-isothermal. The energy balance accounts for heat generation due to adsorption, heat exchanged with ambient air surrounding the packed adsorber, heat accumulation in the column walls, and the heat accumulation within the pellet and fluid phases.
- Adsorption equilibrium is described by the Langmuir isotherm model.
- Adsorption of nitrogen is considered to be negligible when compared to that of carbon dioxide and that a single component model applies. This assumption is fully justified, since it has been shown in our earlier studies that CO_2-N_2 binary adsorption behaviour is fully dominated by CO_2 with 13X as the adsorbent [19].
- The velocity in the bed changes due to adsorption and heat effects.
- Within the pellet particles, the mobile fluid phase in the pellet void and the solid portion of the pellet are assumed to be locally in thermal equilibrium.
- The adsorbent pellets are assumed to be spheres of homogenous size, and the adsorption sites are energetically homogeneous.
- Ideal gas law applies.

- The model accounts for two separate populations of pores, each with their respective mass transfer resistances. The two populations of pores represent respectively pores that are easily accessed and those that are accessed with greater difficulty.

3.1 Mass balance equations

Assuming that the bulk concentration of CO_2 in the column radial direction is constant, the rate of change in concentration of the flowing gas at any axial position along the column is given by Equation (1):

$$\varepsilon_c \frac{\partial C_B}{\partial t} = \varepsilon_c D_Z \frac{\partial^2 C_B}{\partial z^2} - \left(1-\varepsilon_c\right) k_f \frac{3}{r_p}\left(C_B - C_P\big|_{r=r_p}\right) - \varepsilon_c u_G \frac{\partial C_B}{\partial z} \qquad (1)$$

The terms on the right hand side of the equation account for the axial dispersion within column, the CO_2 transferred from the bulk fluid phase to the adsorbent particles (predicted by the linear driving force model), and the CO_2 transferred by convection, respectively.

The mass transfer within the pellet is predicted with a pore diffusion model. CO_2 reaching the surface of the solid from the bulk fluid diffuses, according to Equation (2), along the pores of the pellet due to a concentration gradient. Meanwhile, the concentration of the mobile gas phase within the pores is depleted due to adsorption of CO_2 onto the solid surface of the adsorbent pores. It is assumed that the adsorption of CO_2 onto the surface of the 13X adsorbent can be considered instantaneous in comparison to the other mass transfer mechanisms [21].

$$\varepsilon_p \frac{\partial C_p}{\partial t} = D_M\left(\frac{1}{r^2}\frac{\partial}{\partial r}\left(r^2 \frac{\partial C_p}{\partial r}\right)\right) - (1-\varepsilon_p)\rho_s \frac{\partial q}{\partial t} \qquad (2)$$

Equation (2) was solved twice simultaneously for the two "populations" of pellets (x, y) that represented "easily accessed" (x) and "difficultly accessed"(y) sites. The "easily accessed" sites had the diffusion coefficient, D_x (or) D_m, which was calculated using Equation (5). D_y represented the "difficultly accessed" sites and was estimated by fitting

the model to the experimental data. The Langmuir isotherm model equation is used to describe the equilibrium that exists between the solid and the gas at a particular temperature.

Table 2 gives the list of parameters used in the simulation model of the packed bed adsorber.

3.1.1 Mass transfer correlations

The average external mass transfer coefficient between the flowing gas bulk and the pellet, k_f was calculated using the equation of Wakao and Funazkri [22]:

$$\mathrm{Sh} = 2.0 + 1.1(\mathrm{Re})^{0.6}(Sc)^{0.33} \tag{3}$$

$$\text{i.e., } \frac{k_f D_p}{D_M} = 2.0 + 1.1\left(\frac{D_p \rho_G \vec{u}_G}{\mu_G}\right)^{0.6}\left(\frac{\mu_G}{\rho_G D_M}\right)^{0.33} \tag{4}$$

The molecular diffusion of CO_2 in N_2 was estimated using the Chapman-Enskog equation [12]:

$$D_M = \frac{0.0018583\sqrt{T^3\left(\frac{1}{M_A}+\frac{1}{M_B}\right)}}{P\sigma_{AB}^2\Omega_{AB}} \tag{5}$$

The axial dispersion coefficient was estimated using the following correlation [23].

$$\frac{\varepsilon_c D_Z}{D_M} = 20 + 0.5\,\mathrm{Re}\,Sc \tag{6}$$

Table 2: Parameters used in the simulation model

Model data	Method	Source
C_{ps} (J.kg^{-1}.K^{-1}) = 920	estimated	Cavenati et al., [24]
C_{pG} (J.kmol^{-1}.K^{-1}) = 1023	estimated	A.F. Mills, [25]
C_{pw} (J.kg^{-1}.K^{-1}) = 500	estimated	A.F. Mills, [25]
$D_M = D_x$=(m^2 s^{-1}) = 6.7 x 10^{-5}	calculated	Eq.# 5
D_y (m^2 s^{-1}) = 5.6 x 10^{-8}	optimized[1]	-
D_z (m^2 s^{-1}) = 1.2 x 10^{-4}	calculated	Eq. # 6
FacX^2 = 0.73	optimized[1]	-
h_o (W m^{-2}K^{-1}) = 2.1	calculated	Eq.# 16
h_f (W m^{-2}K^{-1}) =95	calculated	Eq.# 15
k_f (W m^{-1}K^{-1}) = 0.0059	calculated	Eq. # 4
k_g (W m^{-1}K^{-1})= 0.027	calculated	A.F. Mills, [25]
k_{gs} (W m^{-1}K^{-1})= 0.045	optimized[1]	-
k_w (W m^{-1}K^{-1})= 16	estimated	A.F. Mills, [25]
ε_c = 0.35	estimated	Cavenati et al., [24]
ε_p = 0.54	calculated[2]	-
ε_t = 0.7	calculated[2]	-
ρ_p (kg .m^{-3})= 1085	calculated[2]	-
ρ_s (kg adsorbent.m^{-3} bed)= 2359	calculated[2]	-

[1] - Since the exact proportion of the easily accessed sites was unknown and the diffusion coefficient in the difficult sites could not be determined, this parameter was determined by fitting the model to the experimental data such that to minimize the sum of squares of residuals.

[2] - Calculated by estimating the column void and the bulk density of the adsorbent.

3.1.2 Initial and boundary conditions for mass transfer equations

Initially, the packed column adsorber has been regenerated and carbon dioxide is not present such that the fluid and the solid concentrations are zero everywhere within the column:

$$C_B = 0,\ C_P = 0,\ q = 0 \qquad t = 0,\ \forall\,(r, z) \tag{7}$$

This initial condition applies for the bulk fluid concentration as well as the concentration in the pellet. "r" represents both the radial position of the bed and the pellet). Two boundary conditions are required to solve Equation (1). At the entrance to the column, the feed concentration is known and remains constant throughout the experiment.

$$C_B = C_{Feed}\,(\text{i.e., } 25\ \text{mol/m}^3) \qquad z = 0,\ t \geq 0 \tag{8}$$

At the exit of the packed bed, it is assumed that the diffusive flux is equal to zero:

$$\frac{\partial C_B}{\partial z} = 0 \qquad z = L,\ t \geq 0 \tag{9}$$

To solve Equation (2), two boundary conditions are required along with the initial condition given by Equation (7). At the center of the pellet, symmetry prevails whereas at its surface, the rate of diffusion within the pellet must equal the convective mass flux from the bulk fluid.

$$\frac{\partial \boldsymbol{C}_{\boldsymbol{p}}}{\partial \boldsymbol{r}} = 0 \qquad r = 0,\ t \geq 0 \tag{10}$$

$$-D_M \frac{\partial C_p}{\partial r} = k_f \left(C_B - C_p\big|_{r=r_p}\right) \quad r = r_p,\ t \geq 0 \tag{11}$$

3.2 Energy balance equations

The energy balance on the system consists of a balance on the bulk gas phase, a balance on the pellet which is comprised of the solid and the void portions of the pellet, and finally, a balance on the walls of the adsorption column. The energy balance for the bulk gas phase is given by Equation (12):

$$\varepsilon_c \rho_G C_{pG} \frac{\partial T_{bg}}{\partial t} = k_g \frac{\partial^2 T_{bg}}{\partial z^2} \varepsilon_c - (1-\varepsilon_c) h_f \frac{3}{r_p} (T_{bg} - T_P|_{r=r_p}) - u_G \frac{\partial T_{bg}}{\partial z} \varepsilon_c \rho_G C_{pG} - \frac{4}{r_b} h_f (T_{bg} - T_W) \quad (12)$$

This balance accounts for the transfer of energy by axial heat diffusion through the bed, energy transfer between the flowing fluid and the surface of the solid adsorbent due to temperature differences, the energy transfer by convection through the bed due to the bulk movement of gas, and finally, the energy transferred to the wall of the column.

3.2.1 Energy balance on the pellet

Equation (13) accounts for the energy balance on the pellet:

$$(\varepsilon_p \rho_p C_{pG} + (1-\varepsilon_p) \rho_s C_{pS}) \frac{\partial T_p}{\partial t} = k_{gs} \left(\frac{1}{r^2} \frac{\partial}{\partial r} \left(r^2 \frac{\partial T_p}{\partial r} \right) \right) + \Delta H_{ads} \rho_B \frac{\partial q}{dt} \quad (13)$$

Equation (13) accounts for both the void and solid portions of the pellet. As was stated previously, the solid and mobile phases within the pellet are assumed to be in thermal equilibrium at a given radial position. The energy balance states that the local rate of change of temperature within the pellets is caused by energy transfer by thermal diffusion within the pellet and the energy generated within the system due to the exothermic heat of adsorption released when a molecule of CO_2 binds to the surface of the adsorbent.

3.2.2 Energy balance on the wall

Equation (14) represents the energy balance on the column wall [26]. The balance accounts for the heat transfer to the wall from the bulk gas and the heat transfer from the wall to the outside surroundings. The adsorber wall and the coiled coolant tube wall are assumed to be at the same temperature and that the energy balance for the adsorber wall includes the coolant tube wall.

$$\left[\left(\frac{d_2}{d_1} \right)^2 - 1 \right] C_{pw} \rho_w \frac{\partial T_w}{\partial T} = \frac{4}{d_1} h_f (T_{bg} - T_w) - \frac{4}{d_1} \left(\frac{d_2}{d_1} \right) h_o (T_w - T_a) \quad (14)$$

3.2.3 Initial and boundary conditions for heat transfer equations

Initially, the entire column and its contents are at ambient temperature (306 K).

$$T_{bg} = T_p = T_w = 306 \text{ K} \qquad z = 0,\ t \geq 0 \tag{15}$$

Insulation boundary condition is assumed to be valid at the column entrance and exit:

$$\frac{\partial T_{bg}}{\partial z} = 0 \qquad z = 0,\ L;\ t \geq 0 \tag{16}$$

To solve Equation (13), two boundary conditions are required in the pellet, along with the initial condition given by Equation (15). At the center of the pellet, symmetry prevails whereas at its surface, the rate of conduction within the pellet must equal the convective heat flux from the bulk fluid.

$$\frac{\partial T_p}{\partial r} = 0 \qquad r = 0,\ t \geq 0 \tag{17}$$

$$-k_{gs}\frac{\partial T_p}{\partial r} = h_f\left(T_{bg} - T_p\big|_{r=r_p}\right) \quad r = r_p,\ t \geq 0 \tag{18}$$

3.2.4 Heat transfer correlations

Chilton-Colburn analogy [27] was used to estimate the convective heat transfer coefficient for forced convection inside the packed bed:

$$j_D = j_H \Rightarrow Nu = 2.0 + 1.1(\text{Re})^{0.6}(\text{Pr})^{0.33} \tag{19}$$

As the experimental conditions represented a laminar flow of the bulk feed gas through the column, Churchill and Chu correlation [28] was used to deduce the average Nusselt number for laminar flow by Equation (20):

$$Nu = \frac{h_o L}{k_g} = 0.68 + 0.67(Ra \times \psi)^{1/4} \tag{20}$$

$$Ra = \frac{\beta \Delta T g L^3}{\nu^2}\text{Pr} \tag{21}$$

$$\psi = \left[1 + \left(\frac{0.492}{\text{Pr}}\right)^{9/16}\right]^{-16/9} \tag{22}$$

A two-population adsorbent particle model, representing easily accessible adsorbent sites and those sites which are more difficult to access, was solved. An adsorbent particle normally possesses a wide distribution of pore sizes which for simplicity can be grouped into micro-pores and macro-pores having distinct mass transfer resistances. In this investigation, the model was developed in such a way that the two "populations" were solved in parallel and each one was given a weight representing the percentage of sites which were deemed to be "easily accessed" and "difficultly accessed". The population weighting factor (FacX) and the diffusion coefficient for the "difficultly accessed" pores, D_y, were determined by fitting the model to the experimental data. When modelling the temperature profile, only a single parameter, the bulk thermal conductivity of the pellet (k_{gs}), was used to improve the quality of curve fits. All other parameters were determined either experimentally or calculated using the empirical correlations given in this paper.

This model is intended to provide a simplified approach to representing these two types of adsorption sites within the pellet without having to accurately estimate the radius of the zeolite crystals and the intra-crystalline diffusion resistance within the crystal. Similar systems have been modeled in the literature by including these experimentally determined parameters [29, 30].

4.0. Results and discussions

The scope of this study was the experimental determination of adsorption breakthrough behaviour and heat effects for CO_2-N_2 gas mixture (10 % CO_2 by vol. in N_2) using the Ceca 13X adsorbent in the laboratory scale set-up. Desorption and estimation of process performance was not a part of this study. Concentration and temperature breakthrough profiles were determined to understand the adsorbent behaviour. The effects of parameters like the omission of the initial cooling step, feed flow rate, and external cooling during the adsorption step were investigated. A novel approach describing two different populations of the adsorbent pellets was used to develop a simple model for the simulation of non-isothermal adsorption in a fixed bed.

4.1 Omission of the initial cooling step

When the thermal regeneration of the adsorption bed is completed, generally a cooling step follows with a purge gas before adsorption step is implemented. This cooling step generally comprises 10-25% of the total cycle time [31]. There is a significant economic advantage if this step could be omitted entirely without affecting the adsorption performance. Basmadjian [31] derived the criterion mentioned below under which the breakthrough time would be independent of the initial bed temperature using equilibrium theory. The criterion is that the ratio of the equilibrium loading to the feed concentration must be larger than the ratio of adsorbent to gas heat capacity and is given by the following inequality [32]:

$$(q_F / y_F) > C_{ps} / C_{pG} \tag{23}$$

where q_F is the solid phase adsorbate concentration at the feed conditions, y_F is the component molar fraction at the feed conditions, C_{ps} is the solid adsorbent heat capacity and C_{pG} is the gas phase heat capacity. The second and more important criterion based on adiabatic conditions is given by:

$$(q_{pl} / y_F) / (C_{ps} / C_{pG}) > 1.5 \tag{24}$$

where q_{pl} is the solid phase adsorbate concentration at the plateau temperature. This temperature, T_{pl}, is obtained from Equation (25):

$$T_{pl} = T_F - (q_F \Delta H) / (C_{ps}(q_F / y_F) - C_{ps}) \tag{25}$$

where T_F is the inlet feed temperature and ΔH is the heat of adsorption. At the beginning of each experimental run, the bed is still hot due to N_2 adsorption during the pressurisation step. However, these criteria were easily fulfilled in this investigation and confirmed by observations during the concentration and temperature breakthrough experiments. The breakthrough times were similar for the experimental runs that were performed while the bed was hot (55-60^oC) and while the bed was at ambient temperature (40^oC). The effect of parameters like low feed concentration (10% CO_2 bal. N_2), high equilibrium loading of the 13 X adsorbent (at 0.644 atm. partial pressure, q=3.444 mmol/g), high total system pressure (6.44 atm), and a moderate heat of

adsorption (25 kJ/mol) contributed to satisfy this criterion. Therefore, for all the rest of the runs, the initial cooling step was omitted at the beginning of the adsorption cycle.

It was observed that these criteria contributed to the slow movement of the adsorbate concentration front thus allowing the temperature wave to pass ahead. An interesting observation to note was the viable option of using thermocouples only to detect breakthrough behaviour under similar conditions, without the use of sample gas concentration detectors. This is possible for bulk gas separations that exhibit a higher heat of adsorption.

4.2 Effect of feed flow rate

Figure 3 gives the concentration breakthrough curves obtained for CO_2 adsorption from a CO_2/N_2 mixture (10 % CO_2 bal. N_2) on a packed bed of 13X for two different flow rates to see the effect of the feed flow rate at a constant adsorption pressure of 6.44 atm (absolute). The plot gives the concentration of CO_2 in the gas phase as a function of time at the column outlet. A Non-Dispersive Infrared (NDIR) analyzer was used at the column exit to obtain continuous gas concentration measurements. It was observed that a higher feed flow rate of 6.6 SL/min contributed to an early breakthrough since the bed got saturated faster with more CO_2 going through the column compared to a lower feed flow rate of 4 SL/min. For 6.6 SL/min, the mass transfer zone moved quicker and mass transfer coefficient was higher because of the higher Reynolds number.

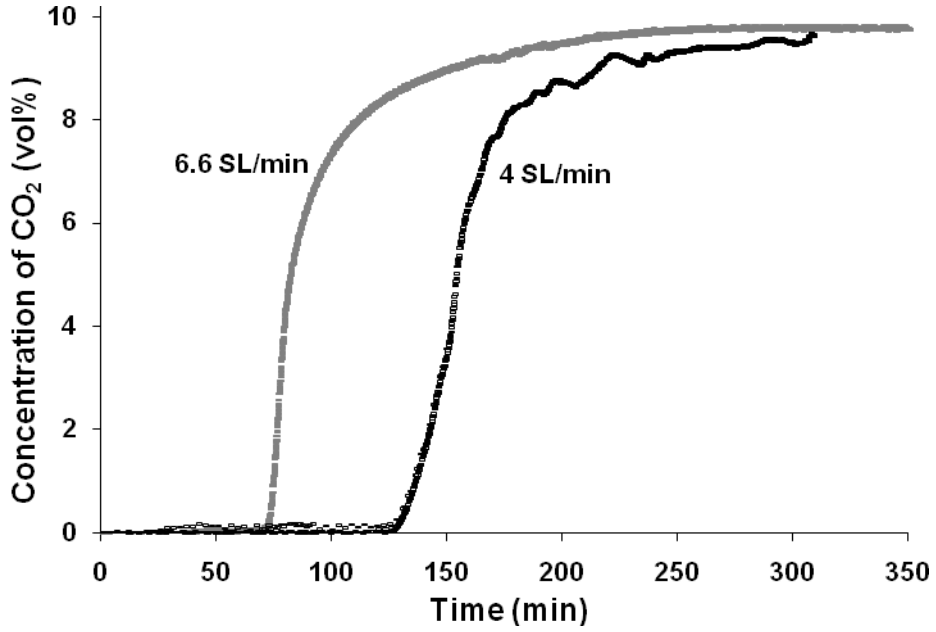

Figure 3 - Effect of flowrate on concentration breakthrough profile for CO_2 adsorption (10% CO_2 bal. N_2) with 13X adsorbent at 6.44 atm column pressure.

Tailing was seen towards the bed exit for both flow rates. This is an indication of the slow intra-particle diffusion within micro-pores of the adsorbent, presence of non-homogeneous particles and varying flow patterns.

4.3 Effect of external cooling

Figure 4 gives the concentration breakthrough curves obtained with and without cooling for CO_2 adsorption from a CO_2/N_2 mixture (10 % CO_2 bal. N_2) on a packed bed of 13X at two different flow rates to see the effect of external cooling at a constant adsorption pressure of 6.44 atm (absolute). The plot gives the concentration of CO_2 in the gas phase as a function of time at the column outlet. During the adsorption step, a mixture of 50:50 (by vol) ethylene glycol and water was circulated as a coolant (at 0^oC) in the copper coils that surround the column. Although this would lead to an increase in the energy consumption, the objective of these runs was to operate the column at the lowest coolant temperature possible (which was 0^oC) and study the breakthrough behaviour at a constant column pressure of 6.44 atm (absolute). For identical feed flow rates, it was observed that the cooling effect made the breakthrough curves steeper, decreasing the mass transfer

zone. Since physical adsorption is exothermic, lower column temperatures contributed to an increase in the capacity of Ceca 13X adsorbent and, as a result, led to a delayed concentration breakthrough when compared to ambient non-isothermal operations.

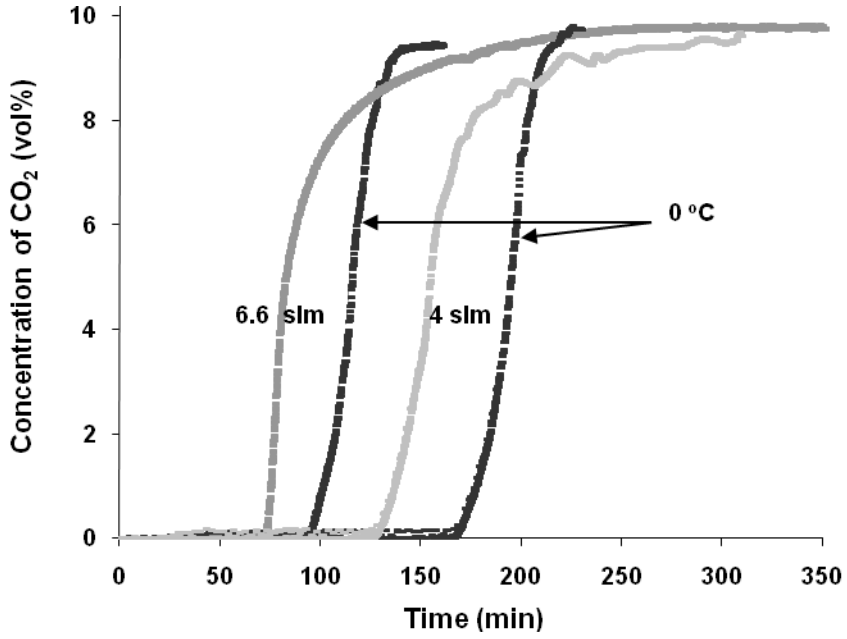

Figure 4 – Effect of cooling during the adsorption cycle on concentration breakthrough profile for CO_2 adsorption (10% CO_2 bal. N_2) with 13X adsorbent at 6.44 atm column pressure. Dark lines indicate the presence of a coolant at 0^oC while grey lines represent experimental runs in the absence of the coolant.

Apart from studying the concentration breakthrough behaviour using an NDIR analyzer, thermocouples were located at different sample ports (at positions 10.2 cm, 30.5 cm and 50.7 cm from column inlet) to study the temperature breakthrough behaviour. The heat of adsorption basically dictates the type of adsorbent regeneration conditions that have to be employed. A higher heat of adsorption requires high temperature and/or lower pressures during regeneration.

Figure 5 gives the temperature breakthrough curves obtained for CO_2 adsorption from a CO_2/N_2 mixture (10 % CO_2 bal. N_2) on a packed bed of Ceca 13X at 4 SL/min to see the effect of external cooling during adsorption step at a constant adsorption pressure of 6.44 atm (absolute). The plot gives the temperatures of the column at different positions as a function of time. The higher heat of adsorption observed for CO_2

on Ceca 13X (25 kJ/mol) contributed to reach a temperature of about 117^{o}C when the column was at room temperature, as observed in Figure 5a. Although more heat was released during the experiments with cooling due to higher capacities at low temperatures, the presence of the coolant resulted in a lower peak temperature (around 98^{o}C). The temperature rise in port #1 (at 10.2 cm from column inlet) was smaller when compared to the ports (#2, #3) closer to the column exit. When the feed gas is introduced, adsorption begins to take place within a narrow mass transfer zone at the entrance of the column. The energy that is released due to adsorption, heats the adsorbent particles as well as the gas within the bed and the column walls near the entrance of the column. Some of the energy that is released will be transferred through convection and axial heat diffusion which begins to warm the downstream column contents. By the time the mass transfer zone has moved down the bed to the downstream sampling ports, the adsorbent particles have already been heated partially due to the energy carried from the upstream sections of the bed due to convection. The heat losses at the end section of the small size adsorber bed also contribute to higher temperatures observed for the second and third peaks. High heat losses are representative of lab scale adsorbers when compared to industrial size adsorbers since they would have a high surface area for heat loss to volume ratio [33]. When energy is released due to adsorption in this section of the bed, a higher peak is attained. This release of energy that is carried along the length of the column also explains the presence of tailing particularly for the experiments in which no cooling is present. When cooling is conducted, less tailing is evident. The coolant provides a higher driving force for energy transfer through the walls of the column due to a larger temperature gradient as opposed to along the length of the column.

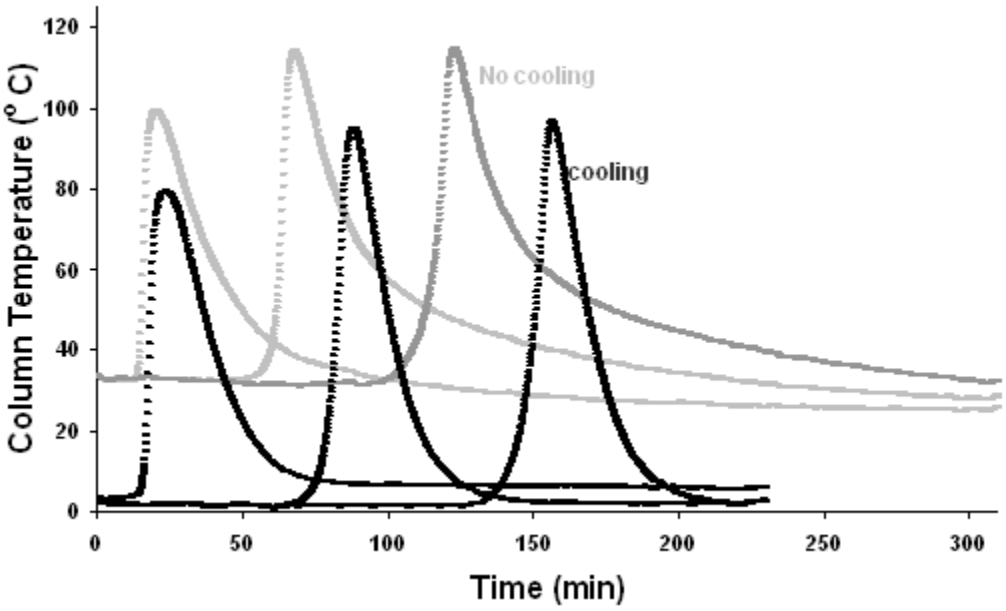

Figure 5a – Effect of cooling/no cooling during adsorption cycle on temperature fronts in column (4 SL/min) for CO_2 adsorption (10% CO_2 bal. N_2) with 13X adsorbent at 6.44 atm column pressure. Dark lines indicate the presence of a coolant at 0^oC while grey lines represent experimental runs in the absence of the coolant.

Similar results were obtained for a higher feed flow rate of 6.6 SL/min as observed in Figure 5b. Temperatures obtained were higher for 6.6 SL/min run, since the quantity of CO_2 being fed into the column was greater than at 4 SL/min (Figure 5a). A higher feed flow also signified a larger Reynolds number and thus a higher mass transfer coefficient which resulted in faster adsorption and thus a higher temperature.

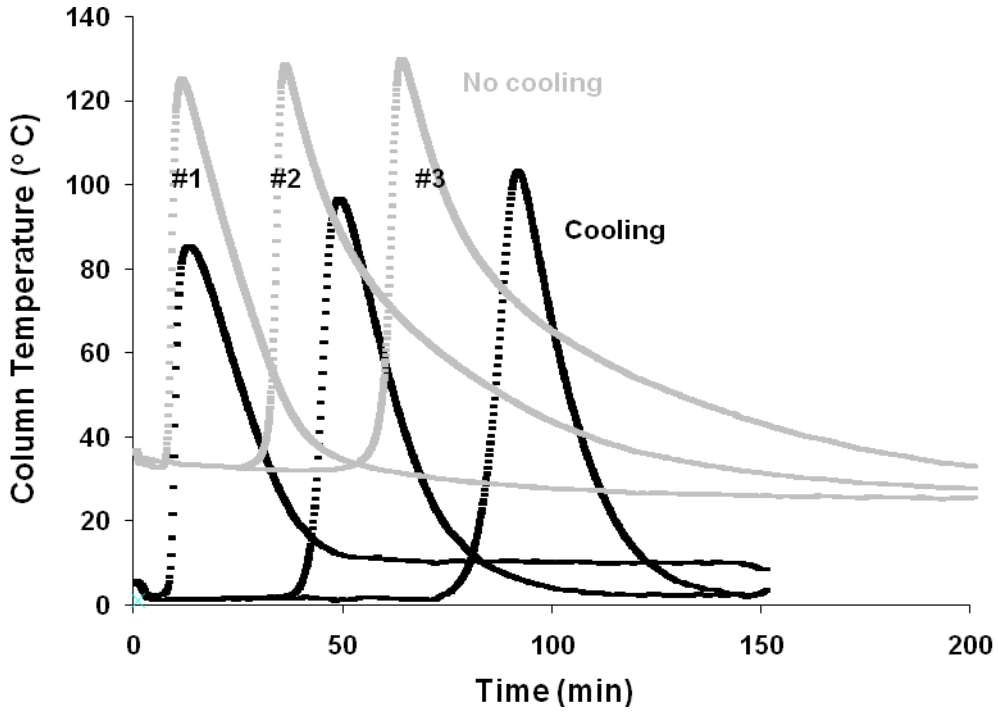

Figure 5b – Effect of cooling during adsorption cycle on temperature fronts in the column for CO_2 adsorption (10% CO_2 bal. N_2) with 13X adsorbent at 6.44 atm column pressure and 6.6 SL/min feed flow-rate. Dark lines indicate the presence of a coolant at 0^oC while grey lines represent experimental runs in the absence of the coolant.

4.4 Modelling

For an experimental feed flow rate of 6.6 SL/min, a constant column pressure of 6.44 atm (absolute) and a feed composition of 10% CO_2 and 90% N_2, samples were obtained at three different positions along the length of the packed column and analysed for their composition by a gas chromatograph (GC) by using the multiposition valve. The experimental concentration vs. time plots obtained for different positions in the column are given in Figure 6 and compared to the same plots from modelling. This figure clearly

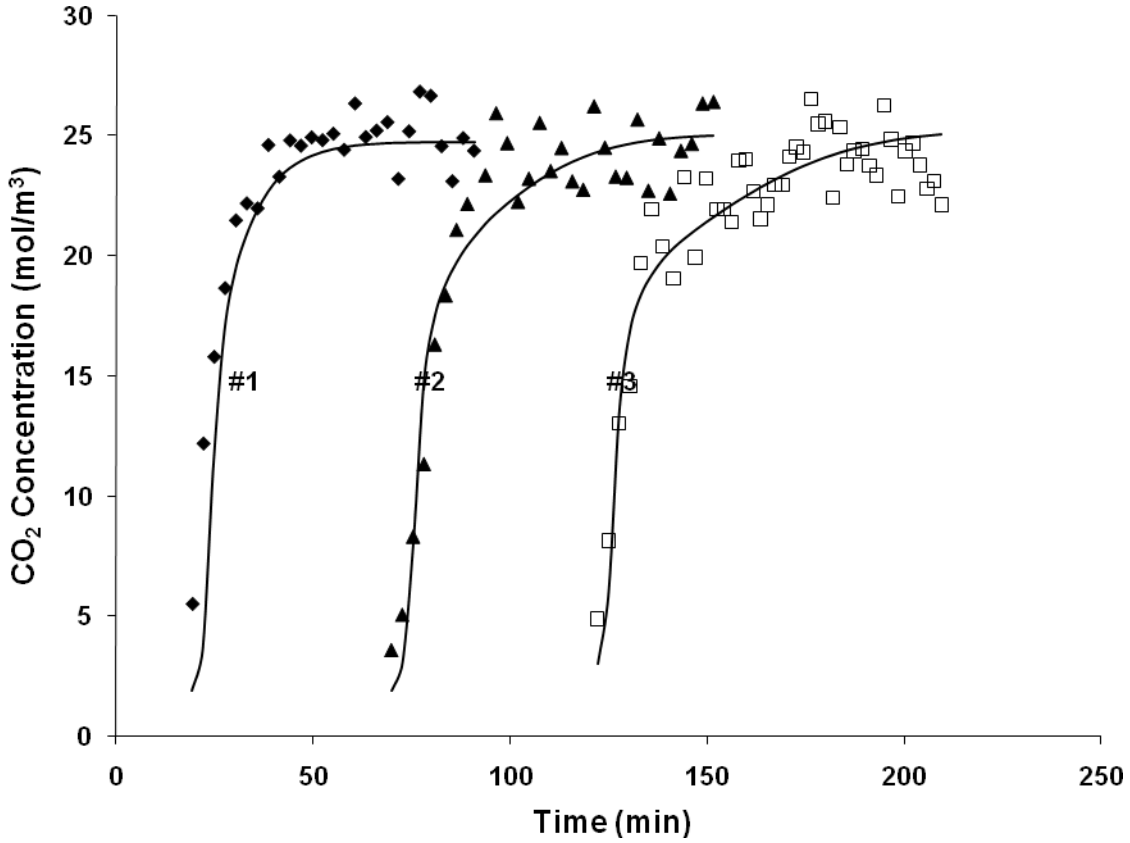

Figure 6 - Concentration profiles at three different locations along the packed adsorption column for CO_2 adsorption from 10% CO_2 bal. N_2 mixture with 13X adsorbent at 6.44 atm column pressure and 6.6 SL/min flow-rate. Points represent experimental data while solid lines represent model fits.

shows that the experimental data are very well represented by the two-population model at all three ports for the duration of the experiment. The experimental data display a significant amount of "tailing" when the feed concentration is approached. Tailing is a common observation in breakthrough experiment in liquid and gas systems [34]. Within the porous adsorbent pellets, there exists a distribution of pores ranging from micro-pores to macro-pores. Typically, the macro-pores which are larger in size are the first to fill with the adsorbate feed gas. The micro-pores which are smaller in diameter tend to fill at slower rates. This difference in the rate of diffusion causes a proportion of the adsorbent sites to remain unsaturated while the other proportion of easily accessed sites saturates quicker. Due to the slower rate at which the pores get saturated, also, since most of adsorption uptake happens in the smaller pores, the width of the mass transfer zone is extended causing the "tailing" characteristics observed in many adsorption systems.

The two-population adsorbent pellet model appears to adequately describe the tailing that is present in the experimental data. The proposed model is considerably less complex in terms of computational resources required to solve the system of differential equations and the type of experiments which are required to determine the intra-crystalline diffusivity.

The temperature changes in the column were also obtained by taking temperature measurements using thermocouples at the same three positions along the length of the packed bed as the concentration measurements. For the experimental conditions of 6.6 SL/min feed flow rate, a constant column pressure of 6.44 atm (absolute) and a feed composition of 10% CO_2 and 90% N_2, the temperature changes measured at three ports in the column along with the predicted model fits are displayed in Figure 7.

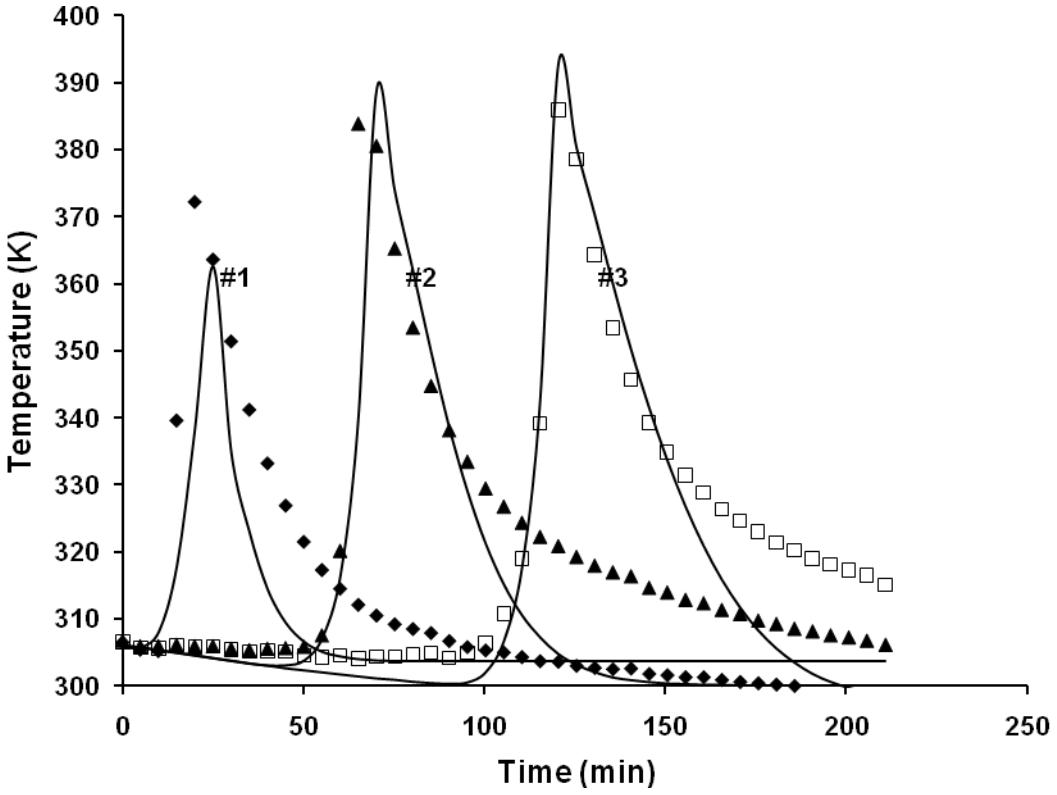

Figure 7 - Temperature profiles at three different locations along the packed adsorption column for CO2 adsorption (10% CO2 bal. N2) with Ceca 13X adsorbent at 6.44 atm column pressure and 6.6 SL/min flow-rate. Points represent experimental data while solid lines represent model fits.

The model predicts the breakthrough time associated with the sharp temperature rise at each port very well. However, the amplitude and the curvature of the temperature changes were not matched exactly. This observed deviation may be caused by use of a constant heat of adsorption for CO_2 in the model and common with gas adsorption systems [24, 35-37].

Figure 8 combines the plots of concentration breakthrough (from Figure 6) and temperature breakthrough profiles (from Figure 7) along the length of the column. Temperature and concentration measurements were performed at the same location in the column. Since there were three different ports, measurements were done at three different positions along the length of the column. This figure clearly shows that the temperature front moves slightly ahead of the concentration front, while concentration breakthrough is observed approximately at the peak of the temperature as the feed gas moves from the column inlet to the outlet.

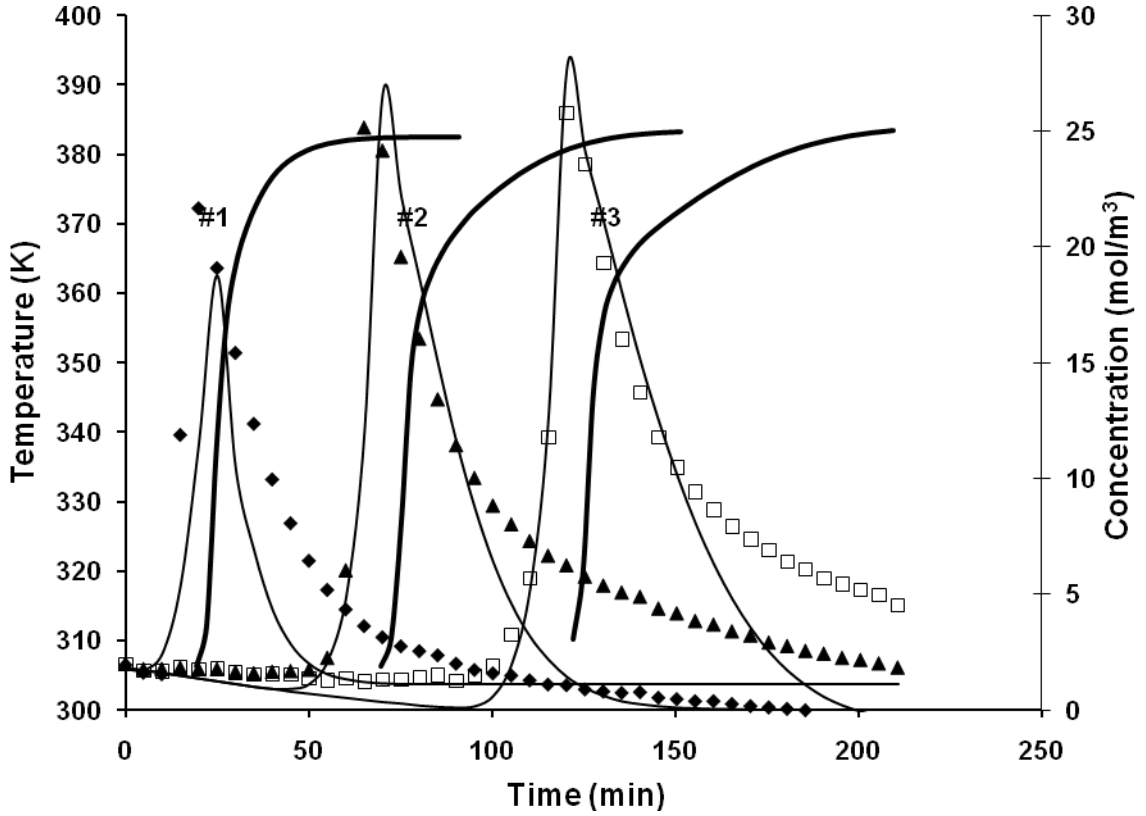

Figure 8 - Temperature and concentration breakthrough at three different locations along the packed adsorption column for CO2 adsorption from a 10% CO2 bal. N2 mixture with 13X adsorbent at 6.44 atm column pressure and 6.6 SL/min flow-rate. Points represent experimental data while solid lines represent model fits

This observation is very significant since it suggests that concentration breakthrough in a column could be easily detected by using thermocouples only. In the case of gas mixtures that exhibit significant heat effects, thermocouples can be used as an indirect method of predicting the concentration breakthrough. An expensive concentration measurement device would not be needed. Similar behaviour was observed for the experimental run with the feed flow rate of 4 SL/min.

By establishing a model which can predict the mass and heat transfer within the fixed bed, we have shown that we can depend on the movement of heat transfer zone in our application and use this to infer about the state of the composition within the packed bed adsorber.

5.0 Conclusions

1. Heat effects are significant for a bulk carbon dioxide separation from a gas mixture of 10 % CO_2 (by vol) in N_2 using Ceca 13X adsorbent.
2. The breakthrough time of Ceca 13X adsorbent is independent of the initial bed temperature resulting in a significant economic advantage without affecting the adsorption performance.
3. An earlier breakthrough time was observed for a higher feed flow rate of 6.6 SL/min compared to 4 SL/min.
4. Cooling during the adsorption cycle decreases the mass transfer zone and leads to a longer breakthrough time.
5. By using the two population model, the curvature of the concentration breakthrough curve including the noted tailing was predicted with good accuracy.
6. The prediction of the energy profile was less accurate by the model. However, the point at which the temperature breakthrough occurs is estimated with good accuracy which is the most important factor for industrial applications.
7. Using online measurements of temperature in the column bed, can predict the concentration breakthrough for mixtures and adsorbents exhibiting high heat effects.

6.0 Acknowledgements

Financial supports received from Ontario Centres of Excellence (OCE), RioTinto Alcan and Air Products & Chemicals Inc., are gratefully acknowledged.

7.0 Nomenclature

Symbols

C_B Concentration of gas in the bulk phase ($mol.m^{-3}$)

C_{FEED} Concentration of the feed ($mol.m^{-3}$)

C_p Concentration in the mobile phase of the pellet ($mol.m^{-3}$)

C_{pG} Heat capacity of the gas ($J.kmol^{-1}.K^{-1}$)

C_{ps} Heat capacity of the adsorbent ($J.kg^{-1}.K^{-1}$)

C_{pw} Heat capacity of the column wall ($J.kg^{-1}.K^{-1}$)

d_1 Internal diameter of the column (m)

d_2 External diameter of the column (m)

D_M Molecular diffusion coefficient of CO_2 in N_2 ($m^2.s^{-1}$)

D_p Particle diameter (m)

D_x Effective diffusion coefficient of the easily accessed sites of the adsorbent ($m^2.s^{-1}$)

D_y Effective diffusion coefficient of the difficultly accessed sites of the adsorbent ($m^2.s^{-1}$)

D_z Axial diffusion coefficient ($m^2.s^{-1}$)

g Acceleration due to gravity (9.81 $m.s^{-2}$)

ΔH Heat of adsorption ($J.mol^{-1}$)

h_f Heat transfer coefficient between gas and wall ($W.m^{-2}.K^{-1}$)

h_o Heat transfer coefficient between wall and surroundings ($W.m^{-2}.K^{-1}$)

j_D Chilton-Colburn j-factor for mass transfer

j_h Chilton-Colburn j-factor for heat transfer

k_f External film mass transfer coefficient ($m.s^{-1}$)

k_g thermal conductivity of gas ($W.m^{-1}.K^{-1}$)

k_{gs} Bulk thermal conductivity of pellet (including pores) ($W.m^{-1}.K^{-1}$)

k_w Thermal conductivity of the column wall ($W.m^{-1}.K^{-1}$)

L Column length (m)

M Molecular weight ($g.mol^{-1}$)

Nu Nusselt number (dimensionless)

P Total pressure (atm)

Pr Prandtl number (dimensionless)

q Adsorbed phase concentration on the solid (adsorbent) ($mol.kg^{-1}$)

q_F Solid phase adsorbate concentration at the feed conditions ($mol.kg^{-1}$)

q_{pl} Solid phase adsorbate concentration at plateau temperature ($mol.kg^{-1}$)

q Equilibrium loading (or) the amount adsorbed (mmol/g)

r Distance in the radial position of the pellet or the packed column (m)

r_b Bed radius (m)

r_p Pellet radius (m)

Ra	Rayleigh number (dimensionless)
Re	Reynolds number (dimensionless)
Sc	Schmidt number (dimensionless)
Sh	Sherwood number (dimensionless)
t	Time (s)
T	Temperature (K)
T_a	Ambient temperature (K)
T_{bg}	Temperature of the bulk gas (K)
T_F	Feed temperature (K)
T_p	Pellet temperature (K)
T_{pl}	Plateau temperature (K)
T_w	Wall temperature (K)
u_G	Superficial velocity ($m.s^{-1}$)
y_F	Component molar fraction at the feed conditions (dimensionless)
z	Distance in the axial direction (m)

Greek letters

β	Volumetric thermal expansion coefficient (equal to T^{-1}) (K^{-1})
ε_c	Bed void (m^3 void.m^{-3} bed)
ε_p	Pellet void fraction (m^3 void.m^{-3} pellet)
ε_t	Total void fraction. $\varepsilon_t = \varepsilon_c + (1-\varepsilon_c)\varepsilon_p$
ρ_B	Bulk density of the adsorbent (kg adsorbent.m^{-3} bed)
ρ_G	Gas mixture density ($kg.m^{-3}$)
ρ_p	Density of the pellet ($kg\ .m^{-3}$)
ρ_S	Solid density (kg solid.m^{-3} solid)
ρ_w	Column wall density ($kg\ .m^{-3}$)
μ_G	Viscosity of gas mixture(Pa.s)
σ	Collision diameter of Lennard Jones (Å)
Ω	Collision integral (dimensionless)

ψ Prandtl number function (dimensionless)

Abbreviations

CCS Carbon dioxide capture and storage

CPC Concentration pulse Chromatography

CO_2 Carbon dioxide

FacX Weighting factor

GC Gas Chromatograph

IEA International Energy Agency

MC Mixing chamber

min Minute

MFC Mass flow controller

NDIR Non dispersive infrared analyzer

N_2 Nitrogen

PID Proportional-Integral-Derivative

SL Standard Litres

SSR Sum of square residuals

UHP Ultra high purity

vol volume

WPFF Working Party on Fossil Fuels

ZET Zero emission technologies

Subscripts

ads adsorption

g gas

A Component A

B Component B

AB Binary component AB

8.0 References

1. International Energy Agency Working Party on Fossil Fuels, "Solutions for the 21st century: Zero emissions technologies for fossil fuels", OECD/IEA, Paris, FR, 1-50, (2002).
2. International Energy Agency Working Party on Fossil Fuels, " CO_2 capture at power stations and other major point sources", OECD/IEA, Paris, FR ,1-12, (2003).
3. Zhang, J., Webley, P.A., and Xiao, P., "Effect of process parameters on power requirements of vacuum swing adsorption technology for CO_2 capture from flue gas", Energy conversion and management, 49, 346-356 (2008).
4. Franchi, R.S., Harlick, P.J.E., and Sayari, A., "Applications of Pore-Expanded Mesoporous Silica. 2. Development of a High-Capacity, Water-Tolerant Adsorbent for CO_2" Ind. Eng. Chem. Res., 44, 8007-8013 (2005).
5. Reynolds, S.P., Mehrotra, A., Ebner, A.D., and Ritter, J.A., "Heavy reflux PSA cycles for CO2 recovery from flue gas: Part I. Performance evaluation", Adsorption, 14, 399-413 (2008)
6. De Witt, J.J., "Recovery of pure CO_2 from flue gases", World Intellectual Property Organization PCT Application WO 02/09849 A2 (2002)
7. Reynolds, S.P., Ebner, A.D., and Ritter, J.A., "New pressure swing adsorption cycles for carbon dioxide sequestration", Adsorption., 11, 531-536 (2005)
8. Li, P and Tezel, F.H., "Adsorption Separation of N_2, O_2, CO_2 and CH_4 Gases by β-Zeolite", Microporous & Mesoporous Materials, 98, 94-101 (2007).
9. Keefer, B. G., J. A. Sawada, E. P. Johannes, S. Roy and M. J. Brown, "Systems and Processes for Providing Hydrogen to Fuel Cells", World Intellectual Property Organization 02/35632 (2002).
10. Ma, X., L. Sun and C. Song, "A New Approach to Deep Desulfurization of Gasoline, Diesel Fuel and Jet Fuel by Selective Adsorption for Ultra-Clean Fuels and for Fuel Cell Applications", Catalysis Today 77, 107-116 (2002)

11. Ruthven, M., Farooq, S., Knaebel, K., "Pressure swing adsorption", John Wiley and Sons Inc., 5-93, (1994).
12. Ruthven, D. M., "Principles of Adsorption and Adsorption Processes", John Wiley and Sons, Inc., New York, NY, 1-433, (1984).
13. Harlick, P.J.E and F.H. Tezel, "An experimental adsorbent screening study for carbon dioxide removal from nitrogen" Microporous Mesoporous Materials. 76, 71-79 (2004).
14. Yon, C.M., and Sherman, J. D., "Adsorption", Kirk Othmer Encyclopaedia of Chemical Technology, John Wiley and Sons (2003)
15. Birbara, P.J., Filburn, T.P., H. Michels and T.A. Nalette, "Sorbent system and method for adsorbing carbon dioxide from the atmosphere of a closed habitable environment", U.S. Patent 6364938 (2002).
16. Kanazirev, V.I., and D.J. Latus, "Composite adsorbents for Air Purifiction", U.S. Patent 6638340 (2003).
17. Xu, X., Song, C., Andressen, J.M., B.G. Miller and A. W. Scaroni, "Preparation and characterization of novel CO_2 molecular basket adsorbents based on polymer modified Mesoporous molecular sieve MCM-41", Microporous Mesoporous Mater. 62, 29-45 (2003).
18. Mulgundmath, V.P., Tezel, F.H, Feifei, H and Golden, T.C., "Binary adsorption behaviour of methane and nitrogen gases", accepted to be published in J. Porous Mater.
19. Mulgundmath, V.P., Tezel, F.H, Saatcioglu, T and Golden, T.C., "Adsorption and separation of CO_2/N_2 and CO_2/CH_4 by 13X zeolite", accepted to be published in Canadian Journal of Chemical Engineering (2011).
20. Ko, D., Kim, M., and Moon, I., "Novel Thermal Swing Adsorption Process with a Cooling Jacket for Benzene-Toluene-*p*-Xylene Purification", Ind. Eng. Chem. Res. *40,* 4973-4982 (2001).
21. Chou, C.T., and Chen, C.Y., "Carbon dioxide recovery by vacuum swing adsorption", Separation and Purification Technology, 39, 51-65 (2004).

22. Wakao, N., Funazkri, T., “Effect of Fluid Dispersion Coefficients on Particle-to-Fluid Mass Transfer Coefficients in Packed Beds.” Chem. Eng. Sci. 33, 1375-1384 (1978).
23. Welty, J.R., Wicks, C.E., Wilson, R.E., and Rorrer, G., “Fundamentals of Momentum, Heat and Mass Transfer”, John Wiley and Sons, New York, (2000).
24. Cavenati, S., Grande, C.A., and Rodrigues, A.E., “Layered Pressure Swing Adsorption for Methane Recovery from $CH_4/CO_2/N_2$ Streams**”,** Adsorption, 11, 549-554 (2005).
25. A.F. Mills, Heat Transfer, Second edition, Prentice Hall, Inc., NJ, USA.
26. Warmuzinski, K and Tanczyk, M., “Multi component pressure swing adsorption. Part I. Modelling of large scale PSA installations”, Chemical Engineering and Processing, 36, 89-99 (1997).
27. Chilton, T. H. and Colburn, A. P., “Mass Transfer (Absorption) Coefficients Prediction from Data on Heat Transfer and Fluid Friction”, Ind. Eng. Chem., 26, 1183-1187 (1934).
28. Churchill, S. W., and Chu, H.H.S., “Correlating equations for laminar and turbulent free convection from a vertical plate” Int. J. Heat Mass Transfer, 18, 1323-1329 (1975).
29. Grande, C.A., and Rodrigues, A.E., “Electric Swing Adsorption for CO_2 removal from flue gases”, International Journal of Greenhouse gas control, 2, 194-202 (2008).
30. Delgado.J.A., Uguina, M.A., Sotela, J.L., and Ruiz, B., “Fixed Bed adsorption of carbon dioxide-helium, nitrogen-helium and carbon dioxide-nitrogen mixtures onto silicalite pellets”, Separation and Purification Technology, 49, 91-100 (2006).
31. Basmadjian, D., “On the possibility of omitting the cooling step in thermal gas adsorption cycles”, The Canadian Journal of Chemical Engineering, 53, 234-238 (1975).
32. Clausse, M., Bonjour, J., and Meunier, F., “Adsorption of gas mixtures in TSA adsorbers under various heat removal conditions”, Chemical Engineering Science, 59, 3657-3670 (2004).

33. Mérel, J., Clausse, M., and Meunier, F., "Experimental Investigation on CO_2 Post-Combustion Capture by Indirect Thermal Swing Adsorption Using 13X and 5A Zeolites", Ind. Eng. Chem. Res. 47, 209-215 (2008).
34. Jones, R., Tezel, F.H. and Thibault, J. "Simulation and validation of ethanol removal from water in an adsorption packed bed: isotherm and mass transfer parameter determination in batch studies", Canadian Journal of Chemical Engineering, 88, 889-898 (2010).
35. Kim, M.B., Bae. Y.S., Choi, D.K., and Lee, C.H., "Kinetic separation of landfill gas by a two-bed pressure swing adsorption process packed with carbon molecular sieve: Non isothermal operation, Ind.Eng. Chem. Res., 45, 5050-5058, (2006).
36. Chue, K. T., J. N. Kim, Y. J. Yoo, S. H. Cho and R. T. Yang, "Comparison of Activated Carbon and Zeolite 13X for CO_2 recovery from flue gas by Pressure Swing Adsorption", Industrial and Engineering Chemistry Research 34, 591-598 (1995).
37. Kim, J., Chue, K., Kim, K., Cho, S., Kim, J., "Non-isothermal adsorption of nitrogen-carbon dioxide mixture in a fixed bed of zeolite-X, J. Chem. Eng. Japan., 27 (1), 45-51 (1994).

Appendix A.2

Microwave regeneration of activated carbon Adsorbents in the production of bioethanol

While the technology of fermenting bio-waste to produce a useable liquid fuel has great potential, there remain technical issues which currently hold back the widespread use of bioethanol as a fuel alternative. Due to ethanol product inhibition, low ethanol yields (3 - 5 wt %) are realized in bioreactors. Because of the relatively small amount of ethanol produced, a distillation separation is required to produce fuel grade ethanol. While the distillation is an effective means of performing the separation, it is not energy efficient and the presence of an azeotrope complicate the separation.

In order to improve the economics of the process, researchers have suggested continuous extraction of ethanol to partly alleviate inhibition. One potential method to reduce product inhibition is to employ the use of an external adsorption column.

The idea is to remove a portion of the fermentation broth and pass it thorough a packed adsorption column. The ethanol would be preferentially loaded into the adsorbent structure as it travels along the length of the column. The broth with lowered ethanol concentration would be returned to the reactor. It is believed this would reduce the inhibition and allow fermentable sugars to be converted into ethanol. Also, the ethanol in the pores of the adsorbent could later be recovered as highly concentrated ethanol product. It is suggested that adsorption technology be used as a precursor to the distillation in order to concentrate the feed in a more economical fashion.

The use of adsorption technology is attractive and is recognized as a process with lower operating costs. However, difficulties still exist. The recovery of ethanol from the pores of the adsorbent once the column has been saturated has proven to be challenging as is the case for most desorption of valuable product. Desorption or regeneration of the

adsorbent is typically performed by lowering the pressure (vacuum accompanied by a sweep gas) or increasing the temperature (steam, hot sweep gas, electrical heating). However, more economical desorption technologies may exist. The use of microwaves to conduct efficient heating to vaporize/desorb the ethanol has to this point been researched on a very limited basis. Microwaves use electromagnetic energy (2450 kHz in North America) to heat dielectric materials. The mechanism of heating depends on the size, shape and properties of the material (Menéndez et al., 1999). The dominant mechanism releases heat is re-orientation loss, a dissipation of heat that is related to the polarity of the substance.

Penetration depth of the microwaves depends on the frequency of the electromagnetic radiation source, as well as the dielectric load that is to be heated. The penetration depth of the microwaves is often very limited, of the order of a few centimetres. For this reason, microwave heating is often non-uniform, with the highest temperatures being reached on the outside of the load being heated and heating being transferred through the load by conduction, convection and radiation. The non-uniform heating of materials is the single biggest design challenge when industrial microwave processes are implemented (Bradshaw et al., 1998)

Microwave heating has been employed in various mineral processing applications. The carbon in pulp process (CIP) which is used for the recovery of gold is one example. In this process, gold-cyanide molecules are concentrated on the surface of activated carbon and later removed by elution. The carbon bed still contains flotation reagents. Typically, these reagents have been removed in a kiln furnace (gas or electric). Both of these methods rely on indirect heating to desorb the flotation reagents. Using microwave direct heating of the activated carbon can be achieved. Pilot studies have shown that microwaves are effective in desorbingflotation reagents from the surface of the carbon. Pilot plant tests by Barrick's Holt-McDermott gold mine in Ontario found that microwave desorption was more energy efficient than conventional desorption technology. The pilot study also showed that activated carbon regenerated using

microwaves had higher capacity on subsequent cycles than activated carbon regenerated by conventional means (Bradshaw et al., 1998)

1.0 Objectives of the study and preliminary results

It was desired to explore the potential of microwaves to provide efficient heating to desorb ethanol and to determine if the regenerated activated carbon could be used for multiple cycles. To achieve these objectives, a series of simple experiments were devised in order to evaluate the technical feasibility of ethanol desorption using microwaves. Activated carbon was saturated with ethanol in a packed adsorption column (feed concentration of 60 g EtOH/L). In each case, the capacity of the carbon was measured and compared to a previously published ethanol isotherm (for virgin activated carbon). Following saturation, the column underwent microwave desorption in a conventional microwave oven. The adsorption-desorption of ethanol in the packed column was continued for five complete cycles. Figure A.2.1 shows the measured ethanol adsorption capacity of the activated carbon for each of the five cycles. The data is plotted alongside the isotherm (solid line) for virgin activated carbon (Jones et al., 2010).

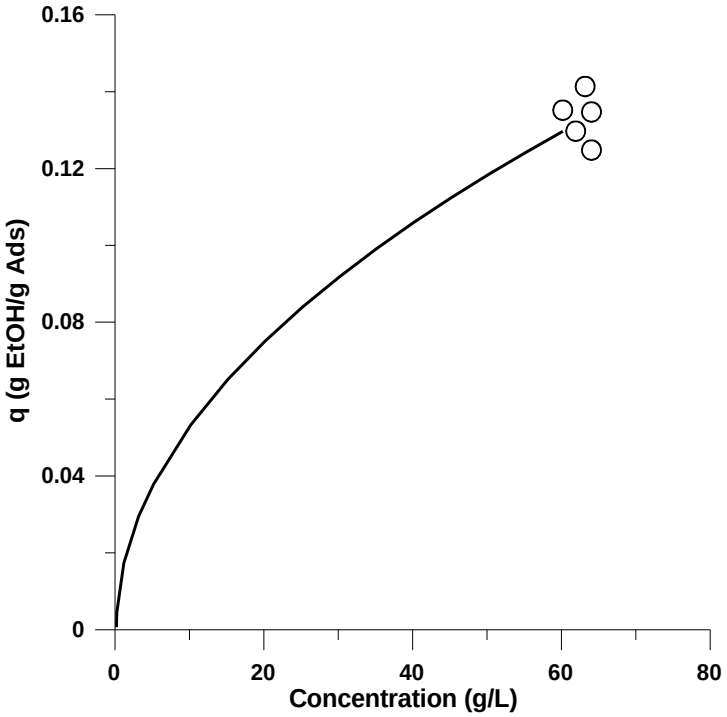

Figure 1 - Measured capacity of five consecutive adsorption runs (following successive microwave desorption runs). Line represent Freundlich Fit from Jones et al., 2010

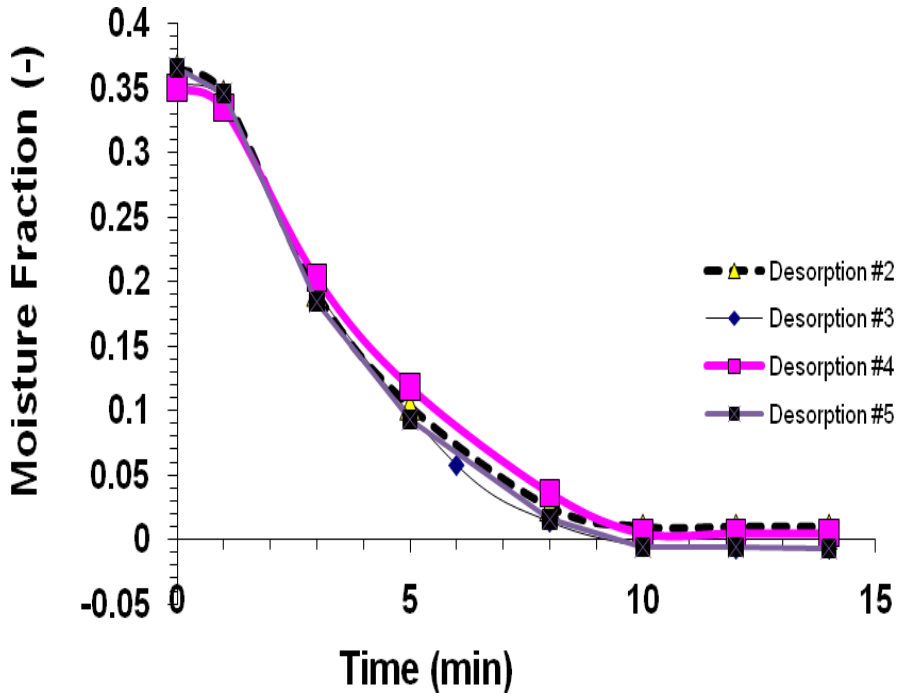

Figure 2 - Moisture fraction of column undergoing microwave desorption as a function of time for desorption cycles 2 through 5.

Complete desorption of ethanol was achieved for each cycle in approximately 10 minutes. The general trend for desorption was a slow desorption when the microwave was started as the activated carbon within the bed as well as the residual liquid is heated. Once the bed reaches a sufficiently high temperature, the unbound liquid molecules can easily evaporate and leave the column. As the application of microwaves continue the amount of liquid left to desorb is lower and the rate of desorption declines. Towards the end of the desorption cycle the most strongly bound molecules are desorbed.

The search for alternative energy sources is a globally relevant issue. Bioethanol from lignocellulosic biomass has great potential but an improvement in the separation technology is required. Selective extraction using adsorbents has been researched. However, a suitable desorption technology needs to be devised to make the process viable. This study confirms that microwaves are effective in regenerating activated carbon that is saturated with ethanol. However, a relevant design is required for further experimentation. Although effective in regenerating small quantity of activated carbon, it should be noted that microwave technology is expensive as most industrial system require custom design. In addition, the regeneration of an industrial-size adsorption bed using microwaves represents a significant challenge.

2.0 References

1. Menéndez, J.A., Menéndez, E.M., Garcia, A., Parra, J.B., Pis, J.J., 1999. Thermal treatment of activated carbons: comparison between microwave and electrical heating. *Inter. Microwave Power.* 34 (3), 137-143.
2. Bradshaw S.M., van Wyk, E.J., de Swardt, J.B., 1998. Microwave heating principles and the application the regeneration of granular activated carbon. *The Journal of South African institute of mining and metallurgy.* 98 (4), 201-210.

Appendix A.3

Additional data

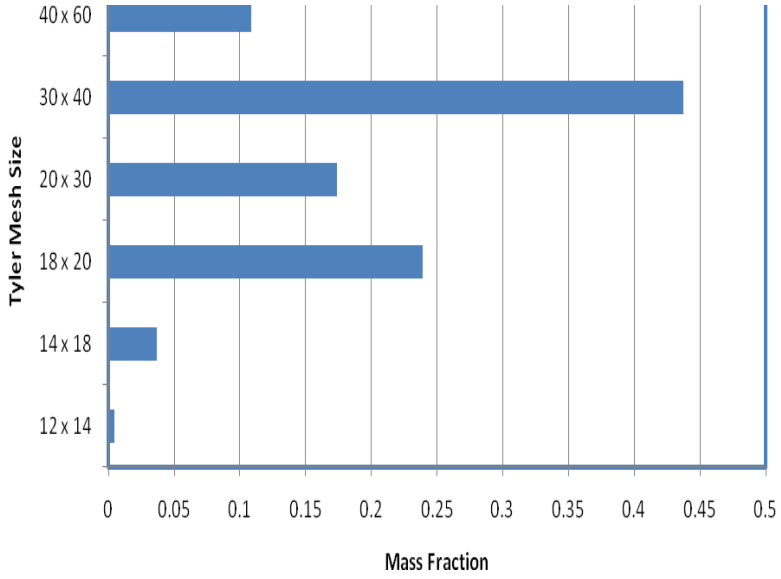

Figure 1: Particle size distribution of F-600 activated carbon acquired from Calgon Corporation.

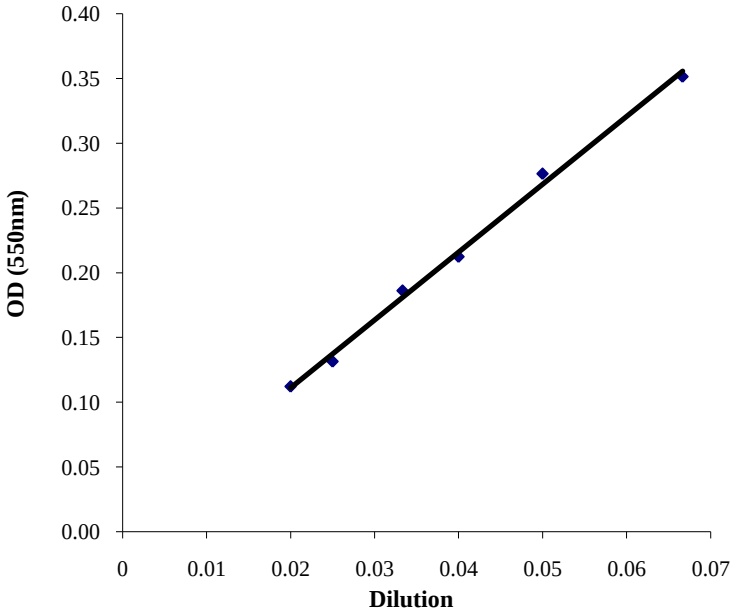

Figure 2: Optical density (OD_{550nm}) of a series diluted fermentation broth samples which were obtained after 6 h cultivation of *Escherichia coli* KO11.

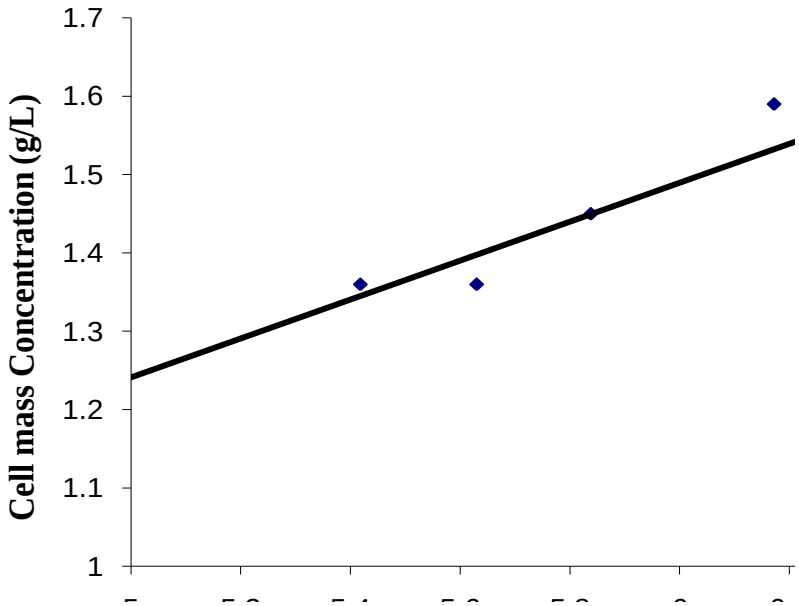

Figure 3: Calibration curve between the dry cell mass and the OD_{550nm} measured using a spectrophotometer.

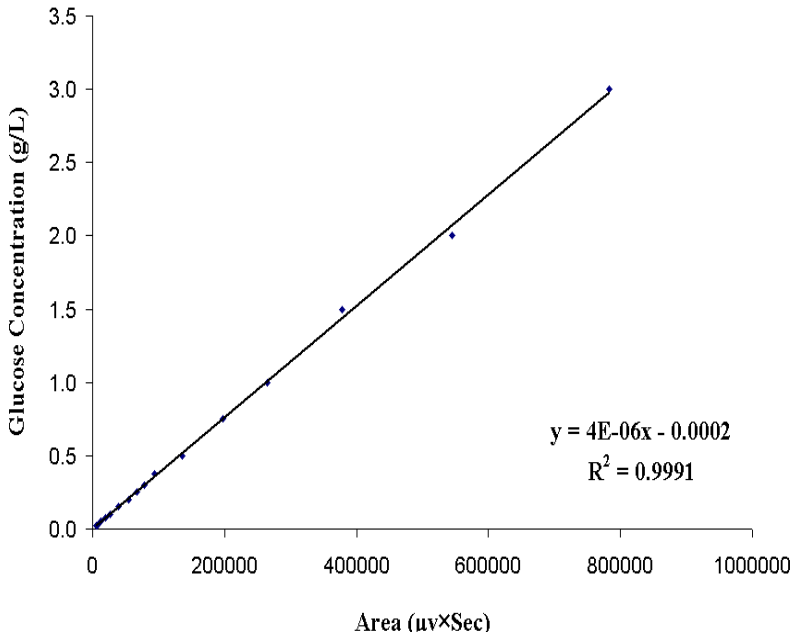

Figure 4: Glucose concentration vs. response area of chromatogram shown for a series of standards

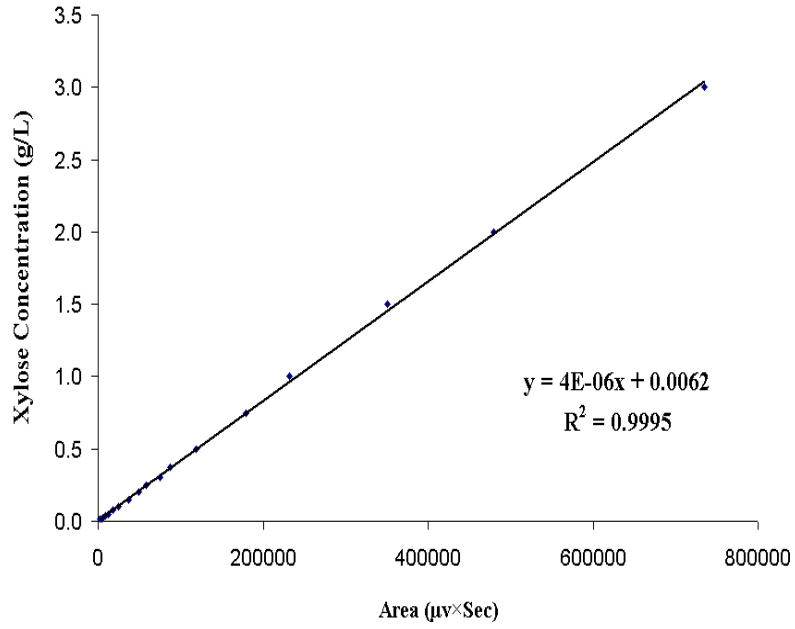

Figure 5: Xylose concentration vs. response area of chromatogram shown for a series of standards

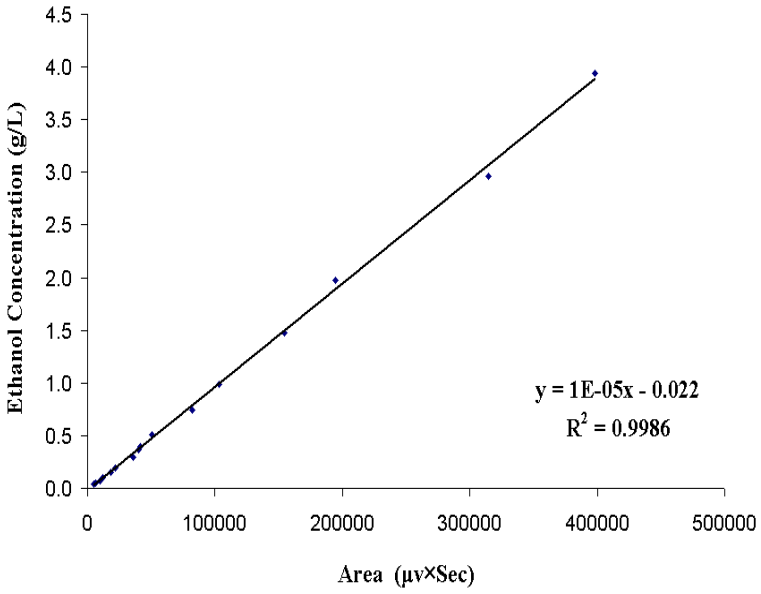

Figure 6: Ethanol concentration vs. response area of chromatogram shown for a series of standards

Appendix A.4

C.V. information

1.0 Paper in refereed journals (Full papers)

1. Jones, R.A., Tezel, F.H., Thibault, J., and Tolan, J.S., 2007, Bioethanol production to be blended with gasoline: Improvements in energy use by adsorption. *Inter. J. of Ener. Res.* 31 (15), 1517-153
2. Jones, R. A., Tezel, F.H., Thibault, J., 2010, Simulation and Validation of Ethanol Removal from Water in an Adsorption Packed Bed: Isotherm and Mass Transfer Parameter Determination in Batch Studies. *Can. J. Chem. Eng.* 88 (5), 889 – 898
3. Jones, R. A., Thibault, J., Tezel, F.H., 2011. Enhanced ethanol production through selective adsorption in bacterial fermentation. *Biotechnol. Bioprocess Eng.* 16 (3), 531-541
4. Morse, G., Jones, R., Thibault, J., Tezel, F.H., 2011, Neural network modelling of adsorption isotherms. *Adsorption.* 17 (2), 303-309
5. Mulgundmath, V.P, Jones, R. A., Tezel, F.H., Thibault, J., 2011, Fixed bed adsorption for the removal of carbon dioxide from nitrogen: breakthrough behaviour and modelling for heat and mass transfer. *Sep. Pur. Technol.*, In press
6. Jones R. A., Thibault, J., Tezel F. H., "Modelling and validation of the continuous production of ethanol with intermittent extraction using a packed bed adsorption column." *App. Eng (submitted:APEN-D-12-00084)*

2.0 Papers in conference proceedings (refereed full papers)

7. R. Jones, F.H. Tezel, and J. Thibault, "Simulating Multi-Component Liquid Phase Adsorption Systems: Ethanol and Residual Sugar", Proceedings of International Green Energy Conference to be held in Eskisehir, Turkey, June 5-9, 12 pages (2011)

8. Jones, R.A., J. A. Gandier, J. Thibault, and F. H. Tezel, "Enhanced ethanol production through selective adsorption in bacterial fermentation", ECOS Conference proceedings, held in Lauzon, 22 pages (June 2010)
9. Jones R., Thibault J., Tezel F.H. and Tolan J.S. "Renewable Energy from Ethanol: Process Improvement Through Selective Adsorption." Proceedings of the XXII Interamerican Congress of Chemical Engineering, Buenos Aires, Argentina, Oct 4 - 10, 19 pages (2006)
10. R. Jones, F.H. Tezel, J. Thibault and J.S. Tolan, "Enhancement of Bio-Ethanol Production by Adsorption", Proceedings of the 2nd International Green Energy Conference (IGEC-2) held in Oshawa, Ontario, Canada, 11 pages (2006)

3.0 Papers in conference proceedings (Abstracts only)

11. Jones, R., Gandier, J.A., Tezel, F.H., and Thibault, "Enhanced production of bioethanol using *E. coli* KO11 with online ethanol extraction by adsorption", presented at the *10th International Conference on Fundamentals of Adsorption* held in Awaji, Hyogo, Japan, May 23-28, 2010
12. Jones, R., Hashi, M., Gandier, J.A., Tezel, F.H., and Thibault, "J. Producción de bioetanol a partir de la biomasa lignocelulosa", presented at *Congreso Nacional de Ingeniería Química de Perú. Trujillo*, Perú, September 28 - October 5, 2009
13. Jones R.A., Gandier, J.A., Tezel F.H., Thibault J., and Poupore, J. "Adsorption of Ethanol from Fermentation Broth: Breakthrough and Equilibrium Behaviour", presented at the *8th World Congress of Chemical Engineering*, Montreal, Canada, August 23-27, 2009
14. Jones R., Gandier J.A., Tezel F.H. and Thibault J. "Enhanced bioethanol production: immobilized *E. coli* KO11 with on-line ethanol extraction activated carbon", presented at *University Industry Partnerships for the Development of Clean Technologies*, Ottawa, Ontario, June 9, 2009
15. Jones, R., J. Poupore, F.H. Tezel, and J. Thibault, "Competitive Ethanol Adsorption: Equilibrium and Dynamic Multi-solute Adsorption Behaviour" , presented at the *58th Canadian Chemical Engineering Conference* held in Ottawa, Ontario, October 19-22, 2008

16. Jones, R., F.H. Tezel, and J. Thibault, "Enhanced Bioethanol Production via Adsorption – Mass Transfer Modelling and Recovery Techniques", presented at the *AIChE Annual meeting* in Salt Lake City, Utah, November 4-9, 2007
17. Jones, R., F.H. Tezel, and J. Thibault, "Enhanced Bioethanol Production via Adsorption – Mass Transfer Modelling and Recovery Techniques", presented at the *57th Canadian Chemical Engineering Conference* in Edmonton, Alberta, October 28-31, 2007
18. Jones R., Tezel F.H. and Thibault J., "In Situ Bioethanol Removal Using a Packed Bed Adsorber", presented at the *13th European Congress on Biotechnology* in Barcelona, Spain, September 16-19, 2007
19. Jones, R., F.H. Tezel, J. Thibault, and J.S. Tolan, "Modelling and Simulation of Dynamic Bioethanol Adsorption", presented at the *AIChE Annual meeting* in San Francisco, California, USA, November 12-17, 2006
20. R. Jones, F.H. Tezel, J. Thibault, R. El-Hawary, and J. Tolan, "Adsorption Separation of Ethanol from Water for Bioethanol Production", presented at the *AIChE Annual meeting* in Cincinnati, Ohio, USA, October 30-November 4, 2005
21. R. Jones, F.H. Tezel, J. Thibault, and R. El-Hawary, "Industrial Bioethanol: Selective Separation via Adsorption" presented at the *55th Canadian Chemical Engineering Conference* in Toronto, Canada, October 16-19, 2005